Dynamic Fracture Problems Involving Highly Transient Crack Growth Histories: An Investigation of Dynamic Failure in Homogeneous and Bimaterial Systems

Thesis by

Cheng Liu

In Partial Fulfillment of the Requirements

for the Degree of

Doctor of Philosophy

California Institute of Technology

Pasadena, California

1994

(Submitted May 2, 1994)

To my parents

To my family

To my homeland, China

Acknowledgments

I always feel lucky of having the opportunity to study and work at Caltech not only for the stimulating research environment but also for the people who made Caltech such a unique scientific community. Among others, my sincere gratitude goes to my advisor, Professor Ares J. Rosakis, for his guidance, support, and encouragement during the entire course of this study. I am very grateful to Professor Rosakis for giving me the opportunity and freedom to pursue the ideas presented in this dissertation. Through the many hours of discussions and sometimes through his scientific intuition, he corrected many of my mistakes and resolved a lot of my confusions. Also, I would like to thank Professors K. Battacharya, W. G. Knauss, and G. Ravichandran for taking time to read this thesis and to provide constructive comments on its content. The work presented in this dissertation bears deep influences from Professor Knowles' lectures on elasticity and Professor Freund's book *Dynamic Fracture Mechanics*. In addition, Professor Ravichandran's emphasis on visualization has proved to be very helpful. They deserve my sincere appreciation as well.

Thanks are also due to all my fellow students in the Solid Mechanics Group of the Graduate Aeronautical Laboratories for their suggestions, comments, and criticism throughout this research. In particular, I greatly appreciate the many fruitful collaborations and useful discussions with Dr. John Lambros. His excellent experimental work provided great motivations to my research. I also want to thank my college classmate and roommate, Professor Y. Huang at The University of Arizona, for the many invaluable conversations we had. It is him who hammered me so hard on the mistakes I made on both concepts and derivations.

The present work was funded by the Office of Naval Research Grant N00014-90-J-1340, the National Science Foundation Grant MSS-9024838, and the Army Research Office Grant DAAH04-93-G-0037. This financial support is gratefully acknowledged.

Finally, I am deeply grateful to my parents, to whom this thesis is dedicated, for their unwavering belief in education and lovely concern during my whole life. I am indebted to my wife, Hong, for her love, encouragement, support, sharing every single up and down, and for her appreciation of my projects which seem too far away from her biological experiments.

Abstract

Highly transient elastodynamic fracture processes in both homogeneous and bimaterial systems have been investigated. It is found that due to the wave character of the mechanical fields during transient and dynamic crack growth, the customarily assumptions of steady state and K^d-dominance may be violated. This may be particularly true during crack growth in laboratory size specimens where crack growth seldom reaches steady state conditions due to the persistence of the initiation transients and the influence of reflected stress waves from the specimen boundaries. By relaxing both restrictions of steady state and of K^d-dominance, and by permitting the crack-tip speed and the dynamic stress intensity factor to be arbitrary functions of time, the transient asymptotic elastodynamic field near the moving crack-tip was established in the form of higher order expansion for both homogeneous solids and bimaterial systems. In homogeneous solids, we considered cracks that propagated along arbitrary smooth paths, while in bimaterial systems, we only considered crack growth along a straight interface. The higher order coefficients of the asymptotic expansion were found to depend on the time derivative of crack-tip speed, the time derivative of the dynamic stress intensity factors, and for crack propagating along curved paths, on the instantaneous value of the local curvature of the crack path.

The issue of K^d-dominance during dynamic crack initiation and transient crack growth was further investigated by solving a particular transient initial/boundary value problem. This corresponds to a planar dilatational wave impinging on a semi-infinite crack in an unbounded elastic solid. The crack initiates under the influence of the wave, and then propagates dynamically. Through comparison of this full field solution and the equivalent K^d-dominant field or the field represented by the higher order transient terms, it is found that even for points which are relatively far away

from the crack-tip, or for times very close to the crack initiation, the higher order transient representation provides a very good description of the actual stress field. The K^d-dominant field, however, is incapable of approximating the complete stress field with any accuracy (lack of K^d-dominance).

The implications of the above observations (possible lack of K^d-dominance) on the interpretability of dynamic fracture experiments are also explored. The interpretation of experimental data in past laboratory investigations of dynamic fracture events is based on the assumption of K^d-dominance. However, as we have seen theoretically this assumption may often fail in laboratory situations. As a result, experimental measurements must be analyzed by techniques that allow for the possibility of the existence of transient higher order term effects. Several types of experiments are considered as examples. Plate impact experiments involving very high rates of loading are first analyzed by both a K_I^d-dominant and a high order transient approach. The results clearly show the strong effects of transients on the interpretation of the data. As a second example, the optical method of caustics is reanalyzed. A new way of extracting the instantaneous value of the dynamic stress intensity factor $K_I^d(t)$, which takes transients into account, is proposed and verified theoretically. For the bimaterial system, the issues are equivalent but much more complicated analytically. Here transient effects are found to be magnified by the material property mismatch between the constituent solids. It is shown however, that the higher order transient analysis can predict accurately the fringe patterns from actual experiment performed by means of the CGS (Coherent Gradient Sensing) technique and high speed photography.

The observations of this thesis suggest that a variety of conclusions made in the literature based on interpretations of experimental data on the basis of steady state or K^d-dominance may be suspect.

Table of Contents

Chapter 1

Introduction

1.1 Motivation

It is inevitable that all engineering structures contain or develop macroscopic cracks, either due to existing natural defects or due to processes of fabrication and assembly. If the applied loads in service are high enough, these macrocracks may grow and, under certain circumstances, become unstable. An unstable crack propagates dynamically in a solid, with a velocity equal to some substantial fraction of the material elastic shear wave speed ($\sim 0.3c_s$). This rapid material separation would seriously damage the integrity and function of the structure, and even lead to catastrophic failure. To prevent the occurrence of such disastrous events, the discipline of dynamic fracture mechanics, which is concerned with problems involving cracks in situations where inertial or strain rate effects are important, has been developed and has become an active area in mechanics during the past decade.

The origin of fracture mechanics is dated back to the 1920's. It is commonly acknowledged that the work of Griffith (1920) represented the birth of quasi-static fracture mechanics as a quantitative science of material behavior. As for dynamic fracture mechanics, the first classical and theoretical contribution seems to be the one by Mott (1948), who included inertial effects into his analysis of rapid crack

growth. Mott's work essentially paralleled that of Griffith and was based on the argument of equilibrium of energies.

Mathematically, if we consider a linearly elastic solid, the governing equation of motion reduces to the linear wave equation (or system of equations). However, for cases of dynamic crack initiation and growth, what we need to deal with is a boundary/initial value problem which is far more complicated than the problem of quasi-static fracture mechanics. This is because part of the boundary — the crack, is moving during the fracture process, and generally the entire history of the moving boundary is not known prior, and it depends on the solution of the governing equations. Inversely the solution also depends on the boundary conditions as well. Consequently, even though the governing equation is linear, the entire problem becomes highly nonlinear. This is called *moving boundary problem* in mathematical physics. For a moving boundary problem involving hyperbolic, second order equation (or equations), no general solution or general procedure to obtain the solution has been discovered yet. Therefore, researchers have to invent various simplifications regarding crack motion so that the mathematical models can be tackled. One of the most famous solutions involving dynamic crack growth was given by Yoffe (1951). She considered a steady state crack propagating in an unbounded elastic solid where the crack length remained a constant. Other solutions which involved transient crack propagation, among others, are those given by Cragg (1960), Broberg (1960), Baker (1962), Achenbach and Nuismer (1971), and Freund (1973). As we have mentioned earlier, in order to make the mathematical problem solvable, these solutions corresponded to very special geometrical configurations (e.g., unbounded bodies) and simple loading conditions.

In contrast to most analytically studied problems, most of the experimental investigations in the laboratory are utilizing finite-sized specimens and the loading histories are much more complicated than most analyses. As a result, it becomes necessary for

the experimentalists to observe near the crack-tip and to interpret data in terms of asymptotic representations of the crack-tip field. The relevant question then becomes what is the universal asymptotic structure of the deformation with respect to an observation position very close to the stationary or moving crack-tip. For a stationary crack subjected to quasi-static load, Irwin (1957) and Williams (1957) observed that the elastic stress field near the crack-tip has a universal spatial structure, and the magnitude of the stress field is controlled by a scalar quantity, the elastic stress intensity factor. For the dynamic moving crack, Freund and Clifton (1974) have provided a standard asymptotic method and have given the leading term of the asymptotic expansion for the boundary/initial value problem of a moving crack. In addition to the most singular asymptotic representation of the stress field, Nishioka and Atluri (1983) and Dally (1987) also studied the higher order asymptotic expression for the stress field near the tip of a moving crack under *steady state* conditions.

The interpretation of the measurement data in most of the experimental investigation of dynamic fracture mechanics is based on the assumption that the near-tip field is represented in terms of the leading term in the asymptotic expansion. This is called the assumption of K^d-dominance. Also, the region where the leading term of the asymptotic expansion can approximate the deformation field sufficiently well, is referred to as the K^d-dominant region. However, recent experimental evidence obtained by means of optical techniques, e.g., the method of caustics (Ravi-Chandar and Knauss, 1984; Krishnaswamy and Rosakis, 1991; Rosakis *et al.*, 1990) and the Coherent Gradient Sensing technique (CGS) (Krishnaswamy *et al.*, 1992), have shown that the assumption of K^d-dominance is often violated during the process of dynamic fracture in laboratory specimens, and K^d-dominance is insufficient to characterize the deformation field near the crack-tip. It was observed that the violation of the assumption of K^d-dominance is often associated with the existence of highly transient crack growth motions as well as with sudden arrivals of stress waves reflected

from the specimen boundaries. It is also believed that many long standing debates in dynamic fracture mechanics may be traced to the transient nature of the fracture event and consequently to the resulting lack of confidence on the conclusions of past experimental studies which assume K^d-dominance.

The possible violation of the assumption of K^d-dominance, raises questions regarding the interpretability of experimental data and partially motivates the theoretical developments described in this thesis.

1.2 Overview of thesis

In Chapter 2, the transient mixed-mode elastodynamic crack growth along arbitrary smoothly varying paths is considered. Asymptotically, the crack-tip stress field is square root singular with the angular variation of the singular term depending weakly on the instantaneous values of the crack-tip speed and on the mode-I and mode-II stress intensity factors. However, for a material particle at a small distance away from the moving crack-tip, the local stress field will depend not only on the instantaneous values of the crack-tip speed and stress intensity factors, but also on the past history of these time dependent quantities. In addition, for cracks propagating along curved paths the stress field is also expected to depend on the nature of the curved crack path. Here, a representation of the crack-tip fields in the form of an expansion about the crack-tip is obtained in powers of radial distance from the tip. The higher order coefficients of this expansion are found to depend on the time derivative of crack-tip speed, the time derivatives of the two stress intensity factors as well as on the instantaneous value of the local curvature of the crack path. It is also demonstrated that even if cracks follow a curved path dictated by the criterion $K_{II}^d = 0$, the stress field may still retain higher order asymmetric components related to non-zero local curvature of the crack path. For the first time, these results will shed new light on

the experimental interpretation of dynamic crack curving and may help to establish the criterion governing the crack growth along an arbitrary curved path.

To illustrate the importance of transient effects on the dynamic crack initiation and growth, in Chapter 3, we revisit the problem of a semi-infinite crack loaded by a planar stress wave. After a finite delay time, the crack starts to extend with a constant speed. In this chapter, we use this particular problem to investigate the question of the region of dominance of the mode-I asymptotic elastodynamic crack-tip fields. The complete full field analytical solution of stresses surrounding the stationary and moving crack-tip is obtained using the procedure outlined by Freund (1973, 1990). This analytical solution is compared to the asymptotic structure obtained in Chapter 2 and the coefficients of the higher order transient asymptotic representation are determined. To demonstrate the importance of transient effects, the normal traction ahead of the moving crack-tip is studied and compared to the field either represented by K_I^d-dominance, or represented by the higher order transient asymptotic expansion (see Chapter 2). The result shows that the higher order transient asymptotic expansion is necessary to describe the near-tip field at a time close to the event of crack initiation, or at a location relatively far away from the crack-tip. This study also concludes that in the event where transient effects are severe and cannot be neglected, the K_I^d-dominant field cannot provide an accurate description of crack-tip fields and should give way to the higher order transient asymptotic representation.

An experimental configuration which involves loading a half plane crack by a planar tensile pulse has been developed by Ravichandran and Clifton (1989). Using this configuration, extensive observations have been made by Prakash and Clifton (1992) on the process of crack initiation and growth in a hardened AISI 4340 VAR steel. Some interesting phenomena regarding the time variation of measured particle velocities, are observed in the work of Prakash and Clifton (1992). These phenomena cannot be explained merely by the K_I^d-dominant representation of the initiating and growing

crack-tip field. The problem studied in Ravichandran and Clifton (1989) and Prakash and Clifton (1992) can be modeled mathematically by the solution given in Chapter 3. In Chapter 4, we provide an interpretation to the experimental observations made by Prakash and Clifton (1992). First, the higher order transient asymptotic representation of the particle velocity field is derived by using the result given in Liu and Rosakis (1992) (also see Chapter 2). Then we simulate the experimental measurements of particle velocity by using the higher order transient representation and by initially assuming constant crack-tip speed. The result of this initial simulation shows that the higher order transient representation successfully captures the crude features of the experimental results. To further investigate the influence of transient effects, we subsequently relax the restriction of constant crack-tip velocity. Motivated by the experimental measurements made by Zehnder and Rosakis (1990), we introduce a fracture criterion that relates the dynamic stress intensity factor to the speed of the propagating crack. By solving the crack-tip equation of motion, all time-dependent quantities in the higher order transient asymptotic representation are determined. The final simulation of the experimental observation shows that the fully transient asymptotic field can describe the measured particle velocities very well. The experimental observation can be interpreted more accurately by including the effects of crack-tip acceleration and rapid changes of the dynamic stress intensity factor associated with crack initiation.

In experimental investigations of dynamic fracture, optical techniques are the mostly used diagnostic methods. Among them, the optical method of caustics has been extensively utilized in the past two decades in studying dynamic crack initiation, propagation and arrest phenomena. However, in analyzing the optical method of caustics, several assumptions need to be made. Some of these assumptions have been addressed and their influence on the interpretation of the caustic patterns have been studied (Rosakis and Zehnder, 1985; Rosakis, 1993). Nevertheless, one of the

important issues that has not been understood is the effect of lack of K_I^d-dominance, resulting from transients, on the interpretation of the caustic patterns. In Chapter 5, the optical method of caustics is re-examined by considering the presence of dynamic non-uniform crack-tip motion histories. Based on the higher order asymptotic transient expansion obtained by Freund and Rosakis (1990, 1991), Rosakis, Liu and Freund (1991), and on the results obtained in Chapter 2, in which dynamic transient effects were included in the near-tip deformation field, the exact mapping equations of caustics are derived for non-uniformly propagating mode-I cracks. The resulting equations indicate that the classical analysis of caustics based on the assumption of K_I^d-dominance, is inadequate to interpret the experimental caustic patterns when dynamic transient effects become significant. In this chapter, an explicit relation between the instantaneous value of the dynamic stress intensity factor $K_I^d(t)$ and the geometrical characteristics of the caustic is established. It is shown that for the case of non-uniformly propagating cracks, the relation between the dynamic stress intensity factor and the geometrical characteristics of the caustic pattern depends on the crack-tip acceleration and on the time derivative of the dynamic stress intensity factor, $\dot{K}_I^d(t)$. It also reduces to the classical relation between $K_I^d(t)$ and the caustic diameter for the case of K_I^d-dominance (when the crack-tip fields are well described by the $r^{-1/2}$ singularity in stresses). Two characteristic lengths of the caustic pattern are proposed to be used in determining the dynamic stress intensity factor of the transiently growing crack. In order to measure these two lengths accurately, a multi-point technique is also developed in this chapter. The Broberg problem (Broberg, 1960) is used as an example problem to check the feasibility of analyzing caustics in the presence of higher order transient terms. It is shown that the value of the dynamic stress intensity factor obtained by the proposed method agrees remarkably well with the exact analytical value while large errors are introduced when the classical analysis (K_I^d-dominant) of the method of caustics is used.

In Chapter 6, we further extend our transient asymptotic analysis to the case of an interfacial crack propagating transiently in a bimaterial system. In this chapter, a higher order asymptotic analysis of the transient deformation field surrounding the tip of a crack running dynamically along a bimaterial interface is presented. An asymptotic methodology is used to reduce the problem to one of the Riemann-Hilbert type. Its solution furnishes displacement potentials which are used to explicitly evaluate the near-tip transient stress field. Crack-tip fields corresponding to crack speeds up to the lower of the two shear wave speeds are investigated. An experimental study of dynamic crack growth in PMMA/steel interfaces using the optical method of CGS and high speed photography, is described and provides motivations for the analysis. Transonic terminal speeds (up to $1.4c_s^{\text{PMMA}}$) and initial accelerations ($\sim 10^8 \text{m/sec}^2$) are reported and discussed in the light of the phenomenon of lack of K^d-dominance. Transient effects are found to be severe and more important than in homogeneous dynamic fracture. For subsonic crack growth, these experiments are used to demonstrate the necessity of employing a fully transient expression in the analysis of optical data to accurately predict the complex dynamic stress intensity factor history.

Finally, in Chapter 7, a summary of work in progress is made.

Chapter 2

Higher Order Asymptotic Analysis of a Non-Uniformly Propagating Crack Along an Arbitrary Path

2.1 Introduction

Since Irwin (1957) and Williams (1957) observed that the elastic stress field near the tip of a static crack has a universal spatial structure, and the magnitude of the stress field is controlled by a scalar quantity, the elastic stress intensity factor, this quantity has played one of the most important roles in linear elastic fracture mechanics. For propagating cracks, the early analytical results of Yoffe (1951), Craggs (1960), Broberg (1960), Baker (1962) and Freund (1972), among others, revealed that the asymptotic stress field near the moving crack-tip has a universal structure as well. As stated by Freund and Clifton (1974), the stress field with reference to a Cartesian coordinate system moving with the crack-tip of "all plane elastodynamic solutions for (smoothly turning) running cracks, for which the total internal energy is finite," can be asymptotically described by the square root singular expression,

$$\sigma_{\alpha\beta} = \frac{K_I^d(t)}{\sqrt{2\pi r}}\Sigma_{\alpha\beta}^I(\theta, v) + \frac{K_{II}^d(t)}{\sqrt{2\pi r}}\Sigma_{\alpha\beta}^{II}(\theta, v) + O(1) \ , \qquad \text{as } r \to 0 \ . \tag{2.1.1}$$

Here (r, θ) is a polar coordinate system traveling with the crack-tip, $\Sigma_{\alpha\beta}^I(\theta, v)$ and $\Sigma_{\alpha\beta}^{II}(\theta, v)$ are known universal functions of θ and crack-tip speed v, and $K_I^d(t)$ and

$K_{II}^d(t)$ are the mode-I and mode-II stress intensity factors, respectively. They are dependent only on the specific geometric and loading conditions of a problem. In addition to the most singular asymptotic representation of the stress field, Nishioka and Atluri (1983) and Dally (1987) also developed the entire higher order asymptotic expression for the stress field near the tip of a dynamically moving straight crack under *steady state* conditions.

Expression (2.1.1) is strictly valid only in the immediate vicinity of the crack-tip. To apply this expression over a region of finite extent, one must show that the asymptotic solution indeed dominates over this region, and this domain is then referred to as a region of K^d-dominance. Recent experimental evidence obtained by means of optical techniques, e.g., the method of caustics (Krishnaswamy and Rosakis, 1991; Rosakis *et al.*, 1990) and the Coherent Gradient Sensor technique (CGS) (Krishnaswamy *et al.*, 1992), have shown that the assumption of K^d-dominance is often violated during the process of dynamic fracture, and that the expression in (2.1.1) is insufficient to characterize the deformation field near the crack-tip. It was observed that the violation of the assumption of K_I^d-dominance is often associated with the existence of highly transient crack growth motions involving crack-tip accelerations as well as fast varying stress intensity factor histories, events that are typical of most laboratory dynamic testing situations.

By using the asymptotic methodology introduced by Freund (1990), and by relaxing the assumption of K_I^d-dominance, Freund and Rosakis (1992) have provided a higher order asymptotic expansion for the first stress invariant (quantity of interest for both caustics and CGS) and showed that this expansion provides an accurate description of crack-tip fields under fairly severe transient conditions. Later, Rosakis *et al.* (1991) obtained the higher order asymptotic stress field near the tip of a non-uniformly propagating mode-I crack. In a related study, Liu *et al.* (1993) have also applied these results to the interpretation of optical caustic patterns and have

confirmed the advantages of the higher order expansion in analyzing experimental data.

Our purpose in this chapter is to understand the nature of the mixed mode asymptotic field that dominates the region near a transiently propagating and curving crack-tip. In this chapter, we develop a new methodology to obtain the higher order transient asymptotic elastodynamic field near the tip of a crack that propagates non-uniformly along an arbitrary and smoothly curved path. Here, we consider crack growth in a homogeneous, isotropic, and linearly elastic material. The deformation is assumed to be plane strain. However, for plane stress similar results can be obtained by changing the expression for some material parameters. By using the asymptotic procedure proposed by Freund (1990) and utilized by Freund and Rosakis (1992), the governing equation is reduced to a series of coupled partial differential equations, and the problem can be further recast into a Riemann-Hilbert problem. Upon solving the Riemann-Hilbert equation, the higher order near-tip transient elastodynamic asymptotic field can be obtained. The results show that the singular terms and the so-called T-stress term have the same spatial form as those obtained under steady state conditions. However, the dynamic stress intensity factors and the crack-tip velocity are now allowed to be functions of time. The third term, on the other hand, depends not only on the instantaneous values of the crack-tip speed and the stress intensity factors, but also on the past history of these time-dependent quantities (i.e., on $\dot{K}_I^d(t)$, $\dot{K}_{II}^d(t)$, and $\dot{v}(t)$). For a crack that propagates along a curved path, the third term also depends on the curvature of the crack path at the crack-tip. Some implications of these analytical results on the interpretation of experimental observations of crack curving are also discussed.

2.2 General formulation

Consider a planar body composed of homogeneous, isotropic, linearly elastic material. In the body, there is an arbitrarily propagating crack. Introduce a fixed orthonormal Cartesian coordinate system (x_1, x_2) so that at a time $t = 0$, the crack-tip happens to be at the origin of the system. For any $t > 0$, the position of the propagating crack-tip is supposed to be given by $(X_1(t), X_2(t))$, see FIGURE 2.1. If the deformation is plane

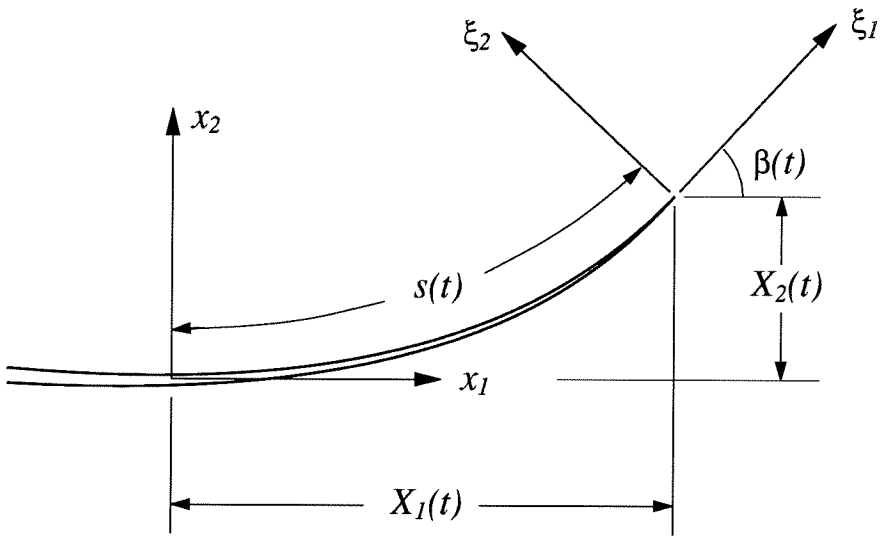

Figure 2.1: Crack growing along a smooth curved path under two-dimensional conditions. The instantaneous crack-tip position is $x_1 = X_1(t)$, $x_2 = X_2(t)$, and the instantaneous crack-tip speed is $v(t)$ in the local ξ_1-direction.

strain, we may consider the two displacement potentials, $\phi(x_1, x_2, t)$ and $\psi(x_1, x_2, t)$, and then the two non-zero displacement components can be expressed by

$$u_\alpha(x_1, x_2, t) = \phi_{,\alpha}(x_1, x_2, t) + e_{\alpha\beta}\psi_{,\beta}(x_1, x_2, t) \ , \tag{2.2.1}$$

where α, $\beta \in \{1, 2\}$ and the summation convention is employed here. $e_{\alpha\beta}$ is the two-dimensional alternative symbol defined by

$$e_{12} = -e_{21} = 1 \ , \qquad e_{11} = e_{22} = 0 \ .$$

The components of stress for the material we consider can be expressed by the displacement potentials like

$$\left.\begin{aligned}\sigma_{11} &= \mu\left[\frac{c_l^2}{c_s^2}\phi_{,\alpha\alpha} - 2\phi_{,22} + 2\psi_{,12}\right] \\ \sigma_{22} &= \mu\left[\frac{c_l^2}{c_s^2}\phi_{,\alpha\alpha} - 2\phi_{,11} - 2\psi_{,12}\right] \\ \sigma_{12} &= \mu\left[2\phi_{,12} + \psi_{,22} - \psi_{,11}\right]\end{aligned}\right\}, \tag{2.2.2}$$

where μ is the shear modulus, and c_l, c_s are the longitudinal and shear wave speeds of the elastic material, respectively. In terms of the shear modulus μ, c_l and c_s are given by

$$c_l = \left\{\frac{\kappa+1}{\kappa-1}\cdot\frac{\mu}{\rho}\right\}^{1/2}, \qquad c_s = \left\{\frac{\mu}{\rho}\right\}^{1/2}, \tag{2.2.3}$$

where $\kappa = 3 - 4\nu$ for plane strain and $\kappa = (3-\nu)/(1+\nu)$ for plane stress, and ρ is the mass density of the material, ν is the Poisson's ratio. By changing the definition for the longitudinal wave speed in equation (2.2.3), the solution corresponding to the plane stress deformation can be obtained. Meanwhile, c_l and c_s in both plane strain and plane stress, are related by

$$\frac{c_s}{c_l} = \left\{\frac{\kappa-1}{\kappa+1}\right\}^{1/2}. \tag{2.2.4}$$

The equation of motion in the absence of body force in the fixed coordinate system, in terms of $\phi(x_1, x_2, t)$ and $\psi(x_1, x_2, t)$ is

$$\left.\begin{aligned}\phi_{,\alpha\alpha}(x_1,x_2,t) - \frac{1}{c_l^2}\ddot{\phi}(x_1,x_2,t) &= 0 \\ \psi_{,\alpha\alpha}(x_1,x_2,t) - \frac{1}{c_s^2}\ddot{\psi}(x_1,x_2,t) &= 0\end{aligned}\right\}. \tag{2.2.5}$$

Now introduce a new moving coordinate system, (ξ_1, ξ_2), so that the origin of the new system is at the moving crack-tip. The ξ_1-axis is tangential to the crack trajectory at the crack-tip and coincides with the direction of crack growth. The angle

between the ξ_1-axis and the fixed x_1-axis is denoted by $\beta(t)$, as shown in FIGURE 2.1. Therefore, the relation between the coordinates in these two systems is

$$\left.\begin{aligned} \xi_1 &= \{x_1 - X_1(t)\}\cos\beta(t) + \{x_2 - X_2(t)\}\sin\beta(t) \\ \xi_2 &= -\{x_1 - X_1(t)\}\sin\beta(t) + \{x_2 - X_2(t)\}\cos\beta(t) \end{aligned}\right\} . \tag{2.2.6}$$

In this new system, the equation of motion (2.2.5) for $\phi(\xi_1, \xi_2, t)$ and $\psi(\xi_1, \xi_2, t)$ will be (Freund, 1990)

$$\left.\begin{aligned} \phi_{,\alpha\alpha} - \frac{1}{c_l^2}\left\{\phi_{,\alpha\beta}\,\dot{\xi}_\alpha\dot{\xi}_\beta + \phi_{,\alpha}\,\ddot{\xi}_\alpha + 2\phi_{,\alpha t}\,\dot{\xi}_\alpha + \phi_{,tt}\right\} &= 0 \\ \psi_{,\alpha\alpha} - \frac{1}{c_s^2}\left\{\psi_{,\alpha\beta}\,\dot{\xi}_\alpha\dot{\xi}_\beta + \psi_{,\alpha}\,\ddot{\xi}_\alpha + 2\psi_{,\alpha t}\,\dot{\xi}_\alpha + \psi_{,tt}\right\} &= 0 \end{aligned}\right\} . \tag{2.2.7}$$

If the length of the trajectory that the crack-tip travels during the time interval $[0, t]$, is denoted by $s(t)$, then the magnitude of the crack-tip speed $v(t)$ will be $\dot{s}(t)$, and the curvature of the crack trajectory at the moving crack-tip, $k(t)$, is given by

$$k(t) = \frac{\mathrm{d}\beta}{\mathrm{d}s} = \frac{\dot{\beta}(t)}{v(t)} . \tag{2.2.8}$$

In terms of the crack-tip speed $v(t)$, and the crack-tip curvature $k(t)$, we have the relation

$$\dot{\xi}_1 = -v(t) + v(t)k(t)\xi_2 , \qquad \dot{\xi}_2 = -v(t)k(t)\xi_1 . \tag{2.2.9}$$

As a result of equation (2.2.9), we can also express the $\ddot{\xi}_\alpha$ in terms of the crack-tip speed and the crack-tip curvature. Now, the equation of motion (2.2.7) can be rewritten as

$$\left.\begin{aligned} &\phi_{,11} + \frac{1}{\alpha_l^2}\phi_{,22} + \frac{2\sqrt{v}}{\alpha_l^2 c_l^2}\left\{\sqrt{v}\phi_{,1}\right\}_{,t} - \frac{1}{\alpha_l^2 c_l^2}\phi_{,tt} \\ &- \frac{v^2 k}{\alpha_l^2 c_l^2}\left\{\phi_{,2} + 2\xi_1\phi_{,12} - 2\xi_2\phi_{,11}\right\} - \frac{2\sqrt{vk}}{\alpha_l^2 c_l^2}\left\{\sqrt{vk}\,(\xi_2\phi_{,1} - \xi_1\phi_{,2})\right\}_{,t} \\ &+ \frac{v^2 k^2}{\alpha_l^2 c_l^2}\left\{\xi_2^2\phi_{,11} - 2\xi_1\xi_2\phi_{,12} + \xi_1^2\phi_{,22} - \xi_1\phi_{,1} - \xi_2\phi_{,2}\right\} = 0 \end{aligned}\right\} , \tag{2.2.10}$$

and

$$\left.\begin{aligned}
&\psi_{,11}+\frac{1}{\alpha_s^2}\psi_{,22}+\frac{2\sqrt{v}}{\alpha_s^2c_s^2}\left\{\sqrt{v}\psi_{,1}\right\}_{,t}-\frac{1}{\alpha_s^2c_s^2}\psi_{,tt}\\
&-\frac{\sqrt{vk}}{\alpha_s^2c_s^2}\left\{\psi_{,2}+2\xi_1\psi_{,12}-2\xi_2\psi_{,11}\right\}-\frac{2\sqrt{vk}}{\alpha_s^2c_s^2}\left\{\sqrt{vk}\left(\xi_2\psi_{,1}-\xi_1\psi_{,2}\right)\right\}_{,t}\\
&+\frac{v^2k^2}{\alpha_s^2c_s^2}\left\{\xi_2^2\psi_{,11}-2\xi_1\xi_2\psi_{,12}+\xi_1^2\psi_{,22}-\xi_1\psi_{,1}-\xi_2\psi_{,2}\right\}\;=\;0
\end{aligned}\right\}\;, \qquad (2.2.11)$$

where the two quantities α_l and α_s depend on crack-tip speed, and therefore depend on time t through

$$\alpha_{l,s}(t)=\left\{1-\frac{v^2(t)}{c_{l,s}^2}\right\}^{1/2}.$$

Notice that in equations (2.2.10) and (2.2.11), the derivative with respect to time, t, is distinct from that in equation (2.2.5). Here, ξ_1,ξ_2 are held fixed, whereas in (2.2.5), x_1,x_2 are held fixed. Throughout this study, we will use $\partial/\partial t$, or $\{\ \}_{,t}$ to denote the differentiation with respect to time, t, where the moving spatial coordinates are held fixed, while using $\{\dot{}\}$ denote the same operation but the fixed spatial coordinates are held fixed.

At this point, we employ the standard asymptotic device used by Freund and Rosakis (1992) for the analysis of transient mode-I crack growth. We assume that $\phi(\xi_1,\xi_2,t)$ and $\psi(\xi_1,\xi_2,t)$ can be asymptotically expanded as

$$\phi(\xi_1,\xi_2,t)=\sum_{m=0}^{\infty}\epsilon^{pm}\phi_m(\eta_1,\eta_2,t)\;,\quad \psi(\xi_1,\xi_2,t)=\sum_{m=0}^{\infty}\epsilon^{pm}\psi_m(\eta_1,\eta_2,t)\;, \qquad (2.2.12)$$

as $r=(\xi_1^2+\xi_2^2)^{1/2}\to 0$, where $\eta_\alpha=\xi_\alpha/\epsilon\;,\alpha\in\{1,2\}$, and ϵ is a small arbitrary positive number. The parameter ϵ is used here so that the region around the crack-tip is expanded to fill the entire field of observation. As ϵ is chosen to be infinitely small, all points in the (ξ_1,ξ_2) plane except those very close to the crack-tip, are pushed out of the field of observation in the (η_1,η_2) plane. If the trajectory of the moving crack is smooth enough, the crack line will occupy the entire negative η_1-axis in this scaled plane. By taking $\epsilon=1$, the above equation will provide the asymptotic representation of the displacement potentials in the unscaled physical plane as $r\to 0$.

In the asymptotic representation (2.2.12), the powers of ϵ are such that

$$p_{m+1} = p_m + \frac{1}{2} , \qquad m = 0, 1, 2, \cdots , \tag{2.2.13}$$

so that the nontrivial solutions for $\phi_m(\eta_1, \eta_2, t)$ exist. Since the displacement should be bounded throughout the region, but the stress may be singular at the crack-tip, p_0 is expected to be in the range $1 < p_0 < 2$. We also should have that

$$\frac{\epsilon^{p_{m+n}} \phi_{m+n}(\eta_1, \eta_2, t)}{\epsilon^{p_m} \phi_m(\eta_1, \eta_2, t)} \to 0 , \qquad \text{as} \quad \epsilon \to 0 , \tag{2.2.14}$$

for any positive integer n. Meanwhile, as we return to the physical plane, we will have

$$\frac{\phi_{m+n}(\xi_1, \xi_2, t)}{\phi_m(\xi_1, \xi_2, t)} \to 0 , \qquad \text{as} \quad r = \sqrt{\xi_1^2 + \xi_2^2} \to 0 , \tag{2.2.15}$$

for any positive integer n, so that in the physical plane, (ξ_1, ξ_2), $\phi_m(\xi_1, \xi_2, t)$ are ordered according to their contributions to the near-tip deformation field. The above properties for ϕ_m hold for ψ_m as well.

Substituting the asymptotic representations for the two displacement potentials $\phi(\xi_1, \xi_2, t)$ and $\psi(\xi_1, \xi_2, t)$, in equation (2.2.12), into the equations of motion (2.2.10) and (2.2.11), we will obtain two equations where the left-hand side is an infinite power series of ϵ. Since ϵ is an arbitrary number, the coefficient of each power of ϵ should be zero. Therefore, the equations of motion reduce to a series of coupled differential equations for $\phi_m(\eta_1, \eta_2, t)$ and $\psi_m(\eta_1, \eta_2, t)$ as follows:

$$\left.\begin{aligned}
\phi_{m,11} + \frac{1}{\alpha_l^2}\phi_{m,22} \;=\; & -\frac{2\sqrt{v}}{\alpha_l^2 c_l^2}\left\{\sqrt{v}\,\phi_{m-2,1}\right\}_{,t} + \frac{1}{\alpha_l^2 c_l^2}\phi_{m-4,tt} \\
& + \frac{(1-\alpha_l^2)k}{\alpha_l^2}\left\{\phi_{m-2,2} + 2\eta_1\phi_{m-2,12} - 2\eta_2\phi_{m-2,11}\right\} \\
& + \frac{2\sqrt{vk}}{\alpha_l^2 c_l^2}\left\{\sqrt{vk}\,(\eta_2\phi_{m-4,1} - \eta_1\phi_{m-4,2})\right\}_{,t} + \frac{(1-\alpha_l^2)k^2}{\alpha_l^2}\left\{\eta_2^2\phi_{m-4,11}\right. \\
& \left. - 2\eta_1\eta_2\phi_{m-4,12} + \eta_1^2\phi_{m-4,22} - \eta_1\phi_{m-4,1} - \eta_2\phi_{m-4,2}\right\}
\end{aligned}\right\} , \tag{2.2.16}$$

and

$$\left.\begin{aligned}
\psi_{m,11}+\frac{1}{\alpha_s^2}\psi_{m,22} \;=\; & -\frac{2\sqrt{v}}{\alpha_s^2 c_s^2}\left\{\sqrt{v}\psi_{m-2,1}\right\}_{,t}+\frac{1}{\alpha_s^2 c_s^2}\psi_{m-4,tt} \\
& +\frac{(1-\alpha_s^2)k}{\alpha_s^2}\left\{\psi_{m-2,2}+2\eta_1\psi_{m-2,12}-2\eta_2\psi_{m-2,11}\right\} \\
& +\frac{2\sqrt{vk}}{\alpha_s^2 c_s^2}\left\{\sqrt{vk}\,(\eta_2\psi_{m-4,1}-\eta_1\psi_{m-4,2})\right\}_{,t}+\frac{(1-\alpha_s^2)k^2}{\alpha_s^2}\left\{\eta_2^2\psi_{m-4,11}\right. \\
& \left.-2\eta_1\eta_2\psi_{m-4,12}+\eta_1^2\psi_{m-4,22}-\eta_1\psi_{m-4,1}-\eta_2\psi_{m-4,2}\right\}
\end{aligned}\right\}, \qquad (2.2.17)$$

for $m = 0, 1, 2, \cdots$, and where

$$\phi_m = \begin{cases} \phi_m & \text{for } m \geq 0 \\ 0 & \text{for } m < 0 \end{cases}, \qquad \psi_m = \begin{cases} \psi_m & \text{for } m \geq 0 \\ 0 & \text{for } m < 0 \end{cases}. \qquad (2.2.18)$$

It is noted that, for a crack propagating along a straight trajectory, $k(t) = 0$, and equations (2.2.16) and (2.2.17) reduce to that given by Rosakis *et al.* (1991). The term "coupled" is used above in the sense that ϕ_m or ψ_m with higher values of m will be affected by the solutions for ϕ_m or ψ_m with lower values of m. Furthermore, for the special case of *steady state* crack growth, the crack-tip velocity, v, will be a constant, and at the same time, $\phi_{m,t} = \psi_{m,t} = 0$, for $m = 0, 1, 2, \cdots$, which means that ϕ_m and ψ_m depend on t only through the spatial coordinate η_1. In such a case, the equations in (2.2.16) and (2.2.17) are not coupled anymore and each one reduces to Laplace's equation in the coordinates $(\eta_1, \alpha_l\eta_2)$ for ϕ_m and $(\eta_1, \alpha_s\eta_2)$ for ψ_m, respectively. The corresponding functions ϕ_m and ψ_m are independent of time in the moving coordinate system. The solution for this case is discussed by Dally (1987) who attributes the original results to G. R. Irwin. However, for the transient case, the crack may propagate along an arbitrary path, the crack-tip velocity, $v(t)$, may be a continuous function of time and so is the crack-tip curvature, $k(t)$. Also, $\phi_m(\eta_1, \eta_2, t)$ and $\psi_m(\eta_1, \eta_2, t)$ may depend on time explicitly in the moving coordinate system. The only uncoupled equations are those for $m = 0$ and $m = 1$. As $m > 1$, we can see from equations (2.2.16) and (2.2.17) that $\phi_m(\eta_1, \eta_2, t)$, or $\psi_m(\eta_1, \eta_2, t)$ is composed by two parts, one is the particular solution which is completely determined

by the previous terms, the other part is the homogeneous solution which satisfies the Laplace's equation in the corresponding scaled coordinate plane. Suppose that there is no traction applied on the crack faces, then the combination of the particular and homogeneous solutions should satisfy the traction free condition on the crack faces. In the following section, we will solve $\phi_m(\eta_1, \eta_2, t)$ and $\psi_m(\eta_1, \eta_2, t)$ for the most general transient situation of a crack propagating along an arbitrary path.

2.3 Solution for the higher order transient problem

As we have discussed in the previous section, in equations (2.2.16) and (2.2.17), the only uncoupled equations are those for $m = 0$ and $m = 1$. As $m > 1$, the solutions for $\phi_m(\eta_1, \eta_2, t)$ and $\psi_m(\eta_1, \eta_2, t)$ will be affected by the solutions with smaller m. Thus, in this section, we consider the situation of $m = 0$ and $m = 1$ first. After we get solutions for $m = 0$ and 1, we will subsequently solve $\phi_m(\eta_1, \eta_2, t)$ and $\psi_m(\eta_1, \eta_2, t)$ for higher order terms.

2.3.1 Solutions for $\phi_m(\eta_1, \eta_2, t)$ and $\psi_m(\eta_1, \eta_2, t)$ for $m = 0$ and 1

For $m = 0$, or 1, the equation of motion (2.2.16) and (2.2.17) reduce to

$$\left.\begin{aligned} \phi_{m,11}(\eta_1, \eta_2, t) + \frac{1}{\alpha_l^2(t)}\phi_{m,22}(\eta_1, \eta_2, t) &= 0 \\ \psi_{m,11}(\eta_1, \eta_2, t) + \frac{1}{\alpha_s^2(t)}\psi_{m,22}(\eta_1, \eta_2, t) &= 0 \end{aligned}\right\} . \tag{2.3.1}$$

They are Laplace's equations in the corresponding scaled plane $(\eta_1, \alpha_l(t)\eta_2)$ for ϕ_m, and $(\eta_1, \alpha_s(t)\eta_2)$ for ψ_m. The most general solutions for equation (2.3.1) can be

expressed as

$$\left.\begin{aligned}\phi_m(\eta_1,\eta_2,t) &= \mathrm{Re}\{F_m(z_l;t)\}\\ \psi_m(\eta_1,\eta_2,t) &= \mathrm{Im}\{G_m(z_s;t)\}\end{aligned}\right\}, \tag{2.3.2}$$

where the complex variables z_l and z_s are given by

$$z_l = \eta_1 + i\alpha_l\eta_2 \ , \qquad z_s = \eta_1 + i\alpha_s\eta_2 \ ,$$

and $i = \sqrt{-1}$. $F_m(z_l;t)$ and $G_m(z_s;t)$ are analytic everywhere in the complex z_l-, or z_s-planes except along the nonpositive real axis. In the analytic functions $F_m(z_l;t)$ and $G_m(z_s;t)$, behind the semicolon, the time t appears as a parameter. This suggests that $\phi_m(\eta_1,\eta_2,t)$ and $\psi_m(\eta_1,\eta_2,t)$ may depend on time t not only through the complex variables, z_l and z_s, but also explicitly through the time t itself.

Associated with these ϕ_m and ψ_m, the contributions to the displacement and stress components are given by

$$\left.\begin{aligned}u_1^{(m)} &= \mathrm{Re}\left\{F_m'(z_l;t) + \alpha_s G_m'(z_s;t)\right\}\\ u_2^{(m)} &= -\mathrm{Im}\left\{\alpha_l F_m'(z_l;t) + G_m'(z_s;t)\right\}\end{aligned}\right\}, \tag{2.3.3}$$

and

$$\left.\begin{aligned}\sigma_{11}^{(m)} &= \mu\mathrm{Re}\left\{\left(1+2\alpha_l^2-\alpha_s^2\right)F_m''(z_l;t) + 2\alpha_s G_m''(z_s;t)\right\}\\ \sigma_{22}^{(m)} &= -\mu\mathrm{Re}\left\{\left(1+\alpha_s^2\right)F_m''(z_l;t) + 2\alpha_s G_m''(z_s;t)\right\}\\ \sigma_{12}^{(m)} &= -\mu\mathrm{Im}\left\{2\alpha_l F_m''(z_l;t) + \left(1+\alpha_s^2\right)G_m''(z_s;t)\right\}\end{aligned}\right\}, \tag{2.3.4}$$

where the prime represents the derivative with respect to the corresponding complex argument.

Denote

$$\left.\begin{aligned}\lim_{\eta_2\to 0^+}\Omega(z) &= \Omega^+(\eta_1)\\ \lim_{\eta_2\to 0^-}\Omega(z) &= \Omega^-(\eta_1)\end{aligned}\right\}, \qquad z = \eta_1 + i\eta_2 \ .$$

As $\eta_1 < 0$ and $\eta_2 \to 0^{\pm}$, the traction free condition on the crack faces implies that $\sigma_{22}^{(m)}(\eta_1, 0^{\pm}, t) = \sigma_{12}^{(m)}(\eta_1, 0^{\pm}, t) = 0$, or, in terms of the complex displacement potentials, $F_m(z_l; t)$ and $G_m(z_s; t)$,

$$\left.\begin{array}{l} \mu(1+\alpha_s^2)\left\{F_m'^{\pm}(\eta_1;t) + \overline{F}_m'^{\mp}(\eta_1;t)\right\} \\ +2\mu\alpha_s\left\{G_m'^{\pm}(\eta_1;t) + \overline{G}_m'^{\mp}(\eta_1;t)\right\} = 0 \\ 2\mu\alpha_l\left\{F_m'^{\pm}(\eta_1;t) - \overline{F}_m'^{\mp}(\eta_1;t)\right\} \\ +\mu(1+\alpha_s^2)\left\{G_m'^{\pm}(\eta_1;t) - \overline{G}_m'^{\mp}(\eta_1;t)\right\} = 0 \end{array}\right\}, \quad \forall\ \eta_1 < 0\ , \tag{2.3.5}$$

where the overline stands for the complex conjugate. Here, it seems that we have four unknown functions, $F_m(z_l; t)$, $\overline{F}_m(z_l; t)$, $G_m(z_s; t)$, and $\overline{G}_m(z_s; t)$, while we only have two independent relations in equation (2.3.5). However, these four functions can be related by the fact that the displacement components and the traction components should be continuous when they cross the real axis ahead of the crack-tip, or in terms of the complex displacement potentials, $F_m(z_l; t)$ and $G_m(z_s; t)$, along $\eta_1 > 0$ and $\eta_2 = 0$, we should have

$$\left.\begin{array}{l} \mu(1+\alpha_s^2)\left\{F_m'^{+}(\eta_1;t) + \overline{F}_m'^{-}(\eta_1;t)\right\} \\ +2\mu\alpha_s\left\{G_m'^{+}(\eta_1;t) + \overline{G}_m'^{-}(\eta_1;t)\right\} \\ -\mu(1+\alpha_s^2)\left\{F_m'^{-}(\eta_1;t) + \overline{F}_m'^{+}(\eta_1;t)\right\} \\ -2\mu\alpha_s\left\{G_m'^{-}(\eta_1;t) + \overline{G}_m'^{+}(\eta_1;t)\right\} = 0 \\ 2\mu\alpha_l\left\{F_m'^{+}(\eta_1;t) - \overline{F}_m'^{-}(\eta_1;t)\right\} \\ +\mu(1+\alpha_s^2)\left\{G_m'^{+}(\eta_1;t) - \overline{G}_m'^{-}(\eta_1;t)\right\} \\ -2\mu\alpha_l\left\{F_m'^{-}(\eta_1;t) - \overline{F}_m'^{+}(\eta_1;t)\right\} \\ -\mu(1+\alpha_s^2)\left\{G_m'^{-}(\eta_1;t) - \overline{G}_m'^{+}(\eta_1;t)\right\} = 0 \end{array}\right\}, \quad \forall\ \eta_1 > 0\ , \tag{2.3.6}$$

and

$$\left.\begin{aligned}
&\left\{F_m'^{+}(\eta_1;t)+\overline{F}_m'^{-}(\eta_1;t)\right\}+\alpha_s\left\{G_m'^{+}(\eta_1;t)+\overline{G}_m'^{-}(\eta_1;t)\right\}\\
&-\left\{F_m'^{-}(\eta_1;t)+\overline{F}_m'^{+}(\eta_1;t)\right\}-\alpha_s\left\{G_m'^{-}(\eta_1;t)+\overline{G}_m'^{+}(\eta_1;t)\right\}=0\\
&\alpha_l\left\{F_m'^{+}(\eta_1;t)-\overline{F}_m'^{-}(\eta_1;t)\right\}+\left\{G_m'^{+}(\eta_1;t)-\overline{G}_m'^{-}(\eta_1;t)\right\}\\
&-\alpha_l\left\{F_m'^{-}(\eta_1;t)-\overline{F}_m'^{+}(\eta_1;t)\right\}-\left\{G_m'^{-}(\eta_1;t)-\overline{G}_m'^{+}(\eta_1;t)\right\}=0
\end{aligned}\right\},\forall\eta_1>0. \quad (2.3.7)$$

For simplicity, define the following matrices

$$\boldsymbol{P}=\begin{bmatrix}\mu(1+\alpha_s^2) & 2\mu\alpha_s\\ 2\mu\alpha_l & \mu(1+\alpha_s^2)\end{bmatrix},\qquad \boldsymbol{Q}=\begin{bmatrix}\mu(1+\alpha_s^2) & 2\mu\alpha_s\\ -2\mu\alpha_l & -\mu(1+\alpha_s^2)\end{bmatrix},$$

and

$$\boldsymbol{U}=\begin{bmatrix}1 & \alpha_s\\ \alpha_l & 1\end{bmatrix},\qquad \boldsymbol{V}=\begin{bmatrix}1 & \alpha_s\\ -\alpha_l & -1\end{bmatrix}.$$

Also define the following complex vector

$$\boldsymbol{f}_m(z;t)=\left(\ F_m(z;t),\ G_m(z;t)\ \right)^{\top},$$

where $z=\eta_1+i\eta_2$. Then, the traction free condition on the crack faces, equation (2.3.5), can be rewritten as

$$\boldsymbol{P}\boldsymbol{f}_m''^{\pm}(\eta_1;t)+\boldsymbol{Q}\overline{\boldsymbol{f}}_m''^{\mp}(\eta_1;t)=\mathbf{o}\ ,\qquad \forall\ \eta_1<0\ , \quad (2.3.8)$$

and the continuity condition of the displacement and traction ahead of the crack-tip, equations (2.3.6) and (2.3.7), become

$$\left.\begin{aligned}
&\boldsymbol{P}\boldsymbol{f}_m''^{+}(\eta_1;t)+\boldsymbol{Q}\overline{\boldsymbol{f}}_m''^{-}(\eta_1;t)-\boldsymbol{P}\boldsymbol{f}_m''^{-}(\eta_1;t)-\boldsymbol{Q}\overline{\boldsymbol{f}}_m''^{+}(\eta_1;t)=\mathbf{o}\\
&\boldsymbol{U}\boldsymbol{f}_m'^{+}(\eta_1;t)+\boldsymbol{V}\overline{\boldsymbol{f}}_m'^{-}(\eta_1;t)-\boldsymbol{U}\boldsymbol{f}_m'^{-}(\eta_1;t)-\boldsymbol{V}\overline{\boldsymbol{f}}_m'^{+}(\eta_1;t)=\mathbf{o}
\end{aligned}\right\},\ \forall\ \eta_1>0. \quad (2.3.9)$$

The continuity conditions in (2.3.9) can be rearranged as

$$\left.\begin{aligned}
&\boldsymbol{P}\boldsymbol{f}_m''^{+}(\eta_1;t)-\boldsymbol{Q}\overline{\boldsymbol{f}}_m''^{+}(\eta_1;t)=\boldsymbol{P}\boldsymbol{f}_m''^{-}(\eta_1;t)-\boldsymbol{Q}\overline{\boldsymbol{f}}_m''^{-}(\eta_1;t)\\
&\boldsymbol{U}\boldsymbol{f}_m'^{+}(\eta_1;t)-\boldsymbol{V}\overline{\boldsymbol{f}}_m'^{+}(\eta_1;t)=\boldsymbol{U}\boldsymbol{f}_m'^{-}(\eta_1;t)-\boldsymbol{V}\overline{\boldsymbol{f}}_m'^{-}(\eta_1;t)
\end{aligned}\right\},\ \forall\ \eta_1>0. \quad (2.3.10)$$

From the above equations, we may define two new functions by

$$\left.\begin{aligned} \boldsymbol{\kappa}_m(z;t) &= \boldsymbol{P}\boldsymbol{f}''_m(z;t) - \boldsymbol{Q}\overline{\boldsymbol{f}}''_m(z;t) \\ \boldsymbol{\theta}_m(z;t) &= \boldsymbol{U}\boldsymbol{f}'_m(z;t) - \boldsymbol{V}\overline{\boldsymbol{f}}'_m(z;t) \end{aligned}\right\} . \tag{2.3.11}$$

$\boldsymbol{\kappa}_m(z;t)$ and $\boldsymbol{\theta}_m(z;t)$ are analytic functions throughout the z-plane except along the cut occupied by the crack. From equation (2.3.11), it can be seen immediately that equation (2.3.9) is satisfied identically. So, the issue now is to find the analytic functions $\boldsymbol{\kappa}_m(z;t)$ and $\boldsymbol{\theta}_m(z;t)$.

Solve for $\boldsymbol{f}''_m(z;t)$ and $\overline{\boldsymbol{f}}''_m(z;t)$ from equation (2.3.11) to get

$$\left.\begin{aligned} \boldsymbol{f}''_m(z;t) &= \boldsymbol{P}^{-1}\boldsymbol{H}^{-1}\left\{\boldsymbol{\theta}'_m(z;t) - \overset{*}{\boldsymbol{L}}\,\boldsymbol{\kappa}_m(z;t)\right\} \\ \overline{\boldsymbol{f}}''_m(z;t) &= \boldsymbol{Q}^{-1}\boldsymbol{H}^{-1}\left\{\boldsymbol{\theta}'_m(z;t) - \boldsymbol{L}\boldsymbol{\kappa}_m(z;t)\right\} \end{aligned}\right\} , \tag{2.3.12}$$

where

$$\boldsymbol{L} = \boldsymbol{U}\boldsymbol{P}^{-1} , \qquad \overset{*}{\boldsymbol{L}} = \boldsymbol{V}\boldsymbol{Q}^{-1} , \qquad \boldsymbol{H} = \boldsymbol{L} - \overset{*}{\boldsymbol{L}} .$$

Here, we have assumed that the inverse matrices $\boldsymbol{P}^{-1}$ and $\boldsymbol{Q}^{-1}$ exist. Notice that the determinants of $\boldsymbol{P}$ and $\boldsymbol{Q}$ are both equal to $D(v)$, where

$$D(v) = 4\alpha_l\alpha_s - \left(1+\alpha_s^2\right)^2 .$$

Therefore, we exclude the situation where the crack propagates with the Rayleigh wave speed of the elastic material. This ensures the existence of $\boldsymbol{P}^{-1}$ and $\boldsymbol{Q}^{-1}$.

Substituting the expressions in equation (2.3.12) into the traction free conditions on the crack faces, (2.3.8), and notice that $\boldsymbol{H} \neq \mathbf{o}$ for $v(t) \neq 0$, we get

$$\left.\begin{aligned} \boldsymbol{\theta}'^{+}_m(\eta_1;t) - \overset{*}{\boldsymbol{L}}\,\boldsymbol{\kappa}^{+}_m(\eta_1;t) + \boldsymbol{\theta}'^{-}_m(\eta_1;t) - \boldsymbol{L}\boldsymbol{\kappa}^{-}_m(\eta_1;t) &= \mathbf{o} \\ \boldsymbol{\theta}'^{-}_m(\eta_1;t) - \overset{*}{\boldsymbol{L}}\,\boldsymbol{\kappa}^{-}_m(\eta_1;t) + \boldsymbol{\theta}'^{+}_m(\eta_1;t) - \boldsymbol{L}\boldsymbol{\kappa}^{+}_m(\eta_1;t) &= \mathbf{o} \end{aligned}\right\} , \quad \forall\ \eta_1 < 0 . \tag{2.3.13}$$

Subtracting the second equation in (2.3.13) from the first one, we obtain

$$\boldsymbol{\kappa}^{+}_m(\eta_1;t) - \boldsymbol{\kappa}^{-}_m(\eta_1;t) = \mathbf{o} , \qquad \forall\ \eta_1 < 0 , \tag{2.3.14}$$

which implies that $\boldsymbol{\kappa}_m(z;t)$ is continuous across the negative real axis except at the crack-tip and therefore $\boldsymbol{\kappa}_m(z;t)$ is analytic in the entire complex plane except at $z = 0$. However, the condition of bounded displacement requires that $\mid \boldsymbol{\kappa}_m(z;t) \mid = O\ (\ |z|^{\alpha}\ )$ for some $\alpha > -1$, as $|z| \to 0$. So that any singularity of $\boldsymbol{\kappa}_m(z;t)$ at the crack-tip is removable. Therefore, $\boldsymbol{\kappa}_m(z;t)$ is an entire function. Now, both equations in (2.3.13) become

$$\boldsymbol{\theta}_m'^{+}(\eta_1;t) + \boldsymbol{\theta}_m'^{-}(\eta_1;t) = \left(\boldsymbol{L} + \overset{*}{\boldsymbol{L}}\right) \boldsymbol{\kappa}_m(\eta_1;t)\ , \qquad \forall\ \eta_1 < 0\ , \tag{2.3.15}$$

where

$$\boldsymbol{\kappa}_m(\eta_1;t) = \boldsymbol{\kappa}_m^{+}(\eta_1;t) = \boldsymbol{\kappa}_m^{-}(\eta_1;t)\ .$$

Equation (2.3.15) constitutes a Riemann-Hilbert problem. Its solution $\boldsymbol{\theta}_m'(z;t)$ is analytic in the cut plane. Along the cut, $\boldsymbol{\theta}_m'(z;t)$ satisfies equation (2.3.15) for some arbitrary entire function $\boldsymbol{\kappa}_m(z;t)$. Also, from the requirement of bounded displacements at the crack-tip, as $|z| \to 0$,

$$\mid \boldsymbol{\theta}_m'(z;t) \mid = O\ (\ |z|^{\alpha}\ )\ , \tag{2.3.16}$$

for some $\alpha > -1$.

In equation (2.3.15), the solution $\boldsymbol{\theta}_m'(z;t)$ is composed by two parts, the homogeneous solution $\overset{\circ}{\boldsymbol{\theta}}{}_m'\ (z;t)$, and the particular solution $\hat{\boldsymbol{\theta}}_m'(z;t)$. The homogeneous solution $\overset{\circ}{\boldsymbol{\theta}}{}_m'\ (z;t)$ can be obtained as (Muskhelishvili, 1953)

$$\overset{\circ}{\boldsymbol{\theta}}{}_m'\ (z;t) = z^{-1/2}\ \overset{\circ}{\boldsymbol{a}}_m\ (z;t)\ , \tag{2.3.17}$$

where $\overset{\circ}{\boldsymbol{a}}_m\ (z;t)$ is an arbitrary entire function. The particular solution $\hat{\boldsymbol{\theta}}_m'(z;t)$ can also be easily constructed by considering that $\boldsymbol{\kappa}_m(z;t)$ is an entire function and by using the identity theorem for analytic functions. The particular solution is given by

$$\hat{\boldsymbol{\theta}}_m'(z;t) = \frac{1}{2}\left(\boldsymbol{L} + \overset{*}{\boldsymbol{L}}\right) \boldsymbol{\kappa}_m(z;t)\ . \tag{2.3.18}$$

The final solution for $\boldsymbol{\theta}'_m(z;t)$ is then

$$\boldsymbol{\theta}'_m(z;t) = z^{-1/2}\, \mathring{\boldsymbol{a}}_m\,(z;t) + \frac{1}{2}\left(\boldsymbol{L} + \overset{*}{\boldsymbol{L}}\right)\boldsymbol{\kappa}_m(z;t)\ . \tag{2.3.19}$$

Substituting equation (2.3.19) into (2.3.12), we have

$$\left.\begin{aligned} \boldsymbol{f}''_m(z;t) &= \boldsymbol{P}^{-1}\left\{z^{-1/2}\boldsymbol{a}_m(z;t) + \boldsymbol{b}_m(z;t)\right\} \\ \overline{\boldsymbol{f}}''_m(z;t) &= \boldsymbol{Q}^{-1}\left\{z^{-1/2}\boldsymbol{a}_m(z;t) - \boldsymbol{b}_m(z;t)\right\} \end{aligned}\right\}\ , \tag{2.3.20}$$

where

$$\boldsymbol{a}_m(z;t) = \boldsymbol{H}^{-1}\, \mathring{\boldsymbol{a}}_m\,(z;t)\ , \qquad \boldsymbol{b}_m(z;t) = \frac{1}{2}\boldsymbol{\kappa}_m(z;t)\ .$$

Suppose that $\boldsymbol{a}_m(z;t)$ and $\boldsymbol{b}_m(z;t)$ have the components like

$$\left.\begin{aligned} \boldsymbol{a}_m(z;t) &= (\ a_m^{(1)}(z;t),\ a_m^{(2)}(z;t)\ )^{\mathsf{T}} \\ \boldsymbol{b}_m(z;t) &= (\ b_m^{(1)}(z;t),\ b_m^{(2)}(z;t)\ )^{\mathsf{T}} \end{aligned}\right\}\ .$$

By comparing the conjugate of $\overline{\boldsymbol{f}}''_m(z;t)$ with $\boldsymbol{f}''_m(z;t)$ in equation (2.3.20), and by using the fact that

$$\boldsymbol{P}\boldsymbol{Q}^{-1} = \begin{bmatrix} 1 & 0 \\ 0 & -1 \end{bmatrix}\ ,$$

we obtain

$$\left.\begin{aligned} a_m^{(1)}(z;t) - \overline{a}_m^{(1)}(z;t) = 0\ , &\qquad a_m^{(2)}(z;t) + \overline{a}_m^{(2)}(z;t) = 0 \\ b_m^{(1)}(z;t) + \overline{b}_m^{(1)}(z;t) = 0\ , &\qquad b_m^{(2)}(z;t) - \overline{b}_m^{(2)}(z;t) = 0 \end{aligned}\right\}\ . \tag{2.3.21}$$

As a result of above relations, the four undetermined entire functions $a_m^{(\alpha)}(z;t)$ and $b_m^{(\alpha)}(z;t)$ $(\alpha = 1,2)$ can be reduced to two by defining

$$\left.\begin{aligned} A_m(z;t) &= \frac{1}{2}\left\{a_m^{(1)}(z;t) + \overline{a}_m^{(1)}(z;t) + a_m^{(2)}(z;t) - \overline{a}_m^{(2)}(z;t)\right\} \\ B_m(z;t) &= \frac{1}{2}\left\{b_m^{(1)}(z;t) - \overline{b}_m^{(1)}(z;t) + b_m^{(2)}(z;t) + \overline{b}_m^{(2)}(z;t)\right\} \end{aligned}\right\}\ . \tag{2.3.22}$$

Now we can express the function $\boldsymbol{f}''_m(z;t)$ in terms of the two undetermined entire functions $A_m(z;t)$ and $B_m(z;t)$ by

$$\left.\begin{aligned} \boldsymbol{f}''_m(z;t) \ &= \ \frac{1}{2}z^{-1/2}\left\{\boldsymbol{P}^{-1}\boldsymbol{\eta}A_m(z;t) + \boldsymbol{Q}^{-1}\boldsymbol{\eta}\overline{A}_m(z;t)\right\} \\ &+ \ \frac{1}{2}\left\{\boldsymbol{P}^{-1}\boldsymbol{\eta}B_m(z;t) - \boldsymbol{Q}^{-1}\boldsymbol{\eta}\overline{B}_m(z;t)\right\} \end{aligned}\right\}\ , \tag{2.3.23}$$

where $\boldsymbol{\eta} = (1,1)^{\top}$. Since $A_m(z;t)$ and $B_m(z;t)$ are entire functions, they can be expanded into Taylor series. Define

$$\left.\begin{aligned}
\frac{1}{2}\left\{A_m(z;t) + \overline{A}_m(z;t)\right\} &= -\sum_{n=0}^{\infty} A_{Im}^{(n)}(t) z^n \\
\frac{1}{2}\left\{A_m(z;t) - \overline{A}_m(z;t)\right\} &= -\,i\sum_{n=0}^{\infty} A_{IIm}^{(n)}(t) z^n \\
\frac{1}{2}\left\{B_m(z;t) + \overline{B}_m(z;t)\right\} &= -\sum_{n=0}^{\infty} B_{Im}^{(n)}(t) z^n \\
\frac{1}{2}\left\{B_m(z;t) - \overline{B}_m(z;t)\right\} &= -\,i\sum_{n=0}^{\infty} B_{IIm}^{(n)}(t) z^n
\end{aligned}\right\}, \tag{2.3.24}$$

where $A_{Im}^{(n)}(t)$, $A_{IIm}^{(n)}(t)$, $B_{Im}^{(n)}(t)$, and $B_{IIm}^{(n)}(t)$ are real functions of time t. Also, by considering the properties of our asymptotic expansion, (2.2.14) and (2.2.15), for $m = 0$ and 1, we have

$$\left.\begin{aligned}
F_0''(z_l;t) &= \sum_{n=0}^{\infty}\left\{\frac{1+\alpha_s^2}{\mu D(v)} A_{I0}^{(n)}(t) z_l^{n-\frac{1}{2}} - \frac{2\alpha_s}{\mu D(v)} B_{I0}^{(n)}(t) z_l^n\right\} \\
&- i\sum_{n=0}^{\infty}\left\{\frac{2\alpha_s}{\mu D(v)} A_{II0}^{(n)}(t) z_l^{n-\frac{1}{2}} - \frac{1+\alpha_s^2}{\mu D(v)} B_{II0}^{(n)}(t) z_l^n\right\} \\
G_0''(z_s;t) &= -\sum_{n=0}^{\infty}\left\{\frac{2\alpha_l}{\mu D(v)} A_{I0}^{(n)}(t) z_s^{n-\frac{1}{2}} - \frac{1+\alpha_s^2}{\mu D(v)} B_{I0}^{(n)}(t) z_s^n\right\} \\
&+ i\sum_{n=0}^{\infty}\left\{\frac{1+\alpha_s^2}{\mu D(v)} A_{II0}^{(n)}(t) z_s^{n-\frac{1}{2}} - \frac{2\alpha_l}{\mu D(v)} B_{II0}^{(n)}(t) z_s^n\right\}
\end{aligned}\right\}, \tag{2.3.25}$$

and

$$\left.\begin{aligned}
F_1''(z_l;t) &= -\sum_{n=0}^{\infty}\left\{\frac{2\alpha_s}{\mu D(v)} B_{I1}^{(n)}(t) z_l^n - \frac{1+\alpha_s^2}{\mu D(v)} A_{I1}^{(n)}(t) z_l^{n+\frac{1}{2}}\right\} \\
&+ i\sum_{n=0}^{\infty}\left\{\frac{1+\alpha_s^2}{\mu D(v)} B_{II1}^{(n)}(t) z_l^n - \frac{2\alpha_s}{\mu D(v)} A_{II1}^{(n)}(t) z_l^{n+\frac{1}{2}}\right\} \\
G_1''(z_s;t) &= \sum_{n=0}^{\infty}\left\{\frac{1+\alpha_s^2}{\mu D(v)} B_{I1}^{(n)}(t) z_s^n - \frac{2\alpha_l}{\mu D(v)} A_{I1}^{(n)}(t) z_s^{n+\frac{1}{2}}\right\} \\
&- i\sum_{n=0}^{\infty}\left\{\frac{2\alpha_l}{\mu D(v)} B_{II1}^{(n)}(t) z_s^n - \frac{1+\alpha_s^2}{\mu D(v)} A_{II1}^{(n)}(t) z_s^{n+\frac{1}{2}}\right\}
\end{aligned}\right\}. \tag{2.3.26}$$

By integrating the above expressions with respect to the corresponding argument z_l or z_s, we can obtain the final expressions of the complex displacement potentials $F_m(z_l;t)$ and $G_m(z_s;t)$ for $m = 0$ and 1. If the crack propagates along a straight path, equation (2.3.25) actually has provided the complete solution for the steady state problem under mixed mode loading conditions, while all coefficients do not depend on time. It can be shown that the coefficients of the most singular terms, $A_{I0}^{(0)}(t)$ and $A_{II0}^{(0)}(t)$, can be rewritten as

$$A_{I0}^{(0)}(t) = \frac{K_I^d(t)}{\sqrt{2\pi}} , \qquad A_{II0}^{(0)}(t) = \frac{K_{II}^d(t)}{\sqrt{2\pi}} , \tag{2.3.27}$$

where $K_I^d(t)$ and $K_{II}^d(t)$ are the mode-I and mode-II dynamic stress intensity factors at the moving crack-tip, respectively.

2.3.2 Solutions for $\phi_m(\eta_1, \eta_2, t)$ and $\psi_m(\eta_1, \eta_2, t)$ for $m = 2$

For $m = 2$, the equations of motion (2.2.16) and (2.2.17) are coupled. They take the form,

$$\left.\begin{aligned}
&\phi_{2,11}(\eta_1,\eta_2,t) + \frac{1}{\alpha_l^2}\phi_{2,22}(\eta_1,\eta_2,t) \;=\; \\
&-\frac{2\sqrt{v}}{\alpha_l^2 c_l^2}\left\{\sqrt{v}\phi_{0,1}\right\}_{,t} + \frac{(1-\alpha_l^2)k}{\alpha_l^2}\left\{\phi_{0,2} + 2\eta_1\phi_{0,12} - 2\eta_2\phi_{0,11}\right\} \\
&\psi_{2,11}(\eta_1,\eta_2,t) + \frac{1}{\alpha_s^2}\psi_{2,22}(\eta_1,\eta_2,t) \;=\; \\
&-\frac{2\sqrt{v}}{\alpha_s^2 c_s^2}\left\{\sqrt{v}\psi_{0,1}\right\}_{,t} + \frac{(1-\alpha_s^2)k}{\alpha_s^2}\left\{\psi_{0,2} + 2\eta_1\psi_{0,12} - 2\eta_2\psi_{0,11}\right\}
\end{aligned}\right\} . \tag{2.3.28}$$

where $\phi_0(\eta_1, \eta_2, t)$ and $\psi_0(\eta_1, \eta_2, t)$ have been given in the previous section.

In order to obtain the next most singular term in $\phi_2(\eta_1, \eta_2, t)$ and $\psi_2(\eta_1, \eta_2, t)$, we should only consider the most singular terms in $\phi_0(\eta_1, \eta_2, t)$ and $\psi_0(\eta_1, \eta_2, t)$. As a result, $\phi_0(\eta_1, \eta_2, t)$ and $\psi_0(\eta_1, \eta_2, t)$ can be written as

$$\phi_0(\eta_1,\eta_2,t) = \mathrm{Re}\left\{K_l(t) z_l^{3/2}\right\} , \qquad \psi_0(\eta_1,\eta_2,t) = \mathrm{Im}\left\{K_s(t) z_s^{3/2}\right\} , \tag{2.3.29}$$

where

$$\left.\begin{aligned} K_l(t) &= \frac{4\,(1+\alpha_s^2)}{3\sqrt{2\pi}\mu D(v)} K_I^d(t) - i\frac{8\alpha_s}{3\sqrt{2\pi}\mu D(v)} K_{II}^d(t) \\ K_s(t) &= -\frac{8\alpha_l}{3\sqrt{2\pi}\mu D(v)} K_I^d(t) + i\frac{4\,(1+\alpha_s^2)}{3\sqrt{2\pi}\mu D(v)} K_{II}^d(t) \end{aligned}\right\} .$$

Substituting equation (2.3.29) into (2.3.28), we get

$$\left.\begin{aligned} \phi_{2,11} + \frac{1}{\alpha_l^2}\phi_{2,22} &= \mathrm{Re}\left\{R_l(t) z_l^{1/2} - S_l(t)\overline{z}_l z_l^{-1/2}\right\} \\ \psi_{2,11} + \frac{1}{\alpha_s^2}\psi_{2,22} &= \mathrm{Im}\left\{R_s(t) z_s^{1/2} - S_s(t)\overline{z}_s z_s^{-1/2}\right\} \end{aligned}\right\} , \qquad (2.3.30)$$

where

$$\left.\begin{aligned} R_{l,s}(t) &= D_{l,s}^1\{K_{l,s}(t)\} + \frac{1}{2}B_{l,s}(t) + M_{l,s}(t) \\ S_{l,s}(t) &= \frac{1}{2}B_{l,s}(t) + N_{l,s}(t) \end{aligned}\right\} ,$$

and

$$\left.\begin{aligned} D_{l,s}^1\{K_{l,s}(t)\} &= -\frac{3\sqrt{v}}{\alpha_{l,s}^2 c_{l,s}^2}\frac{\mathrm{d}}{\mathrm{d}t}\left\{\sqrt{v}K_{l,s}(t)\right\} \\ B_{l,s}(t) &= \frac{3v^2\dot{v}}{2\alpha_{l,s}^4 c_{l,s}^4} K_{l,s}(t) \\ M_{l,s}(t) &= i\frac{3(1-\alpha_{l,s}^2)(1+3\alpha_{l,s}^2)}{4\alpha_{l,s}^3} K_{l,s}(t)k(t) \\ N_{l,s}(t) &= i\frac{3(1-\alpha_{l,s}^2)^2}{4\alpha_{l,s}^3} K_{l,s}(t)k(t) \end{aligned}\right\} .$$

The most general solutions to equation (2.3.30) are

$$\left.\begin{aligned} \phi_2(\eta_1,\eta_2,t) &= \mathrm{Re}\left\{F_2(z_l;t) + \overline{z}_l f_l(z_l;t) + \overline{z}_l^2 g_l(z_l;t)\right\} \\ \psi_2(\eta_1,\eta_2,t) &= \mathrm{Im}\left\{G_2(z_s;t) + \overline{z}_s f_s(z_s;t) + \overline{z}_s^2 g_s(z_s;t)\right\} \end{aligned}\right\} , \qquad (2.3.31)$$

where

$$\left.\begin{aligned} f_{l,s}(z_{l,s};t) &= \frac{1}{6}R_{l,s}(t) z_{l,s}^{3/2} \\ g_{l,s}(z_{l,s};t) &= -\frac{1}{4}S_{l,s}(t) z_{l,s}^{1/2} \end{aligned}\right\} ,$$

and $F_2(z_l;t)$, $G_2(z_s;t)$ are two analytic functions in the corresponding cut planes. It can be seen that $f_{l,s}(z_{l,s};t)$ and $g_{l,s}(z_{l,s};t)$ are totally determined by the solutions $\phi_0(\eta_1,\eta_2,t)$ and $\psi_0(\eta_1,\eta_2,t)$, and they depend on $\dot{K}_I^d(t)$, $\dot{K}_{II}^d(t)$, $\dot{v}(t)$, and for a crack propagates along a curved path, they also depend on the curvature of the path at the crack-tip, $k(t)$.

Associated with $\phi_2(\eta_1,\eta_2,t)$ and $\psi_2(\eta_1,\eta_2,t)$, given in equation (2.3.31), the corresponding components of displacement can be expressed as

$$\left.\begin{aligned} u_1^{(2)} \;=\; & \mathrm{Re}\Big\{ F_2'(z_l;t) + \alpha_s G_2'(z_s;t) \\ & + \left[\overline{z}_l f_l'(z_l;t) + \overline{z}_l^2 g_l'(z_l;t) + f_l(z_l;t) + 2\overline{z}_l g_l(z_l;t)\right] \\ & + \alpha_s\left[\overline{z}_s f_s'(z_s;t) + \overline{z}_s^2 g_s'(z_s;t) - f_s(z_s;t) - 2\overline{z}_s g_s(z_s;t)\right]\Big\} \end{aligned}\right\}, \qquad (2.3.32)$$

$$\left.\begin{aligned} u_2^{(2)} \;=\; & -\mathrm{Im}\Big\{ \alpha_l F_2'(z_l;t) + G_2'(z_s;t) \\ & + \alpha_l\left[\overline{z}_l f_l'(z_l;t) + \overline{z}_l^2 g_l'(z_l;t) - f_l(z_l;t) - 2\overline{z}_l g_l(z_l;t)\right] \\ & + \left[\overline{z}_s f s'(z_s;t) + \overline{z}_s^2 g_s'(z_s;t) + f_s(z_s;t) + 2\overline{z}_s g_s(z_s;t)\right]\Big\} \end{aligned}\right\}. \qquad (2.3.33)$$

The stress components are

$$\left.\begin{aligned} \sigma_{11}^{(2)} \;=\; & \mu\mathrm{Re}\Big\{ \left(1+2\alpha_l^2-\alpha_s^2\right) F_2''(z_l;t) + 2\alpha_s G_2''(z_s;t) \\ & + \left(1+2\alpha_l^2-\alpha_s^2\right)\left[\overline{z}_l f_l''(z_l;t) + \overline{z}_l^2 g_l''(z_l;t) + 2g_l(z_l;t)\right] \\ & + 2\left[\left(1-\alpha_s^2\right) + \frac{2\alpha_l^2\left(\alpha_l^2-\alpha_s^2\right)}{1-\alpha_l^2}\right]\left[f_l'(z_l;t) + 2\overline{z}_l g_l'(z_l;t)\right] \\ & + 2\alpha_s\left[\overline{z}_s f_s''(z_s;t) + \overline{z}_s^2 g_s''(z_s;t) - 2g_s(z_s;t)\right]\Big\} \end{aligned}\right\}, \qquad (2.3.34)$$

$$\left.\begin{aligned}\sigma_{22}^{(2)} &= -\mu \mathrm{Re}\Big\{ \left(1+\alpha_s^2\right) F_2''(z_l;t) + 2\alpha_s G_2''(z_s;t) \\ &+\left(1+\alpha_s^2\right)\left[\overline{z}_l f_l''(z_l;t) + \overline{z}_l^2 g_l''(z_l;t) + 2g_l(z_l;t)\right] \\ &+2\left[\left(1-\alpha_s^2\right) - \frac{2\left(\alpha_l^2-\alpha_s^2\right)}{1-\alpha_l^2}\right]\left[f_l'(z_l;t) + 2\overline{z}_l g_l'(z_l;t)\right] \\ &+ 2\alpha_s\left[\overline{z}_s f_s''(z_s;t) + \overline{z}_s^2 g_s''(z_s;t) - 2g_s(z_s;t)\right]\Big\}\end{aligned}\right\}, \tag{2.3.35}$$

and

$$\left.\begin{aligned}\sigma_{12}^{(2)} &= -\mu \mathrm{Im}\Big\{ 2\alpha_l F_2''(z_l;t) + \left(1+\alpha_s^2\right) G_2''(z_s;t) \\ &+2\alpha_l\left[\overline{z}_l f_l''(z_l;t) + \overline{z}_l^2 g_l''(z_l;t) - 2g_l(z_l;t)\right] \\ &+\left(1+\alpha_s^2\right)\left[\overline{z}_s f_s''(z_s;t) + \overline{z}_s^2 g_s''(z_s;t) + 2g_s(z_s;t)\right] \\ &+ 2\left(1-\alpha_s^2\right)\left[f_s'(z_s;t) + 2\overline{z}_s g_s'(z_s;t)\right]\Big\}\end{aligned}\right\}. \tag{2.3.36}$$

To produce a more compact form of the above expressions, one needs to define the following quantities,

$$\overset{*}{\boldsymbol{P}} = \begin{bmatrix} \mu(1+\alpha_s^2) & -2\mu\alpha_s \\ -2\mu\alpha_l & \mu(1+\alpha_s^2) \end{bmatrix}, \qquad \overset{*}{\boldsymbol{Q}} = \begin{bmatrix} \mu(1+\alpha_s^2) & -2\mu\alpha_s \\ 2\mu\alpha_l & -\mu(1+\alpha_s^2) \end{bmatrix},$$

$$\overset{*}{\boldsymbol{U}} = \begin{bmatrix} 1 & -\alpha_s \\ -\alpha_l & 1 \end{bmatrix}, \qquad \overset{*}{\boldsymbol{V}} = \begin{bmatrix} 1 & -\alpha_s \\ \alpha_l & -1 \end{bmatrix},$$

and

$$\boldsymbol{M} = \begin{bmatrix} \mu\left\{\left(1-\alpha_s^2\right) - \dfrac{2\left(\alpha_l^2-\alpha_s^2\right)}{1-\alpha_l^2}\right\} & 0 \\ 0 & \mu(1-\alpha_s^2) \end{bmatrix},$$

$$\boldsymbol{N} = \begin{bmatrix} \mu\left\{\left(1-\alpha_s^2\right) - \dfrac{2\left(\alpha_l^2-\alpha_s^2\right)}{1-\alpha_l^2}\right\} & 0 \\ 0 & -\mu(1-\alpha_s^2) \end{bmatrix}.$$

Also, let

$$\left.\begin{aligned} \boldsymbol{f}_2(z;t) &= (\ F_2(z;t),\ G_2(z;t)\ )^{\top} \\ \boldsymbol{f}(z;t) &= (\ f_l(z;t),\ f_s(z;t)\ )^{\top} \\ \boldsymbol{g}(z;t) &= (\ g_l(z;t),\ g_s(z;t)\ )^{\top} \end{aligned}\right\} .$$

As in the procedure we used to obtained the complex displacement potentials for $m = 0$ and 1, we may define two new functions $\boldsymbol{\kappa}_2(z;t)$ and $\boldsymbol{\theta}_2(z;t)$, so that the continuity conditions ahead of the crack-tip are satisfied identically, as follows,

$$\left.\begin{aligned} \boldsymbol{\kappa}_2(z;t) &= \boldsymbol{P}\left\{\boldsymbol{f}_2''(z;t) + z\boldsymbol{f}''(z;t) + z^2\boldsymbol{g}''(z;t)\right\} \\ &- \boldsymbol{Q}\left\{\overline{\boldsymbol{f}}_2''(z;t) + z\overline{\boldsymbol{f}}''(z;t) + z^2\overline{\boldsymbol{g}}''(z;t)\right\} \\ &+ 2\boldsymbol{M}\left\{\boldsymbol{f}'(z;t) + 2z\boldsymbol{g}'(z;t)\right\} - 2\boldsymbol{N}\left\{\overline{\boldsymbol{f}}'(z;t) + 2z\overline{\boldsymbol{g}}'(z;t)\right\} \\ &+ 2\overset{*}{\boldsymbol{P}}\,\boldsymbol{g}(z;t) - 2\overset{*}{\boldsymbol{Q}}\,\overline{\boldsymbol{g}}(z;t) \end{aligned}\right\} , \qquad (2.3.37)$$

and

$$\left.\begin{aligned} \boldsymbol{\theta}_2(z;t) &= \boldsymbol{U}\left\{\boldsymbol{f}_2'(z;t) + z\boldsymbol{f}'(z;t) + z^2\boldsymbol{g}'(z;t)\right\} \\ &- \boldsymbol{V}\left\{\overline{\boldsymbol{f}}_2'(z;t) + z\overline{\boldsymbol{f}}'(z;t) + z^2\overline{\boldsymbol{g}}'(z;t)\right\} \\ &+ \overset{*}{\boldsymbol{U}}\left\{\boldsymbol{f}(z;t) + 2z\boldsymbol{g}(z;t)\right\} - \overset{*}{\boldsymbol{V}}\left\{\overline{\boldsymbol{f}}(z;t) + 2z\overline{\boldsymbol{g}}(z;t)\right\} \end{aligned}\right\} , \qquad (2.3.38)$$

where $\boldsymbol{\kappa}_2(z;t)$ and $\boldsymbol{\theta}_2(z;t)$ are analytic in the cut plane. In order to keep our notation short, define a new quantity,

$$\left.\begin{aligned} \boldsymbol{g}_2(z;t) &= \boldsymbol{f}_2''(z;t) + z\boldsymbol{f}''(z;t) + z^2\boldsymbol{g}''(z;t) \\ &+ 2\boldsymbol{P}^{-1}\boldsymbol{M}\left[\boldsymbol{f}'(z;t) + 2z\boldsymbol{g}'(z;t)\right] + 2\boldsymbol{P}^{-1}\,\overset{*}{\boldsymbol{P}}\,\boldsymbol{g}(z;t) \end{aligned}\right\} .$$

Now, the expressions (2.3.37) and (2.3.38) can be simplified to

$$\left.\begin{aligned} \boldsymbol{\kappa}_2(z;t) &= \boldsymbol{P}\boldsymbol{g}_2(z;t) - \boldsymbol{Q}\overline{\boldsymbol{g}}_2(z;t) \\ \boldsymbol{\theta}_2'(z;t) &= \boldsymbol{U}\boldsymbol{g}_2(z;t) - \boldsymbol{V}\overline{\boldsymbol{g}}_2(z;t) - \left[\boldsymbol{q}(z;t) - \overset{*}{\boldsymbol{q}}\,(z;t)\right] \end{aligned}\right\} , \qquad (2.3.39)$$

where

$$\left.\begin{aligned} \boldsymbol{q}(z;t) &= 2\left(\boldsymbol{L}\boldsymbol{M}-\boldsymbol{I}\right)\left[\boldsymbol{f}'(z;t)+2z\boldsymbol{g}'(z;t)\right] \\ &+ 2\left(\boldsymbol{L}\overset{*}{\boldsymbol{P}}-\overset{*}{\boldsymbol{U}}\right)\boldsymbol{g}(z;t) \\ \overset{*}{\boldsymbol{q}}(z;t) &= 2\left(\overset{*}{\boldsymbol{L}}\boldsymbol{N}_k-\boldsymbol{J}\right)\left[\boldsymbol{f}'(z;t)+2z\boldsymbol{g}'(z;t)\right] \\ &+ 2\left(\overset{*}{\boldsymbol{L}}\overset{*}{\boldsymbol{Q}}-\overset{*}{\boldsymbol{V}}\right)\boldsymbol{g}(z;t) \end{aligned}\right\}, \tag{2.3.40}$$

and

$$\boldsymbol{I}=\begin{bmatrix}1 & 0\\ 0 & 1\end{bmatrix}, \qquad \boldsymbol{J}=\begin{bmatrix}1 & 0\\ 0 & -1\end{bmatrix}.$$

By solving equation (2.3.39), we obtained

$$\left.\begin{aligned} \boldsymbol{g}_2(z;t) &= \boldsymbol{P}^{-1}\boldsymbol{H}^{-1}\left\{\boldsymbol{\theta}_2'(z;t)-\overset{*}{\boldsymbol{L}}\,\boldsymbol{\kappa}_2(z;t)+\boldsymbol{q}(z;t)-\overset{*}{\boldsymbol{q}}(z;t)\right\} \\ \overline{\boldsymbol{g}}_2(z;t) &= \boldsymbol{Q}^{-1}\boldsymbol{H}^{-1}\left\{\boldsymbol{\theta}_2'(z;t)-\boldsymbol{L}\boldsymbol{\kappa}_2(z;t)+\boldsymbol{q}(z;t)-\overset{*}{\boldsymbol{q}}(z;t)\right\} \end{aligned}\right\}. \tag{2.3.41}$$

It can be seen that the above equation is very similar to equation (2.3.12), except the term $\boldsymbol{q}(z;t)-\overset{*}{\boldsymbol{q}}(z;t)$ which is totally determined by the solution for $m=0$. On the other hand, it can also be shown that the traction free condition on the crack faces reduces to

$$\boldsymbol{P}\boldsymbol{g}_2^{\pm}(\eta_1;t)+\boldsymbol{Q}\overline{\boldsymbol{g}}_2^{\mp}(\eta_1;t)=\mathbf{o}\,, \qquad \forall\,\eta_1<0\,. \tag{2.3.42}$$

Substituting equation (2.3.41) into the above boundary conditions, and similar to the procedure used in the case for $m=0$ and 1, one can show that $\boldsymbol{\kappa}_2(z;t)$ is an entire function. Meanwhile, conditions (2.2.14) and (2.2.15) require that $|\,\boldsymbol{\kappa}_2(z;t)\,| = O\,(\,|z|\,)$, as $|z|\to 0$. Finally, equation (2.3.42) becomes

$$\boldsymbol{\theta}_2'^{+}(\eta_1;t)+\boldsymbol{\theta}_2'^{-}(\eta_1;t)=\left(\boldsymbol{L}+\overset{*}{\boldsymbol{L}}\right)\boldsymbol{\kappa}_2(\eta_1;t)+\hat{\boldsymbol{\kappa}}(\eta_1;t)\,, \qquad \forall\,\eta_1<0\,, \tag{2.3.43}$$

where

$$\hat{\boldsymbol{\kappa}}(\eta_1;t)=-\left\{\boldsymbol{q}^{+}(\eta_1;t)+\boldsymbol{q}^{-}(\eta_1;t)-\overset{*}{\overline{\boldsymbol{q}}}^{+}(\eta_1;t)-\overset{*}{\overline{\boldsymbol{q}}}^{-}(\eta_1;t)\right\}.$$

By substituting the expressions of $\boldsymbol{q}(z;t)$ and $\overset{*}{\boldsymbol{q}}(z;t)$ into above relation, we can get

$$\hat{\boldsymbol{\kappa}}(\eta_1;t)=\mathbf{o}\,, \qquad \forall\eta_1<0\,.$$

Therefore, the equation that $\boldsymbol{\theta}_2'(z;t)$ should satisfy, is

$$\boldsymbol{\theta}_2'^{+}(\eta_1;t) + \boldsymbol{\theta}_2'^{-}(\eta_1;t) = \left(\boldsymbol{L} + \overset{*}{\boldsymbol{L}}\right) \boldsymbol{\kappa}_2(\eta_1;t) \ , \qquad \forall\ \eta_1 < 0 \ . \tag{2.3.44}$$

This is exactly the same as equation (2.3.15). One basic difference, however, is that from the properties of our asymptotic expansion, (2.2.14) and (2.2.15), as $|z| \to 0$,

$$| \ \boldsymbol{\theta}_2'(z;t) \ | = O \ (\ |z|^{\alpha} \ ) \ , \tag{2.3.45}$$

for some $\alpha > 0$ (recall that before $\alpha > -1$). As a result, the solution of $\boldsymbol{\theta}_2'(z;t)$ will be

$$\boldsymbol{\theta}_2'(z;t) = z^{1/2} \ \overset{\circ}{\boldsymbol{a}}_2 \ (z;t) + \frac{1}{2} \left(\boldsymbol{L} + \overset{*}{\boldsymbol{L}}\right) \boldsymbol{\kappa}_2(z;t) \ , \tag{2.3.46}$$

where $\overset{\circ}{\boldsymbol{a}}_2 \ (z;t)$ is an arbitrary entire function.

In constructing the solution for $\boldsymbol{g}_2(z;t)$, only the leading term in (2.3.46) is considered. This is consistent with the fact that (2.3.29) contains only leading terms of the solution for $m = 0$. The final solution for $\boldsymbol{g}_2(z;t)$ is therefore

$$\boldsymbol{g}_2(z;t) = \frac{1}{2} \left\{ \boldsymbol{P}^{-1} \boldsymbol{\eta} A_2(t) + \boldsymbol{Q}^{-1} \boldsymbol{\eta} \overline{A}_2(t) \right\} z^{1/2} \ , \tag{2.3.47}$$

for some undetermined complex function of time, $A_2(t)$.

Our final target is to find the function $\boldsymbol{f}_2(z;t)$. After some manipulations, we obtain

$$\left.\begin{aligned} \boldsymbol{f}_2(z;t) \ &= \ \frac{2}{15} \left\{ \boldsymbol{P}^{-1} \boldsymbol{\eta} A_2(t) + \boldsymbol{Q}^{-1} \boldsymbol{\eta} \overline{A}_2(t) \right\} z^{5/2} \\ &+ \ \frac{4}{15} \left\{ \boldsymbol{\Gamma} \boldsymbol{\gamma}(t) - \boldsymbol{\Omega} \boldsymbol{\omega}(t) \right\} z^{5/2} \end{aligned}\right\} \ , \tag{2.3.48}$$

where

$$\boldsymbol{\gamma}(t) = (\ R_l(t), \ R_s(t) \ )^{\top} \ , \qquad \boldsymbol{\omega}(t) = (\ S_l(t), \ S_s(t) \ )^{\top} \ ,$$

and

$$\boldsymbol{\Gamma} = \begin{bmatrix} \dfrac{(1+\alpha_s^2)m_l}{D(v)} - \dfrac{1}{8} & -\dfrac{2\alpha_s m_s}{D(v)} \\ -\dfrac{2\alpha_l m_l}{D(v)} & \dfrac{(1+\alpha_s^2)m_s}{D(v)} - \dfrac{1}{8} \end{bmatrix} ,$$

$$\boldsymbol{\Omega} = \begin{bmatrix} \dfrac{(1+\alpha_s^2)m_l}{D(v)} + \dfrac{\overset{*}{D}(v)}{D(v)} + \dfrac{1}{16} & -\dfrac{2\alpha_s m_s}{D(v)} - \dfrac{2\alpha_s(1+\alpha_s^2)}{D(v)} \\ -\dfrac{2\alpha_l m_l}{D(v)} - \dfrac{2\alpha_l(1+\alpha_s^2)}{D(v)} & \dfrac{(1+\alpha_s^2)m_s}{D(v)} + \dfrac{\overset{*}{D}(v)}{D(v)} + \dfrac{1}{16} \end{bmatrix} .$$

In the matrices above, the quantities m_l, m_s, and $\overset{*}{D}(v)$ are given by

$$\left.\begin{aligned} m_l &= \frac{1}{2}\left\{\left(1-\alpha_s^2\right) - \frac{2\left(\alpha_l^2-\alpha_s^2\right)}{1-\alpha_l^2}\right\} \\ m_s &= \frac{1}{2}\left\{1-\alpha_s^2\right\} \\ \overset{*}{D}(v) &= 4\alpha_l\alpha_s + (1+\alpha_s^2)^2 \end{aligned}\right\} . \qquad (2.3.49)$$

In this section, we have provided a procedure which allows us to investigate higher order transient effects systematically. By imposing the boundary conditions along the crack faces and the continuity conditions ahead of the crack-tip on the complex potentials, the problem can be recast into the Riemann-Hilbert methodology and the two complex displacement potentials can therefore be determined. To express these complex potentials in the unscaled physical plane, we redefine the complex variables $z_{l,s}$ and z by

$$z_{l,s} = \xi_1 + i\alpha_{l,s}\xi_2 , \qquad z = \xi_1 + i\xi_2 ,$$

and let

$$\boldsymbol{f}_m(z;t) = \left(F_m(z;t),\ G_m(z;t) \right)^{\top} , \qquad m = 0, 1, 2.$$

Then

$$\left.\begin{aligned} \boldsymbol{f}_0(z;t) &= \frac{1}{2}\left\{\boldsymbol{P}^{-1}\boldsymbol{\eta}A_0(t) + \boldsymbol{Q}^{-1}\boldsymbol{\eta}\overline{A}_0(t)\right\} z^{3/2} \\ \boldsymbol{f}_1(z;t) &= \frac{1}{2}\left\{\boldsymbol{P}^{-1}\boldsymbol{\eta}A_1(t) - \boldsymbol{Q}^{-1}\boldsymbol{\eta}\overline{A}_1(t)\right\} z^{2} \\ \boldsymbol{f}_2(z;t) &= \frac{1}{2}\left\{\boldsymbol{P}^{-1}\boldsymbol{\eta}A_2(t) + \boldsymbol{Q}^{-1}\boldsymbol{\eta}\overline{A}_2(t)\right\} z^{5/2} \\ &+ \frac{4}{15}\left\{\boldsymbol{\Gamma}\boldsymbol{\gamma}(t) - \boldsymbol{\Omega}\boldsymbol{\omega}(t)\right\} z^{5/2} \end{aligned}\right\} . \tag{2.3.50}$$

Notice that since $A_m(t)$ $(m = 0, 1, 2)$ are arbitrary functions of time, we have redefined them in equation (2.3.50). Specifically, $A_0(t)$ is related to the so-called mixed mode dynamic stress intensity factors, $K_I^d(t)$ and $K_{II}^d(t)$, by

$$A_0(t) = -\frac{4}{3\sqrt{2\pi}}\left\{K_I^d(t) + i\ K_{II}^d(t)\right\} . \tag{2.3.51}$$

The corresponding displacement potentials $\phi_m(\xi_1, \xi_2, t)$ and $\psi_m(\xi_1, \xi_2, t)$, will be given by (2.3.2) for $m = 0$ and 1, and (2.3.31) for $m = 2$, respectively. Finally,

$$\left.\begin{aligned} \phi(\xi_1, \xi_2, t) &= \sum_{m=0}^{2} \phi_m(\xi_1, \xi_2, t) + O(r_l^3) \\ \psi(\xi_1, \xi_2, t) &= \sum_{m=0}^{2} \psi_m(\xi_1, \xi_2, t) + O(r_s^3) \end{aligned}\right\} , \tag{2.3.52}$$

where $r_{l,s} = \sqrt{\xi_1^2 + \alpha_{l,s}^2 \xi_2^2}$.

Equation (2.3.52) provides the first three terms of the asymptotic expansion for the two displacement potentials $\phi(\xi_1, \xi_2, t)$ and $\psi(\xi_1, \xi_2, t)$ for a dynamic crack propagating non-uniformly along an arbitrary path. This expansion is based on an assumption that the fields are indeed two dimensional right up to the crack-tip. It is observed that the first two terms are the same as those obtained under the steady state mixed-mode condition and the crack path is straight, except here the coefficients $A_0(t)$ and $A_1(t)$ are arbitrary functions of time and the crack-tip speed takes the instantaneous value at time t. However, generally speaking, under the mixed-mode loading conditions, the crack will no longer propagate along a straight path and it is commonly believed

that the crack will seek the direction where locally the mode-I condition prevails. So the crack will propagate along a curved trajectory for the most general loading conditions. Even if the loading condition is mode-I, and the crack does propagate along a straight path, when the crack-tip speed is sufficiently high, the moving crack will lose its stability and deviate from the original straight path to propagate along a curve. The third term, or the higher order term in (2.3.52), takes into account the recent past history of the mixed-mode stress intensity factors and crack motion. This term involves the time derivatives of the dynamic stress intensity factors, $K_I^d(t)$ and $K_{II}^d(t)$, and crack-tip speed $v(t)$. It also involves the crack-tip curvature $k(t)$ as well. From equations (2.2.16) and (2.2.17), it can be seen that as we go further to the terms with $m > 2$, higher order time derivatives of $K_I^d(t)$, $K_{II}^d(t)$, and crack-tip speed $v(t)$ must be involved, so is the time derivative of the crack-tip curvature $k(t)$. The procedure discussed in this section is constructive and it can be repeated to any order.

2.4 The asymptotic elastodynamic field around a non-uniformly propagating crack-tip

For the planar deformation of a homogeneous, isotropic, linearly elastic material, the ordered array $[u_\alpha, \varepsilon_{\alpha\beta}, \sigma_{\alpha\beta}]$, $\alpha,\ \beta \in \{1,2\}$, is said to be an elastodynamic state in the absence of body force density, if the following conditions are satisfied

$$\left.\begin{aligned} &\varepsilon_{\alpha\beta} = \frac{1}{2}\left(u_{\alpha,\beta} + u_{\beta,\alpha}\right) \\ &\sigma_{\alpha\beta} = 2\mu\varepsilon_{\alpha\beta} + \lambda\varepsilon_{\gamma\gamma}\delta_{\alpha\beta} \\ &\sigma_{\alpha\beta,\beta} = \rho\ddot{u}_\alpha \end{aligned}\right\}, \qquad \alpha,\ \beta \in \{1,2\}\ , \tag{2.4.1}$$

where ρ is the mass density and λ, μ are Lamé constants of the material. In addition, the field quantities $u_\alpha, \varepsilon_{\alpha\beta}$, and $\sigma_{\alpha\beta}$ must satisfy the smoothness requirements outlined

in Wheeler and Sternberg (1968).

In the Cartesian coordinate system (ξ_1, ξ_2), let $\phi_m(\xi_1, \xi_2, t)$ and $\psi_m(\xi_1, \xi_2, t)$ be solutions of equations (2.2.16) and (2.2.17), $m = 0, 1, 2, \cdots$, such that

$$\left.\begin{array}{l} \dfrac{\phi_{m+n}(\xi_1, \xi_2, t)}{\phi_m(\xi_1, \xi_2, t)} \to 0 \\ \dfrac{\psi_{m+n}(\xi_1, \xi_2, t)}{\psi_m(\xi_1, \xi_2, t)} \to 0 \end{array}\right\} , \qquad \text{as } r = \sqrt{\xi_1^2 + \xi_2^2} \to 0 , \qquad m = 0, 1, 2, \cdots \tag{2.4.2}$$

for any positive integer n. Thus, $\phi_m(\xi_1, \xi_2, t)$ and $\psi_m(\xi_1, \xi_2, t)$ will be two asymptotic sequences as $r = (\xi_1^2 + \xi_2^2)^{1/2} \to 0$. Define $\phi(\xi_1, \xi_2, t)$ and $\psi(\xi_1, \xi_2, t)$ by

$$\left.\begin{array}{rcl} \phi(\xi_1, \xi_2, t) & = & \displaystyle\sum_{m=0}^{\infty} \phi_m(\xi_1, \xi_2, t) \\ \psi(\xi_1, \xi_2, t) & = & \displaystyle\sum_{m=0}^{\infty} \psi_m(\xi_1, \xi_2, t) \end{array}\right\} . \tag{2.4.3}$$

Then, the array $[u_\alpha, \varepsilon_{\alpha\beta}, \sigma_{\alpha\beta}]$, $\alpha,\ \beta \in \{1, 2\}$, will constitute an *asymptotic* elastodynamic state as $r = (\xi_1^2 + \xi_2^2)^{1/2} \to 0$, if it satisfies

$$\left.\begin{array}{l} u_\alpha = \phi_{,\alpha} + e_{\alpha\beta}\psi_{,\beta} \\ \varepsilon_{\alpha\beta} = \dfrac{1}{2}\left(u_{\alpha,\beta} + u_{\beta,\alpha}\right) \\ \sigma_{\alpha\beta} = 2\mu\varepsilon_{\alpha\beta} + \lambda\varepsilon_{\gamma\gamma}\delta_{\alpha\beta} \end{array}\right\} , \qquad \alpha,\ \beta \in \{1, 2\} . \tag{2.4.4}$$

Let the two displacement potentials be given by (2.4.3), where each term of the asymptotic series is the solution which has been discussed in the previous section. The asymptotic elastodynamic state near the tip of a non-uniformly propagating crack along an arbitrary path, can therefore be obtained from relations (2.4.4). For its importance in the experimental investigation, here we provide the asymptotic expression of the stress components around the moving crack-tip by using the constitutive relation (2.2.2). With respect to the ξ_1-axis, we can observe that the two

displacement potentials $\phi(\xi_1, \xi_2, t)$ and $\psi(\xi_1, \xi_2, t)$ are composed by two parts,

$$\left.\begin{aligned} \phi(\xi_1, \xi_2, t) &= \phi^{(\mathrm{I})}(\xi_1, \xi_2, t) + \phi^{(\mathrm{II})}(\xi_1, \xi_2, t) \\ \psi(\xi_1, \xi_2, t) &= \psi^{(\mathrm{I})}(\xi_1, \xi_2, t) + \psi^{(\mathrm{II})}(\xi_1, \xi_2, t) \end{aligned}\right\} , \tag{2.4.5}$$

such that

$$\left.\begin{aligned} \phi^{(\mathrm{I})}(\xi_1, -\xi_2, t) &= \phi^{(\mathrm{I})}(\xi_1, \xi_2, t) \\ \phi^{(\mathrm{II})}(\xi_1, -\xi_2, t) &= -\phi^{(\mathrm{II})}(\xi_1, \xi_2, t) \end{aligned}\right\} , \tag{2.4.6}$$

and

$$\left.\begin{aligned} \psi^{(\mathrm{I})}(\xi_1, -\xi_2, t) &= -\psi^{(\mathrm{I})}(\xi_1, \xi_2, t) \\ \psi^{(\mathrm{II})}(\xi_1, -\xi_2, t) &= \psi^{(\mathrm{II})}(\xi_1, \xi_2, t) \end{aligned}\right\} . \tag{2.4.7}$$

This separation is very similar to the decomposition of the deformation field into mode-I, or the symmetric part, and mode-II, or the asymmetric part, when we deal with near-tip deformation field of a straight moving crack and claim that the deformation field is the superposition of these two modes. As a result of this separation, in writing the expression of the stress components $\sigma_{\alpha\beta}(\xi_1, \xi_2, t)$, $\alpha, \beta \in \{1, 2\}$, we may also separate $\sigma_{\alpha\beta}(\xi_1, \xi_2, t)$ into two parts, the part $\sigma^{(\mathrm{I})}_{\alpha\beta}(\xi_1, \xi_2, t)$ associated with the symmetric deformation and the part $\sigma^{(\mathrm{II})}_{\alpha\beta}(\xi_1, \xi_2, t)$ associated with the asymmetric deformation. Then we will have

$$\sigma_{\alpha\beta}(\xi_1, \xi_2, t) = \sigma^{(\mathrm{I})}_{\alpha\beta}(\xi_1, \xi_2, t) + \sigma^{(\mathrm{II})}_{\alpha\beta}(\xi_1, \xi_2, t) , \qquad \alpha, \beta \in \{1, 2\} . \tag{2.4.8}$$

In addition, define the scaled polar coordinates $(r_{l,s}, \theta_{l,s})$ by

$$\left.\begin{aligned} r_{l,s} &= \left(\xi_1^2 + \alpha_{l,s}^2 \xi_2^2\right)^{1/2} \\ \theta_{l,s} &= \tan^{-1} \frac{\alpha_{l,s} \xi_2}{\xi_1} \end{aligned}\right\} .$$

For the problem of a transiently propagating dynamic crack along an arbitrary

path, the asymptotic representation of the displacement potentials will be given by

$$\left.\begin{aligned}
\phi^{(\mathrm{I})}(\xi_1,\xi_2,t) &= -\frac{4K_I^d(t)}{3\mu\sqrt{2\pi}}\frac{1+\alpha_s^2}{D(v)}r_l^{3/2}\cos\frac{3\theta_l}{2}+\frac{2\alpha_s}{\mu D(v)}\mathrm{Re}\{A_1(t)\}r_l^2\cos 2\theta_l \\
&+\mathrm{Re}\left\{\left[-\frac{1+\alpha_s^2}{\mu D(v)}A_2(t)+\frac{4}{15}\left(f_l(t)-\frac{1}{2}S_l(t)\right)\right]\cos\frac{5\theta_l}{2}\right. \\
&\left.+\frac{1}{6}R_l(t)\cos\frac{\theta_l}{2}-\frac{1}{4}S_l(t)\cos\frac{3\theta_l}{2}\right\}r_l^{5/2}+O(r_l^3) \\
\phi^{(\mathrm{II})}(\xi_1,\xi_2,t) &= \frac{4K_{II}^d(t)}{3\mu\sqrt{2\pi}}\frac{2\alpha_s}{D(v)}r_l^{3/2}\sin\frac{3\theta_l}{2}+\frac{1+\alpha_s^2}{\mu D(v)}\mathrm{Im}\{A_1(t)\}r_l^2\sin 2\theta_l \\
&-\mathrm{Im}\left\{\left[\frac{2\alpha_s}{\mu D(v)}A_2(t)+\frac{4}{15}\left(f_l(t)-\frac{1}{2}S_l(t)\right)\right]\sin\frac{5\theta_l}{2}\right. \\
&\left.+\frac{1}{6}R_l(t)\sin\frac{\theta_l}{2}+\frac{1}{4}S_l(t)\sin\frac{3\theta_l}{2}\right\}r_l^{5/2}+O(r_l^3)
\end{aligned}\right\}, \tag{2.4.9}$$

and

$$\left.\begin{aligned}
\psi^{(\mathrm{I})}(\xi_1,\xi_2,t) &= -\frac{4K_I^d(t)}{3\mu\sqrt{2\pi}}\frac{2\alpha_l^2}{D(v)}r_s^{3/2}\sin\frac{3\theta_s}{2}-\frac{1+\alpha_s^2}{\mu D(v)}\mathrm{Re}\{A_1(t)\}r_s^2\sin 2\theta_s \\
&+\mathrm{Re}\left\{\left[\frac{2\alpha_l}{\mu D(v)}A_2(t)+\frac{4}{15}\left(f_s(t)-\frac{1}{2}S_s(t)\right)\right]\sin\frac{5\theta_s}{2}\right. \\
&\left.+\frac{1}{6}R_s(t)\sin\frac{\theta_s}{2}+\frac{1}{4}S_s(t)\sin\frac{3\theta_s}{2}\right\}r_s^{5/2}+O(r_s^3) \\
\psi^{(\mathrm{II})}(\xi_1,\xi_2,t) &= \frac{4K_I^d(t)}{3\mu\sqrt{2\pi}}\frac{1+\alpha_s^2}{D(v)}r_s^{3/2}\cos\frac{3\theta_s}{2}+\frac{2\alpha_l}{\mu D(v)}\mathrm{Im}\{A_1(t)\}r_s^2\cos 2\theta_s \\
&+\mathrm{Im}\left\{\left[-\frac{1+\alpha_s^2}{\mu D(v)}A_2(t)+\frac{4}{15}\left(f_s(t)-\frac{1}{2}S_s(t)\right)\right]\cos\frac{5\theta_s}{2}\right. \\
&\left.+\frac{1}{6}R_s(t)\cos\frac{\theta_s}{2}-\frac{1}{4}S_s(t)\cos\frac{3\theta_s}{2}\right\}r_s^{5/2}+O(r_s^3)
\end{aligned}\right\}. \tag{2.4.10}$$

The stress components associated with the symmetric deformation in equation

(2.4.8) are

$$\left.\begin{aligned}
&\frac{\sigma_{11}^{(\mathrm{I})}}{\mu}=\frac{K_I^d(t)}{\mu\sqrt{2\pi}}\left\{\frac{(1+2\alpha_l^2-\alpha_s^2)(1+\alpha_s^2)}{D(v)}r_l^{-1/2}\cos\frac{\theta_l}{2}-\frac{4\alpha_l\alpha_s}{D(v)}r_s^{-1/2}\cos\frac{\theta_s}{2}\right\}\\
&+\frac{4\alpha_s(\alpha_l^2-\alpha_s^2)}{\mu D(v)}\mathrm{Re}\{A_1(t)\}+\mathrm{Re}\left\{\left[-\frac{15(1+2\alpha_l^2-\alpha_s^2)(1+\alpha_s^2)}{4\mu D(v)}A_2(t)\right.\right.\\
&+(1+2\alpha_l^2-\alpha_s^2)f_l(t)+\left(\frac{1-\alpha_s^2}{2}+\frac{\alpha_l^2(\alpha_l^2-\alpha_s^2)}{1-\alpha_l^2}\right)R_l(t)\Big]\cos\frac{\theta_l}{2}\\
&+\left[\frac{1+2\alpha_l^2-\alpha_s^2}{8}R_l(t)-\left(\frac{1-\alpha_s^2}{2}+\frac{\alpha_l^2(\alpha_l^2-\alpha_s^2)}{1-\alpha_l^2}\right)S_l(t)\right]\cos\frac{3\theta_l}{2}\\
&\left.+\frac{1+2\alpha_l^2-\alpha_s^2}{16}S_l(t)\cos\frac{7\theta_l}{2}\right\}r_l^{1/2}\\
&+2\alpha_s\mathrm{Re}\left\{\left[\frac{15\alpha_l}{2\mu D(v)}A_2(t)+g_s(t)\right]\cos\frac{\theta_s}{2}+\frac{1}{8}R_s(t)\cos\frac{3\theta_s}{2}\right.\\
&\left.+\frac{1}{16}S_s(t)\cos\frac{7\theta_s}{2}\right\}r_s^{1/2}+O(r_{l,s})
\end{aligned}\right\},\tag{2.4.11}$$

$$\left.\begin{aligned}
&\frac{\sigma_{22}^{(\mathrm{I})}}{\mu}=\frac{K_I^d(t)}{\mu\sqrt{2\pi}}\left\{-\frac{(1+\alpha_s^2)^2}{D(v)}r_l^{-1/2}\cos\frac{\theta_l}{2}+\frac{4\alpha_l\alpha_s}{D(v)}r_s^{-1/2}\cos\frac{\theta_s}{2}\right\}\\
&-\mathrm{Re}\left\{\left[-\frac{15(1+\alpha_s^2)^2}{4\mu D(v)}A_2(t)+(1+\alpha_s^2)f_l(t)\right.\right.\\
&+\left(\frac{1-\alpha_s^2}{2}-\frac{\alpha_l^2-\alpha_s^2}{1-\alpha_l^2}\right)R_l(t)\Big]\cos\frac{\theta_l}{2}\\
&+\left[\frac{1+\alpha_s^2}{8}R_l(t)-\left(\frac{1-\alpha_s^2}{2}-\frac{\alpha_l^2-\alpha_s^2}{1-\alpha_l^2}\right)S_l(t)\right]\cos\frac{3\theta_l}{2}\\
&\left.+\frac{1+\alpha_s^2}{16}S_l(t)\cos\frac{7\theta_l}{2}\right\}r_l^{1/2}\\
&-2\alpha_s\mathrm{Re}\left\{\left[\frac{15\alpha_l}{2\mu D(v)}A_2(t)+g_s(t)\right]\cos\frac{\theta_s}{2}+\frac{1}{8}R_s(t)\cos\frac{3\theta_s}{2}\right.\\
&\left.+\frac{1}{16}S_s(t)\cos\frac{7\theta_s}{2}\right\}r_s^{1/2}+O(r_{l,s})
\end{aligned}\right\},\tag{2.4.12}$$

and

$$\left.\begin{aligned}
&\frac{\sigma_{12}^{(\mathrm{I})}}{\mu}=\frac{K_I^d(t)}{\mu\sqrt{2\pi}}\frac{2\alpha_l(1+\alpha_s^2)}{D(v)}\left\{r_l^{-1/2}\sin\frac{\theta_l}{2}-r_s^{-1/2}\sin\frac{\theta_s}{2}\right\}\\
&-2\alpha_l\mathrm{Re}\left\{\left[-\frac{15(1+\alpha_s^2)}{4\mu D(v)}A_2(t)+g_l(t)\right]\sin\frac{\theta_l}{2}-\frac{1}{8}R_l(t)\sin\frac{3\theta_l}{2}\right.\\
&\left.-\frac{1}{16}S_l(t)\sin\frac{7\theta_l}{2}\right\}r_l^{1/2}\\
&-\mathrm{Re}\left\{\left[\frac{15\alpha_l(1+\alpha_s^2)}{2\mu D(v)}A_2(t)+(1+\alpha_s^2)f_s(t)+\frac{1-\alpha_s^2}{2}R_s(t)\right]\sin\frac{\theta_s}{2}\right.\\
&\left.-\left[\frac{1+\alpha_s^2}{8}R_s(t)-\frac{1-\alpha_s^2}{2}S_s(t)\right]\sin\frac{3\theta_s}{2}-\frac{1+\alpha_s^2}{16}S_s(t)\sin\frac{7\theta_s}{2}\right\}r_s^{1/2}\\
&+O(r_{l,s})
\end{aligned}\right\}. \qquad (2.4.13)$$

The stress components associated with the asymmetric deformation in equation (2.4.8) are

$$\left.\begin{aligned}
&\frac{\sigma_{11}^{(\mathrm{II})}}{\mu}=-\frac{2\alpha_s K_{II}^d(t)}{\mu\sqrt{2\pi}}\left\{\frac{1+2\alpha_l^2-\alpha_s^2}{D(v)}r_l^{-1/2}\sin\frac{\theta_l}{2}-\frac{1+\alpha_s^2}{D(v)}r_s^{-1/2}\sin\frac{\theta_s}{2}\right\}\\
&+\mathrm{Im}\left\{\left[-\frac{15\alpha_s(1+2\alpha_l^2-\alpha_s^2)}{2\mu D(v)}A_2(t)-(1+2\alpha_l^2-\alpha_s^2)f_l(t)\right.\right.\\
&\left.-\left(\frac{1-\alpha_s^2}{2}+\frac{\alpha_l^2(\alpha_l^2-\alpha_s^2)}{1-\alpha_l^2}\right)R_l(t)\right]\sin\frac{\theta_l}{2}\\
&+\left[\frac{1+2\alpha_l^2-\alpha_s^2}{8}R_l(t)-\left(\frac{1-\alpha_s^2}{2}+\frac{\alpha_l^2(\alpha_l^2-\alpha_s^2)}{1-\alpha_l^2}\right)S_l(t)\right]\sin\frac{3\theta_l}{2}\\
&\left.+\frac{1+2\alpha_l^2-\alpha_s^2}{16}S_l(t)\sin\frac{7\theta_l}{2}\right\}r_l^{1/2}\\
&+2\alpha_s\mathrm{Im}\left\{\left[\frac{15(1+\alpha_s^2)}{4\mu D(v)}A_2(t)-g_s(t)\right]\sin\frac{\theta_s}{2}+\frac{1}{8}R_s(t)\sin\frac{3\theta_s}{2}\right.\\
&\left.+\frac{1}{16}S_s(t)\sin\frac{7\theta_s}{2}\right\}r_s^{1/2}+O(r_{l,s})
\end{aligned}\right\}, \qquad (2.4.14)$$

$$
\left.
\begin{aligned}
&\frac{\sigma_{22}^{(\mathrm{II})}}{\mu} = \frac{K_{II}^d(t)}{\mu\sqrt{2\pi}} \frac{2\alpha_s(1+\alpha_s^2)}{D(v)} \left\{ r_l^{-1/2} \sin\frac{\theta_l}{2} - r_s^{-1/2} \sin\frac{\theta_s}{2} \right\} \\
&-\mathrm{Im}\left\{ \left[-\frac{15\alpha_s(1+\alpha_s^2)}{2\mu D(v)} A_2(t) - (1+\alpha_s^2) f_l(t) \right.\right. \\
&\left. - \left(\frac{1-\alpha_s^2}{2} - \frac{\alpha_l^2-\alpha_s^2}{1-\alpha_l^2} \right) R_l(t) \right] \sin\frac{\theta_l}{2} \\
&+ \left[\frac{1+\alpha_s^2}{8} R_l(t) - \left(\frac{1-\alpha_s^2}{2} - \frac{\alpha_l^2-\alpha_s^2}{1-\alpha_l^2} \right) S_l(t) \right] \sin\frac{3\theta_l}{2} \\
&\left. + \frac{1+\alpha_s^2}{16} S_l(t) \sin\frac{7\theta_l}{2} \right\} r_l^{1/2} \\
&-2\alpha_s \mathrm{Im}\left\{ \left[\frac{15(1+\alpha_s^2)}{4\mu D(v)} A_2(t) - g_s(t) \right] \sin\frac{\theta_s}{2} + \frac{1}{8} R_s(t) \sin\frac{3\theta_s}{2} \right. \\
&\left. + \frac{1}{16} S_s(t) \sin\frac{7\theta_s}{2} \right\} r_s^{1/2} + O(r_{l,s})
\end{aligned}
\right\}, \qquad (2.4.15)
$$

and

$$
\left.
\begin{aligned}
&\frac{\sigma_{12}^{(\mathrm{II})}}{\mu} = \frac{K_{II}^d(t)}{\mu\sqrt{2\pi}} \left\{ \frac{4\alpha_l\alpha_s}{D(v)} r_l^{-1/2} \cos\frac{\theta_l}{2} - \frac{(1+\alpha_s^2)^2}{D(v)} r_s^{-1/2} \cos\frac{\theta_s}{2} \right\} \\
&-2\alpha_l \mathrm{Im}\left\{ \left[\frac{15\alpha_s}{2\mu D(v)} A_2(t) + g_l(t) \right] \cos\frac{\theta_l}{2} + \frac{1}{8} R_l(t) \cos\frac{3\theta_l}{2} \right. \\
&\left. + \frac{1}{16} S_l(t) \cos\frac{7\theta_l}{2} \right\} r_l^{1/2} \\
&-\mathrm{Im}\left\{ \left[-\frac{15(1+\alpha_s^2)^2}{4\mu D(v)} A_2(t) + \frac{1-\alpha_s^2}{2} R_s(t) \right] \cos\frac{\theta_s}{2} \right. \\
&\left. + \left[\frac{1+\alpha_s^2}{8} R_s(t) - \frac{1-\alpha_s^2}{2} S_s(t) \right] \cos\frac{3\theta_s}{2} + \frac{1+\alpha_s^2}{16} S_s(t) \cos\frac{7\theta_s}{2} \right\} r_s^{1/2} \\
&+O(r_{l,s})
\end{aligned}
\right\}. \qquad (2.4.16)
$$

In the above expressions for components of stress, $K_I^d(t)$ and $K_{II}^d(t)$ are the mixed-mode dynamic stress intensity factors. The complex functions $f_{l,s}(t)$ and $g_{l,s}(t)$ that

appear in the expressions for displacement potentials and stresses, are given by

$$\left.\begin{aligned}
f_l(t) &= \left(\frac{(1+\alpha_s^2)m_l}{D(v)} - \frac{1}{8}\right) R_l(t) - \left(\frac{(1+\alpha_s^2)m_l}{D(v)} + \frac{\overset{*}{D}(v)}{D(v)} + \frac{9}{16}\right) S_l(t) \\
&\quad - \frac{2\alpha_s m_s}{D(v)} R_s(t) + \left(\frac{2\alpha_s m_s}{D(v)} + \frac{2\alpha_s(1+\alpha_s^2)}{D(v)}\right) S_s(t) \\
f_s(t) &= -\frac{2\alpha_l m_l}{D(v)} R_l(t) + \left(\frac{2\alpha_l m_l}{D(v)} + \frac{2\alpha_l(1+\alpha_s^2)}{D(v)}\right) S_l(t) \\
&\quad + \left(\frac{(1+\alpha_s^2)m_s}{D(v)} - \frac{1}{8}\right) R_s(t) - \left(\frac{(1+\alpha_s^2)m_s}{D(v)} + \frac{\overset{*}{D}(v)}{D(v)} + \frac{9}{16}\right) S_s(t) \\
g_l(t) &= \left(\frac{(1+\alpha_s^2)m_l}{D(v)} - \frac{1}{8}\right) R_l(t) - \left(\frac{(1+\alpha_s^2)m_l}{D(v)} + \frac{\overset{*}{D}(v)}{D(v)} - \frac{7}{16}\right) S_l(t) \\
&\quad - \frac{2\alpha_s m_s}{D(v)} R_s(t) + \left(\frac{2\alpha_s m_s}{D(v)} + \frac{2\alpha_s(1+\alpha_s^2)}{D(v)}\right) S_s(t) \\
g_s(t) &= -\frac{2\alpha_l m_l}{D(v)} R_l(t) + \left(\frac{2\alpha_l m_l}{D(v)} + \frac{2\alpha_l(1+\alpha_s^2)}{D(v)}\right) S_l(t) \\
&\quad + \left(\frac{(1+\alpha_s^2)m_s}{D(v)} - \frac{1}{8}\right) R_s(t) - \left(\frac{(1+\alpha_s^2)m_s}{D(v)} + \frac{\overset{*}{D}(v)}{D(v)} - \frac{7}{16}\right) S_s(t)
\end{aligned}\right\}, \tag{2.4.17}$$

where m_l, m_s, and $\overset{*}{D}(v)$ are functions of the crack-tip speed and are given in equation (2.3.49). Also, more explicitly, we can express the quantities $S_{l,s}(t)$ and $R_{l,s}(t)$ in terms of the mixed-mode dynamic stress intensity factors $K_I^d(t)$ and $K_{II}^d(t)$, the time derivative of the crack-tip speed $\dot{v}(t)$, and the curvature of the trajectory at the crack-tip $k(t)$ as follows:

$$\left.\begin{aligned}
S_l(t) &= \left\{\frac{v^2(1+\alpha_s^2)}{\mu\sqrt{2\pi}D(v)\alpha_l^4 c_l^4} K_I^d(t)\dot{v}(t) + \frac{2\alpha_s(1-\alpha_l^2)^2}{\mu\sqrt{2\pi}D(v)\alpha_l^3} K_{II}^d(t)k(t)\right\} \\
&\quad - i\left\{\frac{2v^2\alpha_s}{\mu\sqrt{2\pi}D(v)\alpha_l^4 c_l^4} K_{II}^d(t)\dot{v}(t) - \frac{(1+\alpha_s^2)(1-\alpha_l^2)^2}{\mu\sqrt{2\pi}D(v)\alpha_l^3} K_I^d(t)k(t)\right\} \\
S_s(t) &= -\left\{\frac{2v^2\alpha_l}{\mu\sqrt{2\pi}D(v)\alpha_s^4 c_s^4} K_I^d(t)\dot{v}(t) + \frac{(1+\alpha_s^2)(1-\alpha_s^2)^2}{\mu\sqrt{2\pi}D(v)\alpha_s^3} K_{II}^d(t)k(t)\right\} \\
&\quad + i\left\{\frac{v^2(1+\alpha_s^2)}{\mu\sqrt{2\pi}D(v)\alpha_s^4 c_s^4} K_{II}^d(t)\dot{v}(t) - \frac{2\alpha_l(1-\alpha_s^2)^2}{\mu\sqrt{2\pi}D(v)\alpha_s^3} K_I^d(t)k(t)\right\}
\end{aligned}\right\}, \tag{2.4.18}$$

and

$$
\left.
\begin{aligned}
R_l(t) = &-\frac{1}{\mu\sqrt{2\pi}}\left\{\frac{4\sqrt{v}}{\alpha_l^2 c_l^2}\frac{\mathrm{d}}{\mathrm{d}t}\left[\frac{\sqrt{v}(1+\alpha_s^2)}{D(v)}K_I^d(t)\right] - \frac{v^2(1+\alpha_s^2)}{D(v)\alpha_l^4 c_l^4}K_I^d(t)\dot{v}(t)\right. \\
&\left. -\frac{2\alpha_s(1-\alpha_l^2)(1+3\alpha_l^2)}{D(v)\alpha_l^3}K_{II}^d(t)k(t)\right\} \\
&+ i\frac{1}{\mu\sqrt{2\pi}}\left\{\frac{8\sqrt{v}}{\alpha_l^2 c_l^2}\frac{\mathrm{d}}{\mathrm{d}t}\left[\frac{\sqrt{v}\alpha_s}{D(v)}K_{II}^d(t)\right] - \frac{2v^2\alpha_s}{D(v)\alpha_l^4 c_l^4}K_{II}^d(t)\dot{v}(t)\right. \\
&\left. +\frac{(1+\alpha_s^2)(1-\alpha_l^2)(1+3\alpha_l^2)}{D(v)\alpha_l^3}K_I^d(t)k(t)\right\} \\
R_s(t) = &\frac{1}{\mu\sqrt{2\pi}}\left\{\frac{8\sqrt{v}}{\alpha_s^2 c_s^2}\frac{\mathrm{d}}{\mathrm{d}t}\left[\frac{\sqrt{v}\alpha_l}{D(v)}K_I^d(t)\right] - \frac{2v^2\alpha_l}{D(v)\alpha_s^4 c_s^4}K_I^d(t)\dot{v}(t)\right. \\
&\left. -\frac{(1+\alpha_s^2)(1-\alpha_s^2)(1+3\alpha_s^2)}{D(v)\alpha_s^3}K_{II}^d(t)k(t)\right\} \\
&- i\frac{1}{\mu\sqrt{2\pi}}\left\{\frac{4\sqrt{v}}{\alpha_s^2 c_s^2}\frac{\mathrm{d}}{\mathrm{d}t}\left[\frac{\sqrt{v}(1+\alpha_s^2)}{D(v)}K_{II}^d(t)\right] - \frac{v^2(1+\alpha_s^2)}{D(v)\alpha_s^4 c_s^4}K_{II}^d(t)\dot{v}(t)\right. \\
&\left. +\frac{2\alpha_l(1-\alpha_s^2)(1+3\alpha_s^2)}{D(v)\alpha_s^3}K_I^d(t)k(t)\right\}
\end{aligned}
\right\}. \quad (2.4.19)
$$

In the expressions of the components of asymptotic stress field near the moving crack-tip, (2.4.11) through (2.4.16), $R_l(t)$ and $R_s(t)$ depend not only on the mixed-mode dynamic stress intensity factors, $K_I^d(t)$ and $K_{II}^d(t)$, and the crack-tip speed, $v(t)$, but also on the time derivatives of these quantities. Meanwhile, $R_l(t)$ and $R_s(t)$ also depend on the trajectory curvature at the crack-tip $k(t)$, as shown in equation (2.4.19). $S_l(t)$ and $S_s(t)$ also have these properties, but they do not depend on the time derivatives of the mixed-mode dynamic stress intensity factors. In most of the experiments, the study of the dynamic crack growth is under mode-I loading conditions and the crack propagates along a straight path. Under this circumstance, $k(t) = 0$, $K_{II}^d(t) = 0$, and all quantities of the form $\mathrm{Im}\{\ \cdot\ \}$ disappear, and the deformation field is symmetric. At this point, equations (2.4.11) through (2.4.13) provide the stress field of a non-uniformly propagating mode-I crack. This is the same as that given by Rosakis *et al.* (1991). If the crack-tip velocity, $v(t)$, is a

constant, i.e., $\dot{v}(t) = 0$, and therefore, $S_l(t) = S_s(t) = 0$, we can obtain the asymptotic stress field corresponding to transient crack growth with constant velocity and varying stress intensity factor (see Freund and Rosakis, 1992). A classical example of such a transient crack problem is the one analyzed by Broberg (1960). Furthermore, if the time derivative of the dynamic stress intensity factor, $\dot{K}_I^d(t)$, is also zero, so are $R_l(t)$ and $R_s(t)$; we obtain the familiar asymptotic stress field for the steady state situation up to the third term. This is the case considered by Nishioka and Atluri (1983), and Dally (1987).

2.5 Discussion

In this chapter, a procedure for obtaining the higher order transient asymptotic representation of the elastodynamic field around the tip of a propagating crack has been developed. The crack propagates transiently along a smooth but otherwise arbitrary path. The material is considered to be homogeneous, isotropic and linearly elastic. The formulation is based on the two displacement potentials, $\phi(\xi_1, \xi_2, t)$ and $\psi(\xi_1, \xi_2, t)$. These two potentials can be expressed in terms of the real and imaginary parts of some complex functions, respectively. By imposing the continuity condition ahead of the crack-tip and the traction free boundary condition along the crack faces, the problem can be recast into a Riemann-Hilbert problem. Upon solving the Riemann-Hilbert problem, the two displacement potentials are obtained. Meanwhile, the transient asymptotic representation of the near-tip stress field up to the third term is also provided. The transient effects and the geometrical characteristic of the crack path are included in this analysis.

The general form of the near-tip stress field, equations (2.4.11) through (2.4.16), exhibits some noteworthy features. First, it is noted that the spatial structure in the *radial direction* of the transient elastodynamic field is the same as that under

the steady state conditions. The differences between the results for the transient and the steady state analyses appear in the angular distribution. Secondly, it is observed that the angular distribution for a mixed-mode curving crack is identical to the one corresponding to a mixed-mode crack propagating along a straight line (see Freund and Rosakis, 1992; and Rosakis *et al.*, 1991). The information regarding the path curvature $k(t)$ only appears in the coefficients of the expansion. It should be also observed that in the local coordinate system (ξ_1, ξ_2), the two components of the crack-tip acceleration vector are ($\dot{v}(t)$, $k(t)v^2(t)$) at any instant. The above results, as expected, contain both components of crack-tip acceleration in the coefficients of the transient high order terms. In the case of a mode-I crack propagating along a straight line (Freund and Rosakis, 1992; and Rosakis *et al.*, 1991), only $\dot{v}(t)$ appears in these coefficients.

Suppose that a crack propagates along a straight path, then $k(t) = 0$ at any time during the propagation. Under this situation, (2.4.11) through (2.4.16) provide the customarily mixed-mode stress field for a mode-I and a mode-II straight crack, respectively. However, as we have mentioned earlier, under the most general loading conditions, the crack will grow along a curved path. When this happens, even though the deformation field can be separated into a symmetric part and an asymmetric part, the so-called mode-I and mode-II types will be coupled together. This happens since in the higher order contributions to the expression of the stress components associated with the symmetric deformation, the crack-tip curvature $k(t)$ always appears as a product with $K_{II}^d(t)$ which is the dynamic stress intensity factor for mode-II. Similarly, in the asymmetric deformation field, the crack-tip curvature $k(t)$ always appears in a product with $K_I^d(t)$ where $K_I^d(t)$ is the dynamic stress intensity factor for mode-I. An interesting consequence of the above observation is the following. Suppose that the propagating crack follows the path of $K_{II}^d(t) = 0$ for any time (as proposed by Cotterell and Rice (1980) for the quasi-statically growing crack). Then since $k(t)$ will

not be zero, the asymmetric part of the stresses will in general survive even if the first term disappears. This may produce an experimental illusion of the existence of a nonzero K_{II}^d, if the experimental data are recorded at some distance away from the crack-tip. Rossmanith (1983) has studied the rapid curved crack propagation using the dynamic photoelastic method. In the interpretation of his experimental data, Rossmanith used the singular (or the K^d-dominant) stress representation. He found that the values of K_I^d and K_{II}^d depend on the positions of measurement (or depend on fringe order). By using the extrapolation, he observed that as the distance from the moving crack-tip $r \to 0$, or the fringe order tends to infinity, K_I^d tends to a finite value while K_{II}^d becomes infinitely small. Similar experimental observations have been reported by Chona and Shukla (1986), and by Shukla and Chona (1988), who conducted extensive studies of this phenomenon. They also used dynamic photoelasticity to investigate dynamic crack growth along a curved path. Although their isochromatic data were analyzed on the basis of a mixed-mode, *steady state* higher order expansion, they reported very small values of K_{II}^d (up to 10% of K_I^d at each time). They observed that even if they force K_{II}^d to vanish in their expansion, they can still fit the higher order asymmetric isochromatic patterns by adjusting the coefficient of the third ($r^{1/2}$) term in their expansion. This is exactly the term that in the transient expansion involves the product $k(t)K_I^d(t)$ which appears in equations (2.4.14) – (2.4.16).

To visualize the above discussions, consider the following special situation. Suppose that at time t, locally, the crack-tip undergoes mode-I deformation which conforms to the criterion proposed by Cotterell and Rice (1980). This criterion requires that the crack will follow the path which will assure that $K_{II}^d = 0$. Meanwhile, assume that at this time, the crack-tip acceleration, the time derivatives of the stress intensity factors, and the higher order coefficient $A_2(t)$ all vanish. In addition, suppose that the crack propagates along a curved path, so that the instantaneous crack-tip curva-

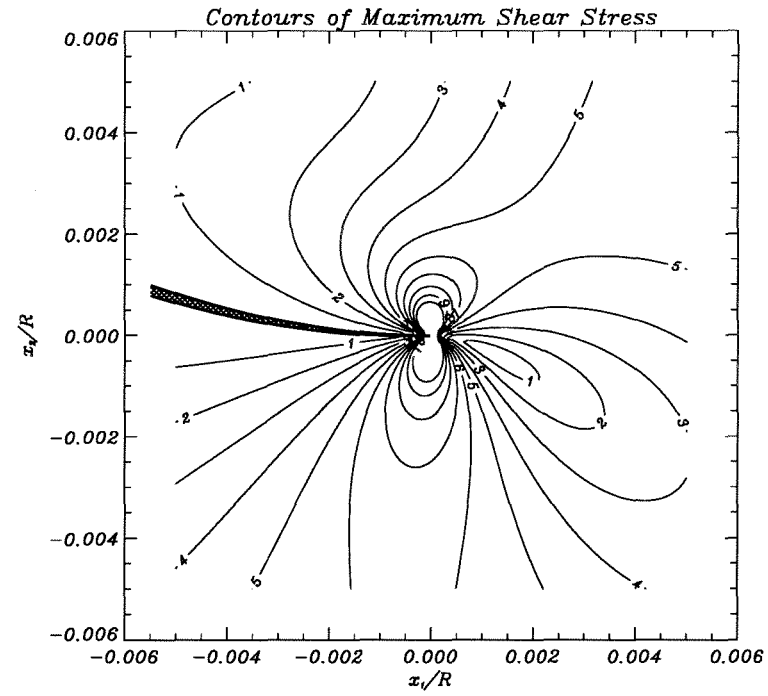

(a)

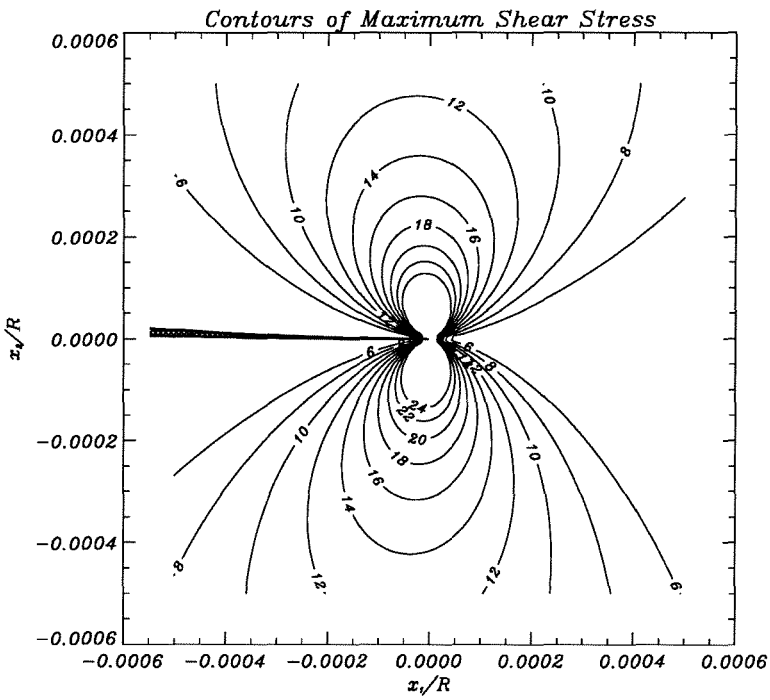

(b)

Figure 2.2: Simulated photoelastic fringe patterns surrounding the tip of a crack propagating along a curved path, (a) larger observation region, (b) observation in the region very close to the crack-tip.

ture is not zero. By using the higher order transient asymptotic stress representations obtained in previous sections, the contours of the following field

$$m(\xi_1, \xi_2) = \frac{1}{2} \cdot \frac{\sigma_1 - \sigma_2}{K_I^d(t)/\sqrt{2\pi R(t)}}, \tag{2.5.1}$$

are plotted. In (2.5.1), σ_1 and σ_2 are the two principal stresses, and $R(t)$ is such that $k(t) = 1/R(t)$. Notice that the contours of the field $m(\xi_1, \xi_2)$ actually simulate normalized photoelastic fringe patterns surrounding the moving crack-tip. These simulated fringe patterns are given in FIGURE 2.2 where the Poisson's ratio for the solid has been chosen as $\nu = 0.3$ and the crack-tip speed has been set to $v/c_s = 0.35$. FIGURE 2.2(a) shows the fringe pattern observed in a relatively large region. The fringe pattern is apparently mixed-mode. However, by recalling that locally, the crack-tip field is pure mode-I, this apparent mixed-mode fringe pattern is due to the "mode-coupling" that stems from the geometrical shape of the curved crack which results in non-zero asymmetric higher order transient contributions. Although in this case, the tangential acceleration of the crack-tip, $\dot{v}(t)$, is zero, the instantaneous angular acceleration is finite and equal to $k(t)v^2(t)$. FIGURE 2.2(b) represents a view of the same fringe pattern taken much closer to the crack-tip than the view in FIGURE 2.2(a). FIGURE 2.2(b) clearly shows that the near-tip field is indeed symmetric. The above observations suggests that the accurate measurement of the dynamic stress intensity factors at a moving crack-tip requires that data points should be chosen either very close to the crack-tip, so that K^d-dominance is valid and can be used, or otherwise a complete higher order transient asymptotic representation should be used to interpret the measurements.

In conclusion we should point out that the field presented above contains, for the first time, both the transient and the geometric features of crack growth. In this sense, it is hoped that it may prove useful in studying crack-tip kinking or curving even in laboratory situations where specimen size and geometry make the existence of transients unavoidable.

Chapter 3

Dynamic Crack Initiation and Transient Crack Growth under Stress Wave Loading Conditions – Revisited

3.1 Introduction

In the last decade, extensive theoretical and experimental studies have been carried out on the subject of dynamic fracture under stress wave loading conditions. Due to the high loading rates which exist during a dynamic fracture event, the effects of material inertia and strain rate sensitivity cannot be neglected, and as a result the material may exhibit totally different fracture behavior than the one exhibited under quasi-static loading regimes. Because of the complex transient nature of the crack initiation, growth and arrest problems, complete analytical solutions of even elastodynamic problems are very scarce. Moreover, these analytical solutions are only for those situations corresponding to very special geometrical configurations and loading conditions so that the mathematical models are tractable. Some of the theoretical and experimental studies on the subject are described below.

Baker (1962) studied the transient problem of a semi-infinite crack suddenly appearing in a pre-stretched elastic body and simultaneously propagating with a constant speed. He used the Laplace transforms and the Wiener-Hopf technique to

obtain the distribution of normal tractions ahead of the moving crack-tip, as well as the asymptotic leading term of the stress field surrounding the crack-tip. This leading term which is square root singular in stresses and whose amplitude is the dynamic stress intensity factor $K_I^d(t)$, will be referred to in this investigation as the "K_I^d-dominant field." Achenbach and Nuismer (1971) observed that Baker's result was essentially the solution for the case of a planar step-stress wave with a wavefront parallel to the semi-infinite crack impinging on the initially stationary crack. When the stress wave hits the crack, the crack begins to grow with a constant speed. They then extended the solution to include incident waves of arbitrary stress profile, and also to include the case of oblique incidence. The unrealistic restriction of instant crack growth when the incident stress wave reaches the crack-tip in the above solutions was relaxed by Freund (1973), who introduced a finite delay time between the two events of stress wave arrival at the crack and the onset of crack extension. By using an elegant superposition procedure, Freund obtained the expression for the dynamic stress intensity factor at the running crack-tip, and also generalized this expression to the case of non-uniform crack growth speeds. He found that for an unbounded body subjected to time-independent loading conditions, the dynamic stress intensity factor at the running crack-tip can be expressed as a universal function of instantaneous crack-tip speed multiplied by the equilibrium stress intensity factor for the given applied loading and the instantaneous amount of crack growth.

Since these early theoretical studies have revealed that the stress field near the tip of a propagating crack can be represented in terms of a dynamic stress intensity factor, analogous to that for a static crack, a large number of experimental investigations has attempted to measure this parameter for various specimen configurations and for various loading conditions. The eventual goal of these studies was to use the dynamic stress intensity factor concept in the formulation of a dynamic fracture criterion. From the experimental point of view, Ravi-Chandar and Knauss (1982) studied

the dynamic fracture of a semi-infinite crack in an unbounded body subjected to a uniform step pressure applied on the crack faces. The solution of this problem can be obtained from the solution for the problem studied by Freund (1973) and described above. By using the optical method of caustics, and by interpreting the experimental results on the assumption of the existence of a K_I^d-dominant field, they found that when the crack starts to propagate, a discrepancy exists between experimentally inferred dynamic stress intensity factors and the theoretical predictions. For the same problem studied by Ravi-Chandar and Knauss, Ma and Freund (1986) observed that for a point which is fixed with respect to the moving crack-tip, a surprisingly long time is needed for the stress intensity factor controlled field (K_I^d-dominant field) to be fully established. Their observation suggested that optical measurements (by caustics or otherwise) performed at finite distances from the crack-tip and at times close to crack initiation should not be interpreted on the basis of the assumption of the existence of a K_I^d-dominant field. The fact that the classical analysis of caustics assumes K_I^d-dominance for a deformation field which does not conform with this assumption, provided an explanation in the discrepancy between the theoretical and the experimentally inferred stress intensity factors in the experiments by Ravi-Chandar and Knauss (1982). A similar problem was studied experimentally by Kim (1985) using the technique of Stress-Intensity Factor Tracer (SIFT). Other geometrical and loading configurations were explored by Kalthoff *et al.* (1979), Kobayashi and Dally (1980), and Rosakis *et al.* (1984) who utilized the double cantilever specimen, and by Zehnder and Rosakis (1990) who utilized the three point bend specimen. More recently, a bifocal caustics arrangement was utilized by Krishnaswamy and Rosakis (1991) to investigate the accuracy of caustics in measuring dynamic stress intensity factors in the presence of transients. However, with the suspicion of the lack of K_I^d-dominance, as further emphasized by Krishnaswamy and Rosakis (1991), the dependability of stress intensity factor histories measured from various experimental techniques is still questionable.

By relaxing the assumption of K_I^d-dominance, Freund and Rosakis (1992) and Rosakis *et al.* (1991) have recently obtained a higher order transient asymptotic expansion for the stress field surrounding the mode-I moving crack-tip. The leading term of this expansion corresponds to the classical square root singular field (K_I^d-dominant field). The higher order, less singular terms in this interpretation are found to involve coefficients that are functions of the time derivatives of crack-tip speed as well as the time derivatives of $K_I^d(t)$. When highly transient conditions exist, there exist regions near the crack-tip where the higher order terms may be as important as the leading square root singular contribution, and if so, K_I^d-dominance will be absent. Such cases are typically ones involving large crack-tip accelerations or sudden crack initiation or crack arrest events that may be a result of discrete stress wave arrivals. Based on these results, Liu *et al.* (1993) re-examined the optical method of caustics and provided a new interpretation technique for the analysis of caustic patterns and the accurate inference of the dynamic stress intensity factors in the presence of transients, in cases where strict K_I^d-dominance is absent. The analysis of Freund and Rosakis (1992) was generalized for the case of a mixed-mode crack propagating along an arbitrarily curved path by Liu and Rosakis (1992). This analysis provided the higher order transient asymptotic representation of the elastodynamic field surrounding the crack-tip. The higher order terms were found to depend on the time derivatives of the complex dynamic stress intensity factor $K_I^d + iK_{II}^d$, the crack-tip acceleration, as well as on the local value of the crack path curvature. For generally anisotropic solids the same issues for a transiently propagating mode-I crack were addressed by Willis (1992). The asymptotic analyses described above provide the spatial structure of the field near the crack-tip when transient conditions exist. As a result, they are necessary for the accurate interpretation of optical high speed photography measurements performed in laboratory specimens of finite size where steady state conditions are usually the exception rather than the rule. Such measurements may be performed by means of optical techniques such as photoelasticity, caustics or

the Coherent Gradient Sensor (CGS). A discussion of the experimental verification of the existence and the influence of transient higher order terms in dynamic fracture is given by Krishnaswamy *et al.* (1992) and by Rosakis (1993).

The desire of producing very high loading rates and easily interpretable dynamic crack initiation and growth experiments has recently motivated Ravichandran and Clifton (1989) to devise a plate impact experimental configuration for the investigation of dynamic fracture. This configuration is capable of producing extremely high loading rates $\dot{K}_I^d \sim 10^8 \text{MPa}\sqrt{\text{m}} \cdot \text{sec}^{-1}$ under stress wave loading and plane strain conditions. The specimen configuration and loading condition they used, simulates the problem of a plane strain semi-infinite crack subjected to a planar stress pulse of finite duration. Consequently the experimental observations can be directly compared with the analytical results given by Freund (1973). By monitoring the particle velocity at a point some distance away from the initial crack-tip, Prakash and Clifton (1992) have observed some interesting phenomena which cannot be explained merely by the existence of a pure K_I^d-dominant elastodynamic field.

The ultimate purpose of this study is to provide an interpretation to the observation made by Prakash and Clifton (1992) for a suddenly initiating and transiently propagating crack, within the framework of linear elastic dynamic fracture mechanics. In this chapter, we revisit the problem studied by Freund (1973). Here, in addition to the dynamic stress intensity factor history, we also try to obtain the full field analytical solution for the stresses around the crack-tip. From the full field solution, the coefficients of the higher order terms which appear in Rosakis *et al.* (1991) and Liu and Rosakis (1992) are determined for this specific problem. To demonstrate the existence of transient effects, we also study the normal traction ahead of the moving crack-tip and compare it to the equivalent traction of the K_I^d-dominant field and the field represented by the higher order transient terms. The result shows that even for a point which is relatively far away from the crack-tip, or for times very close to crack

initiation, the higher order transient representation provides a very good description of the actual stress field while the K_I^d-dominant field is incapable of representing the stress field with any accuracy. In next chapter, we use the result obtained in this chapter to interpret the experimental observations of Prakash and Clifton (1992) and to thus provide further evidence of the existence of measurable transient effects in dynamic fracture. In the process we also provide indirect evidence supporting a particular fracture criterion governing dynamic crack growth. This provides an additional example of the influence of transient effects in a new and important specimen configuration for dynamic fracture studies under very high loading rate conditions.

3.2 Description of the problem

Let $\mathcal{R}$ be an unbounded two-dimensional region occupied by an isotropic, homogeneous, linearly elastic body. The region $\mathcal{R}$ contains a straight semi-infinite crack. Let (x_1, x_2) be an orthonormal Cartesian coordinate system such that the crack occupies the entire $-\infty < x_1 \leq 0,\ x_2 = 0$, see FIGURE 3.1. Initially, the material surrounding

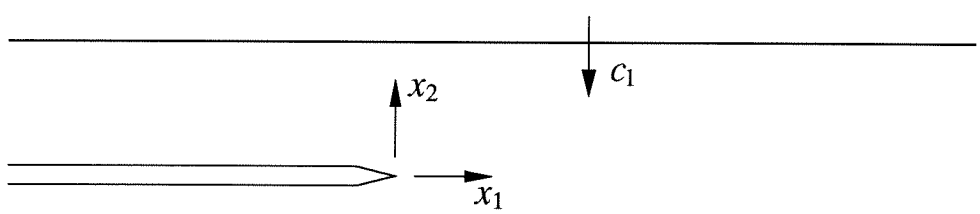

Figure 3.1: A semi-infinite crack loaded by a planar longitudinal wave.

the crack is at rest and stress free, and the crack-tip remains stationary. A planar

longitudinal tension wave with a constant amplitude σ^*, propagates toward the crack and the wavefront is parallel to the crack plane. At time $t = 0$, the stress wave strikes the crack and is partially reflected and partially diffracted. The diffracted waves radiate from the crack-tip and propagate into the body. If the material occupying the body is of limited strength, then the crack will start to grow at some later time, say $t = \tau$. In order to obtain the complete full field analytical solution for this transient problem, we assume that the rate of crack growth v is a constant, but we will relax this restriction in the second part of this study. If the deformation is assumed to be plane strain, the displacement field surrounding the crack-tip may be generated from two displacement potentials, $\phi(x_1, x_2, t)$ and $\psi(x_1, x_2, t)$, by the following relation,

$$u_\alpha(x_1, x_2, t) = \phi_{,\alpha}(x_1, x_2, t) + e_{\alpha\beta}\psi_{,\beta}(x_1, x_2, t) \ , \tag{3.2.1}$$

where $\alpha, \ \beta \in \{1, 2\}$ and the summation convention has been used. $e_{\alpha\beta}$ is the two-dimensional alternator defined by

$$e_{12} = -e_{21} = 1 \ , \qquad e_{11} = e_{22} = 0 \ .$$

The components of stress associated with this deformation can be expressed in terms of the displacement potentials as

$$\left.\begin{aligned} \sigma_{11} &= \mu\left\{\frac{c_l^2}{c_s^2}\phi_{,\alpha\alpha} - 2\phi_{,22} + 2\psi_{,12}\right\} \\ \sigma_{22} &= \mu\left\{\frac{c_l^2}{c_s^2}\phi_{,\alpha\alpha} - 2\phi_{,11} - 2\psi_{,12}\right\} \\ \sigma_{12} &= \mu\left\{2\phi_{,12} + \psi_{,22} - \psi_{,11}\right\} \end{aligned}\right\} \ , \tag{3.2.2}$$

where μ is the shear modulus, and c_l, c_s are the longitudinal and shear wave speeds of the elastic material, respectively.

The equation of motion in the absence of body forces and in terms of $\phi(x_1, x_2, t)$ and $\psi(x_1, x_2, t)$, reduces to

$$\left.\begin{aligned} \phi_{,\alpha\alpha}(x_1, x_2, t) - a^2\ddot{\phi}(x_1, x_2, t) &= 0 \\ \psi_{,\alpha\alpha}(x_1, x_2, t) - b^2\ddot{\psi}(x_1, x_2, t) &= 0 \end{aligned}\right\} \ , \tag{3.2.3}$$

where $a = 1/c_l$ and $b = 1/c_s$.

The crack faces remain traction free during the entire process, therefore the boundary conditions will be

$$\sigma_{2\alpha}(x_1, 0^{\pm}, t) = 0 \ , \qquad -\infty < x_1 < v(t-\tau)H(t-\tau) \ , \quad \alpha \in \{1, 2\} \ , \tag{3.2.4}$$

where $H(\cdot)$ is the Heaviside step function.

At time $t = 0$, we can write the stress field inside the two-dimensional body as

$$\left.\begin{aligned} \sigma_{11}(x_1, x_2, 0) &= \frac{\nu\sigma^*}{1-\nu} H(x_2) \\ \sigma_{22}(x_1, x_2, 0) &= \sigma^* H(x_2) \\ \sigma_{12}(x_1, x_2, 0) &= 0 \end{aligned}\right\} \ , \qquad \forall\ (x_1, x_2) \in \mathcal{R} \ , \tag{3.2.5}$$

where ν is the Poisson's ratio of the elastic body.

To solve the above problem and obtain the complete full field solution, we will use the procedure outlined by Freund (1973 and 1990), namely the method of linear superposition. As discussed by Freund, we consider the following four separate problems shown FIGURE 3.2. In problem A, the incident planar longitudinal stress wave with a constant amplitude σ^*, propagates through a body without a crack. This stress wave will induce a traction on the plane which will be occupied by the initial crack shown as the dashed lines in FIGURE 3.2. In problem B, we consider a body containing a stationary semi-infinite crack subjected to a uniform pressure on its surfaces. The magnitude of the pressure is equal to the amplitude of the plane wave considered in problem A. The combination of solutions for these two problems provides the solution for the problem of diffraction of a planar stress wave by a stationary crack. As a result of the stress wave diffraction at the crack-tip, a traction distribution is generated along the plane ahead of the crack-tip. In order to extend, the crack must in effect negate this traction distribution. Accordingly, in problem C,

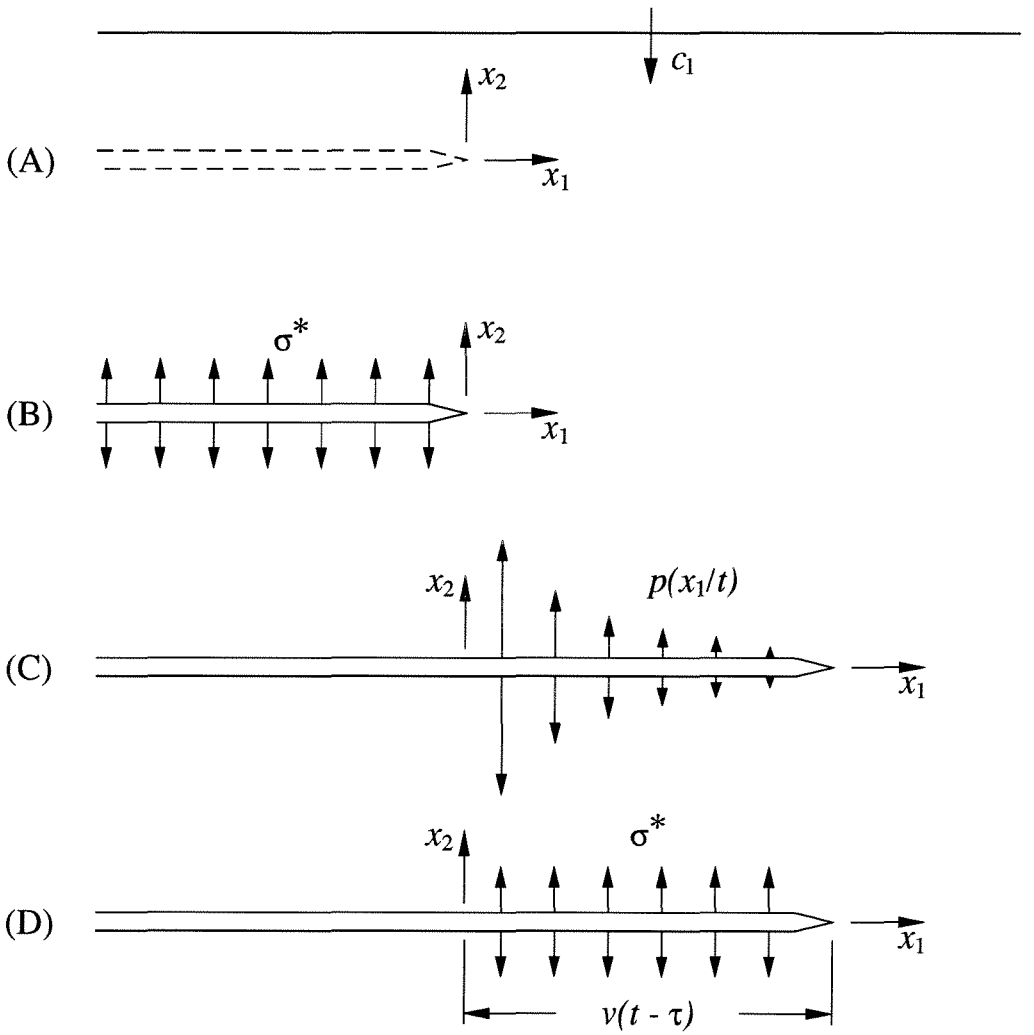

Figure 3.2: Schematic representation of the various boundary value problems considered in constructing the solution for constant speed crack growth under stress wave loading conditions.

we study the case of the crack starting to grow with a constant speed v, at some finite delay time τ after the diffraction has occurred. During the growing process, a traction distribution will appear on the newly formed crack surface and this traction distribution will be equal but opposite to the traction distribution ahead of the crack-

tip in problem B. Finally, in problem D, the crack propagates with the same constant speed v as in problem C, and a uniform pressure with the magnitude σ^* is applied on the newly created crack faces. The sum of solutions of these four problems provides the final solution for the problem we considered in this study, i.e., the one that corresponds to the case of a planar wave which strikes the crack and then, after some finite time, the crack extends at a constant speed.

In the following section, we will give the analytical results pertinent to the problems discussed above with little development. Nevertheless, besides the history of the dynamic stress intensity factor at the stationary and the moving crack-tips, which has drawn most of the attentions in previous studies, we will also provide the full field solution for the stresses surrounding the stationary and moving crack-tips. Due to length limitation, we will omit most of the details in getting those solutions, however, the reader can acquire these details from Freund (1972, 1973, and 1990), and Achenbach (1973).

3.3 Analytical solution for the elastodynamic stress field

In this section, we study the four problems discussed in the last section separately. The solutions of these four problems will provide the final solution for our initial problem.

3.3.1 Problem A: Plane wave in an unbounded body

In this problem, we consider a planar longitudinal stress wave with a constant amplitude σ^*, which propagates in an unbounded two-dimensional region. In the Cartesian coordinate system shown in FIGURE 3.2, the wave front is parallel to the x_1-axis, and

the wave propagates in the direction of negative x_2-axis. The wave speed is c_l and the moment that the wave front reaches the plane $x_2 = 0$, is designated as $t = 0$. For this problem, we can write the in plane stress components $\sigma^{(A)}_{\alpha\beta}(x_1, x_2, t)$ as follows:

$$\left.\begin{aligned} \sigma^{(A)}_{11}(x_1, x_2, t) &= \frac{\nu\sigma^*}{1-\nu} H(t + c_l x_2) \\ \sigma^{(A)}_{22}(x_1, x_2, t) &= \sigma^* H(t + c_l x_2) \\ \sigma^{(A)}_{12}(x_1, x_2, t) &= 0 \end{aligned}\right\}, \qquad \forall\ (x_1, x_2) \in \mathcal{R}\ . \tag{3.3.1}$$

Once again, $H(\cdot)$ is the Heaviside step function.

3.3.2 Problem B: Stationary crack subjected to suddenly applied pressure

Let's consider the unbounded two-dimensional region $\mathcal{R}$. The Cartesian coordinate system is chosen as in FIGURE 3.2, and the semi-infinite crack occupies the semi-infinite line of $-\infty < x_1 \leq 0,\ x_2 = 0$. For time $t < 0$, the body is stress free and at rest everywhere. At time $t = 0$, a uniformly distributed pressure with magnitude σ^*, is applied on the crack faces. From the symmetry of this loading condition, we can see that the deformation is mode-I type. Thus, we only need to consider the half plane $\overset{+}{\mathcal{R}}$, where

$$\overset{+}{\mathcal{R}} = \{\ (x_1, x_2)\ |\ -\infty < x_1 < \infty,\ 0 < x_2 < \infty\ \}\ .$$

Let the two displacement potentials associated with this problem be $\phi^{(B)}(x_1, x_2, t)$ and $\psi^{(B)}(x_1, x_2, t)$, then they will satisfy the equation of motion (3.2.3) in the region $\overset{+}{\mathcal{R}}$. The boundary conditions are

$$\left.\begin{aligned} \sigma^{(B)}_{22}(x_1, 0^+, t) &= -\sigma^* H(t)\ , && -\infty < x_1 \leq 0 \\ \sigma^{(B)}_{12}(x_1, 0^+, t) &= 0\ , && -\infty < x_1 < \infty \\ u^{(B)}_2(x_1, 0^+, t) &= 0\ , && 0 < x_1 < \infty \end{aligned}\right\}, \qquad \forall\ t > 0\ . \tag{3.3.2}$$

The initial conditions are

$$\left.\begin{aligned}\phi^{(\mathrm{B})}(x_1,x_2,0)&=\psi^{(\mathrm{B})}(x_1,x_2,0)=0\\ \dot{\phi}^{(\mathrm{B})}(x_1,x_2,0)&=\dot{\psi}^{(\mathrm{B})}(x_1,x_2,0)=0\end{aligned}\right\},\qquad \forall\,(x_1,x_2)\in\overset{+}{\mathcal{R}}\ . \tag{3.3.3}$$

Meanwhile, since the displacement should be bounded throughout the region, or the mechanical energy density should be integrable, but the stress may be singular at the crack-tip, we also have

$$\int_{\mathcal{R}'}\left(\sigma^{(\mathrm{B})}_{\alpha\beta}\epsilon^{(\mathrm{B})}_{\alpha\beta}+\rho\dot{u}^{(\mathrm{B})}_{\alpha}\dot{u}^{(\mathrm{B})}_{\alpha}\right)\mathrm{d}A<\infty\ ,\qquad \forall\,\mathcal{R}'\subset\overset{+}{\mathcal{R}}\ . \tag{3.3.4}$$

In solving the above initial/boundary value problem, a one-side Laplace transform with respect to time t, and a two-side Laplace transform with respect to the coordinate x_1 are used. The transformed solution for the two displacement potentials can be expressed as (Freund, 1990),

$$\left.\begin{aligned}\Phi^{(\mathrm{B})}(\zeta,x_2,s)&=\frac{\sigma^*}{\mu}\cdot\frac{P^{(\mathrm{B})}(\zeta)}{s^4}e^{-s\alpha^{(\mathrm{B})}(\zeta)x_2}\\ \Psi^{(\mathrm{B})}(\zeta,x_2,s)&=\frac{\sigma^*}{\mu}\cdot\frac{Q^{(\mathrm{B})}(\zeta)}{s^4}e^{-s\beta^{(\mathrm{B})}(\zeta)x_2}\end{aligned}\right\},\quad \forall\ x_2\in(0,\infty)\ , \tag{3.3.5}$$

where

$$P^{(\mathrm{B})}(\zeta)=\frac{b^2-2\zeta^2}{\zeta R^{(\mathrm{B})}(\zeta)}\cdot\frac{F^{(\mathrm{B})}_{+}(0)}{F^{(\mathrm{B})}_{+}(\zeta)}\ ,\qquad Q^{(\mathrm{B})}(\zeta)=\frac{2\alpha^{(\mathrm{B})}(\zeta)}{R^{(\mathrm{B})}(\zeta)}\cdot\frac{F^{(\mathrm{B})}_{+}(0)}{F^{(\mathrm{B})}_{+}(\zeta)}\ , \tag{3.3.6}$$

and

$$\left.\begin{aligned}R^{(\mathrm{B})}(\zeta)&=\left(b^2-2\zeta^2\right)^2+4\zeta^2\alpha^{(\mathrm{B})}(\zeta)\beta^{(\mathrm{B})}(\zeta)\\ \alpha^{(\mathrm{B})}(\zeta)&=\left(a^2-\zeta^2\right)^{1/2},\qquad \beta^{(\mathrm{B})}(\zeta)=\left(b^2-\zeta^2\right)^{1/2}\\ F^{(\mathrm{B})}_{+}(\zeta)&=\frac{\alpha^{(\mathrm{B})}_{+}(\zeta)}{(c+\zeta)S^{(\mathrm{B})}_{+}(\zeta)}\end{aligned}\right\}.$$

In the above expressions, appropriate branch cuts have been chosen. Also, $\alpha^{(\mathrm{B})}_{+}(\zeta)=(a+\zeta)^{1/2}$, $c=1/c_R$ where c_R is the Rayleigh wave speed of the elastic material, and

$$S^{(\mathrm{B})}_{+}(\zeta)=\exp\left\{-\frac{1}{\pi}\int_a^b\tan^{-1}\left[\frac{4\eta^2\sqrt{(\eta^2-a^2)(b^2-\eta^2)}}{(b^2-2\eta^2)^2}\right]\frac{\mathrm{d}\eta}{\eta+\zeta}\right\}\ .$$

The subscript + indicates that the function is analytic in the half plane Re $\zeta > -a$, and this comes from the Wiener-Hopf procedure used to solve this problem.

In order to obtain the stress field surrounding the stationary crack-tip, we need to perform the inverse transforms of those transformed stress components which can be obtained from the expressions in equation (3.3.5). However, from the constitutive relation (3.2.2), it can be seen that the stress components are related to the second derivatives of the two displacement potentials, $\phi^{(\mathrm{B})}(x_1, x_2, t)$ and $\psi^{(\mathrm{B})}(x_1, x_2, t)$. Let $\Phi^{(\mathrm{B})}_{\alpha\beta}(\zeta, x_2, s)$ and $\Psi^{(\mathrm{B})}_{\alpha\beta}(\zeta, x_2, s)$ be the transforms of $\phi^{(\mathrm{B})}_{,\alpha\beta}(x_1, x_2, t)$ and $\psi^{(\mathrm{B})}_{,\alpha\beta}(x_1, x_2, t)$, respectively. Then, we can write that

$$\left.\begin{aligned} \Phi^{(\mathrm{B})}_{\alpha\beta}(\zeta, x_2, s) &= \frac{\sigma^*}{\mu} \cdot \frac{P^{(\mathrm{B})}_{\alpha\beta}(\zeta)}{s^2} e^{-s\alpha^{(\mathrm{B})}(\zeta)x_2} \\ \Psi^{(\mathrm{B})}_{\alpha\beta}(\zeta, x_2, s) &= \frac{\sigma^*}{\mu} \cdot \frac{Q^{(\mathrm{B})}_{\alpha\beta}(\zeta)}{s^2} e^{-s\beta^{(\mathrm{B})}(\zeta)x_2} \end{aligned}\right\}, \qquad \forall\, x_2 \in (0, \infty)\,, \tag{3.3.7}$$

where

$$\left.\begin{aligned} P^{(\mathrm{B})}_{11}(\zeta) &= \zeta^2 P^{(\mathrm{B})}(\zeta) \\ P^{(\mathrm{B})}_{22}(\zeta) &= \left(a^2 - \zeta^2\right) P^{(\mathrm{B})}(\zeta) \\ P^{(\mathrm{B})}_{12}(\zeta) &= -\zeta\alpha^{(\mathrm{B})}(\zeta) P^{(\mathrm{B})}(\zeta) \end{aligned}\right\}, \qquad \left.\begin{aligned} Q^{(\mathrm{B})}_{11}(\zeta) &= \zeta^2 Q^{(\mathrm{B})}(\zeta) \\ Q^{(\mathrm{B})}_{22}(\zeta) &= \left(b^2 - \zeta^2\right) Q^{(\mathrm{B})}(\zeta) \\ Q^{(\mathrm{B})}_{12}(\zeta) &= -\zeta\beta^{(\mathrm{B})}(\zeta) Q^{(\mathrm{B})}(\zeta) \end{aligned}\right\}.$$

Several observations can be made at this point: i) $P^{(\mathrm{B})}_{11}(\zeta)$ and $P^{(\mathrm{B})}_{12}(\zeta)$ are analytic in the strip $-a <$ Re $\zeta < a$; $P^{(\mathrm{B})}_{22}(\zeta)$ is analytic in the strip $-a <$ Re $\zeta < a$, but has a simple pole at $\zeta = 0$; ii) $Q^{(\mathrm{B})}_{\alpha\beta}(\zeta)$ are analytic the strip $-b <$ Re $\zeta < a$, where $\alpha, \beta \in \{1, 2\}$; iii) All singularities and branch cuts lie along the real axis.

By using the Cagniard-de Hoop technique to the transformed second derivatives in equation (3.3.7) and by using the above observations for the regions of analyticity for each function, the second derivatives of the displacement potential associated with

the longitudinal wave, $\phi^{(\mathrm{B})}(x_1, x_2, t)$, can be expressed as (see Appendix)

$$\left.\begin{aligned}
\phi^{(\mathrm{B})}_{,11}(x_1,x_2,t) &= \frac{\sigma^*}{\pi\mu}\int_{ar}^{t} \mathrm{Im}\left\{P_{11}^{(\mathrm{B})}(\zeta_l^{(\mathrm{B})})\frac{\partial\zeta_l^{(\mathrm{B})}}{\partial\tau}\right\}\mathrm{d}\tau\cdot H(t-ar)\\
\phi^{(\mathrm{B})}_{,22}(x_1,x_2,t) &= \frac{\sigma^*}{\pi\mu}\int_{-\omega_l^*}^{x_1} \mathrm{Im}\left\{\zeta_l^{(\mathrm{B})*}P_{22}^{(\mathrm{B})}(\zeta_l^{(\mathrm{B})*})\frac{\partial\zeta_l^{(\mathrm{B})*}}{\partial t}\right\}\mathrm{d}x_1^*\cdot H(t-ar)\\
\phi^{(\mathrm{B})}_{,12}(x_1,x_2,t) &= \frac{\sigma^*}{\pi\mu}\int_{ar}^{t} \mathrm{Im}\left\{P_{12}^{(\mathrm{B})}(\zeta_l^{(\mathrm{B})})\frac{\partial\zeta_l^{(\mathrm{B})}}{\partial\tau}\right\}\mathrm{d}\tau\cdot H(t-ar)
\end{aligned}\right\}, \qquad (3.3.8)$$

where

$$\zeta_l^{(\mathrm{B})}(x_1,x_2,t) = -\frac{t}{r}\cos\theta + i\sqrt{\frac{t^2}{r^2}-a^2}\sin\theta\ , \qquad (3.3.9)$$

and (r,θ) are the polar coordinates centered at the crack-tip. $\zeta_l^{(\mathrm{B})*}(x_1^*, x_2, t)$ has the same form as that in equation (3.3.9) except that x_1 should be replaced by x_1^*. Also

$$\omega_l^* = \left(\frac{t^2}{a^2} - x_2^2\right)^{1/2}\ .$$

Similarly, the second derivatives of the displacement potential associated with the transverse wave, $\psi^{(\mathrm{B})}(x_1, x_2, t)$, can be expressed as (see Appendix B)

$$\left.\begin{aligned}
\psi^{(\mathrm{B})}_{,\alpha\beta}(x_1,x_2,t) = \frac{\sigma^*}{\pi\mu}\Bigg\{&\int_{br}^{t}\mathrm{Im}\left[Q_{\alpha\beta}^{(\mathrm{B})}(\zeta_s^{(\mathrm{B})})\frac{\partial\zeta_s^{(\mathrm{B})}}{\partial\tau}\right]\mathrm{d}\tau\cdot H(t-br)\\
&+\int_{a}^{\lambda^{(\mathrm{B})}(\theta)}\mathrm{Im}\left[Q_{\alpha\beta}^{(\mathrm{B})+}(\eta)\right]h^{(\mathrm{B})}(\eta)\mathrm{d}\eta\cdot H(\theta-\theta_{\mathrm{H}}^{(\mathrm{B})})\Bigg\}
\end{aligned}\right., \qquad (3.3.10)$$

where $\alpha, \beta \in \{1, 2\}$, and

$$\zeta_s^{(\mathrm{B})}(x_1,x_2,t) = -\frac{t}{r}\cos\theta + i\sqrt{\frac{t^2}{r^2}-b^2}\sin\theta\ . \qquad (3.3.11)$$

In addition, in equation (3.3.10), $\lambda^{(\mathrm{B})}(\theta) = -b\cos\theta$, and $\theta_{\mathrm{H}}^{(\mathrm{B})} = \pi - \cos^{-1}(a/b)$. Also,

$$h^{(\mathrm{B})}(\eta) = H\left(t - [\beta^{(\mathrm{B})}(\eta)x_2 - \eta x_1]\right)\ , \qquad a < \eta \le \lambda^{(\mathrm{B})}(\theta)\ .$$

It should be noted that the second part of the right-hand side in equation (3.3.10) provides information inside the head wave region.

By substituting equations (3.3.8) and (3.3.10) into the constitutive relation (3.2.2), we can get the stress field surrounding the stationary crack-tip for problem B. As an

input to problem C, we need to know the normal traction $\sigma_+^{(B)}(x_1,t)$, ahead of the stationary crack-tip in problem B. It can be shown that (Freund, 1990)

$$\sigma_+^{(B)}(x_1,t)=\frac{\sigma^*}{\pi}\left\{\int_{ax_1}^{t}\mathrm{Im}\left[\frac{F_+^{(B)}(0)}{F_+^{(B)+}(-\eta/x_1)}\right]\frac{\mathrm{d}\eta}{\eta}\right\}\cdot H(t-ax_1)\ , \tag{3.3.12}$$

or $\sigma_+^{(B)}(x_1,t)$ may also be expressed as

$$p(u)=\frac{\sigma^*}{\pi}\left\{\int_{a}^{1/u}\mathrm{Im}\left[\frac{F_+^{(B)}(0)}{F_+^{(B)+}(-\omega)}\right]\frac{\mathrm{d}\omega}{\omega}\right\}\cdot H\left(\frac{1}{u}-a\right)\ , \tag{3.3.13}$$

where $u=x_1/t$. It must be pointed out that the normal traction ahead of the stationary crack-tip, $\sigma_+^{(B)}(x_1,t)$, or $p(x_1/t)$, is a homogeneous function of x_1 and t of degree zero. Finally, the dynamic stress intensity factor at the stationary crack-tip for problem B is

$$K_I^{d(B)}(t)=\frac{2\sigma^*}{1-\nu}\sqrt{\frac{(1-2\nu)c_l t}{\pi}}\ . \tag{3.3.14}$$

3.3.3 Problem C: Moving crack with varying traction applied on its new surface

In this problem, we study the semi-infinite crack configuration considered in problem B. At time $t=\tau$, the crack starts to extend with a constant speed v. At the same time, a compressive normal traction of magnitude of $p(x_1/t)$, given in (3.3.13), is applied on the newly created crack faces, $0<x_1<v(t-\tau)$. Since the traction distribution (3.3.13) has the property of homogeneity, any fixed stress level in the scattered field radiates out along the x_1-axis at constant speed. As a result of this observation, the solution for problem C can be further generated by the so-called fundamental solution (Freund, 1990).

Consider the region $\mathcal{R}$ and a semi-infinite crack lying along the entire negative x_1–axis in the Cartesian coordinate system, (x_1,x_2). As time $t<0$, the body is stress free and at rest everywhere. At $t=0$, a pair of concentrated forces $p(t)$, of the form,

$$p(t)=p_0+p_1 t\ ,$$

where p_0 and p_1 are constants, is applied at the crack-tip and tends to open the crack. At the same time, the crack begins to propagate with a constant speed v. Meanwhile, the concentrated force $p(t)$ also propagates with a constant velocity $u < v$ toward the moving crack-tip. Let $\phi^{(\mathrm{F})}(x_1, x_2, t)$ and $\psi^{(\mathrm{F})}(x_1, x_2, t)$ be the two displacement potentials for the fundamental problem. Then, $\phi^{(\mathrm{F})}(x_1, x_2, t)$ and $\psi^{(\mathrm{F})}(x_1, x_2, t)$ will satisfy the equation of motion (3.2.3) and the same initial conditions (3.3.3). The boundary conditions are

$$\left.\begin{aligned} \sigma_{22}^{(\mathrm{F})}(x_1, 0^+, t) &= -\left(p_0 + p_1 t\right)\delta(x_1 - ut)H(t)\ , && -\infty < x_1 \le vt \\ \sigma_{12}^{(\mathrm{F})}(x_1, 0^+, t) &= 0\ , && -\infty < x_1 < \infty \\ u_2^{(\mathrm{F})}(x_1, 0^+, t) &= 0\ , && vt < x_1 < \infty \end{aligned}\right\}, \quad \forall\, t > 0, \tag{3.3.15}$$

where $\delta(\cdot)$ is the Dirac delta function. By defining the moving coordinates (ξ_1, ξ_2) through $\xi_1 = x_1 - vt$, $\xi_2 = x_2$, and applying the Laplace transforms with respect to t and ξ_1, the solutions in the transformed plane will be

$$\left.\begin{aligned} \Phi^{(\mathrm{F})}(\zeta, \xi_2, s) &= \frac{p_0}{\mu}\cdot\frac{P_0(\zeta)}{s^3}e^{-s\alpha(\zeta)\xi_2} - \frac{p_1}{\mu}\cdot\frac{P_1(\zeta)}{s^4}e^{-s\alpha(\zeta)\xi_2} \\ \Psi^{(\mathrm{F})}(\zeta, \xi_2, s) &= \frac{p_0}{\mu}\cdot\frac{Q_0(\zeta)}{s^3}e^{-s\beta(\zeta)\xi_2} - \frac{p_1}{\mu}\cdot\frac{Q_1(\zeta)}{s^4}e^{-s\beta(\zeta)\xi_2} \end{aligned}\right\}, \ \forall\, \xi_2 \in (0, \infty), \tag{3.3.16}$$

where

$$\left.\begin{aligned} P_0(\zeta) &= \frac{w\left\{\beta^2(\zeta) - \zeta^2\right\}}{(\zeta - w)R(\zeta)}\cdot\frac{F_+(w)}{F_+(\zeta)} \\ Q_0(\zeta) &= \frac{2w\zeta\alpha(\zeta)}{(\zeta - w)R(\zeta)}\cdot\frac{F_+(w)}{F_+(\zeta)} \end{aligned}\right\}, \quad \left.\begin{aligned} P_1(\zeta) &= \frac{w^2\left\{\beta^2(\zeta) - \zeta^2\right\}}{R(\zeta)F_+(\zeta)}\cdot\left[\frac{F_+(w)}{\zeta - w}\right]' \\ Q_1(\zeta) &= \frac{2w^2\zeta\alpha(\zeta)}{R(\zeta)F_+(\zeta)}\cdot\left[\frac{F_+(w)}{\zeta - w}\right]' \end{aligned}\right\}. \tag{3.3.17}$$

In the above expressions, prime denotes the derivative with respect to the argument w, where $w = 1/(v - u)$, and

$$\begin{aligned} R(\zeta) &= 4\zeta^2\alpha(\zeta)\beta(\zeta) + \left\{\beta^2(\zeta) - \zeta^2\right\}^2\ , \\ \alpha(\zeta) &= \left(a^2 - \zeta^2 + \frac{a^2\zeta^2}{h^2} - \frac{2a^2\zeta}{h}\right)^{1/2}\ , \end{aligned}$$

$$\beta(\zeta) = \left(b^2 - \zeta^2 + \frac{b^2\zeta^2}{h^2} - \frac{2b^2\zeta}{h}\right)^{1/2} ,$$

$$F_+(\zeta) = \frac{\alpha_+(\zeta)}{(c_- + \zeta)\, S_+(\zeta)} , \quad \alpha_+(\zeta) = \left\{a + \left(1 - \frac{a}{h}\right)\zeta\right\}^{1/2} ,$$

$$S_+(\zeta) = \exp\left\{-\frac{1}{\pi}\int_{a_-}^{b_-} \tan^{-1}\left[\frac{4\eta^2\beta(-\eta)|\alpha(-\eta)|}{[\beta^2(-\eta) - \eta^2]^2}\right]\frac{\mathrm{d}\eta}{\eta + \zeta}\right\} ,$$

in which $h = 1/v$. Also,

$$a_\pm = \frac{a}{1 \pm a/h} , \qquad b_\pm = \frac{b}{1 \pm b/h} , \qquad c_\pm = \frac{c}{1 \pm c/h} .$$

Similar to the procedure used in problem B, by defining

$$\left.\begin{aligned} &P_{11}^{(k)}(\zeta) = \zeta^2 P_k(\zeta) , \quad P_{22}^{(k)}(\zeta) = \alpha^2(\zeta) P_k(\zeta) , \quad P_{12}^{(k)}(\zeta) = -\zeta\alpha(\zeta) P_k(\zeta) \\ &Q_{11}^{(k)}(\zeta) = \zeta^2 Q_k(\zeta) , \quad Q_{22}^{(k)}(\zeta) = \beta^2(\zeta) Q_k(\zeta) , \quad Q_{12}^{(k)}(\zeta) = -\zeta\beta(\zeta) Q_k(\zeta) \end{aligned}\right\} ,$$

where $k \in \{0, 1\}$, the second derivatives of the displacement potential, $\phi^{(\mathrm{F})}(\xi_1, \xi_2, t)$, can be expressed as

$$\left.\begin{aligned} \phi^{(\mathrm{F})}_{,\alpha\beta}(\xi_1, \xi_2, t) &= \frac{p_0}{\pi\mu}\mathrm{Im}\left\{P_{\alpha\beta}^{(0)}(\zeta_l)\frac{\partial\zeta_l}{\partial t}\right\} \cdot H\left(t - \omega_l(r_l, \theta_l)\right) \\ &- \frac{p_1}{\pi\mu}\int_{\omega_l(r_l,\theta_l)}^{t} \mathrm{Im}\left\{P_{\alpha\beta}^{(1)}(\zeta_l)\frac{\partial\zeta_l}{\partial\tau}\right\}\mathrm{d}\tau \cdot H\left(t - \omega_l(r_l, \theta_l)\right) \end{aligned}\right\} , \quad (3.3.18)$$

where $\alpha, \beta \in \{1, 2\}$, and

$$\left.\begin{aligned} \zeta_l(\xi_1, \xi_2, t) &= -\left(\frac{t}{r_l} - \frac{a_- - a_+}{2}\cos\theta_l\right)\cos\theta_l - \frac{a_- - a_+}{2} \\ &+ i\left\{\left(\frac{t}{r_l} - \frac{a_- - a_+}{2}\cos\theta_l\right)^2 - \left(\frac{a_- + a_+}{2}\right)^2\right\}^{1/2}\sin\theta_l \\ \omega_l(r_l, \theta_l) &= r_l\left(\frac{a_- - a_+}{2}\cos\theta_l + \frac{a_- + a_+}{2}\right) \end{aligned}\right\} .$$

The second derivative of the displacement potential, $\psi^{(\mathrm{F})}(\xi_1, \xi_2, t)$, can be expressed

as

$$\left.\begin{aligned}\psi^{(\mathrm{F})}_{,\alpha\beta}(\xi_1,\xi_2,t) &= \frac{p_0}{\pi\mu}\left\{\mathrm{Im}\left[Q^{(0)}_{\alpha\beta}(\zeta_s)\frac{\partial\zeta_s}{\partial t}\right]\cdot H\left(t-\omega_s(r_s,\theta_s)\right)\right.\\ &+ \left.\int_{a_+}^{\lambda(\theta_s)}\left[\mathrm{Im}\left(Q^{(0)+}_{\alpha\beta}(\eta)\right)d(\eta)\right]\mathrm{d}\eta\cdot H\left(\theta_s-\theta_{\mathrm{H}}\right)\right\}\\ &- \frac{p_1}{\pi\mu}\left\{\int_{\omega_s(r_s,\theta_s)}^{t}\mathrm{Im}\left[Q^{(1)}_{\alpha\beta}(\zeta_s)\frac{\partial\zeta_s}{\partial\tau}\right]\mathrm{d}\tau\cdot H\left(t-\omega_s(r_s,\theta_s)\right)\right.\\ &+ \left.\int_{a_+}^{\lambda(\theta_s)}\left[\mathrm{Im}\left(Q^{(1)+}_{\alpha\beta}(\eta)\right)h(\eta)\right]\mathrm{d}\eta\cdot H\left(\theta_s-\theta_{\mathrm{H}}\right)\right\}\end{aligned}\right\}, \tag{3.3.19}$$

where $\alpha,\beta\in\{1,2\}$. In equation (3.3.19),

$$\left.\begin{aligned}\zeta_s(\xi_1,\xi_2,t) &= -\left(\frac{t}{r_s}-\frac{b_- - b_+}{2}\cos\theta_s\right)\cos\theta_s-\frac{b_- - b_+}{2}\\ &\quad + i\left\{\left(\frac{t}{r_s}-\frac{b_- - b_+}{2}\cos\theta_s\right)^2-\left(\frac{b_- + b_+}{2}\right)^2\right\}^{1/2}\sin\theta_s\\ \omega_s(r_s,\theta_s) &= r_s\left(\frac{b_- - b_+}{2}\cos\theta_s+\frac{b_- + b_+}{2}\right)\end{aligned}\right\},$$

and

$$\lambda(\theta_s)=-\left(\frac{b_- + b_+}{2}\cos\theta_s+\frac{b_- - b_+}{2}\right),\quad \theta_{\mathrm{H}}=\pi-\cos^{-1}\left(\frac{2a_+}{b_- + b_+}+\frac{b_- - b_+}{b_- + b_+}\right).$$

Also,

$$\left.\begin{aligned}d(\eta) &= \delta\left(t-[\beta(\eta)\xi_2-\eta\xi_1]\right)\\ h(\eta) &= H\left(t-[\beta(\eta)\xi_2-\eta\xi_1]\right)\end{aligned}\right\},\qquad a_+\le\eta\le\lambda(\theta_s).$$

In equations (3.3.18) and (3.3.19), $(r_{l,s},\theta_{l,s})$ are two scaled polar coordinate systems defined by

$$r_{l,s}=\left\{\xi_1^2+\alpha_{l,s}^2\xi_2^2\right\}^{1/2},\qquad \theta_{l,s}=\tan^{-1}\frac{\alpha_{l,s}\xi_2}{\xi_1},$$

where

$$\alpha_l=\left(1-\frac{a^2}{h^2}\right)^{1/2},\qquad \alpha_s=\left(1-\frac{b^2}{h^2}\right)^{1/2}.$$

The components of stress field for the fundamental problem can be obtained by using the constitutive relation (3.2.2).

Returning to problem C, let $q^{(\mathrm{F})}(\xi_1, \xi_2, t; w)$ be any element of the fundamental solution, such as the stress components, particle velocity, etc., and the dependence of the fundamental solution on the parameter w is made explicitly here. Following the analysis given by Freund (1973 and 1990), the corresponding element $q^{(\mathrm{C})}(\xi_1, \xi_2, t)$ for problem C will be given by

$$q^{(\mathrm{C})}(\xi_1, \xi_2, t) = \int_h^{h^*} q^{(\mathrm{F})}\left(\xi_1, \xi_2, \frac{\tau}{h}(h^* - w); w\right) \frac{p^*(w)}{w^2} \mathrm{d}w \ , \quad \forall\ (\xi_1, \xi_2) \in \overset{+}{\mathcal{R}} \ , \tag{3.3.20}$$

where $p^*(w) = p((vw - 1)/w)$. It should be pointed out that in equation (3.3.20), quantities p_0 and p_1 that appear in the fundamental solutions have been changed to $\tau w/h$ and 1, respectively. Finally, the dynamic stress intensity factor at the moving crack-tip in problem C is given by

$$K_I^{d(\mathrm{C})}(t) = 2\sigma^* k(v)\sqrt{\frac{2}{\pi}} \left\{ \frac{\sqrt{2c_l t(1-2\nu)}}{2(1-\nu)} - \sqrt{v(t-\tau)} \right\}, \quad \forall\ t > \tau \ , \tag{3.3.21}$$

where $k(v)$ is a universal function of the crack-tip speed given by

$$k(v) = \frac{1 - c/h}{S_+(h)\sqrt{1 - a/h}} \ . \tag{3.3.22}$$

3.3.4 Problem D: Moving crack with uniform pressure applied on its new surface

Similar to problem C, we study the semi-infinite crack configuration considered in problem B. At time $t = \tau$, the crack starts to extend with a constant speed v. However, at the same time, a uniform pressure of magnitude of σ^*, is applied on the newly created crack faces, $0 < x_1 < v(t - \tau)$. Let $\phi^{(\mathrm{D})}(x_1, x_2, t)$ and $\psi^{(\mathrm{D})}(x_1, x_2, t)$ be the displacement potentials of this problem. For analysis convenience, consider that the crack-tip starts to extend at $t = 0$ and obtain the displacement potentials for

this new problem, denoted as problem M. Therefore, $\phi^{(M)}(x_1, x_2, t)$ and $\psi^{(M)}(x_1, x_2, t)$ satisfy the equation of motion (3.2.3), and the boundary conditions are

$$\left.\begin{aligned} \sigma_{22}^{(M)}(x_1, 0^+, t) &= -\sigma^* H(x_1) H(vt - x_1) H(t) \ , && -\infty < x_1 \le vt \\ \sigma_{12}^{(M)}(x_1, 0^+, t) &= 0 \ , && -\infty < x_1 < \infty \\ u_2^{(M)}(x_1, 0^+, t) &= 0 \ , && vt < x_1 < \infty \end{aligned}\right\}, \quad \forall\, t > 0. \tag{3.3.23}$$

In the moving coordinate system (ξ_1, ξ_2), after the Laplace transforms are applied, the solutions are

$$\left.\begin{aligned} \Phi^{(M)}(\zeta, \xi_2, s) &= \frac{\sigma^*}{\mu} \cdot \frac{P^{(M)}(\zeta)}{s^4} e^{-s\alpha(\zeta)\xi_2} \\ \Psi^{(M)}(\zeta, \xi_2, s) &= \frac{\sigma^*}{\mu} \cdot \frac{Q^{(M)}(\zeta)}{s^4} e^{-s\beta(\zeta)\xi_2} \end{aligned}\right\}, \quad \forall\, \xi_2 \in (0, \infty), \tag{3.3.24}$$

where

$$P^{(M)}(\zeta) = \frac{\beta^2(\zeta) - \zeta^2}{(\zeta - h) R(\zeta)} \cdot \frac{F_+(h)}{F_+(\zeta)} \ , \qquad Q^{(M)}(\zeta) = \frac{2\zeta\alpha(\zeta)}{(\zeta - h) R(\zeta)} \cdot \frac{F_+(h)}{F_+(\zeta)} \ , \tag{3.3.25}$$

where all quantities that appear in the above expressions have been given in the solutions for problem C. By defining

$$\left.\begin{aligned} P_{11}^{(M)}(\zeta) &= \zeta^2 P^{(M)}(\zeta) \\ P_{22}^{(M)}(\zeta) &= \alpha^2(\zeta) P^{(M)}(\zeta) \\ P_{12}^{(M)}(\zeta) &= -\zeta\alpha(\zeta) P^{(M)}(\zeta) \end{aligned}\right\}, \qquad \left.\begin{aligned} Q_{11}^{(M)}(\zeta) &= \zeta^2 Q^{(M)}(\zeta) \\ Q_{22}^{(M)}(\zeta) &= \beta^2(\zeta) Q^{(M)}(\zeta) \\ Q_{12}^{(M)}(\zeta) &= -\zeta\beta(\zeta) Q^{(M)}(\zeta) \end{aligned}\right\},$$

the second derivatives of $\phi^{(M)}(\xi_1, \xi_2, t)$ and $\psi^{(M)}(\xi_1, \xi_2, t)$ will be

$$\left.\begin{aligned} \phi^{(M)}_{,\alpha\beta}(\xi_1, \xi_2, t) &= \frac{\sigma^*}{\pi\mu} \int_{\omega_l(r_l, \theta_l)}^{t} \mathrm{Im}\left\{ P_{\alpha\beta}^{(M)}(\zeta_l) \frac{\partial \zeta_l}{\partial \tau} \right\} \mathrm{d}\tau \cdot H\left(t - \omega_l(r_l, \theta_l)\right) \\ \psi^{(M)}_{,\alpha\beta}(\xi_1, \xi_2, t) &= \frac{\sigma^*}{\pi\mu} \left\{ \int_{\omega_s(r_s, \theta_s)}^{t} \mathrm{Im}\left[Q_{\alpha\beta}^{(M)}(\zeta_s) \frac{\partial \zeta_s}{\partial \tau} \right] \mathrm{d}\tau \cdot H\left(t - \omega_s(r_s, \theta_s)\right) \right. \\ &\quad + \left. \int_{a_+}^{\lambda(\theta_s)} \left[\mathrm{Im}\left(Q_{\alpha\beta}^{(M)+}(\eta) \right) h(\eta) \right] \mathrm{d}\eta \cdot H\left(\theta_s - \theta_{\mathrm{H}}\right) \right\} \end{aligned}\right\}. \tag{3.3.26}$$

For problem D, we can get

$$\phi^{(\mathrm{D})}_{,\alpha\beta}(\xi_1,\xi_2,t)=\phi^{(\mathrm{M})}_{,\alpha\beta}(\xi_1,\xi_2,t-\tau)\ ,\quad \psi^{(\mathrm{D})}_{,\alpha\beta}(\xi_1,\xi_2,t)=\psi^{(\mathrm{M})}_{,\alpha\beta}(\xi_1,\xi_2,t-\tau)\ . \tag{3.3.27}$$

The components of stress can be obtained from the constitutive relation (3.2.2). The dynamic stress intensity factor at the moving crack-tip in problem D, is given by

$$K_I^{d(\mathrm{D})}(t)=2\sigma^* k(v)\sqrt{\frac{2v(t-\tau)}{\pi}}\ ,\qquad t>\tau\ . \tag{3.3.28}$$

Up to this point, we have obtained the analytical full field solution for each problem. Returning to our original problem which corresponds to a planar longitudinal stress wave of constant amplitude σ^* which strikes a semi-infinite crack, and after some time τ, the crack extends at a constant speed v, we can construct the final solution. For $0<t\leq\tau$, the solution is given by the sum of problems A and B. For $t>\tau$, the solution is given by the sum of all four problems. Particularly, the dynamic stress intensity factors at the stationary and moving crack-tips are

$$K_I^d(t)=\begin{cases}\dfrac{2\sigma^*}{1-\nu}\sqrt{\dfrac{(1-2\nu)c_l t}{\pi}}\ , & \forall\ 0<t\leq\tau\ ,\\[2ex] \dfrac{2\sigma^* k(v)}{1-\nu}\sqrt{\dfrac{(1-2\nu)c_l t}{\pi}}\ , & \forall\ t>\tau\ .\end{cases} \tag{3.3.29}$$

It is clear from equation (3.3.29) that for an unbounded body under time-independent loading conditions, the dynamic stress intensity factor at the running crack-tip can be expressed as a universal function of instantaneous crack-tip speed multiplied by the equilibrium stress intensity factor for the given applied loading and the instantaneous amount of crack growth. It should be pointed out that the sum of problems B and C will give the solution for the problem studied by Ravi-Chandar and Knauss (1982) and analyzed by Ma and Freund (1986). However, since the problem is no longer self-similar, the dynamic stress intensity factor at the moving crack-tip corresponding to this problem will not have the property stated above.

3.4 Higher order transient asymptotic representation of the elastodynamic field surrounding the moving crack-tip

In the previous section, we have derived the full field analytical solution for the problem stated in Section 3.2. This solution has considered the transient nature of the problem. As one can see that the expressions for the solution are complicated. In order to use the solution in comparison with experimental observations, one is interested in the asymptotic structure of this elastodynamic field, or the field very close to the moving crack-tip. Recently, Freund and Rosakis (1992) and Liu and Rosakis (1992) have developed the structure of the higher order transient asymptotic representation for the stress field around a transiently extending crack-tip in homogeneous and isotropic linear elastic materials. Their asymptotic representation involves coefficients which are complicated functions of time that cannot be completely determined by the asymptotic analysis. The crack problem under consideration here is highly transient. As such it is a good candidate to be used for obtaining the coefficients of the higher order transient asymptotic representation of the elastodynamic field surrounding the moving crack-tip. A comparison of the transient expansion with the actual full field solution will give us an indication of how well this transient asymptotic representation describes the actual field.

To obtain the asymptotic expansion of the elastodynamic field derived in the previous section, we consider the quantity $\phi_{,\alpha\alpha}(\xi_1, \xi_2, t)$. For problem A, as $t > 0$,

$$\phi^{(\mathrm{A})}_{,\alpha\alpha}(\xi_1, 0^+, t) = \frac{\sigma^*}{\mu} \cdot \frac{1-2\nu}{2(1-\nu)} . \tag{3.4.1}$$

In problem B, for finite $t > \tau$, by expanding the quantity $\phi^{(\mathrm{B})}_{,\alpha\alpha}(x_1, 0^+, t)$ into a power series of ξ_1 where $x_1 = \xi_1 + v(t-\tau)$, we get

$$\phi^{(\mathrm{B})}_{,11}(\xi_1 + v(t-\tau), 0^+, t) = \frac{\sigma^*}{\mu} \cdot \frac{1}{\pi\sqrt{1-\nu}} \Omega^{(\mathrm{B})}_1(t) + O(\xi_1), \quad \text{as } \xi_1 \to 0^+, \tag{3.4.2}$$

where

$$\left.\begin{aligned}\Omega_1^{(\mathrm{B})}(t) &= \int_a^b \frac{a^2(\eta-c)(b^2-2\eta^2)^3 S_+^{(\mathrm{B})}(-\eta)}{\eta\sqrt{b(\eta-a)}\,\{(b^2-2\eta^2)^4+16\eta^4(\eta^2-a^2)(b^2-\eta^2)\}}\mathrm{d}\eta \\ &+ \int_b^{\frac{ht}{t-\tau}} \frac{a^2(\eta-c)(b^2-2\eta^2)S_+^{(\mathrm{B})}(-\eta)}{\eta\sqrt{b(\eta-a)}\left\{(b^2-2\eta^2)^2-4\eta^2\sqrt{\eta^2-a^2}\sqrt{\eta^2-b^2}\right\}}\mathrm{d}\eta\end{aligned}\right\},$$

and the function $S_+^{(\mathrm{B})}(\zeta)$ has been defined in Section 3.3.2.

For the fundamental problem, it can be shown that

$$\left.\begin{aligned}\phi_{,\alpha\alpha}^{(\mathrm{F})}(\xi_1,0^+,t) &= \frac{(1-\alpha_l^2)(1+\alpha_s^2)}{\mu D(v)}\left\{\frac{K_I^{d(\mathrm{F})}(t;w)}{\sqrt{2\pi\xi_1}}\right. \\ &-\frac{1}{\pi}\sqrt{\frac{a_-}{a}}\left[\left(\omega_0(v)+\frac{w}{h}\right)\left(p_0\frac{hwF_+(w)}{t^{3/2}}+2p_1\frac{hw^2F_+'(w)}{t^{1/2}}\right)\right. \\ &\left.\left.+2p_1\frac{w^2F_+(w)}{t^{1/2}}\right]\xi_1^{1/2}+O(\xi_1^{3/2})\right\}\cdot H(t-a_-\xi_1)\end{aligned}\right\},\quad \text{as } \xi_1\to 0^+ ,$$

(3.4.3)

where

$$\omega_0(v)=\frac{c_-}{h}-\frac{a_-}{2h}-\frac{4\alpha_s^2}{1+\alpha_s^2}+R_0(v)+S_0(v) ,$$

and

$$\left.\begin{aligned}R_0(v) &= \frac{4}{D(v)}\left\{\left(1-\alpha_s^4\right)-\frac{\alpha_l^2+\alpha_s^2-2\alpha_l^2\alpha_s^2}{\alpha_l\alpha_s}\right\} \\ S_0(v) &= -\frac{1}{\pi h}\int_{a_-}^{b_-}\tan^{-1}\left[\frac{4\eta^2\beta(-\eta)|\alpha(-\eta)|}{[\beta^2(-\eta)-\eta^2]^2}\right]\mathrm{d}\eta \\ D(v) &= 4\alpha_l\alpha_s-\left(1+\alpha_s^2\right)^2\end{aligned}\right\}.$$

From this result, as $t>\tau$, we can get the corresponding expansion for problem C by using relation (3.3.20). After some manipulations and using the property of the Heaviside function in (3.4.3), it can be shown that

$$\left.\begin{aligned}\phi_{,\alpha\alpha}^{(\mathrm{C})}(\xi_1,0^+,t) &= \frac{(1-\alpha_l^2)(1+\alpha_s^2)}{D(v)}\cdot\frac{K_I^{d(\mathrm{C})}(t)}{\mu\sqrt{2\pi\xi_1}} \\ &+\frac{\sigma^*}{\mu}\cdot\frac{2(1-\alpha_l^2)(1+\alpha_s^2)}{D(v)}\cdot\sqrt{\frac{h}{b}}\cdot\frac{k(v)\Omega_2^{(\mathrm{C})}(t)}{\pi}\sqrt{\frac{\xi_1}{c_s\tau}}+O(\xi_1^{3/2})\end{aligned}\right\},\quad \text{as } \xi_1\to 0^+,$$

(3.4.4)

where $K_I^{d(\mathrm{C})}(t)$ has been given in equation (3.3.21) and

$$\Omega_2^{(\mathrm{C})}(t) = \frac{\sqrt{2(1-2\nu)}}{2(1-\nu)}\sqrt{\frac{h}{a}}\cdot\frac{\omega_0(v)}{\sqrt{t/\tau}} - \frac{\omega_0(v)+1}{\sqrt{t/\tau-1}}\,.$$

For problem D, it can be shown that as $t > \tau$,

$$\left.\begin{aligned}\phi_{,\alpha\alpha}^{(\mathrm{D})}(\xi_1,0^+,t) &= \frac{(1-\alpha_l^2)(1+\alpha_s^2)}{D(v)}\cdot\frac{K_I^{d(\mathrm{D})}(t)}{\mu\sqrt{2\pi\xi_1}} \\ &+\frac{\sigma^*}{\mu}\cdot\frac{2(1-\alpha_l^2)(1+\alpha_s^2)}{D(v)}\cdot\sqrt{\frac{h}{b}}\cdot\frac{k(v)\Omega_2^{(\mathrm{D})}(t)}{\pi}\sqrt{\frac{\xi_1}{c_s\tau}}+O(\xi_1^{3/2})\end{aligned}\right\},\quad \text{as } \xi_1\to 0^+, \tag{3.4.5}$$

where $K_I^{d(\mathrm{D})}(t)$ has been given in equation (3.3.28) and

$$\Omega_2^{(\mathrm{D})}(t) = \frac{\omega_0(v)+1}{\sqrt{t/\tau-1}}\,.$$

Finally, by superposing the above asymptotic expressions for the four constituent problems, the asymptotic representation of the quantity $\phi_{,\alpha\alpha}(\xi_1,0^+,t)$ of our original problem near the extending crack-tip is

$$\left.\begin{aligned}\phi_{,\alpha\alpha}(\xi_1,0^+,t) &= \frac{(1-\alpha_l^2)(1+\alpha_s^2)}{D(v)}\cdot\frac{K_I^d(t)}{\mu\sqrt{2\pi\xi_1}}+\frac{\sigma^*}{\mu}\Omega_1(t) \\ &+\frac{\sigma^*}{\mu}\cdot\frac{2(1-\alpha_l^2)(1+\alpha_s^2)}{D(v)}\cdot\sqrt{\frac{h}{b}}\cdot\frac{k(v)\Omega_2(t)}{\pi}\sqrt{\frac{\xi_1}{c_s\tau}}+O(\xi_1^{3/2})\end{aligned}\right\},\quad \text{as } \xi_1\to 0^+, \tag{3.4.6}$$

where $K_I^d(t)$ has been given in equation (3.3.29) and

$$\left.\begin{aligned}\Omega_1(t) &= \frac{1-2\nu}{2(1-\nu)}+\frac{1}{\pi\sqrt{1-\nu}}\Omega_1^{(\mathrm{B})}(t) \\ \Omega_2(t) &= \frac{\sqrt{2(1-2\nu)}}{2(1-\nu)}\sqrt{\frac{h}{a}}\cdot\frac{\omega_0(v)}{\sqrt{t/\tau}}\end{aligned}\right\}.$$

For a transiently propagating mode-I crack in a homogeneous, isotropic, linearly elastic material, Freund and Rosakis (1992) have provided the higher order transient

asymptotic representation for the first stress invariant. By using the notation of Liu and Rosakis (1992), for a mode-I crack growing with a constant speed v, we have

$$\left.\begin{aligned}\phi_{,\alpha\alpha}(\xi_1,0^+,t) &= -\frac{3(1-\alpha_l^2)(1+\alpha_s^2)}{4\mu D(v)}A_0(t)\xi_1^{-1/2}\\ &+\frac{4\alpha_s(1-\alpha_l^2)}{\mu D(v)}A_1(t)+\left\{-\frac{15(1-\alpha_l^2)(1+\alpha_s^2)}{4\mu D(v)}A_2(t)\right.\\ &+\left[\frac{(1-\alpha_l^2)(1+\alpha_s^2)m_l}{D(v)}+\frac{1+\alpha_l^2}{2}\right]D_l^1\{A_0(t)\}\\ &\left.-\frac{2\alpha_s(1-\alpha_l^2)m_s}{D(v)}D_s^1\{A_0(t)\}\right\}\xi_1^{1/2}+O(\xi_1^{3/2})\end{aligned}\right\},\quad \text{as } \xi_1\to 0^+, \qquad (3.4.7)$$

where

$$\left.\begin{aligned}D_l^1\{A_0(t)\} &= \frac{3v(1+\alpha_s^2)}{\mu\alpha_l^2c_l^2D(v)}\dot{A}_0(t)\\ D_s^1\{A_0(t)\} &= -\frac{6v\alpha_l}{\mu\alpha_s^2c_s^2D(v)}\dot{A}_0(t)\end{aligned}\right\},\qquad \left.\begin{aligned}m_l &= \frac{1}{2}\left\{\left(1-\alpha_s^2\right)-\frac{2\left(\alpha_l^2-\alpha_s^2\right)}{1-\alpha_l^2}\right\}\\ m_s &= \frac{1}{2}\left(1-\alpha_s^2\right)\end{aligned}\right\}.$$

In equation (3.4.7), $A_0(t)$, $A_1(t)$, and $A_2(t)$ are undetermined functions of time. They cannot be determined by the asymptotic analysis itself. However, for the specific problem at hand, these undetermined functions of time can be obtained by comparing equations (3.4.6) and (3.4.7). This comparison yields:

$$\left.\begin{aligned}A_0(t) &= -\frac{\sigma^*\sqrt{c_s\tau}}{\pi}\cdot\frac{\sqrt{2(1-2\nu)}}{2(1-\nu)}\cdot\frac{8k(v)}{3}\sqrt{\frac{b}{a}}\sqrt{\frac{t}{\tau}}\\ A_1(t) &= \sigma^*\cdot\frac{D(v)\Omega_1(t)}{4\alpha_s(1-\alpha_l^2)}\\ A_2(t) &= -\frac{\sigma^*}{\pi\sqrt{c_s\tau}}\cdot\frac{\sqrt{2(1-2\nu)}}{2(1-\nu)}\cdot\frac{k_2(v)}{\sqrt{t/\tau}}\end{aligned}\right\},\qquad \forall\, t>\tau\,, \qquad (3.4.8)$$

where

$$k_2(v)=\frac{8}{15}\left\{\frac{2(1-\alpha_l^2)(1+\alpha_s^2)m_l}{\alpha_l^2D(v)}+\frac{8\alpha_l(1-\alpha_s^2)m_s}{\alpha_s(1+\alpha_s^2)D(v)}+\frac{1+\alpha_l^2}{\alpha_l^2}+\omega_0(v)\right\}\frac{hk(v)}{\sqrt{ab}}\,.$$

The variation of the dynamic stress intensity factor $K_I^d(t)$ with time t is plotted in FIGURE 3.3 for different crack-tip speeds. In this figure, the dynamic stress intensity

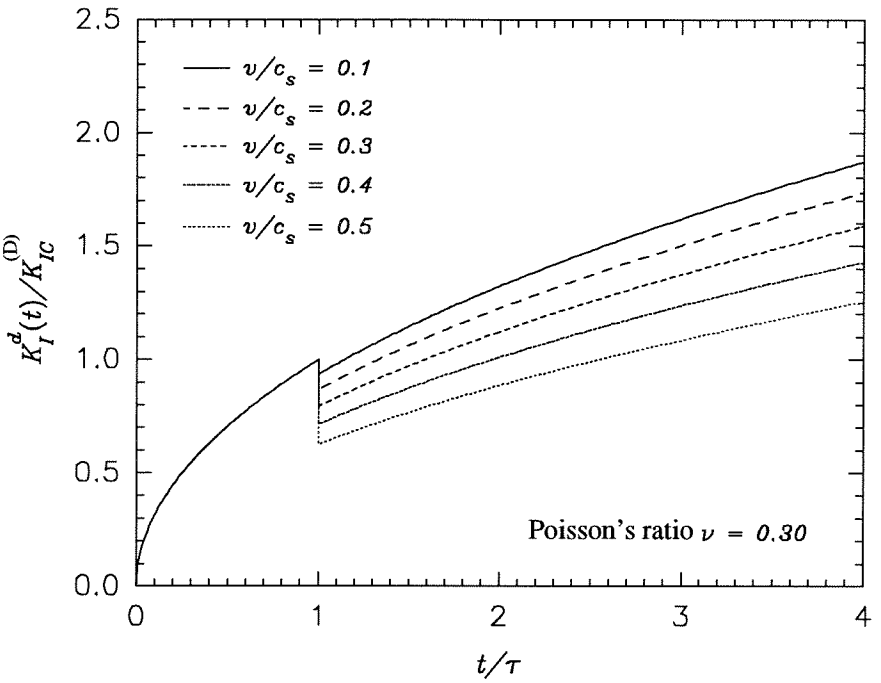

Figure 3.3: The dynamic stress intensity factor history for the stationary and propagating crack under stress wave loading conditions.

factor is normalized by the critical value of the stress intensity factor at which the stationary crack begins to extend, and the time t is normalized by the delay time τ. These numerical results are obtained by setting the Poisson's ratio $\nu = 0.3$. Before crack initiation, the dynamic stress intensity factor is a monotonic function of time. After crack initiation, the dynamic stress intensity factor monotonically increases with time as well. Although the crack-tip speed is constant, the problem we studied here is characterized as transient, because as the crack starts to grow, the time derivative of the dynamic stress intensity factor is not zero which is contrast with the steady state situation. Notice that in FIGURE 3.3, at the time of crack initiation, there is a sudden drop in the value of the dynamic stress intensity factor. This is due to the release of deformation energy by the formation of new crack surfaces associated with crack extension. In addition, the time histories of the coefficients in the higher order transient asymptotic representation of a propagating crack, $A_1(t)$ and $A_2(t)$, are presented in FIGURES 3.4 and 3.5 for different crack-tip speeds. Once again, their

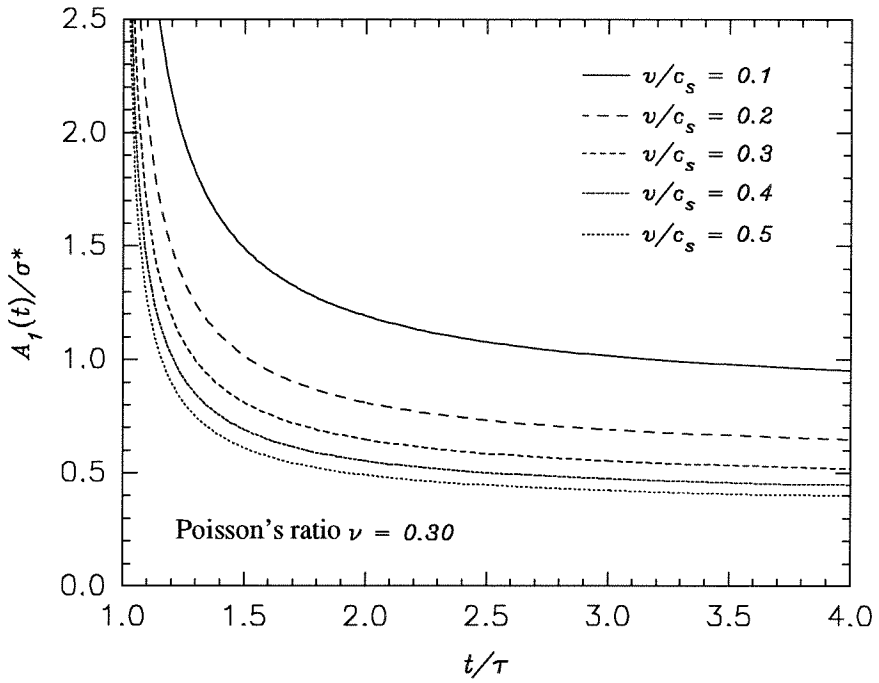

Figure 3.4: Time history of the coefficient $A_1(t)$ in the higher order transient asymptotic expansion for the moving crack under stress wave loading conditions.

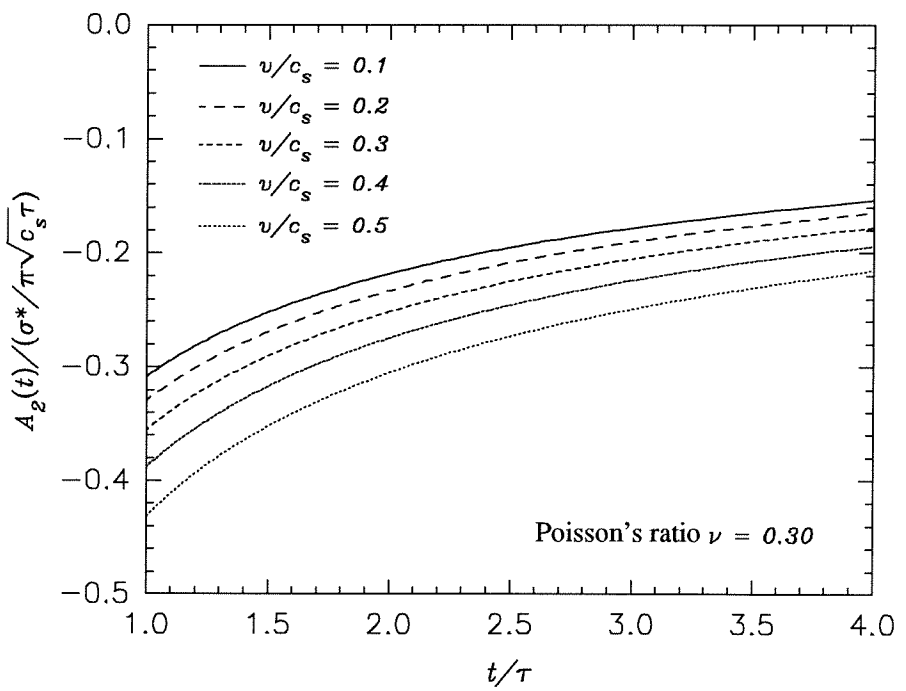

Figure 3.5: Time history of the coefficient $A_2(t)$ in the higher order transient asymptotic expansion for the moving crack under stress wave loading conditions.

time derivatives are not zero due to the transient nature of the problem.

3.5 An observation of the normal traction ahead of the moving crack-tip

In previous sections, we have obtained the complete full field solution for the stresses for the problem described in Section 2. We also obtained the coefficients $A_1(t)$ and $A_2(t)$ of the higher order transient asymptotic expansion. In order to examine whether the full field transient field is representable by either a K_I^d-dominant field or a higher order transient asymptotic field, we will investigate the normal traction ahead of the propagating crack-tip. In other words, we want to investigate the region of dominance of the lowest order and the higher order asymptotic solutions.

By using the analytical results given in Section 3.3 regarding the stresses surrounding the moving crack-tip, the normal traction ahead of the crack-tip, $\sigma_+(\xi_1, t)$ can be calculated from the full field solution. Meanwhile, the normal traction can also be represented by its asymptotic form (up to three terms) as

$$\sigma_+^{(\mathrm{A})}(\xi_1, t) = \frac{K_I^d(t)}{\sqrt{2\pi}}\xi_1^{-1/2} - \frac{15}{4}A_2(t)\xi_1^{1/2} + O(\xi_1) \ , \quad \text{as } \xi_1 \to 0 \ , \tag{3.5.1}$$

where the dynamic stress intensity factor $K_I^d(t)$ and the higher order coefficient $A_2(t)$ have been given in the last section. Here, we have two choices for the asymptotic representation. In regions near the crack-tip where the field is *indeed* K_I^d-dominant, the first term on the right-hand side of equation (3.5.1) will adequately describe the field. Otherwise higher order terms should be included in order to deal with the lack of K_I^d-dominance.

In FIGURE 3.6, the distribution of the normal traction ahead of the moving crack-tip is shown at different instants of time. It is calculated from the full field analytical solutions presented in previous sections. Here, we have chosen that the Poisson's ratio

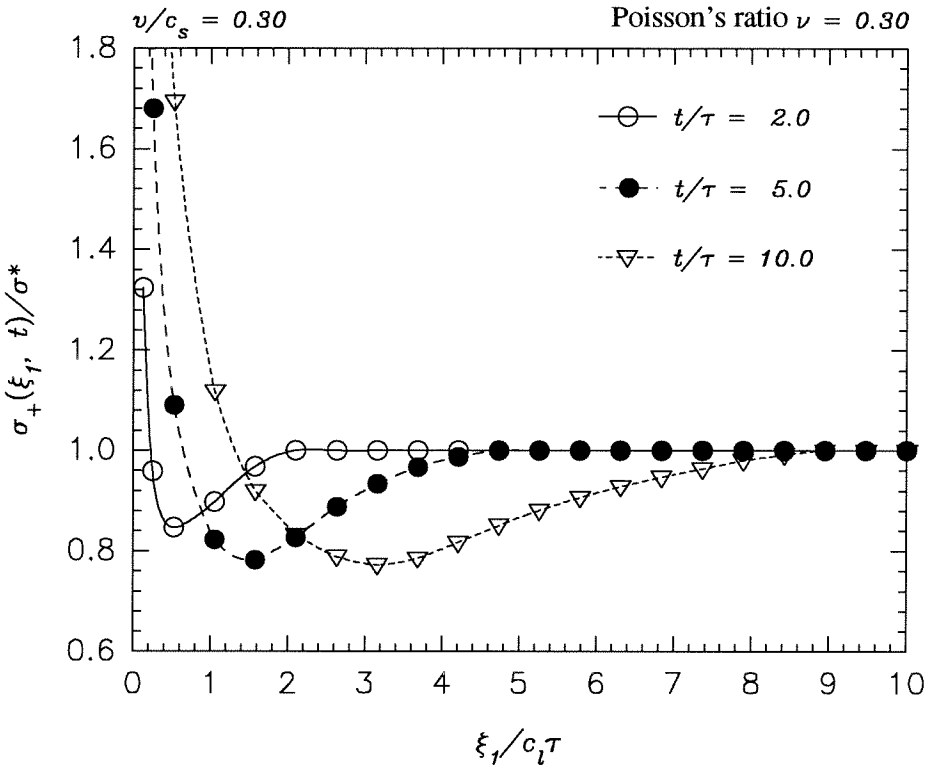

Figure 3.6: Distribution of normal traction ahead of the moving crack-tip at different instants of time.

$\nu = 0.3$ and the crack-tip speed $v = 0.3c_s$.

Quantitative comparisons of the near tip transient field with either the K_I^d-dominant field or the higher order transient asymptotic field (three term expansion) are given in FIGURES 3.7 and 3.8. In both figures, the normal traction ahead of the moving crack-tip calculated from the analytical result is normalized by its asymptotic representation. The Poisson's ratio is chosen to be 0.3 and the crack-tip speed v is set to be equal to $0.3c_s$. In FIGURES 3.7, the variation of the ratio $\sigma_+(\xi_1, t)/\sigma_+^{(A)}(\xi_1, t)$ with respect to the nondimensional parameter $\xi_1/c_l\tau$ which represents the distance from the moving crack-tip, is presented. Results for different instants of time after the crack initiation are also presented in this figure. The hollow circles are the value obtained by using the K_I^d-dominant representation, while the solid ones are those obtained by using the higher order transient representation as the asymptotic description (3.5.1).

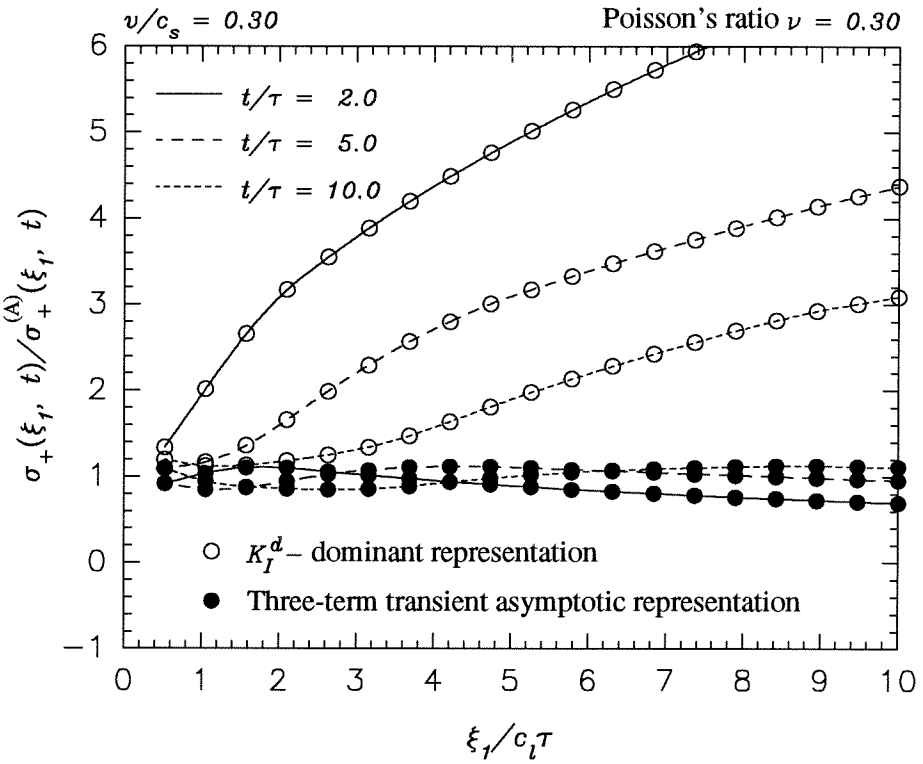

Figure 3.7: Comparison of the K_I^d-dominant and the higher order transient asymptotic distributions of normal traction ahead of the moving crack-tip at different instant of time after crack initiation.

To adequately describe the near tip field, the ratio $\sigma_+(\xi_1, t)/\sigma_+^{(A)}(\xi_1, t)$ should be close to 1. However, from FIGURES 3.7, we can see that the K_I^d-dominant field deviates substantially from the actual field even when the observation position is at a small distance away from the crack-tip. For the establishment of the fully K_I^d-dominant field near the crack-tip, a rather long time is needed. For example, at the position $\xi_1 = 2c_l\tau$, the time for the K_I^d-dominant field to be established is about $t = 10\tau$. However, the higher order transient asymptotic representation can be seen to approximate the near tip field much closer than the K_I^d-dominant field. Here, even at short times after crack initiation, say $t = 2\tau$, and within a distance $\xi_1 \leq 6c_l\tau$, the result obtained from the higher order transient asymptotic field is about 90/observation can be made in FIGURE 3.8. Here, the variation of the ratio $\sigma_+(\xi_1, t)/\sigma_+^{(A)}(\xi_1, t)$ is plotted against the nondimensional time t/τ for different positions ahead of the moving crack-tip. In this

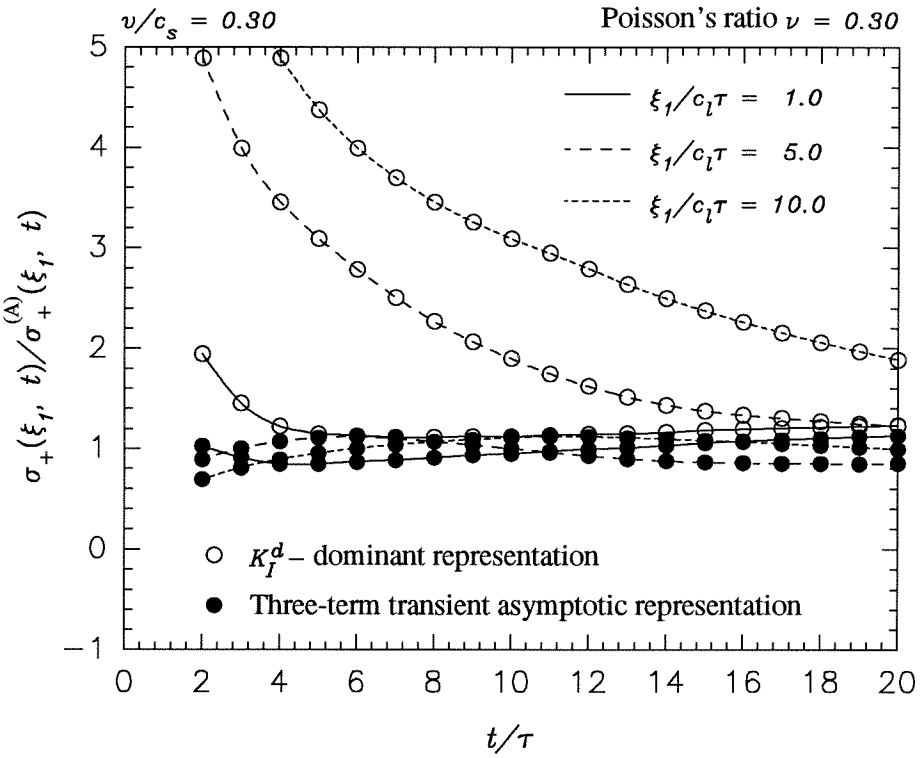

Figure 3.8: Comparison of the time histories of the K_I^d-dominant and the higher order transient asymptotic representation of normal traction ahead of the moving crack-tip at different distances from the crack-tip.

figure, attention is focused on a moving point which is at a fixed distance relative to the crack-tip. The time required for the K_I^d-dominant field to be established is then calculated. Once again, long times are required for the K_I^d-dominant field to approach the actual field, while at a fixed position relative to the crack-tip the field is well described by the higher order transient representation even at times very close to the crack initiation. Based on these observations, we conclude that conditions of K_I^d-dominance exist either extremely close to the crack-tip or are eventually established at long times after crack initiation. However, the higher order transient asymptotic representation is more successful in describing the actual field even at times close to the event of crack initiation or at distances relatively far away from the moving crack-tip. Similar observations were also made by Ma and Freund (1986). They considered the problem of a semi-infinite crack subjected to a uniform step pressure

on its surface. After a finite delay time, the crack starts to propagate with a constant speed.

3.6 Discussion and conclusions

Since Yoffe (1951) mathematically determined the stress field around the tip of a steadily propagating crack with constant length, substantial progress has been made in the areas of theoretical and numerical analysis of dynamic fracture events in brittle materials. The uniqueness of the near tip stress field of a running crack was proved by Freund and Clifton (1974). Their work also established that for a running crack the *near tip* stress state can be characterized by a single parameter – the dynamic stress intensity factor. However, interpretation of the stress field near the edge of a crack in a loaded body in terms of a stress intensity factor must always be based on the assumption that the dimensions of the body and the details of the loading are such that a stress intensity factor controlled (K_I^d-dominant) field does indeed exist and the size of this K_I^d-dominant field is sufficiently small compared to the crack length, distance to the nearest boundary, or any other characteristic dimension of the body. In addition to the limitation noted above concerning overall body dimensions and crack length, the zone of influence of three-dimensional effects around the crack edge should also be small compared to the K_I^d-dominant field, especially when the case of a through thickness crack in a plate is considered. Typically, the plane stress assumption is valid only for points at half of the plate thickness away from the crack edge (Rosakis and Ravi-Chandar, 1986; Yang and Freund, 1985).

If a cracked body is subjected to stress wave loading and the crack growth process is dynamic, there is yet another important factor which complicates the application of the stress intensity factor idea under conditions of plane deformation. This factor is due to the wave character of the mechanical fields in the body during crack growth.

Consider, for example, the case studied in the previous sections. This corresponds to a semi-infinite crack in an otherwise unbounded elastic body subjected to stress wave loading conditions. Even though this semi-infinite configuration strictly satisfies all of the size requirements mentioned above, the application of the K_I^d-dominant field is still limited. For the crack before initiation, when the incoming stress wave hits the crack, the stress wave will diffract around the crack-tip. A cylindrical longitudinal wave and a cylindrical shear wave will be emitted from the crack-tip and will propagate into the body. The K_I^d-dominant assumption is valid only for points much closer to the crack-tip than the distance of the cylindrical shear wave front from the crack-tip. After crack initiation, the situation becomes even more complicated because stress waves are continuously emitted from the moving crack-tip. This can be seen by observing that the internal stress in the elastic body at a point on the prospective fracture plane will gradually build up as the crack-tip approaches and that this gradually accumulated stress is then suddenly released with the passage of the crack-tip. As a result, the transient fields must radiate out continuously through the region surrounding the crack-tip. This lack of K_I^d-dominance was studied theoretically by Ma and Freund (1986) and was observed experimentally by Krishnaswamy and Rosakis (1991) and Krishnaswamy *et al.* (1992) by using a bifocal caustics arrangement and the optical method of CGS.

By studying the specific problem of a stress wave loaded semi-infinite precrack which eventually extends with a constant speed, we show that the assumption of K_I^d-dominance is inadequate in describing the near tip stress state at short times after crack initiation. For this problem, the transient effect is manifested through the time derivative of the dynamic stress intensity factor even if the crack-tip speed is constant. This study suggests that the use of the higher order transient asymptotic representation provided by Freund and Rosakis (1992), and by Liu and Rosakis (1992) is necessary to represent the actual field near the moving crack-tip. Section 4 clearly

shows that the coefficients of this expansion depend on the time derivative of the dynamic stress intensity factor. It is further shown that by including this higher order term in the asymptotic expansion, the nature of the near tip stress field is indeed captured. Because of the loss of K_I^d-dominance, even when the body is unbounded and the crack is semi-infinite, this study also suggests that the transient effects should be considered when any attempt is made to interpret experimental measurements performed at finite distances away from the moving crack-tip. In the second part of this study, we will use the results obtained in this paper to interpret the experimental observation made by Prakash and Clifton (1992) where crack initiation and growth was studied under extremely high loading rates.

Appendix

A Inversion of Laplace transforms – Cagniard-de Hoop technique

Consider a quantity $G(\zeta, x_2, s)$ with the form

$$G(\zeta, x_2, s) = \frac{A(\zeta)}{s^2} e^{-s\alpha^{(\mathrm{B})}(\zeta)x_2} \ , \tag{A.1}$$

where $A(\zeta)$ is analytic in the strip $-a < \mathrm{Re}\ \zeta < a$. The inversion of $G(\zeta, x_2, s)$ is given by

$$\hat{g}(x_1, x_2, s) = \frac{1}{2\pi si} \int_{\zeta_0 - i\infty}^{\zeta_0 + i\infty} A(\zeta) e^{-\{\alpha^{(\mathrm{B})}(\zeta)x_2 - \zeta x_1\}s} \mathrm{d}\zeta \ , \tag{A.2}$$

where ζ_0 is real and $-a < \zeta_0 < a$. Set

$$\alpha^{(\mathrm{B})}(\zeta)x_2 - \zeta x_1 = \tau > 0 \ , \tag{A.3}$$

and solve equation (A.3) for ζ, we obtain

$$\zeta_{l\pm}^{(\mathrm{B})} = -\frac{\tau}{r}\cos\theta \pm i\sqrt{\frac{\tau^2}{r^2} - a^2}\sin\theta \ , \tag{A.4}$$

where

$$r = \sqrt{x_1^2 + x_2^2} \ , \qquad \theta = \tan^{-1}\frac{x_2}{x_1} \ .$$

Notice that

$$\left.\begin{array}{ll} \mathrm{Im}\ \zeta_{l\pm}^{(\mathrm{B})} = 0 \ , & \text{as } \tau = ar \\ \dfrac{\mathrm{Im}\ \zeta_{l\pm}^{(\mathrm{B})}}{\mathrm{Re}\ \zeta_{l\pm}^{(\mathrm{B})}} = \mp\tan\theta \ , & \text{as } \tau \to \infty \end{array}\right\} \ . \tag{A.5}$$

From FIGURE 3.9 and the analysis above, we can see that the original integral contour Γ_i can be distorted into new integral contours $\zeta_{l+}^{(\mathrm{B})}$ and $\zeta_{l-}^{(\mathrm{B})}$, and the new contour will not intersect with the branch cuts as θ changing from 0 to π.

Now, we can express $\hat{g}(x_1, x_2, s)$ as

$$\hat{g}(x_1, x_2, s) = \frac{1}{2\pi si} \int_{ar}^{\infty} \left\{ A(\zeta_{l+}^{(\mathrm{B})}) \frac{\partial \zeta_{l+}^{(\mathrm{B})}}{\partial \tau} - A(\zeta_{l-}^{(\mathrm{B})}) \frac{\partial \zeta_{l-}^{(\mathrm{B})}}{\partial \tau} \right\} e^{-s\tau} \mathrm{d}\tau \ . \tag{A.6}$$

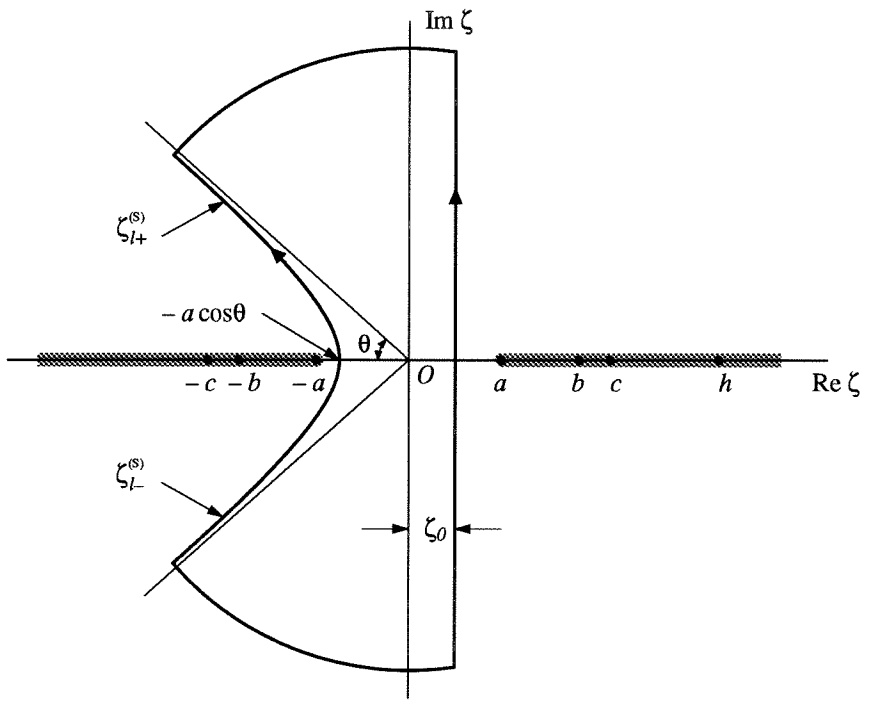

Figure 3.9: Distortion of the integral contour to evaluate the inversion of $G(\zeta, x_2, s)$.

Notice that $\zeta_{l-}^{(B)} = \overline{\zeta}_{l+}^{(B)}$. If $A(\zeta)$ has the property $\overline{A(\zeta)} = A(\overline{\zeta})$, then

$$\hat{g}(x_1, x_2, s) = \frac{1}{\pi s} \int_{ar}^{\infty} \mathrm{Im}\left\{ A(\zeta_{l+}^{(B)}) \frac{\partial \zeta_{l+}^{(B)}}{\partial \tau} \right\} e^{-s\tau} \mathrm{d}\tau \ . \tag{A.7}$$

Furthermore,

$$g(x_1, x_2, t) = \frac{1}{2\pi i} \int_{\sigma - i\infty}^{\sigma + i\infty} \hat{g}(x_1, x_2, s) e^{st} \mathrm{d}s \ . \tag{A.8}$$

After some manipulations, it can be shown that

$$g(x_1, x_2, t) = \frac{1}{\pi} \int_{ar}^{t} \mathrm{Im}\left\{ A(\zeta_{l+}^{(B)}) \frac{\partial \zeta_{l+}^{(B)}}{\partial \tau} \right\} \mathrm{d}\tau \cdot H(t - ar) \ , \tag{A.9}$$

where $\zeta_{l+}^{(B)}(x_1, x_2, t)$ is given by equation (A.4), from which $\partial \zeta_{l+}^{(B)} / \partial \tau$ can also be calculated.

On the other hand, if $G(\zeta, x_2, s)$ has the form

$$G(\zeta, x_2, s) = \frac{A(\zeta)}{s^2 \zeta} e^{-s\alpha^{(B)}(\zeta) x_2} \ , \tag{A.10}$$

where $A(\zeta)$ is analytic in the strip $-a < \mathrm{Re}\ \zeta < a$. Write

$$A(\zeta, x_2, s) = \frac{A(\zeta)}{s} e^{-s\alpha^{(\mathrm{B})}(\zeta)x_2} ,$$

then the inversion of $A(\zeta, x_2, s)$ can be obtained by using the Cagniard-de Hoop technique we just discussed. It is

$$\hat{a}(x_1, x_2, s) = \frac{1}{\pi} \int_{ar}^{\infty} \mathrm{Im} \left\{ A(\zeta_{l+}^{(\mathrm{B})}) \frac{\partial \zeta_{l+}^{(\mathrm{B})}}{\partial \tau} \right\} e^{-s\tau} \mathrm{d}\tau . \tag{A.11}$$

Notice that for the Heaviside function $H(x_1)$, we have

$$\int_{-\infty}^{\infty} H(x_1) e^{-s\zeta x_1} \mathrm{d}x_1 = 1 , \quad \text{for } \mathrm{Re}\ \zeta > 0 .$$

From the composition product relation (van der Pol and Bremmer, 1955), the inversion of $G(\zeta, x_2, s)$ which can be rewritten as

$$G(\zeta, x_2, s) = \frac{A(\zeta, x_2, s)}{s\zeta} \cdot 1 ,$$

is given by

$$\hat{g}(x_1, x_2, s) = \int_{-\infty}^{\infty} \hat{a}(x_1^*, x_2, s) H(x_1 - x_1^*) \mathrm{d}x_1^* , \tag{A.12}$$

or

$$\hat{g}(x_1, x_2, s) = \frac{1}{\pi} \int_{-\infty}^{x_1} \left\{ \int_{ar^*}^{\infty} \mathrm{Im} \left[A(\zeta_{l+}^{(\mathrm{B})*}) \frac{\partial \zeta_{l+}^{(\mathrm{B})*}}{\partial \tau} \right] e^{-s\tau} \mathrm{d}\tau \right\} \mathrm{d}x_1^* , \tag{A.13}$$

where

$$\zeta_{l+}^{(\mathrm{B})*} = -\frac{\tau}{r^*} \cos\theta^* + i \sqrt{\frac{\tau^2}{r^{*2}} - a^2} \sin\theta^* ,$$

and

$$r^* = \sqrt{x_1^{*2} + x_2^2} , \qquad \theta^* = \tan^{-1} \frac{x_2}{x_1^*} .$$

Also, by performing the inversion of the Laplace transform with respect to parameter s, we can get

$$g(x_1, x_2, t) = \frac{1}{\pi} \int_{-\infty}^{x_1} \mathrm{Im} \left\{ A(\zeta_{l+}^{(\mathrm{B})*}) \frac{\partial \zeta_{l+}^{(\mathrm{B})*}}{\partial t} \right\} H(t - ar^*) \mathrm{d}x_1^* , \tag{A.14}$$

or

$$g(x_1, x_2, t) = \frac{1}{\pi} \int_{-\omega_l}^{\mathrm{Min}(x_1, \omega_l)} \mathrm{Im} \left\{ A(\zeta_{l+}^{(\mathrm{B})*}) \frac{\partial \zeta_{l+}^{(\mathrm{B})*}}{\partial t} \right\} \mathrm{d}x_1^* , \tag{A.15}$$

where

$$\omega_l = \left(\frac{t^2}{a^2} - x_2^2\right)^{1/2} .$$

Finally, we have

$$g(x_1, x_2, t) = \frac{1}{\pi}\int_{-\omega_l}^{x_1} \mathrm{Im}\left\{A(\zeta_{l+}^{(\mathrm{B})*})\frac{\partial \zeta_{l+}^{(\mathrm{B})*}}{\partial t}\right\} \mathrm{d}x_1^* \cdot H(t - ar) . \tag{A.16}$$

Consider another quantity $W(\zeta, x_2, s)$ with the form

$$W(\zeta, x_2, s) = \frac{B(\zeta)}{s^2} e^{-s\beta^{(\mathrm{B})}(\zeta)x_2} , \tag{A.17}$$

where $B(\zeta)$ is analytic in the strip $-b < \mathrm{Re}\ \zeta < a$. By definition,

$$\hat{w}(x_1, x_2, s) = \frac{1}{2\pi si}\int_{\zeta_0 - i\infty}^{\zeta_0 + i\infty} B(\zeta) e^{-\{\beta^{(\mathrm{B})}(\zeta)x_2 - \zeta x_1\}s} \mathrm{d}\zeta , \tag{A.18}$$

where ζ_0 is real and $-b < \zeta_0 < a$. Similar to previous discussions, we may set

$$\beta^{(\mathrm{B})}(\zeta)x_2 - \zeta x_1 = \tau > 0 , \tag{A.19}$$

and solve equation (A.19) for ζ. Then

$$\zeta_{s\pm}^{(\mathrm{B})} = -\frac{\tau}{r}\cos\theta \pm i\sqrt{\frac{\tau^2}{r^2} - b^2}\sin\theta . \tag{A.20}$$

We also have the property that

$$\left.\begin{array}{ll} \mathrm{Im}\ \zeta_{s\pm}^{(\mathrm{B})} = 0 , & \text{as } \tau = br \\ \dfrac{\mathrm{Im}\ \zeta_{s\pm}^{(\mathrm{B})}}{\mathrm{Re}\ \zeta_{s\pm}^{(\mathrm{B})}} = \mp\tan\theta , & \text{as } \tau \to \infty \end{array}\right\} . \tag{A.21}$$

But it can be seen that as $\tau = br$,

$$\zeta_{s\pm}^{(\mathrm{B})} = -b\cos\theta = \lambda^{(\mathrm{B})}(\theta) ,$$

and as a result, when θ is changing from 0 to π, $\lambda^{(\mathrm{B})}(\theta)$ is in the range

$$-b \le \lambda^{(\mathrm{B})}(\theta) \le b .$$

So, as θ is greater than angle $\theta_{\rm H}^{\rm (B)} = \pi - \cos^{-1}(a/b)$, the distorted integral contour will intersect with the branch cut, and we need to consider two cases separately.

For $0 \le \theta \le \theta_{\rm H}^{\rm (B)}$, we can directly apply the same procedure for $G(\zeta, x_2, s)$, and if $B(\zeta)$ satisfies that $\overline{B(\zeta)} = B(\overline{\zeta})$, then

$$w(x_1, x_2, t) = \frac{1}{\pi} \int_{br}^{t} \mathrm{Im} \left\{ B(\zeta_{s+}^{\rm (B)}) \frac{\partial \zeta_{s+}^{\rm (B)}}{\partial \tau} \right\} \mathrm{d}\tau \cdot H(t - br) \ , \tag{A.22}$$

where $\zeta_{s+}^{\rm (B)}(x_1, x_2, t)$ is given by equation (A.20), from which $\partial \zeta_{s+}^{\rm (B)} / \partial \tau$ can be calculated.

For $\theta_{\rm H}^{\rm (B)} \le \theta \le \pi$, from FIGURE 3.10, we have

$$\hat{w}(x_1, x_2, s) = \hat{w}_0(x_1, x_2, s) + \hat{w}_H(x_1, x_2, s) \ , \tag{A.23}$$

where by assuming that $\overline{B(\zeta)} = B(\overline{\zeta})$,

$$\hat{w}_0(x_1, x_2, s) = \frac{1}{\pi s} \int_{br}^{\infty} \mathrm{Im} \left\{ B(\zeta_{s+}^{\rm (B)}) \frac{\partial \zeta_{s+}^{\rm (B)}}{\partial \tau} \right\} e^{-s\tau} \mathrm{d}\tau \ ,$$

and

$$\hat{w}_H(x_1, x_2, s) = \frac{1}{\pi s} \int_{a}^{\lambda^{\rm (B)}(\theta)} \mathrm{Im} \left\{ B^{+}(\eta) \right\} e^{-\{\beta^{\rm (B)}(\eta) x_2 - \eta x_1\} s} \mathrm{d}\eta \ .$$

Moreover, it can be shown that

$$w_0(x_1, x_2, t) = \frac{1}{\pi} \int_{br}^{t} \mathrm{Im} \left\{ B(\zeta_{s+}^{\rm (B)}) \frac{\partial \zeta_{s+}^{\rm (B)}}{\partial \tau} \right\} \mathrm{d}\tau \cdot H(t - br) \ , \tag{A.24}$$

and

$$w_H(x_1, x_2, t) = \frac{1}{\pi} \int_{a}^{\lambda^{\rm (B)}(\theta)} \mathrm{Im} \left\{ B^{+}(\eta) \right\} h^{\rm (B)}(\eta) \mathrm{d}\eta \ , \tag{A.25}$$

where

$$h^{\rm (B)}(\eta) = H\left(t - [\beta^{\rm (B)}(\eta) x_2 - \eta x_1]\right) \ , \qquad a < \eta \le \lambda^{\rm (B)}(\theta) \ .$$

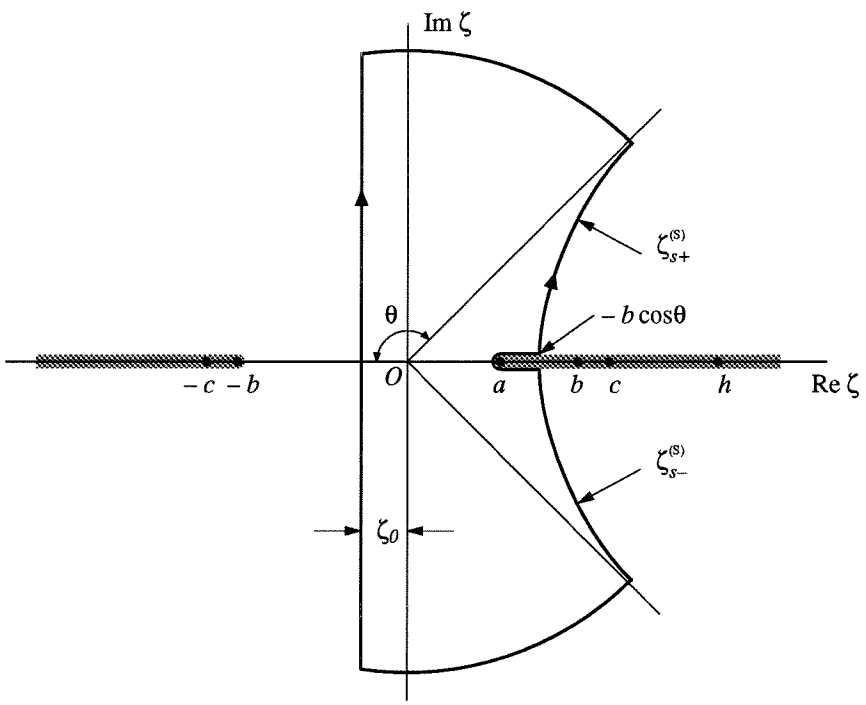

Figure 3.10: Distortion of the integral contour to evaluate the inversion of $W(\zeta, x_2, s)$.

Summarize the results for above two cases, we can write

$$w(x_1,x_2,t) = \frac{1}{\pi}\left\{\begin{array}{l}\displaystyle\int_{br}^{t} \mathrm{Im}\left[B(\zeta_{s+}^{(\mathrm{B})})\frac{\partial\zeta_{s+}^{(\mathrm{B})}}{\partial\tau}\right]\mathrm{d}\tau\cdot H(t-br) \\ + \displaystyle\int_{a}^{\lambda^{(\mathrm{B})}(\theta)} \mathrm{Im}\left[B^{+}(\eta)\right]h^{(\mathrm{B})}(\eta)\mathrm{d}\eta\cdot H(\theta-\theta_{\mathrm{H}}^{(\mathrm{B})})\end{array}\right\}. \qquad \text{(A.26)}$$

As a matter of fact, the second part in the right-hand side of equation (A.26) provides the information inside the region of head wave. By denoting $\zeta_{l,s+}^{(\mathrm{B})}$ as $\zeta_{l,s}^{(\mathrm{B})}$, expressions in (3.3.8) and (3.3.10) are obtained. By using the same technique, expressions in (3.3.18) and (3.3.19) can also be obtained.

Chapter 4

Comparison of the Theoretical Prediction to High Loading Rate Plate Impact Fracture Experiments in AISI 4340 Steel

4.1 Introduction

As a material parameter, the fracture toughness can only be obtained through experimental measurements. Meanwhile, the fracture resistance of materials is generally understood to vary with environmental conditions under which the experiment is conducted, and with loading rates to which the specimen is subjected. Under impact loading conditions, high loading rates are caused at the pre-existing crack-tip. In dynamic fracture experiments, a parameter is defined to characterize the loading rate under which the specimen is loaded, and it is

$$\dot{K}_I = \frac{K_{IC}}{t_C} \ , \tag{4.1.1}$$

where K_{IC} is the mode-I critical stress intensity factor at the instant of crack initiation (fracture toughness) and t_C denotes the time from the beginning of loading to the instant at which fracture initiation occurs. Usually, the crack-tip loading rates range from $\dot{K}_I \sim 1$ MPa$\sqrt{\text{m}} \cdot \text{sec}^{-1}$ for quasi-static loading to as high as $\dot{K}_I \sim 10^8$ MPa$\sqrt{\text{m}} \cdot \text{sec}^{-1}$ for impact loading. Due to the presence of material inertia and strain rate, the material may exhibit totally different behaviors from those under

quasi-static loading conditions. To understand the mechanism of crack initiation, propagation, and arresting, various specimen configurations and loading devices have been designed, and extensive research has been carried out for various materials by using different experimental techniques. Using the method of optical caustics, Kalthoff *et al.* (1979) have studied rapid crack propagation and arrest in double-cantilever beam specimen made of Araldite B. Using the same experimental technique and specimen configuration, Rosakis *et al.* (1984) studied crack growth in 4340 steel. Kobayashi and Dally (1980) investigated the crack growth in double cantilever beam 4340 steel specimen but using the method of dynamic photoelasticity. Ravi-Chandar and Knauss (1982) studied the dynamic fracture in Homalite 100 material under stress wave loading. Zehnder and Rosakis (1990) have conducted studies on crack initiation and propagation in 4340 steel using a three point bend configuration impacted by a drop weight hammer.

The interpretation of experimental observations involving dynamic fracture under stress wave loading has been proved to be difficult. This is because the specimen configurations commonly used in laboratory testing, cannot be completely modeled by existing mathematical methods, even when the material response is linear elastic. In most experimental observations of dynamic fracture, finite-sized specimens are used. The stress waves generated either by the external loading or by radiation from the extending crack-tip, reflect back and forth inside the specimen so that the stress state surrounding the crack-tip is too complicated to be analyzed. Even though Beinert and Kalthoff (1983) have designed a specimen configuration which minimizes the dynamic effects caused by wave reflection, direct mathematical analysis is still impossible.

So far, the only geometrical configurations for which it is possible to obtain the exact solutions for the elastodynamic fields by solving an initial/boundary value problem, are ones involving infinite straight cracks and unbounded bodies. For the prob-

lem of semi-infinite crack loaded by a planar stress wave which after a finite delay time starts to extend with a constant speed, the procedure of getting the complete transient solution has been discussed by Freund (1973 and 1990). The time history of the dynamic stress intensity factor was also obtained and was generalized to include the situation where the crack propagates with a nonuniform speed. In Chapter 3, we have revisited this problem and obtained the full field analytical solution for the stresses surrounding the stationary and moving crack-tip. In addition, we have also obtained the expressions for the coefficients that appear in a newly developed higher order transient asymptotic representation of the near tip field of a transiently growing crack (Freund and Rosakis, 1992; Liu and Rosakis, 1992). We have shown that this higher order transient representation is able to describe the actual near tip field very well.

Ravichandran and Clifton (1989) have developed a novel experimental configuration which involves loading a half plane crack by a planar tensile pulse. This experimental method is designed to provide comparatively straightforward interpretation of experimental observation within the framework of dynamic fracture mechanics. In this configuration, a disc containing a pre-fatigued edge crack in its mid-plane is impacted by a thin flyer plate of the same material. The resulting compressive pulse propagates through the specimen and reflects from the rear surface as a step, tensile pulse with a duration of about 1 μsec. This plane wave loads the crack and causes dynamic initiation and propagation of the crack. Within the duration of loading and the extension of the crack, no unloading waves reach the crack-tip. Therefore, this loading condition corresponds to a semi-infinite crack subjected to a finite duration plane pulse. By using this experimental technique, one can attain loading rates of approximately $\dot{K}_I \sim 10^8$ MPa$\sqrt{\text{m}} \cdot \text{sec}^{-1}$. This unique configuration allows for the study of dynamic fracture processes which occur when the loading times are in the submicrosecond range.

Prakash and Clifton (1992) studied the process of crack initiation in a hardened AISI 4340 VAR steel by using the high loading rate plate impact experimental procedure described above. The total time period of their experiment was approximately 1μsec. They monitored the motion of the rear surface of the disc at four different points simultaneously during the experiment by using a multiple beam laser interferometer system. An important observation they made in these experiments is the appearance of a clearly marked change in the free surface velocity at all four points at times that correspond to the arrival of waves emanating from the crack-tip during fracture initiation. Meanwhile, they also simulated the dynamic process numerically using a visco-plastic finite difference code. The measured normal velocity of the rear surface of the specimen at a typical monitoring point agrees well with computed scattered fields except for the appearance of a sharp spike in the experimental data of a very short duration. To provide an interpretation for the existence of these spikes, Prakash *et al.* (1992) developed a mathematical model where they assumed that at the moment of initiation, a small, but with finite size, hole suddenly appears at the crack-tip. The stress field associated with this small hole radiates out into the body, and the dominant singularity of this field is $O(r^{-3/2})$ which is stronger than the singularity caused by the sharp crack itself as the crack-tip is approached. In this case, the jump in the particle velocity on the wavefront is infinite, a fact that is consistent with the existence of a spike. However, one should recall that the measurements in their experiments were carried out at points relatively far away from the initial crack-tip. In such points, the information associated with the stronger singularity would die out even faster than the term corresponding to the K_I^d-dominant field. This observation has motivated us to seek a second, possible explanation for this phenomenon which lies totally within the realm of classical transient elastodynamics of crack initiation and growth.

In this chapter, we provide an alternative interpretation to the experimental ob-

servations made by Prakash and Clifton (1992). In Chapter 3, we have obtained the full field analytical solution for stresses surrounding the crack-tip. In addition, the coefficients in the higher order transient asymptotic representation developed by Freund and Rosakis (1992) and by Liu and Rosakis (1992), have also been calculated. Based on these results, we simulate the experimental observation by using some parameters provided in the experiments. In the next section, the experimental technique and procedure are briefly described. In Section 4.3, the higher order transient asymptotic representation of the particle velocity field is derived by using the result given in Liu and Rosakis (1992). In this asymptotic representation, transient effects including the time derivative of the dynamic stress intensity factor and the crack-tip acceleration are taken into account. In the same section, we use parameters from the experimental measurement, namely, the delay time for crack initiation τ and the amplitude of the incident stress pulse σ^*, to simulate the experimental output. This is done by using the higher order transient representation and by initially assuming constant crack-tip speed. The result shows that the higher order transient representation successfully captures the crude feature of the experimental observation, i.e., a finite jump at the time of crack initiation is observed. To predict the experimental observations more accurately, we subsequently relax the restriction of constant crack-tip speed. To do so, in Section 4.4, we first introduce a fracture criterion that relates the dynamic stress intensity factor to the speed of the propagating crack. The fracture criterion is motivated by the experimental measurements made by Zehnder and Rosakis (1990) on the same steel. By solving the crack-tip equation of motion, all time-dependent quantities in the higher order transient asymptotic representation are determined. The simulation of the experimental observation shows that the fully transient asymptotic field can describe the actual field very well. The information regarding the changes of the dynamic stress intensity factor and the crack-tip acceleration associated with crack initiation that are carried out by the term with $r^{1/2}$, attribute to the formation of the spikes seen in the experiments. Finally, some discussions are made and conclusions

are drawn in the last section.

4.2 Description of the experiment

A very detailed description of the experiment has been provided by Ravichandran and Clifton (1989) and by Prakash and Clifton (1992). The experiment is designed to load a semi-infinite crack by a planar longitudinal tensile wave impinging at normal incidence. The specimen consists of a round disc of 63mm in diameter and 8mm in thickness, which contains a pre-fatigued edge crack that has propagated half way across the diameter. The crack is situated at the mid-plane of the disc. The specimen is impacted by a plate flyer made of the same material as the specimen. The thickness of the flyer is 3mm. Compressive waves of uniaxial strain are generated by the impact. The wave propagating through the specimen reflects from the rear surface and subjects the crack plane to a step tensile pulse. As the incident tensile pulse hits the crack, part of it is reflected from the crack surface as a compressive wave and part of it is diffracted at the crack-tip. The wave patterns of diffraction and reflection are shown in FIGURE 4.1. As we can see from this figure, the transmitted wave ahead of the crack-tip will be reflected from the front surface of the specimen and the reflected compressive wave will be reflected from the rear surface of the specimen. Before these two waves reach the crack-tip, the stress state near the crack-tip can be modeled as a planar wave diffracted by a semi-infinite crack in an unbounded body.

The material used in the experiments is AISI 4340 VAR steel. This is a high-strength, low-ductility, structural alloy having reduced levels of phosphorus and sulfur to enhance the fracture toughness. Consequently, the choice of material allows the experimental results to be interpreted within the framework of elastodynamic fracture mechanics. The specimen is cut from a notched cylindrical bar in which a fatigue crack has been grown by subjecting the bar to cyclical bending. In order to produce

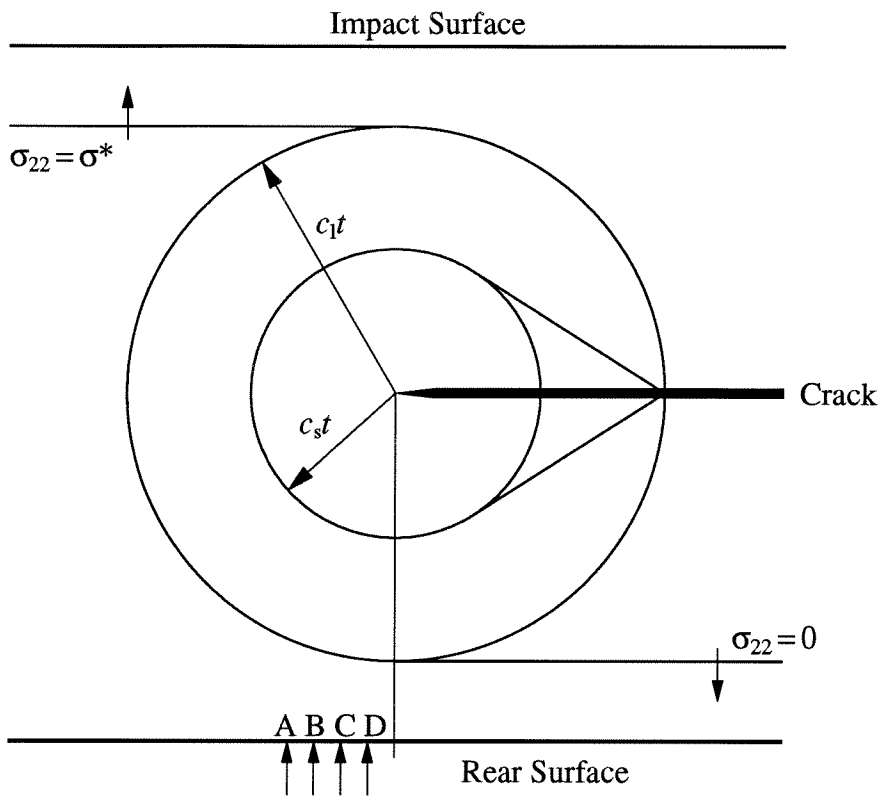

Figure 4.1: Wavefronts for the diffraction of a planar wave by a semi-infinite crack.

a homogeneous martinsitic microstructure, special care has been taken in the process of heat treatment of the material.

The motion of four different points on the rear surface of the specimen is monitored by using the interferometric technique. The experimental configuration is shown in FIGURE 4.2. A fiberglass projectile which carries the flyer plate is accelerated by the nitrogen gas releasing at prescribed pressure and is propelled down the gas gun barrel. The velocity of impact is measured within an accuracy of 1% so that the amplitude of the stress pulse σ^* can be determined fairly accurate. The impact signal triggers the recording system and the motion history of each point monitored on the rear surface of the specimen is obtained. The duration of loading is determined by the thickness of the flyer plate. For this special design of the experimental configuration and the

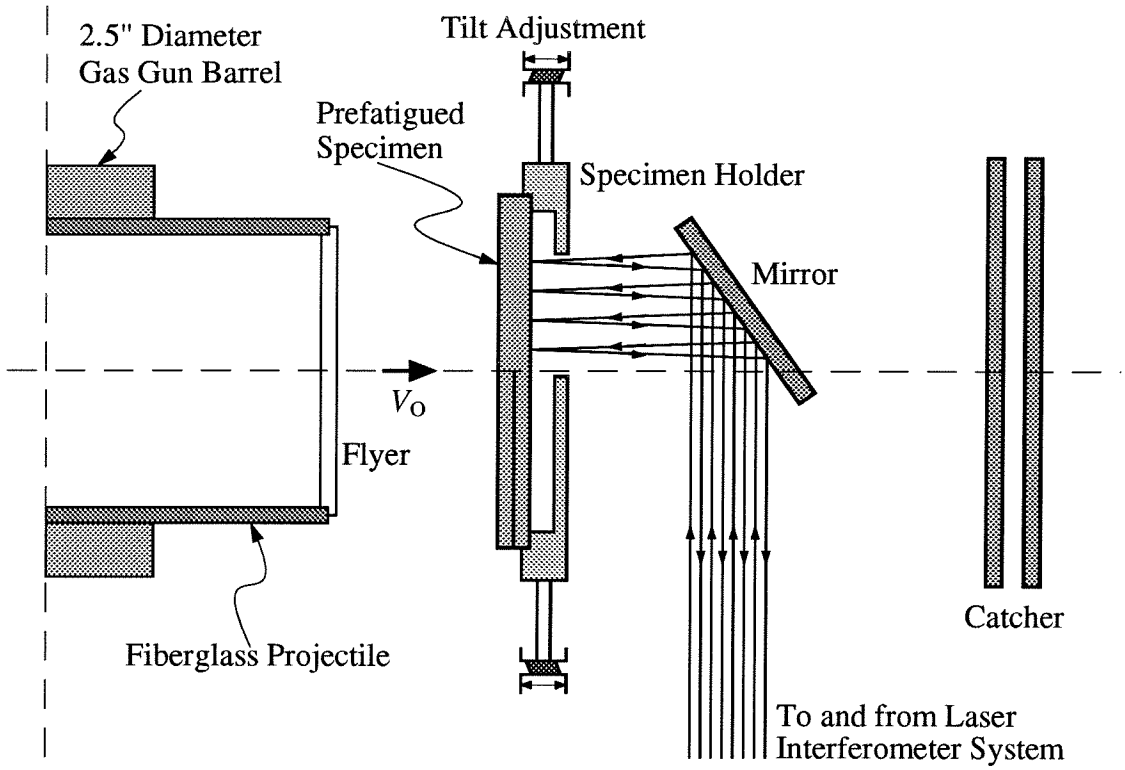

Figure 4.2: Schematic of the experimental configuration.

specimen material, the loading duration is approximately 1μsec. Meanwhile, the design of the experimental configuration ensures that within the duration of loading, no unloading waves reach the crack-tip (see Ravichandran and Clifton, 1989; Prakash and Clifton, 1992).

A typical recording of the experiment obtained by Prakash and Clifton (1992) is shown in FIGURE 4.3. This figure shows the particle velocity-time profiles of the rear surface motion at the four monitoring points ahead of the crack-tip. The horizontal axis has been normalized by the characteristic time H/c_l, where c_l is the longitudinal wave speed of the AISI 4340 VAR steel and H is the half thickness of the specimen.

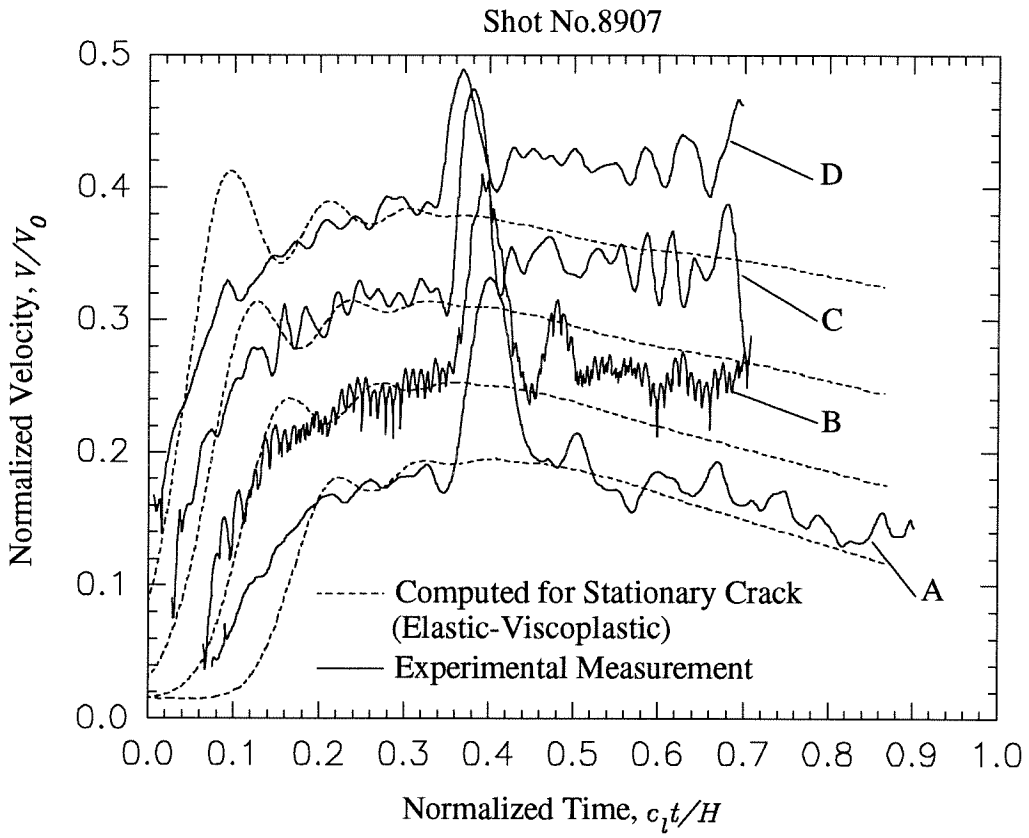

Figure 4.3: Experimental and numerical predicted (stationary crack) velocity-time profiles at four different monitoring points, from Prakash and Clifton, 1992.

The measured particle velocity has also been normalized by the impact velocity V_0 which is 0.0854mm/μsec for this particular experiment. The closest monitoring point is located 0.68mm ahead of the crack-tip. The remaining three monitoring points are spaced at 0.48mm intervals. In the figure, the solid lines correspond to the recorded velocity-time profiles at those four monitoring points from A to D, which get closer and closer to the crack-tip. The dashed curves correspond to the numerical simulation of the experiment using the elastic-viscoplastic model of the material described in Ravichandran and Clifton (1989), which assumes that the crack remains stationary. Agreement between the computed and experimentally obtained particle velocity histories at the four monitoring points is seen to be very good up to the time which

is understood to correspond to the instant of crack initiation. After this time, the experimental and computed velocity-time profiles deviate. An interesting observation from this figure is the appearance of sharp spikes of very short duration at instant corresponding to the crack initiation. As the stress wave emitted due to the crack growth reaches the observation point, the particle velocity increases drastically and then drops very quickly. In the following sections, we will provide an interpretation of these spikes by using the analytical results obtained in Chapter 3 and the higher order transient asymptotic representation developed by Freund and Rosakis (1992) and by Liu and Rosakis (1992).

4.3 Higher order transient asymptotic representation of the particle velocity field

By using the asymptotic methodology introduced by Freund (1990), and by relaxing the assumptions of K_I^d-dominance and steady state, Freund and Rosakis (1992) have provided a higher order asymptotic expansion for the first stress invariant and have shown that this expansion provides an accurate description of crack-tip fields under fairly severe transient conditions. Rosakis *et al.* (1991) have also obtained all of the components of the higher order asymptotic stress field near the tip of a non-uniformly propagating mode-I crack. For the most general transient situation, i.e., a crack propagates transiently along an arbitrary path, the asymptotic elastodynamic field has been obtained by Liu and Rosakis (1992). In this section, we provide the higher order transient asymptotic representation for the particle velocity field surrounding the moving crack-tip. Based on this representation, we will further offer a possible interpretation for the experimental observations described in the previous section.

By using the notation introduced in Liu and Rosakis (1992), for mode-I deformation, the two components of the higher order transient asymptotic representation for

the particle velocity field surrounding a transiently moving crack-tip are:

$$\left.\begin{aligned}
&\dot{u}_1(\xi_1,\xi_2,t) = -\frac{vK_I^d(t)}{\mu\sqrt{2\pi}}\left\{\frac{1+\alpha_s^2}{D(v)}r_l^{-1/2}\cos\frac{\theta_l}{2} - \frac{2\alpha_l\alpha_s}{D(v)}r_s^{-1/2}\cos\frac{\theta_s}{2}\right\}\\
&-\frac{2v\alpha_s(1-\alpha_s^2)}{\mu D(v)}A_1(t) - v\left\{\left[-\frac{15(1+\alpha_s^2)}{4\mu D(v)}A_2(t) + f_l(t)\right]\cos\frac{\theta_l}{2}\right.\\
&+\left[\frac{1}{8}D_l^1\{A_0(t)\} - \frac{3+\alpha_l^2}{16(1-\alpha_l^2)}B_l(t)\right]\cos\frac{3\theta_l}{2} + \frac{1}{32}B_l(t)\cos\frac{7\theta_l}{2}\left.\right\}r_l^{1/2}\\
&-v\alpha_s\left\{\left[\frac{15\alpha_l}{2\mu D(v)}A_2(t) + g_s(t)\right]\cos\frac{\theta_s}{2}\right.\\
&+\left[\frac{1}{8}D_s^1\{A_0(t)\} + \frac{1-5\alpha_s^2}{16(1-\alpha_s^2)}B_s(t)\right]\cos\frac{3\theta_s}{2} + \frac{1}{32}B_s(t)\cos\frac{7\theta_s}{2}\left.\right\}r_s^{1/2}\\
&+O(r_{l,s})
\end{aligned}\right\}, \qquad (4.3.1)$$

and

$$\left.\begin{aligned}
&\dot{u}_2(\xi_1,\xi_2,t) = -\frac{vK_I^d(t)}{\mu\sqrt{2\pi}}\left\{\frac{\alpha_l(1+\alpha_s^2)}{D(v)}r_l^{-1/2}\sin\frac{\theta_l}{2} - \frac{2\alpha_l}{D(v)}r_s^{-1/2}\sin\frac{\theta_s}{2}\right\}\\
&+v\alpha_l\left\{\left[-\frac{15(1+\alpha_s^2)}{4\mu D(v)}A_2(t) + g_l(t)\right]\sin\frac{\theta_l}{2}\right.\\
&-\left[\frac{1}{8}D_l^1\{A_0(t)\} + \frac{1-5\alpha_l^2}{16(1-\alpha_l^2)}B_l(t)\right]\sin\frac{3\theta_l}{2} - \frac{1}{32}B_l(t)\sin\frac{7\theta_l}{2}\left.\right\}r_l^{1/2}\\
&+v\left\{\left[\frac{15\alpha_l}{2\mu D(v)}A_2(t) + f_s(t)\right]\sin\frac{\theta_s}{2}\right.\\
&-\left[\frac{1}{8}D_s^1\{A_0(t)\} - \frac{3+\alpha_s^2}{16(1-\alpha_s^2)}B_s(t)\right]\sin\frac{3\theta_s}{2} - \frac{1}{32}B_s(t)\sin\frac{7\theta_s}{2}\left.\right\}r_s^{1/2}\\
&+O(r_{l,s})
\end{aligned}\right\}. \qquad (4.3.2)$$

In expressions (4.3.1) and (4.3.2), $v(t)$ is the time dependent crack-tip speed, $K_I^d(t)$ is the dynamic stress intensity factor at the moving crack-tip for mode-I deformation, and $A_1(t)$, $A_2(t)$ are unknown coefficients of higher order terms. Functions $f_{l,s}(t)$ and

$g_{l,s}(t)$ are defined by

$$\left.\begin{aligned}
f_l(t) &= \left\{\frac{(1+\alpha_s^2)m_l}{D(v)} + \frac{3+\alpha_l^2}{8(1-\alpha_l^2)}\right\} D_l^1\{A_0(t)\} - \frac{2\alpha_s m_s}{D(v)} D_s^1\{A_0(t)\} \\
&- \frac{1}{2}\left\{\frac{\overset{*}{D}(v)}{D(v)} + \frac{9}{16} - \frac{\alpha_l^2(1+\alpha_l^2)}{8(1-\alpha_l^2)}\right\} B_l(t) + \frac{\alpha_s(1+\alpha_s^2)}{D(v)} B_s(t) \\
f_s(t) &= \left\{\frac{(1+\alpha_s^2)m_s}{D(v)} + \frac{3+\alpha_s^2}{8(1-\alpha_s^2)}\right\} D_s^1\{A_0(t)\} - \frac{2\alpha_l m_l}{D(v)} D_l^1\{A_0(t)\} \\
&- \frac{1}{2}\left\{\frac{\overset{*}{D}(v)}{D(v)} + \frac{9}{16} - \frac{\alpha_s^2(1+\alpha_s^2)}{8(1-\alpha_s^2)}\right\} B_s(t) + \frac{\alpha_l(1+\alpha_s^2)}{D(v)} B_l(t) \\
g_l(t) &= \left\{\frac{(1+\alpha_s^2)m_l}{D(v)} - \frac{1-5\alpha_l^2}{8(1-\alpha_l^2)}\right\} D_l^1\{A_0(t)\} - \frac{2\alpha_s m_s}{D(v)} D_s^1\{A_0(t)\} \\
&- \frac{1}{2}\left\{\frac{\overset{*}{D}(v)}{D(v)} - \frac{5}{16} - \frac{\alpha_l^2(5-3\alpha_l^2)}{8(1-\alpha_l^2)^2}\right\} B_l(t) + \frac{\alpha_s(1+\alpha_s^2)}{D(v)} B_s(t) \\
g_s(t) &= \left\{\frac{(1+\alpha_s^2)m_s}{D(v)} - \frac{1-5\alpha_s^2}{8(1-\alpha_s^2)}\right\} D_s^1\{A_0(t)\} - \frac{2\alpha_l m_l}{D(v)} D_l^1\{A_0(t)\} \\
&- \frac{1}{2}\left\{\frac{\overset{*}{D}(v)}{D(v)} - \frac{5}{16} - \frac{\alpha_s^2(5-3\alpha_s^2)}{8(1-\alpha_s^2)^2}\right\} B_s(t) + \frac{\alpha_l(1+\alpha_s^2)}{D(v)} B_l(t)
\end{aligned}\right\}, \qquad (4.3.3)$$

where

$$\left.\begin{aligned}
A_0(t) &= -\frac{4}{3\sqrt{2\pi}} K_I^d(t) \\
D_l^1\{A_0(t)\} &= -\frac{4\sqrt{v}}{\sqrt{2\pi}\mu\alpha_l^2 c_l^2} \cdot \frac{\mathrm{d}}{\mathrm{d}t}\left\{\frac{\sqrt{v}(1+\alpha_s)}{D(v)} K_I^d(t)\right\} \\
D_s^1\{A_0(t)\} &= \frac{8\sqrt{v}}{\sqrt{2\pi}\mu\alpha_s^2 c_s^2} \cdot \frac{\mathrm{d}}{\mathrm{d}t}\left\{\frac{\sqrt{v}\alpha_l}{D(v)} K_I^d(t)\right\} \\
B_l(t) &= \frac{2v^2(1+\alpha_s^2)\dot{v}}{\sqrt{2\pi}\mu D(v)\alpha_l^4 c_l^4} K_I^d(t) \\
B_s(t) &= -\frac{4v^2\alpha_l\dot{v}}{\sqrt{2\pi}\mu D(v)\alpha_s^4 c_s^4} K_I^d(t)
\end{aligned}\right\}, \qquad (4.3.4)$$

and

$$\left.\begin{aligned} D(v) &= 4\alpha_l\alpha_s - (1+\alpha_s^2)^2 \\ \overset{*}{D}(v) &= 4\alpha_l\alpha_s + (1+\alpha_s^2)^2 \\ m_l &= \frac{1}{2}\left\{\left(1-\alpha_s^2\right) - \frac{2\left(\alpha_l^2-\alpha_s^2\right)}{1-\alpha_l^2}\right\} \\ m_s &= \frac{1}{2}\left\{1-\alpha_s^2\right\} \end{aligned}\right\} . \tag{4.3.5}$$

$(r_{l,s}, \theta_{l,s})$ are two scaled polar coordinate systems traveling with the crack-tip and are defined by

$$r_{l,s} = \left\{\xi_1^2 + \alpha_{l,s}^2(t)\xi_2^2\right\}^{1/2} , \qquad \theta_{l,s} = \tan^{-1}\frac{\alpha_{l,s}(t)\xi_2}{\xi_1} ,$$

where the functions of time $\alpha_{l,s}(t)$ are defined by

$$\alpha_{l,s}(t) = \left\{1 - \frac{v^2(t)}{c_{l,s}^2}\right\}^{1/2} ,$$

and c_l, c_s are the longitudinal and shear wave speeds of the elastic solid, respectively. As we can see from equations (4.3.1) and (4.3.2), the *first terms* in the asymptotic particle velocity field have the same form as those under the steady state conditions and have $r^{-1/2}$ singularities. However, here the crack-tip velocity takes the instantaneous value at each moment and the dynamic stress intensity factor $K_I^d(t)$ may be an arbitrary function of time. In the component $\dot{u}_1$, the second term (spatially constant term) also takes the form of steady state, but $A_1(t)$ may depend on time explicitly. The third terms, which are proportional to $r^{1/2}$, are totally different from the steady state results for $\dot{u}_1$ and $\dot{u}_2$ not only in their coefficients, but also in their angular distributions. Here, the coefficient $A_2(t)$ may be an explicit function of time. From the definitions, we also see that the differential operators $D_{l,s}^1\{A_0(t)\}$ depend on the instantaneous values of the crack-tip speed and the dynamic stress intensity factor, as well as their time derivatives. Meanwhile, $B_{l,s}(t)$ not only depend on the instantaneous values of the crack-tip speed and the dynamic stress intensity factor, but also depend linearly on the crack-tip acceleration. In addition, the dynamic stress intensity factor $K_I^d(t)$ and the higher order coefficients $A_1(t)$ and $A_2(t)$ cannot be

determined by the asymptotic analysis itself. They can only be determined by the specific boundary and initial conditions of the problem. If the crack-tip speed $v(t)$ is constant, i.e., if $\dot{v}(t) = 0$, then $B_{l,s}(t) = 0$, and $D^1_{l,s}\{A_0(t)\}$ will linearly depend on the time derivative of the dynamic stress intensity factor. Under such circumstance, expressions (4.3.1) and (4.3.2) correspond to transient crack growth with constant velocity and varying stress intensity factor. This is still a transient problem. The problem we solved in Chapter 3 belongs to this category. Furthermore, if the time derivative of the dynamic stress intensity factor is also zero, then $D^1_{l,s}\{A_0(t)\} = 0$ as well. In this case, the higher order steady state expansion is obtained. However, the coefficients A_1 and A_2 are now time independent.

For the problem at hand, we have obtained the full field analytical solution for the elastodynamic field surrounding the crack-tip in Chapter 3. Also, we have obtained the coefficients of the higher order terms $A_1(t)$ and $A_2(t)$ for this problem. Therefore, for the case of constant crack-tip velocity but varying dynamic stress intensity factor, we can use expressions (4.3.1) and (4.3.2), with $B_{l,s}(t) = 0$ for this case, to predict the particle velocity at any position and at any moment. To simulate the observations given in FIGURE 4.3, we only need expression (4.3.2). However, since the measurement is carried out at the traction free surface of the specimen and equation (4.3.2) is for a point inside unbounded body (traction free condition is not met), the value of the particle velocity $\dot{u}_2$ obtained from equation (4.3.2) has to be multiplied by a factor of two to provide a proper comparison between the analytical and the experimental results. For the particular test (shot No.8907, Prakash and Clifton, 1992), the following parameters obtained from the experiment have been used in the simulation: Impact velocity $V_0 = 0.0854\text{mm}/\mu\text{sec}$, Amplitude of the incident stress pulse $\sigma^* = 1941\text{MPa}$, Delay time $\tau = 0.1905\mu\text{sec}$, Material mass density $\rho = 7600\text{Kg} \cdot \text{m}^{-3}$, Poisson's ratio $\nu = 0.3$, Longitudinal wave speed $c_l = 5.983\text{mm}/\mu\text{sec}$, and Shear wave speed $c_s = 3.124\text{mm}/\mu\text{sec}$.

By using the parameters given above, FIGURE 4.4 shows analytical predictions in which we have used the higher order asymptotic representation for the transiently propagating crack with constant speed, to simulate the particle velocity at monitoring point D. In FIGURE 4.4, the circles represent the experimental data while the various

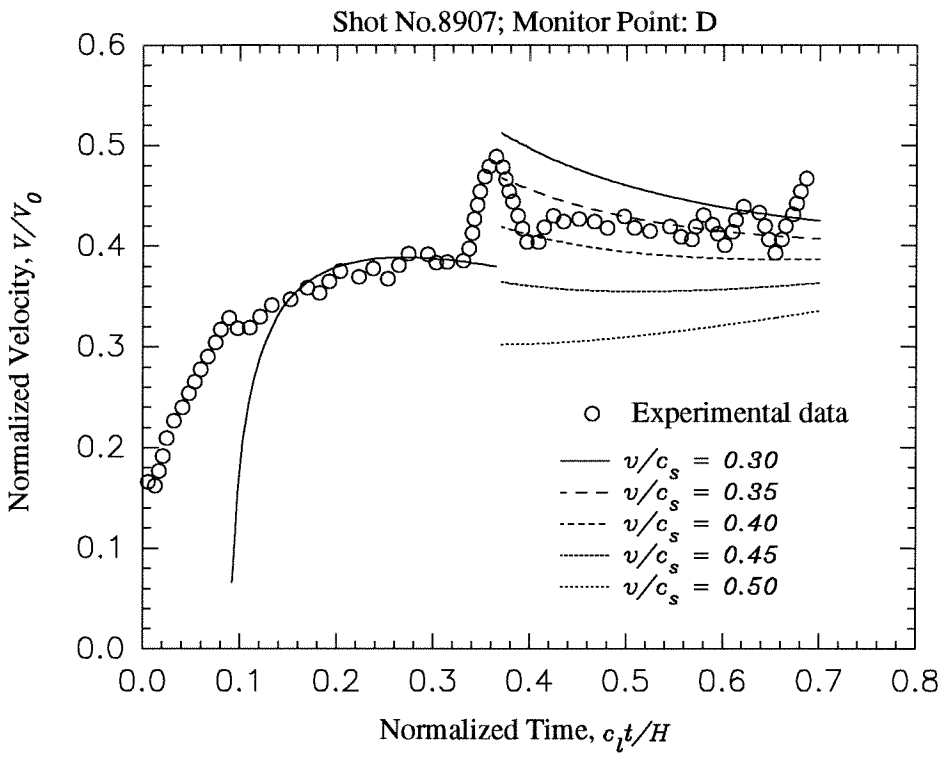

Figure 4.4: Analytical simulation of the experimental measurement at monitoring point D by Prakash and Clifton (1992), shot No. 8907. Before crack initiation, full field expression for the particle velocity is used. After crack initiation, three-term transient asymptotic representation given in equation (4.3.2) with constant crack-tip speed has been used.

lines stand for the simulated values. It should be pointed out that in FIGURE 4.4, before crack initiation, the simulated particle velocity is calculated from the full field analytical solution obtained in Chapter 3, while after crack initiation, expression (4.3.2) is used. It can be seen that before crack initiation,the particle velocity calculated by using the analytical solution, agrees well with the measurements. At the very beginning, however, deviation exists between the theoretical prediction and the experimental measurement. This is due to the fact that the specimen is preloaded by

a compressive pulse resulting from the initial impact while the mathematical model assumes that the body is loaded directly by a tensile stress pulse. After crack initiation, the velocity-time profile at point D is simulated by the three-term transient asymptotic representation given in equation (4.3.2). Here, $B_{l,s}(t) = 0$, $K_I^d(t)$ and $A_2(t)$ have been given in Chapter 3 (see equations (3.3.29) and (3.4.8) in Chapter 3). One can see from this figure that by including the transient effect (through the time derivative of the dynamic stress intensity factor $K_I^d(t)$), we are able to capture the most important feature in the experimental observations for a particular choice of crack-tip velocity, i.e., $v \sim 0.33c_s$. At the instant of crack initiation, the particle velocity at the monitoring point does not transit smoothly from the value corresponding to the stationary crack to the value corresponding to the extending crack. This velocity has a jump at the moment associated with crack initiation and this jump depends on the magnitude of the speed of crack growth.

At this point, some qualitative observations can be made from FIGURE 4.4. At the instant of crack initiation, the crack first jumps from stationary to a velocity about $0.3c_s$ after that the crack-tip speed increases quickly and approaches the value of $0.4c_s$. After crack initiation, the crack-tip speed oscillates about the level of $0.35c_s$. It seems that because of the applied stress pulse, deformation energy is accumulated at the tip of the original semi-infinite stationary crack, and if the material is of limited strength, the crack will start to grow and the deformation energy will be released. Part of this released energy is consumed to form new crack surface, another part becomes the kinematic energy of the crack-tip. However, this process is not steady. The extending crack continuously increases its speed to approach a "steady" state, i.e., the crack-tip speed approaches a constant value. Therefore, the formation of the spikes in the experimental observations is attributed to the process of crack initiation and then approaching the steady speed in a very short period of time. This description is only a qualitative speculation and does not provide a complete picture

about the dynamic crack initiation and transient crack growth since we have assumed that the crack-tip velocity is constant when we simulate the experimental observation in FIGURE 4.4, while change of velocity has been involved in this process. Notice that in the higher order transient asymptotic representation of the field of particle velocity, equations (4.3.1) and (4.3.2), the crack-tip acceleration plays a prominent role. Therefore, if we can provide more accurate information regarding the crack-tip speed during the extension, the picture of the transient crack growth will become more complete. However, unlike the fracture experiments based on optical caustics and CGS, the plate impact experimental technique cannot provide an independent crack-tip velocity history. For this reason, in the next section, we will introduce a criterion regarding dynamic crack growth first, and then we can predict the histories of the crack-tip speed by solving the crack-tip equation of motion. After that, we will simulate the experimental observation again by including all of the transient effects (i.e., terms involving both $\dot{K}_I^d(t)$ and $\dot{v}(t)$).

4.4 Crack-tip equation of motion

If the history of the crack-tip motion is specified, then the surrounding mechanical fields in an elastic body can be obtained in principle within the context of linear elastic continuum mechanics, as long as the configuration of the body and the details of the loading are also specified. However, since the motion of crack-tip is totally controlled by the deformation state inside the surrounding material, the motion of the crack-tip should not be specified a priori. Due to the fact that the constitutive equation for the material does not include the possibility of material separation, we need a mathematical statement of a crack growth criterion to be added into the governing equations. Such criterion must be stated as a physical postulate on material behavior and at the same level as the kinematical theorems governing deformation, momentum balance principles, as well as the constitutive relation describing material response.

The most common form for such a criterion is the requirement that the crack must grow in such a way that some parameter defined as part of the crack-tip field maintains a value that is specific to the material. This value, representing the resistance of the material to the advance of the crack, is called the fracture toughness of the material, and it can be determined through experimental measurements only.

During the process of crack growth, if the small scale yielding condition prevails, a possible fracture criterion stipulates

$$K_I^d(t) = K_{IC}^d \ , \tag{4.4.1}$$

where the left-hand side is the dynamic stress intensity factor (in principle entirely determined through an analysis of a boundary/initial value problem) and the right-hand side represents a material quantity called the *dynamic fracture toughness* which can only be determined through experiments. The dynamic stress intensity factor $K_I^d(t)$ is known to be a function of crack length $a(t)$, crack-tip speed $v(t)$, and some generalized measure of the applied load $P(t)$. It has also been suggested that the dynamic fracture toughness must be dependent on crack-tip velocity (Freund, 1990; Rosakis, Duffy, and Freund, 1984; Zehnder and Rosakis, 1990). Thus the fracture criterion as given in (4.4.1) becomes

$$K_I^d\left(a(t), v(t), P(t), t\right) = K_{IC}^d\left(v(t), \cdots\right) \ . \tag{4.4.2}$$

Equation (4.4.2) is an evolution equation for crack growth, i.e., a crack-tip equation of motion, since it represents a nonlinear, first order differential equation for the crack length $a(t)$.

For the specific problem at hand, the dynamic stress intensity factor for the propagating crack is given by

$$K_I^d(t) = k(v) K_{IC}^{(\mathrm{D})} \sqrt{\frac{t}{\tau}} \ , \tag{4.4.3}$$

where $K_{IC}^{(\mathrm{D})}$ is the value of the dynamic stress intensity factor at the instant of crack initiation (dynamic initiation toughness) and τ is the delay time between the instant

of stress wave arrival at the crack and the onset of crack extension (see Chapter 3). $k(v)$ is a universal function of the crack-tip speed v, such that $k(v) = 1$ at $v = 0$ and $k(v) = 0$ at $v = c_R$, where c_R is the Rayleigh wave speed of the material. As for the dynamic fracture toughness, one usually assumes that it is only dependent on the crack-tip velocity and on material characteristics. We can thus express K_{IC}^d as

$$K_{IC}^d(v) = K_{IC}^{(\mathrm{S})} f(v) \ , \tag{4.4.4}$$

where $K_{IC}^{(\mathrm{S})}$ is the quasi-static crack growth fracture toughness for the material (steady state value of the resistance curve). $f(v)$ is a function of crack-tip speed such that $f(v) = 1$ at $v = 0$. The relation between the dynamic initiation toughness $K_{IC}^{(\mathrm{D})}$ and $K_{IC}^{(\mathrm{S})}$ that appear in equations (4.4.3) and (4.4.4) is supposed to be

$$K_{IC}^{(\mathrm{D})} = \alpha K_{IC}^{(\mathrm{S})} \ , \tag{4.4.5}$$

where $\alpha \geq 1$. Since $K_{IC}^{(\mathrm{S})}$ corresponds to the quasi-static conditions, it represents the situation where the loading rate is close to zero. Here, several effects have been included into the number α. First, it has been observed that the critical value of the dynamic stress intensity factor at crack initiation increases as the loading rate increases. Secondly, in the laboratory situations, the crack-tip cannot be mathematically sharp, and the bluntness of the crack-tip will also increase the critical value for initiation. Even for high strength materials like AISI 4340 steel, some initial plasticity is expected to blunt the fatigue precrack. As a result, the number α is assigned to accommodate the effects of loading rate and initial crack-tip bluntness.

Now the crack-tip equation of motion (4.4.2) becomes

$$\alpha k(v) \sqrt{\frac{t}{\tau}} = f(v) \ . \tag{4.4.6}$$

The form of the universal function $k(v)$ can be simplified as (Freund, 1990)

$$k(v) = \frac{1 - v/c_R}{\sqrt{1 - v/c_l}} \ . \tag{4.4.7}$$

Also for the purpose of present study and from previous experimental observations regarding the relation between the dynamic fracture toughness and the crack-tip speed, we choose the form of the function $f(v)$ as

$$f(v) = \frac{1 + \frac{1}{M} \tan\left(\frac{\pi}{2} \cdot \frac{v}{v_m}\right)}{\sqrt{1 - v/c_l}} , \tag{4.4.8}$$

where M and v_m are two material constants. Notice that $f(v) \to 1$ as $v \to 0$ and $f(v) \to \infty$ as $v \to v_m$, so that v_m represents a "terminal speed" that a crack can achieve in this particular solid. In most of the dynamic fracture experimental measurements, the terminal speed of a mode-I crack in the homogeneous material is about $0.3 \sim 0.5 c_R$. To determine the constants M and v_m for the material AISI 4340 VAR steel used in the experimental observations, we compare the curves given by equation (4.4.8) to the experimental measurements obtained by Rosakis *et al.* (1984) and by Zehnder and Rosakis (1990). These experimental measurements are shown here in FIGURE 4.5. In this figure, the circles represent the value obtained from the experiments, and the various lines are obtained from (4.4.8) for different value of M. From this figure, we can see that $v_m \sim 0.34 c_s$. In the same figure, it seems that $M = 10$ is best fitting for the experimental values. However, one should notice that the material that the experiment used is 4340 steel (see Rosakis *et al.*, 1984; Zehnder and Rosakis, 1990) which is slightly different from the material used in Prakash and Clifton (1992). The heat treatment processes are also different for these two materials. As a result, the material used by Prakash and Clifton (1992) is more brittle than the material used in Zehnder and Rosakis (1990). Another reason for this conclusion is that the loading rates in the experiments by Prakash and Clifton (1992) are much higher than the rate in Zehnder and Rosakis (1990). Under high strain rate, material will also become more brittle. Previous experiments have shown that the more brittle the material is, the more abrupt the $K_I^d - v$ curve becomes. This suggests that larger value of M should be used to simulate the experimental observations in Prakash and Clifton (1992).

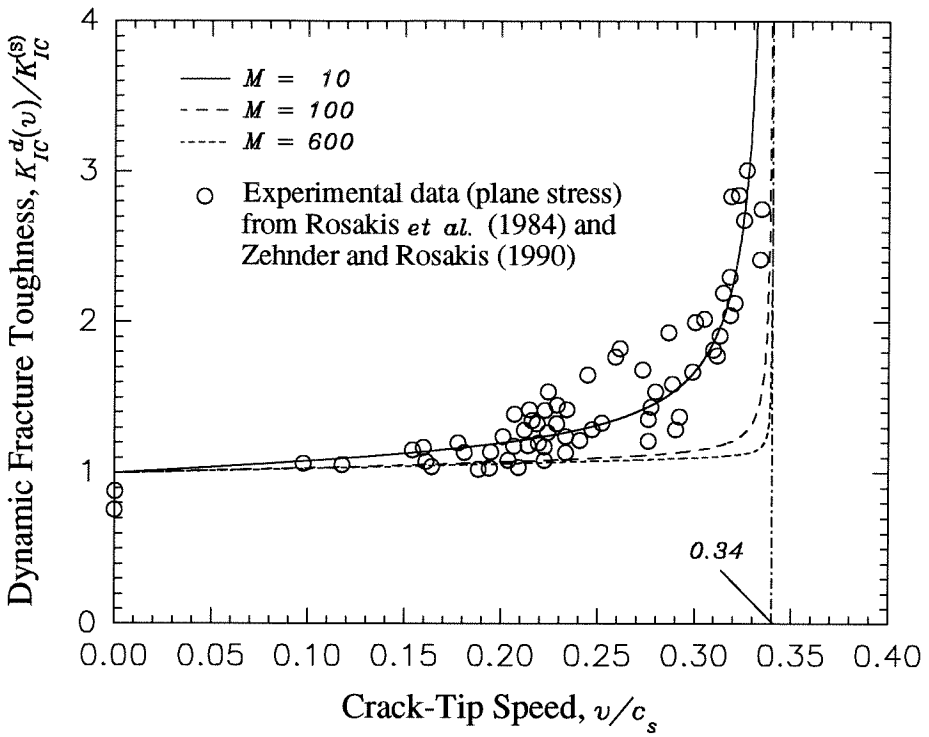

Figure 4.5: Comparison of the relationship between the dynamic fracture toughness and the crack-tip speed. Different lines represent the prediction using equation (4.4.8) and circles are the experimental results obtained by Rosakis *et al.* (1984) and Zehnder and Rosakis (1990).

By substituting the expressions for $k(v)$ and $f(v)$ into the crack-tip equation of motion (4.4.6), we get

$$1 + \frac{1}{M} \tan\left(\frac{\pi}{2} \cdot \frac{v}{v_m}\right) - \alpha\left(1 - \frac{v}{c_R}\right)\sqrt{\frac{t}{\tau}} = 0 \,, \tag{4.4.9}$$

from which the time history $v(t)$ of the crack-tip speed can be obtained. Once the crack-tip speed history is determined, the crack-tip acceleration can also be obtained by differentiating the crack-tip speed profile. From equation (4.4.9), we can express the crack-tip acceleration in terms of crack-tip velocity and time t as:

$$\dot{v}(t) = -\frac{\alpha c_R}{2\tau} \cdot \frac{g(v)}{\sqrt{t/\tau}} \,, \tag{4.4.10}$$

where

$$g(v) = \frac{\left\{1 + \left(\frac{\pi}{2} \cdot \frac{v}{v_m}\right)^2\right\}\left(1 - \frac{v}{c_R}\right)^2}{\frac{\pi}{2M} \cdot \frac{c_R}{v_m}\left(1 - \frac{v}{c_R}\right) + \left\{1 + \frac{1}{M}\tan\left(\frac{\pi}{2} \cdot \frac{v}{v_m}\right)\right\}\left\{1 + \left(\frac{\pi}{2} \cdot \frac{v}{v_m}\right)^2\right\}} \ .$$

Freund (1973) has shown that for an unbounded body under time-independent loading conditions, the dynamic stress intensity factor at the running crack-tip can be expressed as a universal function of instantaneous crack-tip speed times the equilibrium stress intensity factor for the given applied loading and the instantaneous amount of crack growth. Therefore, for the problem we considered in Chapter 3, even when the crack propagates with nonuniform velocity, the dynamic stress intensity factor $K_I^d(t)$ is still given by equation (4.4.3), where the velocity v takes the instantaneous value at each instant of time. As a result, the time derivative of the dynamic stress intensity factor under this circumstance will be expressed in terms of the crack-tip speed, acceleration, and the time t as:

$$\dot{K}_I^d(t) = K_I^d(t)\left\{\frac{1}{2t} + \frac{k'(v)}{k(v)}\dot{v}(t)\right\} \ . \tag{4.4.11}$$

By applying the crack growth criterion (4.4.2), we have been able to determine the time histories of crack-tip speed, crack-tip acceleration, and the time derivative of the dynamic stress intensity factor. Consequently, the quantities that appear in the higher order transient asymptotic representation of the particle velocity field surrounding the moving crack-tip, i.e., $D_{l,s}^1\{A_0(t)\}$ and $B_{l,s}(t)$ in equation (4.3.4), can be determined as well. However, the explicit expression for the higher order coefficient $A_2(t)$ is obtained under the condition that the crack propagates with a constant velocity (see Chapter 3). Nevertheless, if we expand the field for the stationary crack subjected to stress pulse (superposition of problems A and B in Chapter 3) to the third term and compare this term to our expression for $A_2(t)$, we found that $A_2(t)$ has the same property as the dynamic stress intensity factor, i.e., $A_2(t)$ can be expressed as a

function of instantaneous crack-tip speed times the equilibrium value of the third term for the given applied loading and the instantaneous amount of crack growth. Based on this observation, we conclude that for a crack propagating with a nonuniform speed, the coefficient of higher order term, $A_2(t)$, has the same form as that for constant velocity except that the crack-tip speed takes the instantaneous value at each instant of time.

The initiation and propagation of a semi-infinite crack subjected to the stress wave loading conditions can be described by FIGURE 4.6. In FIGURE 4.6, the solid

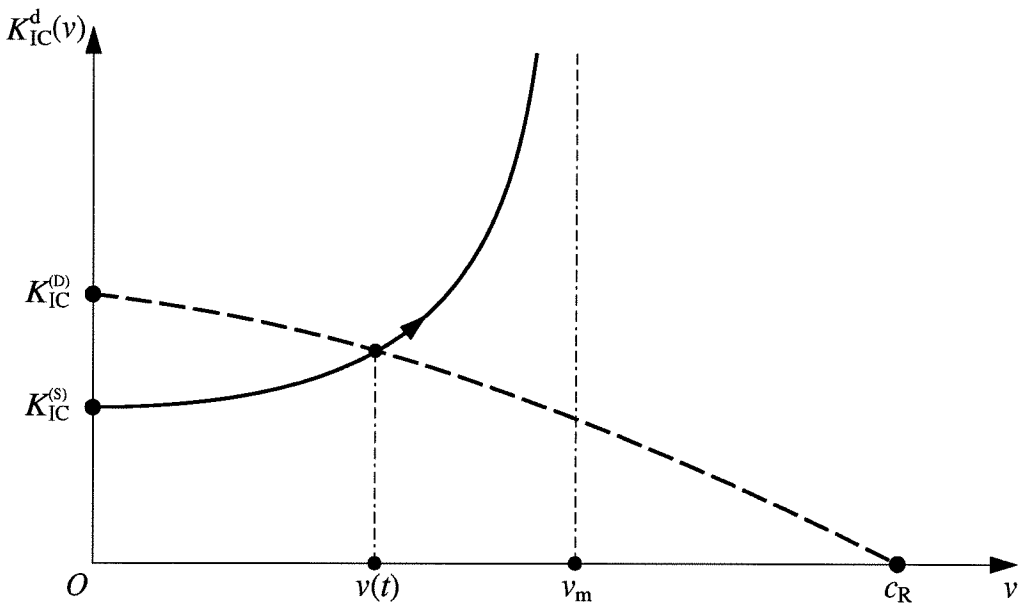

Figure 4.6: Schematic description of dynamic crack initiation and propagation.

line represents the relation between the dynamic fracture toughness K^d_{IC} and the crack-tip propagating speed $v(t)$. The intersection of this curve to the vertical axis is the value of the critical stress intensity factor of crack initiation under quasi-static conditions, i.e., $K^{(S)}_{IC}$. Also, this curve asymptotically approaches the vertical line denoting the terminal speed of the crack-tip in this material. In the same figure, the dashed line gives the relationship between the dynamic stress intensity factor $K^d_I(t)$ at

the moving crack-tip and the crack-tip speed $v(t)$. The point corresponding to $v = 0$ provides the value of the dynamic stress intensity factor at the stationary crack-tip under stress wave loading. As $v = c_R$, the dynamic stress intensity factor of the moving crack will be zero. At the time $t = \tau$, the initial crack-tip speed and the new value of the dynamic stress intensity factor just after initiation are determined by the intersection point of the solid and dashed lines. As we can see from this geometrical construction, the dynamic stress intensity factor suffers a drop relative to its value immediately before initiation. For this particular loading condition and specimen configuration, the initial crack-tip speed and the drop of the dynamic stress intensity factor are completely determined by the shape of the solid line. In other words, they are determined by the material property described by the crack growth criterion. After crack initiation, since $K_I^d(t)$ is an increasing function of time t, the intersection point will move upward along the crack growth criterion curve. The crack-tip speed will increase as well and finally approach the terminal speed. In FIGURE 4.7, the profiles of the crack-tip speed and crack-tip acceleration are plotted. Here, we have chosen $\alpha = 2.0$ and $M = 600$ to simulate a brittle material experiencing high strain rate, and as the result of Zehnder and Rosakis (1990) suggested, we have also chosen that the terminal speed $v_m = 0.34c_s$.

By using the crack-tip velocity and acceleration histories given in FIGURE 4.7 which results from imposing the crack growth criterion depicted in FIGURE 4.5, and by using the expressions for $A_2(t)$ obtained in Chapter 3, we simulate the particle velocity at the monitoring point D again for the experiment presented in FIGURE 4.3. This simulation is compared to the experimental results in FIGURE 4.8. In this figure, we can see that the theoretical prediction is much closer to the experimental measurement than the theoretical prediction obtained under the assumption of constant crack-tip speed. By imposing the crack growth criterion, the crack-tip first jumps to a relatively low initiation velocity and then quickly approaches its terminal speed. As a result,

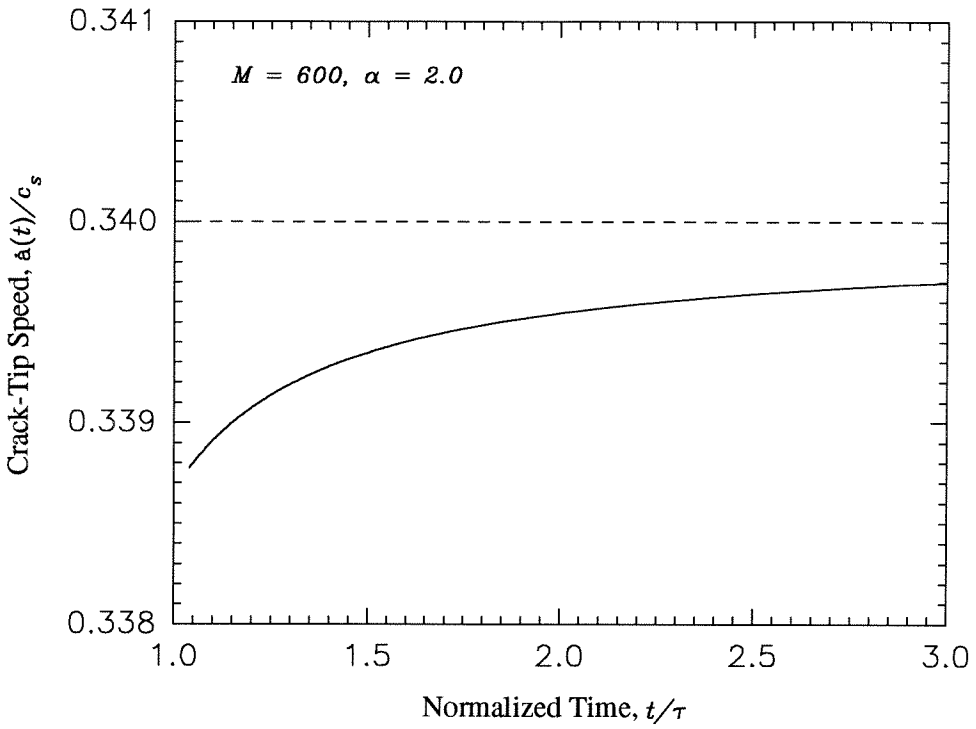

(a)

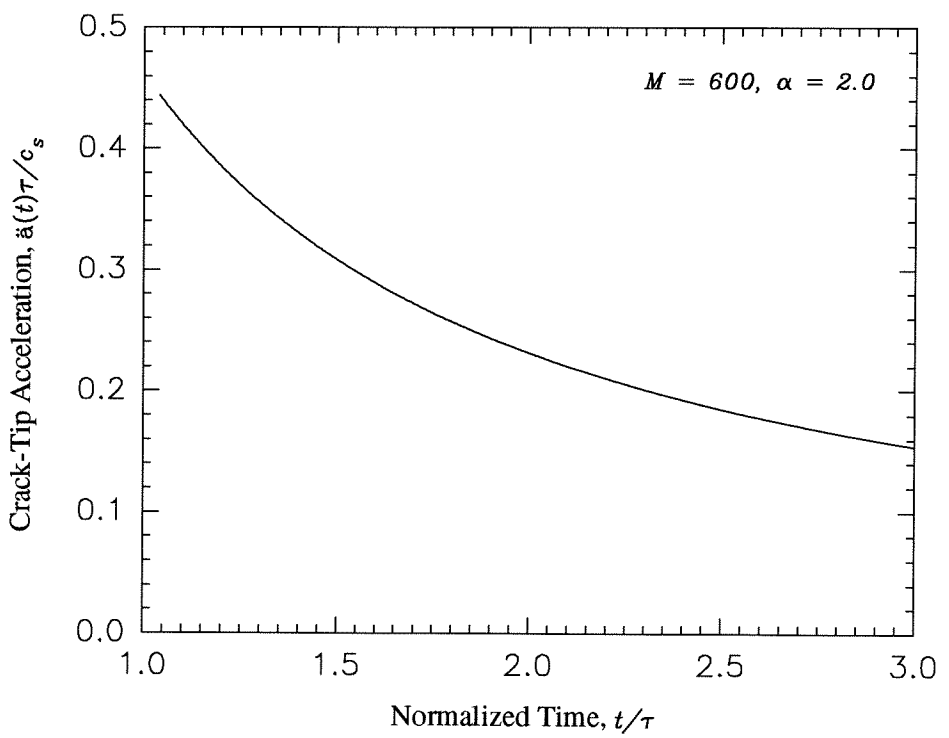

(b)

Figure 4.7: Time histories of the crack-tip speed (a), and crack-tip acceleration (b), where $\alpha = 2.0$ and $M = 600$ have been chosen.

the particle velocity at the observation point D also jumps to a high value at the moment of crack initiation at first, and then quickly decreases to the average value of the particle velocity measured from the experiment at that point. Notice that even though the theoretical prediction by our current higher order transient asymptotic analysis has captured the essential feature of the experimental observation, the decay of the particle velocity obtained from calculation is not as fast as the experimental result. The reason for this difference is probably due to the fact that the measuring point is relatively far away from the crack-tip, therefore even higher order terms in the asymptotic expansion need to be used.

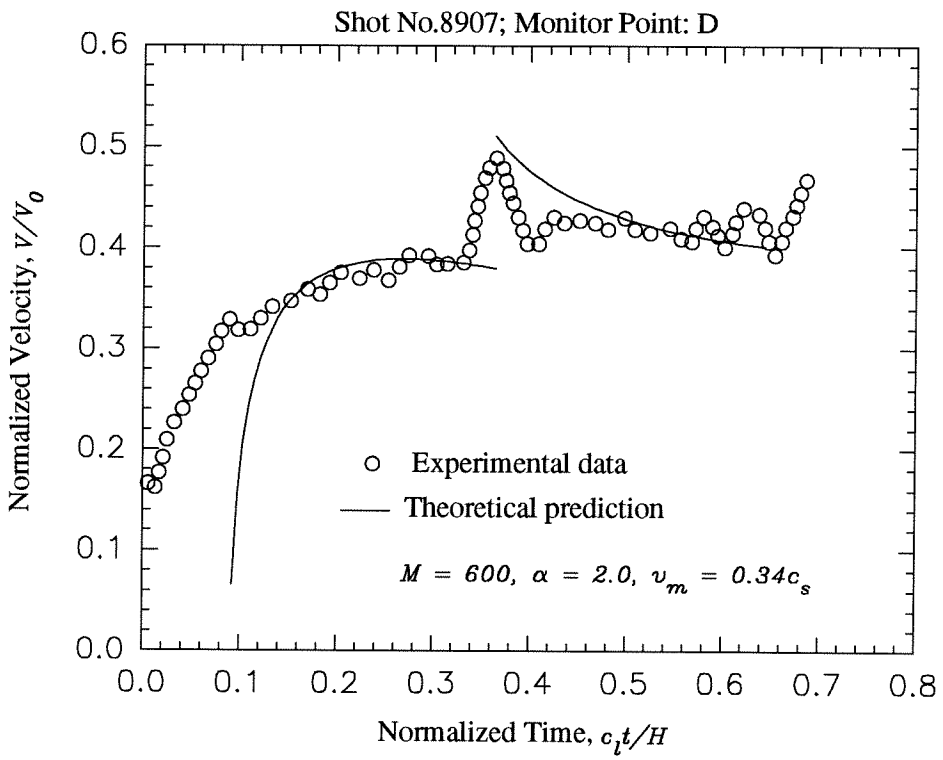

Figure 4.8: Analytical simulation of the experimental measurement at monitoring point D by Prakash and Clifton (1992), shot No. 8907. Before crack initiation, full field expression for the particle velocity is used. After crack initiation, three-term fully transient asymptotic representation given in equation (4.3.2) has been used.

In the theoretical simulations in the present and the previous sections, we choose to compare the theoretical prediction and the experimental observation from point

D only. For other points, like points A, B, and C in FIGURE 4.3, the results from theoretical calculation and experimental measurements deviate progressively as the distance from point D is increased. In particular, the further the horizontal distance away from the crack-tip becomes, the larger is the deviation between the theoretical prediction and the experimental measurement. The explanation for this deviation is that when the stress wave diffracts at the stationary crack-tip, or emanates from the moving crack-tip, cylindrical waves radiate from the crack-tip and propagate towards the boundaries of the specimen. As these waves reach the boundary, various kinds of waves are generated from the reflection of the incident wave. If the incident cylindrical wave is longitudinal or transverse, both longitudinal and shear type of reflection waves are generated depending on the incident angle. At the same time, surface waves are generated as well. So the effects of these reflection waves influence the experimental measurements. However, in our mathematical model, the specimen is considered to be unbounded and the theoretical prediction cannot include the free boundary reflection effects. The only point that an accurate simulation can be expected from the theoretical model, is the point just below the crack-tip on the boundary (see FIGURE 4.1). At this point, the reflection effect can be accounted for, by multiplying the theoretical value by a factor of two. Unfortunately, there is no further experimental data from such points available for our simulation. As a result, a complete numerical simulation of the experiment is necessary. In such a simulation, the data obtained from points just below the crack-tip can be compared with our theoretical predictions.

4.5 Discussion and conclusions

In this chapter, the experimental observations made by Prakash and Clifton (1992) are reinterpreted on the basis of the newly developed higher order transient asymptotic analysis by Freund and Rosakis (1992) and by Liu and Rosakis (1992). In this

transient asymptotic representation, the leading term in the expansion of the local stress field is the familiar stress intensity factor distribution, that is, it is square root singular in the radial distance from the moving crack-tip and its coefficient is proportional to the instantaneous value of the dynamic stress intensity factor, $K_I^d(t)$. The higher order terms, on the other hand, take into account the recent past history of the stress intensity factor and crack motion. Therefore, the transient nature of the local field is reflected in these higher order terms. It should be noted that from the view point of asymptotic expansion, the coefficient of each term of the asymptotic expansion carries different information about the deformation field. The coefficient of the first term, $K_I^d(t)$, purely represents the intensity or the amplitude of the local stress and deformation fields, and this coefficient depends on the overall specimen configuration and loading condition. The coefficient of the second term, $A_1(t)$, also possesses these properties. Inside the coefficients of the higher order terms, however, more information will be present. One part of the information, like $A_2(t)$, etc. still relates to the overall specimen configuration and loading condition. The other part will relate to the crack-tip acceleration, time derivatives of the coefficients of the lower order terms, and if the crack propagates along a curved path, as being shown in Liu and Rosakis (1992) and in Chapter 2, it also relates to the shape of the crack trajectory. At this point, we have clearly known the asymptotic structure of the deformation field near a transiently moving crack-tip. Because each term in the expansion is associated with certain function of the radial distance from the crack-tip, therefore, in order to correctly interpret the observation data in an experimental investigation, either we can change the observation position continuously so that we can pick up one specific information we are interested in, or we cannot choose the observation point freely so that we have to resolve various information from the data we get. The dependence of the leading term on the radial distance is $r^{-1/2}$, so the effects of this term are restrained inside the region very close to the moving crack-tip. However, the dependence of the higher order terms on the radial distance is $r^{1/2}$ or higher.

As a result, as the observation position is relatively far away from the crack-tip, the effects of the higher order terms will become profound and cannot be neglected in any attempt to interpret data obtained at that position.

The experimental configuration developed by Ravichandran and Clifton (1989) and by Prakash and Clifton (1992) has the great advantage of being correlated to the existing analytical results for two-dimensional dynamic fracture problems. However, the technique utilized by Ravichandran and Clifton (1989) and by Prakash and Clifton (1992) cannot access the crack-tip, so that the direct information about the crack-tip speed and the intensity or the amplitude of the local stress and deformation fields can only be inferred from the information obtained at positions far away from the moving crack-tip. Nevertheless, this experimental configuration is still a very good candidate for the study of dynamic fracture behavior of materials under very high loading rates while the transient effects associated with the crack growth should be taken into account in the interpretation.

In Chapter 3, the mathematical problem by which the experimental and loading configuration can be modeled, is revisited, and the full field solution for the stresses is obtained. Meanwhile, the coefficients that appear in the transient asymptotic representation of the deformation field are also be obtained for the situation of crack propagating with constant speed. By including the higher order terms in the theoretical simulation, the result agrees fairly well with the experimental observations (see FIGURE 4.4). We can conclude from FIGURE 4.4 that the near tip deformation field is well described by the higher order transient asymptotic expansion, at least qualitatively. Since the experimental technique cannot provide the complete histories of the crack motion, we have to suppose that the crack growth is governed by a criterion which relates the critical dynamic stress intensity factor and the moving speed of the crack-tip. The mathematical form of this criterion is motivated by previous experimental measurements. Through solving the crack-tip equation of motion, the

history of crack-tip motion can be determined, so are those quantities related to the transient effects. When all of these transient effects related quantities are cooperated into the asymptotic representation of the particle velocity near the crack-tip, the simulation has become very close to the experimental observation. The meaning of this simulation has two folds. One shows again the necessity of applying the higher order asymptotic expansion which includes the transient history of the crack growth to describe the near tip deformation fields. The other one shows that the crack growth is indeed controlled by a material related criterion. This criterion gives the unique relationship between the dynamic fracture toughness K_{IC}^d and the crack-tip speed v. The existence of such a criterion in this simulation is supported by using the higher order transient expansion, while the lack of the uniqueness of a relationship between K_{IC}^d and v has been observed when the K_I^d-dominant assumption or the steady state higher order expansion is used (see Kobayashi and Mall, 1978, and Ravi-Chandar and Knauss, 1984). Therefore, the lack of the uniqueness of correspondence between K_{IC}^d and v may be attributed by the fact that there is no K_I^d-dominant deformation field surrounding the crack-tip close to the crack initiation as has been prevailed in Chapter 3 and the study by Ma and Freund (1986).

However, some difficulties still exist preventing the complete simulation of the experimental observations by using the existing analytical solutions. This is due to the presence of free boundary in the experimental configuration. Complicated wave reflections will occur when the stress waves emanated from the stationary or the moving crack-tip reach the boundary. These reflections impose new difficulty for obtaining complete analytical solution. As a result, in order to deepen the understanding of the mechanism of dynamic crack initiation and growth, detailed numerical simulation should be performed.

Chapter 5

Interpretation of Optical Caustics in the Presence of Non-Uniform Crack-Tip Motion Histories

5.1 Introduction

In experimental investigation of dynamic fracture, the inherent time dependence of crack propagating process requires that many sequential measurements of the field quantities be made in an extremely short time, and these measurements should not interfere with the crack propagating process itself. Therefore, most experimental techniques for measuring crack-tip stress and deformation fields during rapid fracture are based on optics. Optical techniques have a number of advantages for dynamic, local crack-tip measurements. The specimen is observed continuously and crack paths need not be known prior. There is no coupling between the optical and mechanical processes, i.e., the method of measurement does not interfere with the process being examined. The time response of the optical techniques is virtually instantaneous compared to the time scale of the mechanical response. Finally, due to the local nature of the measurements, optical methods can be expected to be sensitive enough to detect local events such as the onset of crack initiation or arrest.

In the past few decades, a number of optical methods based on the principles

of light wave interference have been introduced for the study of stress and strain fields. Such techniques include photoelasticity, moiré deflectometry, coherent gradient sensing (CGS), Twyman-Green interferometry, optical caustics, etc. However, each optical method is characterized by a different set of restrictions in its applicability. The application of photoelasticity, for example, is confined to transparent materials, or to opaque materials with transparent coatings. Other methods require complicated optical arrangements, or sophisticated image processing systems. As a result, they suffer from severe light limitations and are not suitable for high-speed photography applications.

The optical method of caustics, a technique based on geometrical optics, has several advantages over the other optical methods which are mainly related to its simplicity. It requires a simple optical set-up which does not involve the use of diffraction optics. It can be used easily either in transmission or in reflection arrangements. Data analysis is simple and does not require the use of complicated image processing techniques. The simplicity of the technique makes it an ideal candidate for high-speed photography applications. In particular, the fact that the physical principle of caustics does not hinge on the availability of a coherent, monochromatic light source, has allowed for the use of high-speed camera systems which utilize white light illumination such as the Cranz-Schardin type cameras. In addition, the lack of complicated optical components, such as diffraction gratings, beam splitters, etc., in a caustic set-up ensures minimal light intensity losses which are crucial for successful high-speed photography, especially when the exposure time is in the order of nanoseconds.

The method of caustics has been initially introduced by Schardin (1959) and Manogg (1964). Manogg used caustics in a transmission arrangement and gave the first quantitative analysis. He was able to record changes in the optical path of rays traveling through transparent plate at the vicinity of a crack-tip, where the elastic stress field introduces changes in the refractive index as well as changes of plate

thickness. The resulting difference in optical path produces a caustic pattern on a screen placed behind the specimen. He showed that the geometrical characteristics of the caustic depend on the nature and intensity of the crack-tip singularity and was able to measure the intensity of the near-tip stress field.

After Manogg's work, the method of caustics was extensively used by Theocaris, who was also the first one to use this method in a reflection arrangement (Theocaris, 1970 and 1971). Later, Theocaris and Gdoutos (1974) applied the method of caustics in reflection to experimentally examine the deformation fields near the tips of stationary cracks in metal plates, and this is the first application of the method to the investigation of fracture in metals. Unlike the method of photoelasticity which gives the information of the distribution of the maximum shear stress in a domain, the method of caustics is directly related to the in-plane components of the *gradient* of the first stress invariant, so it is much more sensitive to the singular stress distribution than photoelasticity. Due to this advantage, the method of caustics is a very good candidate to be applied to investigating the phenomenon of stress concentration at any singular region, especially, at the vicinity of the crack-tip. Since the beginning of 1970's, the optical method of caustics has been developed into a successful experimental stress analysis method and found wide applications, especially for the analysis of dynamic fracture mechanics problems.

There are two sets of simplifying assumptions that are customarily made in the various applications of the method of caustics. One regards the analysis of the optical process (transmission or reflection) and the other regards the nature of the mechanical fields under study. In each of them, assumptions and simplifications are made in order to interpret the caustic pattern quantitatively. The limitations introduced by the simplifications in the optical analysis of the method of caustics as well as an exact geometrical optics interpretation of the technique were thoroughly discussed by Rosakis and Zehnder (1985) and Rosakis (1993). However the corresponding issue

regarding the assumptions made about the mechanical fields under study is more complicated and troublesome.

In linearly elastic dynamic fracture mechanics, the method of caustics was first used in experiments involving very rapid crack propagation and stress wave loading by Kalthoff *et al.* (1976), Katsamanis *et al.* (1977), Theocaris (1978), and Goldsmith and Katsamanis (1979). In each case, it was assumed that the elastic stress field at the vicinity of a rapidly propagating crack-tip has precisely the same spatial variation as the elastic stress field near the tip of a stationary crack. That is, the influence of inertial effects on the spatial distribution of the crack-tip field was not taken into account. Kalthoff *et al.* (1978) introduced an approximate correction factor to account for the error introduced when the static local field is used in the interpretation of caustic patterns. Rosakis (1980) presented the exact equations of the caustic envelope for elastic specimen containing a rapidly growing crack. He also presented the caustic equations for the case of mixed mode plane stress crack propagation. The above analyses all assume that the deformation field near the propagating crack-tip is K_I^d-dominant. This means that the stress field at a finite region near the crack-tip can be approximated accurately by the elastodynamic asymptotic singular solution (to within some acceptable error). Based on this assumption, many experimental investigations of the dynamic crack initiation, propagation and arrest have been carried out since then.

Recent experimental investigation by Krishnaswamy and Rosakis (1991) and analytical results by Freund and Rosakis (1990, 1992) have found that the analysis of caustics based on K_I^d-dominance may not always adequately characterize the behavior of the deformation field at the vicinity of a transiently propagating dynamic crack-tip. Indeed the assumption of K_I^d-dominance is often violated during dynamic crack growth. By relaxing the assumption of K_I^d-dominance, Freund and Rosakis (1992) have suggested that under fairly severe transient conditions, a representation

of the crack-tip field in the form of a higher order expansion (involving time derivatives of crack-tip velocity and stress intensity factor) should be used to interpret the experimental observations.

In this chapter, we will re-examine the optical method of caustics by considering non-uniform crack growth histories. In Section 5.2, the formation of the caustic image is briefly reviewed. In the following section, the exact mapping equations of caustics and the initial curve equation are derived for a non-uniformly propagating mode-I crack. This derivation is based on the theoretical results of Freund and Rosakis (1990, 1992), Rosakis *et al.* (1991), and the results given in Chapter 2, which allow both the crack-tip speed and the dynamic stress intensity factor to be arbitrary differentiable functions of time. Then the explicit relation between the dynamic stress intensity factor, $K_I^d(t)$, and two geometrical dimensions of the caustic pattern, is established. It is shown that the classical analysis of caustics is a special case of this result under the condition of strict K_I^d-dominance. In Section 5.4, a multi-point measurement technique is established to accurately measure the two geometrical dimensions used in the transient interpretation of the caustic pattern. In order to verify the accuracy of the analysis developed in Sections 5.3 and 5.4, the Broberg problem is considered as an example problem of transient crack growth in Section 5.5. The exact caustic patterns are generated by using the solution of Broberg problem. These patterns are subsequently analyzed by using both the classical analysis and the newly modified method proposed in the previous sections. The results show that the value of the dynamic stress intensity factor obtained by the modified method agrees remarkably well with the exact analytical value while large errors are introduced when the classical analysis (K_I^d-dominance) of the method of caustics is used. In the final section, some comments and discussions are made.

5.2 Method of caustics

5.2.1 Mapping equations

Consider a plate specimen of uniform thickness, h, in the undeformed state. Let its mid-plane occupy the (x_1, x_2) plane of an orthonormal Cartesian coordinate system. As the specimen is subjected to applied loads, non-uniform gradients in the optical path of light transmitted through it, or reflected from its surface, are generated. For a transparent specimen, the gradients in the optical path are due to non-uniform changes in the thickness of the plate and also due to stress induced gradients in the refractive index of the material in the specimen interior. For an opaque specimen, the gradients in the optical path are due to non-uniform surface elevations of the plate.

Consider further a collimated beam of light traveling in the x_3-direction, normally incident on the plate, as illustrated in FIGURE 5.1. Under certain stress gradients, the

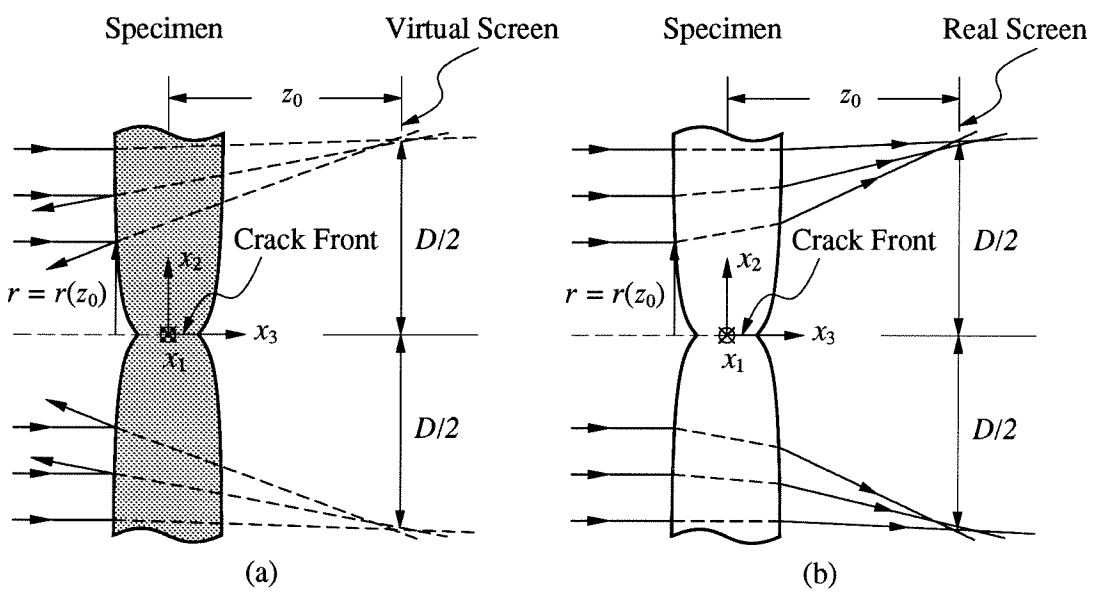

Figure 5.1: Caustic formation in (a) reflection, (b) transmission.

reflected or refracted rays will deviate from parallelism and form an envelope in the

form of a three-dimensional surface in space. This surface, which is called the *caustic surface*, is the locus of points of maximum luminosity in the reflected or transmitted light fields.

The deflected rays are tangent to the caustic surface. If a screen is positioned parallel to the $x_3 = 0$ plane so that it intersects the caustic surface, then the cross-section of the surface can be observed on the screen as a bright curve (the *caustic curve*) bordering a dark region (the *shadow spot*). Suppose that the incident ray, which is reflected from or transmitted through point $p(x_1, x_2)$ on the specimen, intersects the screen at the image point $P(X_1, X_2)$. The (X_1, X_2) coordinate system is identical to the (x_1, x_2) system, except that the origin of the former has been translated by a distance z_0 to the screen (z_0 can be either positive or negative). The position of the image point P will depend on the gradient of the optical path change $\Delta S(x_1, x_2)$ introduced by the specimen as well as on the distance z_0 and is given by (Rosakis and Zehnder, 1985):

$$\underset{\sim}{X} = \underset{\sim}{x} + z_0 \nabla(\Delta S(x_1, x_2)) \ , \tag{5.2.1}$$

where $\underset{\sim}{X} = X_\alpha \underset{\sim}{e_\alpha}$, $\underset{\sim}{x} = x_\alpha \underset{\sim}{e_\alpha}$, $\alpha \in \{1, 2\}$, $\underset{\sim}{e_\alpha}$ denote unit vectors, and '∇' denotes the two-dimensional gradient operator. Relation (5.2.1) describes the mapping of the points on the specimen onto the points on the screen.

5.2.2 The initial curve and its significance

If the screen intersects the caustic surface, then the resulting caustic curve on the screen is the optical mapping of the locus of points for which the determinant of the Jacobian matrix of mapping equation (5.2.1) must vanish on the specimen, i.e.,

$$J(x_1, x_2; z_0) = \det \left\{ X_{\alpha/\beta}(x_1, x_2, z_0) \right\} = \det \left\{ \delta_{\alpha\beta} + z_0 (\Delta S)_{,\alpha\beta} \right\} = 0 \ . \tag{5.2.2}$$

Equation (5.2.2) is a necessary and sufficient condition for the existence of a caustic curve. The locus of points on the reference plane $(x_1, x_2, x_3 = 0)$ for which the

Jacobian vanishes is called the *initial curve* whose geometry is described by equation (5.2.2). All points on the initial curve map onto the caustic curve. In addition, all points inside and outside this curve map *outside* the caustic (Rosakis and Zehnder, 1985). Since the light transmitted through or reflected from both the interior and the exterior of the initial curve maps only outside the caustic, the area within the caustic remains dark and is customarily referred to as the shadow spot. Also since the light that forms the caustic curve originates from the initial curve, essential information conveyed by the caustic comes from that curve only.

Equation (5.2.2), defining the initial curve, depends parametrically on z_0. Thus, by varying z_0, we may vary the initial curve position. If z_0 is large, the initial curve will be far from the crack-tip. If z_0 is small, the initial curve will be close to the crack-tip. Variation of z_0 can easily be achieved experimentally by simply varying the focal plane of the recording camera system. This is an essential property of the method of caustics, and it can be utilized to "scan" the near-tip region to obtain information regarding the nature of the deformation field at different distances from the crack-tip. This property has been used by Krishnaswamy and Rosakis (1991) in the bifocal caustic technique to study the extent of K_I^d-dominant region. For the present work, we require that the initial curve is located outside the near-tip plastic and three-dimensional zones.

5.3 Interpretation of caustic patterns in the presence of transient effects

5.3.1 Caustics generated by non-uniformly propagating cracks

For opaque specimens, caustics are formed by the reflection of light rays from the polished specimen surface. The shape of the caustic curve depends on the near-tip normal displacement u_3 of the plate surface, initially at $x_3 = h/2$, where h is the undeformed specimen thickness. For transparent specimens the optical path change ΔS depends on both local changes in thickness and on local changes in refractive index. The change in the refractive index Δn is given by the Maxwell relation,

$$\Delta n(x_1, x_2) = D_1 \{\sigma_{11} + \sigma_{22} + \sigma_{33}\} \ , \tag{5.3.1}$$

where D_1 is the stress optic constant and σ_{ij} are the nominal stress components. The above relation is strictly true for mechanically and optically isotropic linear elastic solids.

For a cracked linear elastic plate of uniform thickness and finite in-plane dimensions, the optical path difference ΔS, in general will depend on the details of the three-dimensional elastostatic or elastodynamic stress state that would exist at the vicinity of the crack-tip. This will be a function of the applied loading, in-plane dimensions and thickness of the specimen. In the present work, we assume that the two-dimensional asymptotic analyses may provide adequate approximation for $\Delta S(x_1, x_2)$. In particular, it has been suggested that conditions of generalized plane stress will dominate in thin cracked plates at distances from the crack-tip larger than half of the specimen thickness (Rosakis and Ravi-Chandar, 1986; Yang and Freund, 1985), which implies that if the initial curve is kept outside the near-tip three dimensional zone, the resulting caustic could be interpreted on the basis of a generalized

plane stress analysis. Furthermore, in this chapter, we also assume that the initial curve is always kept outside the plastic and the fracture process zones, and this enables that the asymptotic elastic analysis can be employed to interpret the caustic pattern.

Under the aforementioned conditions, the optical path difference $\Delta S(x_1, x_2)$ will be (Rosakis, 1993)

$$\Delta S(x_1, x_2) = ch\left\{\hat{\sigma}_{11}(x_1, x_2) + \hat{\sigma}_{22}(x_1, x_2)\right\} \ , \tag{5.3.2}$$

where

$$c = \begin{cases} \left(D_1 - \dfrac{\nu}{E}(n-1)\right) = c_\sigma \ , & \text{for transmission} \\ \dfrac{\nu}{E} \ , & \text{for reflection} \end{cases}$$

and E and ν are the Young's modulus and Poisson's ratio of the material, respectively, c_σ is called the stress-optical coefficient, and $\hat{\sigma}_{11}$ and $\hat{\sigma}_{22}$ are thickness averages of the stress components in the solid. These stress components will be provided by the generalized plane stress solution of the elastostatic or elastodynamic problem under investigation.

Consider a planar, mode-I crack that grows through a two-dimensional, homogeneous, isotropic, linearly elastic solid, with a non-uniform speed $v(t)$, along the positive x_1-direction. Let (ξ_1, ξ_2) be the coordinate system which translates with the moving crack-tip and the ξ_1-axis coincides with the crack propagating direction. The asymptotic stress field around the tip of a non-uniformly propagating dynamic mode-I crack has been presented by Rosakis *et al.* (1991), which can also be obtained from the stress field given in Chapter 2 by imposing the conditions of mode-I straight crack. By using the notations defined in Chapter 2, for generalized plane stress, the thickness averaged sum of the two normal stress components is

$$\left.\begin{aligned}
&\frac{\hat{\sigma}_{11}+\hat{\sigma}_{22}}{2\rho(c_l^2-c_s^2)} = \frac{3v^2}{4c_l^2}\hat{A}_0(t)r_l^{-1/2}\cos\frac{\theta_l}{2} + \frac{2v^2}{c_l^2}\hat{A}_1(t) \\
&+\left\{\frac{15v^2}{4c_l^2}\hat{A}_2(t)\cos\frac{\theta_l}{2} + D_l^1\{A_0(t)\}\left[\left(1-\frac{v^2}{2c_l^2}\right)\cos\frac{\theta_l}{2} + \frac{v^2}{8c_l^2}\cos\frac{3\theta_l}{2}\right]\right. \\
&\left.+\frac{1}{2}B_l(t)\left[\left(1-\frac{v^2}{c_l^2}\right)\cos\frac{\theta_l}{2} - \left(1-\frac{5v^2}{8c_l^2}\right)\cos\frac{3\theta_l}{2} + \frac{v^2}{16c_l^2}\cos\frac{7\theta_l}{2}\right]\right\} r_l^{1/2} \\
&+O(r_l)
\end{aligned}\right\}, \quad (5.3.3)$$

where in terms of the dynamic stress intensity factor $K_I^d(t)$,

$$\begin{aligned}
\hat{A}_0(t) &= \frac{4}{3\mu\sqrt{2\pi}}\frac{1+\alpha_s^2}{D(v)}K_I^d(t)\,, \\
D_l^1\{A_0(t)\} &= -\frac{4v^{\frac{1}{2}}(t)}{\mu\sqrt{2\pi}\alpha_l^2 c_l^2}\frac{\mathrm{d}}{\mathrm{d}t}\left\{v^{\frac{1}{2}}(t)\frac{1+\alpha_s^2}{D(v)}K_I^d(t)\right\}\,, \\
B_l(t) &= \frac{2v^2(t)\dot{v}(t)}{\mu\sqrt{2\pi}\alpha_l^4 c_l^4}\frac{1+\alpha_s^2}{D(v)}K_I^d(t)\,, \\
D(v) &= 4\alpha_l\alpha_s - (1+\alpha_s^2)^2\,,
\end{aligned}$$

and ρ and μ are the mass density and the shear modulus of the elastic material, respectively. Notice that for making the notation short, here the undetermined functions of time have been redefined as $\hat{A}_0(t)$, $\hat{A}_1(t)$, and $\hat{A}_2(t)$, where $\hat{A}_0(t)$ can be directly related to the dynamic stress intensity factor $K_I^d(t)$.

By substituting the above expression for the first stress invariant into the optical path difference relation (5.3.2), the mapping equation (5.2.1) becomes

$$\left.\begin{aligned}
X_1 &= r_l\cos\theta_l + z_0 ch\rho(c_l^2-c_s^2)\left[\frac{3v^2}{4c_l^2}\hat{A}_0(t)r_l^{-3/2}\cos\frac{3\theta_l}{2}\right. \\
&-\left\{D_l^1\{A_0(t)\}\left[\left(1-\frac{v^2}{4c_l^2}\right)\cos\frac{\theta_l}{2} - \frac{v^2}{8c_l^2}\cos\frac{5\theta_l}{2}\right]\right. \\
&-\frac{1}{2}B_l(t)\left[\left(1-\frac{v^2}{4c_l^2}\right)\cos\frac{\theta_l}{2} - \left(1-\frac{3v^2}{8c_l^2}\right)\cos\frac{5\theta_l}{2} + \frac{3v^2}{16c_l^2}\cos\frac{9\theta_l}{2}\right] \\
&\left.\left.+\frac{15v^2}{4c_l^2}\hat{A}_2(t)\cos\frac{\theta_l}{2}\right\} r_l^{-1/2}\right]
\end{aligned}\right\}, \quad (5.3.4)$$

and

$$X_2 = \frac{r_l \sin\theta_l}{\alpha_l} + \alpha_l z_0 ch\rho(c_l^2 - c_s^2)\left[\frac{3v^2}{4c_l^2}\hat{A}_0(t) r_l^{-3/2}\sin\frac{3\theta_l}{2}\right.$$
$$- \left\{D_l^1\{A_0(t)\}\left[\left(1-\frac{3v^2}{4c_l^2}\right)\sin\frac{\theta_l}{2} - \frac{v^2}{8c_l^2}\sin\frac{5\theta_l}{2}\right]\right.$$
$$+ \frac{1}{2}B_l(t)\left[3\left(1-\frac{3v^2}{4c_l^2}\right)\sin\frac{\theta_l}{2} + \left(1-\frac{7v^2}{8c_l^2}\right)\sin\frac{5\theta_l}{2} - \frac{3v^2}{16c_l^2}\sin\frac{9\theta_l}{2}\right]$$
$$\left.\left. + \frac{15v^2}{4c_l^2}\hat{A}_2(t)\sin\frac{\theta_l}{2}\right\} r_l^{-1/2}\right] \Bigg\} . \qquad (5.3.5)$$

The initial curve defined by equation (5.2.2) is then

$$1 + z_0 ch\rho(c_l^2 - c_s^2)\left\{-\frac{9v^4}{8c_l^4}\hat{A}_0(t) r_l^{-5/2}\cos\frac{5\theta_l}{2} + \left[\frac{15v^4}{8c_l^4}\hat{A}_2(t)\cos\frac{3\theta_l}{2}\right.\right.$$
$$\left.\left. - D_l^1\{A_0(t)\}\left(f_{11}^d(\theta_l) + \alpha_l^2 f_{22}^d(\theta_l)\right) + B_l(t)\left(f_{11}^b(\theta_l) - \alpha_l^2 f_{22}^b(\theta_l)\right)\right] r_l^{-3/2}\right\}$$
$$+\alpha_l^2\left[z_0 ch\rho(c_l^2 - c_s^2)\right]^2\left\{-\left(\frac{9v^2}{8c_l^2}\hat{A}_0(t)\right)^2 r_l^{-5} + \frac{9v^2}{8c_l^2}\hat{A}_0(t)\left[\frac{15v^2}{4c_l^2}\hat{A}_2(t)\cos\theta_l\right.\right.$$
$$\left. - D_l^1\{A_0(t)\}g_1^d(\theta_l) + B_l(t)g_1^b(\theta_l)\right] r_l^{-4} + \left[-\left(\frac{15v^2}{8c_l^2}\hat{A}_2(t)\right)^2\right.$$
$$+\frac{15v^2}{8c_l^2}\hat{A}_2(t)D_l^1\{A_0(t)\}g_2^d(\theta_l) + \left(D_l^1\{A_0(t)\}\right)^2\left[f_{11}^d(\theta_l)f_{22}^d(\theta_l) - (f_{12}^d(\theta_l))^2\right]$$
$$-B_l(t)\left\{\frac{15v^2}{8c_l^2}\hat{A}_2(t)g_2^b(\theta_l) + D_l^1\{A_0(t)\}\left[f_{22}^d(\theta_l)f_{11}^b(\theta_l) - f_{11}^d(\theta_l)f_{22}^b(\theta_l)\right.\right.$$
$$\left.\left.\left. - 2f_{12}^d(\theta_l)f_{12}^b(\theta_l)\right]\right\} - B_l^2(t)\left[f_{11}^b(\theta_l)f_{22}^b(\theta_l) + (f_{12}^b(\theta_l))^2\right]\Bigg] r_l^{-3}\Bigg\} = 0 \qquad (5.3.6)$$

where

$$g_1^d(\theta_l) = \left(f_{11}^d(\theta_l) - f_{22}^d(\theta_l)\right)\cos\frac{5\theta_l}{2} + 2f_{12}^d(\theta_l)\sin\frac{5\theta_l}{2} ,$$
$$g_1^b(\theta_l) = \left(f_{11}^b(\theta_l) + f_{22}^b(\theta_l)\right)\cos\frac{5\theta_l}{2} + 2f_{12}^b(\theta_l)\sin\frac{5\theta_l}{2} ,$$
$$g_2^d(\theta_l) = \left(f_{11}^d(\theta_l) - f_{22}^d(\theta_l)\right)\cos\frac{3\theta_l}{2} + 2f_{12}^d(\theta_l)\sin\frac{3\theta_l}{2} ,$$

$$
\begin{aligned}
g_2^b(\theta_l) &= \left(f_{11}^b(\theta_l) + f_{22}^b(\theta_l)\right)\cos\frac{3\theta_l}{2} + 2f_{12}^b(\theta_l)\sin\frac{3\theta_l}{2}\ , \\
f_{11}^d(\theta_l) &= -\frac{1}{2}\cos\frac{3\theta_l}{2} + \frac{3v^2}{16c_l^2}\cos\frac{7\theta_l}{2}\ , \\
f_{11}^b(\theta_l) &= -\frac{3}{4}\left(1-\frac{v^2}{3c_l^2}\right)\cos\frac{3\theta_l}{2} + \frac{3}{4}\left(1-\frac{v^2}{8c_l^2}\right)\cos\frac{7\theta_l}{2} - \frac{15v^2}{64c_l^2}\cos\frac{11\theta_l}{2}\ , \\
f_{22}^d(\theta_l) &= \frac{1}{2}\left(1-\frac{v^2}{c_l^2}\right)\cos\frac{3\theta_l}{2} - \frac{3v^2}{16c_l^2}\cos\frac{7\theta_l}{2}\ , \\
f_{22}^b(\theta_l) &= \frac{5}{4}\left(1-\frac{4v^2}{5c_l^2}\right)\cos\frac{3\theta_l}{2} + \frac{3}{4}\left(1-\frac{9v^2}{8c_l^2}\right)\cos\frac{7\theta_l}{2} - \frac{15v^2}{64c_l^2}\cos\frac{11\theta_l}{2}\ , \\
f_{12}^d(\theta_l) &= -\frac{1}{2}\left(1-\frac{v^2}{2c_l^2}\right)\sin\frac{3\theta_l}{2} + \frac{3v^2}{16c_l^2}\sin\frac{7\theta_l}{2}\ , \\
f_{12}^b(\theta_l) &= \frac{1}{4}\left(1-\frac{v^2}{2c_l^2}\right)\sin\frac{3\theta_l}{2} + \frac{3}{4}\left(1-\frac{5v^2}{8c_l^2}\right)\sin\frac{7\theta_l}{2} - \frac{15v^2}{64c_l^2}\sin\frac{11\theta_l}{2}\ .
\end{aligned}
$$

In the expressions above, $\hat{A}_0(t)$ is determined by the dynamic stress intensity factor history, $K_I^d(t)$, and the propagating speed of the crack-tip, $v(t)$. $D_l^1\{A_0(t)\}$ depends not only on $K_I^d(t)$ and $v(t)$, but also on the time derivatives of these quantities. Besides $K_I^d(t)$ and $v(t)$, $B_l(t)$ also depends on the acceleration of the crack-tip. From the first stress invariant, equation (5.3.3), we can see that the dynamic transient effects, $D_l^1\{A_0(t)\}$ and $B_l(t)$ inter the expression only through the third terms. If we also want to investigate the higher order time derivatives of $K_I^d(t)$ and $v(t)$, we have to use higher order terms in the asymptotic expansion of stress. The coefficients $\hat{A}_0(t)$, $\hat{A}_1(t)$ and $\hat{A}_2(t)$ cannot be determined by the asymptotic analysis. Their values can only be determined for particular initial/boundary value problems. It should be observed at this point that the θ_l variation of the higher order terms in relation (5.3.3) is different from that of the steady state higher order expansion presented by Dally *et al.* (1985). Relation (5.3.3) reduces to the steady state case only if both K_I^d and v are constant.

We can also see from above expressions that if the crack-tip speed $v(t)$ is a constant, i.e., $\dot{v}(t) = 0$, and therefore, $B_l(t) = 0$, equations (5.3.4), (5.3.5), and (5.3.6),

give the caustic mapping equation and the initial curve equation corresponding to transient crack growth under constant velocity and varying stress intensity factor. Furthermore, if the time derivative of the dynamic stress intensity factor, $\dot{K}_I^d(t)$ is also zero, $D_l^1\{A_0(t)\}$ will be zero. In such a case, equations (5.3.4), (5.3.5), and (5.3.6) describe the caustic curves corresponding to steady state crack growth evaluated on the basis of a three term steady state expansion for the stresses. If in addition, $\hat{A}_2$ vanishes, these relations exactly reduce to the results obtained under the assumption of K_I^d-dominance (Rosakis, 1980). For stationary cracks ($v = 0$), $D_l^1\{A_0(t)\}$ and $B_l(t)$ all vanish even if $\dot{K}_I \neq 0$. Depending on whether the loading is dynamic or not, $\hat{A}_2$ may be either a constant or a function of time. If $\hat{A}_2$ happens to be vanish, then a situation of K_I-dominance is established outside the near-tip three dimensional zone and the equations of the caustics reduce to those of an epicycloid (Theocaris, 1981).

5.3.2 Relation between the dynamic stress intensity factor and the geometrical dimensions of caustics

For a given specimen with a straight mode-I crack, if the initial conditions and the boundary conditions are prescribed, and also if the crack propagation history, i.e., the propagating velocity of the crack-tip $v(t)$, is known, then the history of the dynamic stress intensity factor, $K_I^d(t)$, can be determined. Consequently, $D_l^1\{A_0(t)\}$ and $B_l(t)$, which depend on the dynamic stress intensity factor and the crack tip velocity as well as on their time derivatives, can also be determined, and so can the coefficients $\hat{A}_1(t)$ and $\hat{A}_2(t)$. According to equations (5.3.4), (5.3.5), and (5.3.6), the shape of the initial curve and the caustic pattern corresponding to this dynamic crack propagation process for each instant of time, can be calculated. However, in laboratory situations the inverse problem is encountered. That is the values of $K_I^d(t)$, $D_l^1\{A_0(t)\}$, $B_l(t)$, $\hat{A}_1(t)$, and $\hat{A}_2(t)$ have to be determined from the caustic pattern. Indeed, in dynamic fracture experiments we need to establish a method of inferring the stress intensity

factor history from local near-tip measurements, since the boundary/initial value problem is usually too difficult to solve. In this section, we provide the main steps of the derivation of the relation between the dynamic stress intensity factor and some experimentally measurable quantities (i.e., geometrical characteristics of caustic and crack-tip velocity).

Since the caustic mapping equations (5.3.4) and (5.3.5), and the initial curve equation (5.3.6) are too complicated, we now make the assumption that $v/c_l \ll 1$. This assumption is realistic since in most solids terminal crack growth velocities do not exceed a speed of $0.2c_l$, or approximately $0.5c_R$ before branching. c_R is the material Rayleigh wave speed in plane stress. It is thus felt that assuming $v/c_l \ll 1$ will lead to a useful and accurate simplification for the mapping equations. By making this simplification, equations (5.3.4) and (5.3.5) become

$$\left.\begin{aligned} X_1 &= r_l\cos\theta_l + \hat{K}(t)r_l^{-3/2}\cos\frac{3\theta_l}{2} - \hat{A}(t)r_l^{-1/2}\cos\frac{\theta_l}{2} \\ &- \frac{1}{2}\hat{B}(t)r_l^{-1/2}\left(\cos\frac{\theta_l}{2} - \cos\frac{5\theta_l}{2}\right) \\ X_2 &= \frac{r_l\sin\theta_l}{\alpha_l} + \alpha_l\left\{\hat{K}(t)r_l^{-3/2}\sin\frac{3\theta_l}{2} - \hat{A}(t)r_l^{-1/2}\sin\frac{\theta_l}{2}\right. \\ &+ \left.\frac{1}{2}\hat{B}(t)r_l^{-1/2}\left(3\sin\frac{\theta_l}{2} + \sin\frac{5\theta_l}{2}\right)\right\} \end{aligned}\right\}, \tag{5.3.7}$$

and the initial curve equation associated with the above mapping equations are obtained by requiring that the Jacobian of the above transformation vanishes, i.e.,

$$\left.\begin{aligned} &\left\{1 - \frac{3}{2}(1-\alpha_l^2)\hat{K}(t)r_l^{-5/2}\cos\frac{5\theta_l}{2} - \frac{9}{4}\alpha_l^2\hat{K}^2(t)r_l^{-5}\right\} \\ &+\left\{\frac{1}{2}(1-\alpha_l^2)\hat{A}(t)r_l^{-3/2}\cos\frac{3\theta_l}{2} + \frac{3}{2}\alpha_l^2\hat{K}(t)\hat{A}(t)r_l^{-4}\cos\theta_l - \frac{1}{4}\alpha_l^2\hat{A}^2(t)r_l^{-3}\right\} \\ &-\hat{B}(t)\left\{\frac{1}{4}\left[(3+5\alpha_l^2)\cos\frac{3\theta_l}{2} - 3(1-\alpha_l^2)\cos\frac{7\theta_l}{2}\right]r_l^{-3/2} - 3\alpha_l^2\hat{K}(t)r_l^{-4}\cos\theta_l\right. \\ &+\left.\frac{1}{4}\hat{A}(t)(1+3\cos 2\theta_l)r_l^{-3} + \frac{1}{8}\hat{B}(t)(1+3\cos 2\theta_l - 4\cos 3\theta_l)r_l^{-3}\right\} = 0 \end{aligned}\right\}, \tag{5.3.8}$$

where

$$\left.\begin{aligned}
\hat{K}(t) &= \frac{z_0 ch F(v)}{\sqrt{2\pi}} K_I^d(t) \\
\hat{A}(t) &= z_0 ch\rho(c_l^2 - c_s^2)\left\{\frac{15v^2}{4c_l^2}\hat{A}_2(t) + D_l^1\{A_0(t)\}\right\} \\
\hat{B}(t) &= z_0 ch\rho(c_l^2 - c_s^2) B_l(t) \\
F(v) &= \frac{(\alpha_l^2 - \alpha_s^2)(1+\alpha_s^2)}{4\alpha_l\alpha_s - (1+\alpha_s^2)^2}
\end{aligned}\right\} .$$

For given experimentally obtained caustic patterns and an appropriate numerical scheme, equations (5.3.7) and (5.3.8) can be used to obtain the values of $\hat{K}(t)$, $\hat{A}(t)$, and $\hat{B}(t)$ as functions of time.

Since the initial curve equation (5.3.8) is still too complicated to use, and in an attempt to retain some of the simplicity of the classical analysis of caustics one can introduce a simplifying assumption regarding the nature of the initial curve by assuming that the initial curve remains a circle of radius $r_0(t)$ in the scaled polar coordinate plane (r_l, θ_l), i.e.,

$$r_l = \left\{\frac{3}{2}\alpha_l \hat{K}(t)\right\}^{2/5} = r_0(t) , \tag{5.3.9}$$

which implies that the size of the initial curve is only determined by the instantaneous value of the dynamic stress intensity factor, as well as the propagating velocity of the crack-tip, rather than the time derivatives of these quantities. By substituting $r_l = r_0(t)$ into the mapping equation (5.3.7), the parametric equations of the caustic are obtained as follows:

$$\left.\begin{aligned}
\frac{X_1}{r_0} &= \cos\theta_l + \frac{2}{3\alpha_l}\left\{\cos\frac{3\theta_l}{2} - \frac{\hat{A}(t)r_0}{\hat{K}(t)}\cos\frac{\theta_l}{2} - \frac{\hat{B}(t)}{2\hat{K}(t)}\left(\cos\frac{\theta_l}{2} - \cos\frac{5\theta_l}{2}\right)\right\} \\
\frac{X_2}{r_0} &= \frac{\sin\theta_l}{\alpha_l} + \frac{2}{3}\left\{\sin\frac{3\theta_l}{2} - \frac{\hat{A}(t)r_0}{\hat{K}(t)}\sin\frac{\theta_l}{2} + \frac{\hat{B}(t)r_0}{2\hat{K}(t)}\left(3\sin\frac{\theta_l}{2} + \sin\frac{5\theta_l}{2}\right)\right\}
\end{aligned}\right\} . \tag{5.3.10}$$

For $\hat{A}(t)r_0/\hat{K}(t) \to 0$ and $\hat{B}(t)r_0/\hat{K}(t) \to 0$, equation (5.3.10) reduce to the parametric equation for dynamic caustics obtained on the basis of K_I^d-dominance (Rosakis,

1980). The validity of the assumption regarding the circularity of the initial curve will be justified in section 5.5 in connection to the Broberg problem.

The two caustic curve dimensions chosen in this analysis are the maximum transverse diameter D of the caustic and the distance between the point of intersection of this diameter with the X_1-axis and the front point of the caustic. This length will be denoted by X. These lengths are shown in FIGURE 5.2. If the end point of the

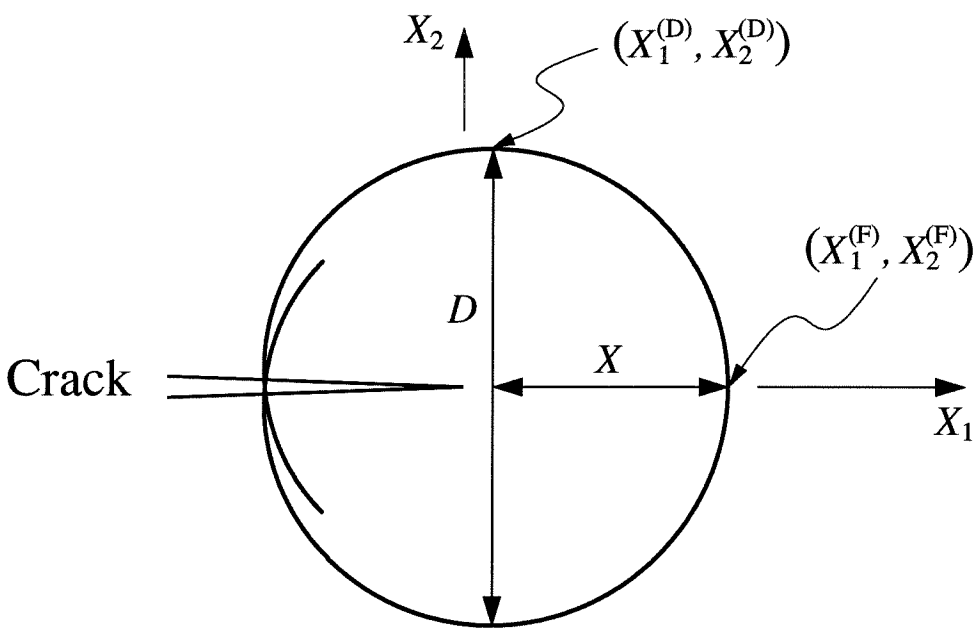

Figure 5.2: Evaluation of the dynamic stress intensity factor $K_I^d(t)$ by measuring two geometrical dimensions, D and X.

caustic diameter has coordinates $X_1^{(D)}$ and $X_2^{(D)}$, respectively, and if the front point of the caustic curve, has coordinates $X_1^{(F)}$ and $X_2^{(F)} = 0$, then one can use the mapping equation (5.3.10) to write

$$\left.\begin{aligned} X_1^{(F)} &= r_0 + \hat{K}(t) r_0^{-3/2} - \hat{A}(t) r_0^{-1/2} \\ X_2^{(F)} &= 0 \end{aligned}\right\}, \tag{5.3.11}$$

and

$$\left.\begin{aligned} X_1^{(\mathrm{D})} &= r_0 \cos\theta_l^{(\mathrm{D})} + \hat{K}(t) r_0^{-3/2} \cos\frac{3\theta_l^{(\mathrm{D})}}{2} - \hat{A}(t) r_0^{-1/2} \cos\frac{\theta_l^{(\mathrm{D})}}{2} \\ &- \frac{1}{2}\hat{B}(t) r_0^{-1/2} \left(\cos\frac{\theta_l^{(\mathrm{D})}}{2} - \cos\frac{5\theta_l^{(\mathrm{D})}}{2} \right) \\ X_2^{(\mathrm{D})} &= \frac{r_0 \sin\theta_l^{(\mathrm{D})}}{\alpha_l} + \alpha_l \left\{ \hat{K}(t) r_0^{-3/2} \sin\frac{3\theta_l^{(\mathrm{D})}}{2} - \hat{A}(t) r_0^{-1/2} \sin\frac{\theta_l^{(\mathrm{D})}}{2} \right. \\ &+ \left. \frac{1}{2}\hat{B}(t) r_0^{-1/2} \left(3\sin\frac{\theta_l^{(\mathrm{D})}}{2} + \sin\frac{5\theta_l^{(\mathrm{D})}}{2} \right) \right\} \end{aligned}\right\} , \qquad (5.3.12)$$

where $\theta_l^{(\mathrm{D})}$ is the angular coordinate of the point $(r_0, \theta_l^{(\mathrm{D})})$ on the initial curve that maps onto the point $(X_1^{(\mathrm{D})}, X_2^{(\mathrm{D})})$, where X_2 is a maximum. Since at this point, X_2 is a local maximum, the following condition has to be met

$$\frac{\partial X_2}{\partial \theta_l} = 0 , \qquad \text{as} \quad \theta_l = \theta_l^{(\mathrm{D})} . \qquad (5.3.13)$$

The relations between the experimentally measurable quantities, D and X, and the points $(X_1^{(\mathrm{D})}, X_2^{(\mathrm{D})})$ and $(X_1^{(\mathrm{F})}, X_2^{(\mathrm{F})})$, are

$$D = 2X_2^{(\mathrm{D})} , \qquad X = X_1^{(\mathrm{F})} - X_1^{(\mathrm{D})} . \qquad (5.3.14)$$

Then, the relations that should be used to obtain the unknown coefficients, are

$$\left.\begin{aligned} \frac{D}{r_0} &= 2\left(\frac{\sin\theta_l^{(\mathrm{D})}}{\alpha_l} + \frac{2}{3}\sin\frac{3\theta_l^{(\mathrm{D})}}{2} \right) - 2\alpha_l \hat{A}(t) r_0^{-3/2} \sin\frac{\theta_l^{(\mathrm{D})}}{2} \\ &+ \alpha_l \hat{B}(t) r_0^{-3/2} \left(3\sin\frac{\theta_l^{(\mathrm{D})}}{2} + \sin\frac{5\theta_l^{(\mathrm{D})}}{2} \right) \\ \frac{X}{r_0} &= \left(1 + \frac{2}{3\alpha_l} - \cos\theta_l^{(\mathrm{D})} - \frac{2}{3\alpha_l}\cos\frac{3\theta_l^{(\mathrm{D})}}{2} \right) - \hat{A}(t) r_0^{-3/2} \left(1 - \cos\frac{\theta_l^{(\mathrm{D})}}{2} \right) \\ &+ \frac{1}{2}\hat{B}(t) r_0^{-3/2} \left(\cos\frac{\theta_l^{(\mathrm{D})}}{2} - \cos\frac{5\theta_l^{(\mathrm{D})}}{2} \right) \end{aligned}\right\} , \qquad (5.3.15)$$

and

$$\left.\begin{aligned}\frac{1}{r_0}\left(\frac{\partial X_2}{\partial\theta_l}\right)_{\theta_l=\theta_l^{(\mathrm{D})}} &= \left(\frac{\cos\theta_l^{(\mathrm{D})}}{\alpha_l}+\cos\frac{3\theta_l^{(\mathrm{D})}}{2}\right)-\frac{1}{2}\alpha_l\hat{A}(t)r_0^{-3/2}\cos\frac{\theta_l^{(\mathrm{D})}}{2}\\ &+\frac{1}{4}\alpha_l\hat{B}(t)r_0^{-3/2}\left(3\cos\frac{\theta_l^{(\mathrm{D})}}{2}+5\cos\frac{5\theta_l^{(\mathrm{D})}}{2}\right)=0\end{aligned}\right\}. \qquad (5.3.16)$$

In the above expressions, relation (5.3.9) between $\hat{K}(t)$ and r_0 has been used. It seems that there are only three equations in (5.3.15) and (5.3.16), but four undetermined parameters, r_0(or $\hat{K}(t)$), $\theta_l^{(\mathrm{D})}$, $\hat{A}(t)$, and $\hat{B}(t)$. However, if the crack propagating velocity, $v(t)$ and thus $\dot{v}(t)$ are independently known, then $\hat{B}(t)$ is related to $\hat{K}(t)$ by

$$\hat{B}(t)=\frac{2\dot{v}(t)}{\alpha_l^4 c_l^2}\hat{K}(t)\ ,$$

and thus $\hat{B}(t)$ and $\hat{K}(t)$ are not independent variables. So actually there are only three undetermined parameters, and they can be obtained by solving the equations (5.3.15) and (5.3.16). By eliminating $\hat{A}(t)$, and $\hat{B}(t)$ from equations (5.3.15) and (5.3.16), we obtain the relations

$$\left.\begin{aligned}\frac{D}{r_0} &= \left\{g_1(\theta_l^{(\mathrm{D})})-2g_1'(\theta_l^{(\mathrm{D})})\tan\frac{\theta_l^{(\mathrm{D})}}{2}\right\}\\ &+\frac{2\dot{v}(t)D}{\alpha_l^4 c_l^2}\left\{g_2(\theta_l^{(\mathrm{D})})-2g_2'(\theta_l^{(\mathrm{D})})\tan\frac{\theta_l^{(\mathrm{D})}}{2}\right\}\frac{r_0}{D}\\ \frac{X}{r_0} &= f_1(\theta_l^{(\mathrm{D})})+\frac{2\dot{v}(t)X}{\alpha_l^4 c_l^2}f_2(\theta_l^{(\mathrm{D})})\frac{r_0}{X}\end{aligned}\right\}, \qquad (5.3.17)$$

where

$$\begin{aligned}g_1(\theta_l^{(\mathrm{D})}) &= 2\left(\frac{\sin\theta_l^{(\mathrm{D})}}{\alpha_l}+\frac{2}{3}\sin\frac{3\theta_l^{(\mathrm{D})}}{2}\right)\ ,\\ g_2(\theta_l^{(\mathrm{D})}) &= \frac{2}{3}\left(3\sin\frac{\theta_l^{(\mathrm{D})}}{2}+\sin\frac{5\theta_l^{(\mathrm{D})}}{2}\right)\ ,\\ f_1(\theta_l^{(\mathrm{D})}) &= 1+\frac{2}{3\alpha_l}-\left\{1+\frac{2}{\alpha_l^2}\left(\sec\frac{\theta_l^{(\mathrm{D})}}{2}-1\right)\right\}\cos\theta_l^{(\mathrm{D})}\\ &+\frac{2}{\alpha_l}\left(\frac{2}{3}-\sec\frac{\theta_l^{(\mathrm{D})}}{2}\right)\cos\frac{3\theta_l^{(\mathrm{D})}}{2}\ ,\\ f_2(\theta_l^{(\mathrm{D})}) &= \frac{1}{3\alpha_l}\left\{\left(4-3\sec\frac{\theta_l^{(\mathrm{D})}}{2}\right)\cos\frac{\theta_l^{(\mathrm{D})}}{2}+\left(4-5\sec\frac{\theta_l^{(\mathrm{D})}}{2}\right)\cos\frac{5\theta_l^{(\mathrm{D})}}{2}\right\}\ .\end{aligned}$$

In equation (5.3.17), the prime denotes the differentiation with respect to the argument, $\theta_l^{(\mathrm{D})}$. Consequently, when D and X are measured, r_0 and $\theta_l^{(\mathrm{D})}$ can be obtained by solving equation (5.3.17), and therefore, the dynamic stress intensity factor, $K_I^d(t)$, can be obtained from relation (5.3.9).

To be more explicit, we solve the first equation in (5.3.17) for r_0, which then can be expressed as

$$r_0 = \frac{D}{g_1(\theta_l^{(\mathrm{D})})}\left\{1 - \frac{2g_1'(\theta_l^{(\mathrm{D})})}{g_1(\theta_l^{(\mathrm{D})})}\tan\frac{\theta_l^{(\mathrm{D})}}{2}\right\}^{-1}\left\{\frac{1}{2} + \sqrt{\frac{1}{4} + \frac{2\dot{v}(t)D}{\alpha_l^4 c_l^2}\cdot\frac{G_2(\theta_l^{(\mathrm{D})})}{[G_1(\theta_l^{(\mathrm{D})})]^2}}\right\}^{-1}, \tag{5.3.18}$$

where

$$G_1(\theta_l^{(\mathrm{D})}) = g_1(\theta_l^{(\mathrm{D})}) - 2g_1'(\theta_l^{(\mathrm{D})})\tan\frac{\theta_l^{(\mathrm{D})}}{2}, \quad G_2(\theta_l^{(\mathrm{D})}) = g_2(\theta_l^{(\mathrm{D})}) - 2g_2'(\theta_l^{(\mathrm{D})})\tan\frac{\theta_l^{(\mathrm{D})}}{2}.$$

By using equations (5.3.9) and (5.3.18), the dynamic stress intensity factor can be expressed as

$$\begin{aligned} K_I^d(t) \;=\; & \frac{2\sqrt{2\pi}}{3\alpha_l c h z_0 F(v)}\left\{\frac{D}{g_1(\theta_l^{(\mathrm{D})})}\right\}^{5/2}\left\{1 - \frac{2g_1'(\theta_l^{(\mathrm{D})})}{g_1(\theta_l^{(\mathrm{D})})}\tan\frac{\theta_l^{(\mathrm{D})}}{2}\right\}^{-5/2} \\ & \times\left\{\frac{1}{2} + \sqrt{\frac{1}{4} + \frac{2\dot{v}(t)D}{\alpha_l^4 c_l^2}\cdot\frac{G_2(\theta_l^{(\mathrm{D})})}{\left[G_1(\theta_l^{(\mathrm{D})})\right]^2}}\right\}^{-5/2}\Bigg\}. \end{aligned} \tag{5.3.19}$$

The above expression still contains an undetermined parameter, $\theta_l^{(\mathrm{D})}$. However, if the second equation in (5.3.17) is solved for r_0, we can get that

$$r_0 = \frac{X}{f_1(\theta_l^{(\mathrm{D})})}\left\{\frac{1}{2} + \sqrt{\frac{1}{4} + \frac{2\dot{v}(t)X}{\alpha_l^4 c_l^2}\cdot\frac{f_2(\theta_l^{(\mathrm{D})})}{\left[f_1(\theta_l^{(\mathrm{D})})\right]^2}}\right\}^{-1}.$$

Consequently, the angle $\theta_l^{(\mathrm{D})}$ that appears in equation (5.3.19) is the root of the

following trigonometric equation,

$$\frac{X}{D} = \frac{f_1(\theta_l^{(D)})}{G_1(\theta_l^{(D)})} \left\{ \frac{1}{2} + \sqrt{\frac{1}{4} + \frac{2\dot{v}(t)X}{\alpha_l^4 c_l^2} \cdot \frac{f_2(\theta_l^{(D)})}{\left[f_1(\theta_l^{(D)})\right]^2}} \right\} \times \left\{ \frac{1}{2} + \sqrt{\frac{1}{4} + \frac{2\dot{v}(t)D}{\alpha_l^4 c_l^2} \cdot \frac{G_2(\theta_l^{(D)})}{\left[G_1(\theta_l^{(D)})\right]^2}} \right\}^{-1} \Bigg\} . \tag{5.3.20}$$

Under the fully transient dynamic condition, equations (5.3.19) and (5.3.20) give the final relation between the dynamic stress intensity factor, $K_I^d(t)$, and the experimentally measurable quantities, D and X.

It should be pointed out that for the case of non-uniformly propagating crack, the dynamic stress intensity factor, $K_I^d(t)$ measured from the caustic patterns, is explicitly related to the crack-tip acceleration, $\dot{v}(t)$. It is also implicitly related (through $\theta_l^{(D)}$) to $\dot{K}_I^d(t)$. The coefficient $\hat{A}_2(t)$ can also be obtained in the following way,

$$\hat{A}(t) = \frac{1}{\alpha_l} \sec\frac{\theta_l^{(D)}}{2} \left\{ g_1'(\theta_l^{(D)}) \left(\frac{r_0}{D}\right)^{3/2} + \frac{2\dot{v}(t)D}{\alpha_l^4 c_l^2} g_2'(\theta_l^{(D)}) \left(\frac{r_0}{D}\right)^{5/2} \right\} D^{3/2} , \tag{5.3.21}$$

and

$$\hat{A}_2(t) = \frac{4c_l^2}{15v^2} \left\{ \frac{\hat{A}(t)}{z_0 ch\rho(c_l^2 - c_s^2)} + \frac{8v^{1/2}(t)}{3\alpha_l^2} \cdot \frac{\mathrm{d}}{\mathrm{d}t} \left[\frac{v^{-3/2}(t)}{\alpha_l} \left(\frac{r_0}{D}\right)^{5/2} D^{5/2} \right] \right\} , \tag{5.3.22}$$

where r_0/D is given by equation (5.3.18) and $\theta_l^{(D)}$ by equation (5.3.20) in terms of the measurable quantities X and D. Once the caustic diameter D is measured at different times, $\hat{A}_2(t)$ is determined from (5.3.22), provided that many sequential measurements of caustic patterns are available and if the time derivative in the formula can be evaluated by some numerical procedures.

In an experimental situation, caustic patterns are photographed and D and X are measured. Equation (5.3.20) is then used to obtain $\theta_l^{(D)}$, substitute it into equation (5.3.19) and thus obtain $K_I^d(t)$. From equations (5.3.21) and (5.3.22), coefficient $\hat{A}_2(t)$ can also be determined.

For the case of constant velocity, $\hat{B}(t) = 0$ ($\dot{v}(t) = 0$), equation (5.3.19) corresponds to transient crack growth under constant velocity and varying stress intensity factor. Equation (5.3.20) then gives an explicit relation between X/D and $\theta_l^{(D)}$. If the time derivative of the stress intensity factor, $\dot{K}_I^d(t)$, is also zero (steady state), then $D_l^1\{A_0(t)\} = 0$. For both $\dot{v}(t) = 0$ and steady state, the relation between the dynamic stress intensity factor, $K_I^d(t)$, and the caustic diameter, D, has the same form. The only difference comes in the value of $\theta_l^{(D)}$, which is directly related to the ratio X/D. For the transient constant velocity case ($\dot{v}(t) = 0$, $\dot{K}_I^d(t) \neq 0$),

$$\hat{A}_2(t) = \frac{4c_l^2}{15v^2}\left\{\frac{\hat{A}(t)}{z_0 ch\rho(c_l^2 - c_s^2)} + \frac{8}{3\alpha_l^3 v}\cdot\frac{\mathrm{d}}{\mathrm{d}t}\left[\left(\frac{D}{G_1(\theta_l^{(D)})}\right)^{5/2}\right]\right\} . \tag{5.3.23}$$

For the steady state case ($\dot{v}(t) = 0$, $\dot{K}_I^d(t) = 0$),

$$\hat{A}_2 = \frac{4c_l^2}{15v^2}\cdot\frac{\hat{A}}{z_0 ch\rho(c_l^2 - c_s^2)} , \tag{5.3.24}$$

or, in this case, $\hat{A}_2$ is directly related to the caustic diameter.

Furthermore, if we only retain the singular term in the asymptotic stress expansion, then in the caustic mapping equation (5.3.7) and the initial curve equation (5.3.8) $\hat{A}(t)$ and $\hat{B}(t)$ will be zero, and equations (5.3.7) and (5.3.8) reduce to the same equations used in the classical analysis (Rosakis, 1980). If we still make the assumption of (5.3.9), the unknown parameters will reduce to two (i.e., $K_I^d(t)$ and $\theta_l^{(D)}$), and so we only need to measure one quantity from the caustic pattern, say the diameter, D. By using the first equation in (5.3.15) and equation (5.3.16), the dynamic stress intensity factor corresponding to the classical analysis can be determined. Now equation (5.3.19) becomes

$$K_I^d(t) = \frac{2\sqrt{2\pi}}{3\alpha_l ch z_0 F(v)}\left\{\frac{D}{g_1(\theta_l^{(D)})}\right\}^{5/2} . \tag{5.3.25}$$

Also, if $\hat{A}(t)$ and $\hat{B}(t)$ are set equal to zero, the maximum condition (5.3.16) requires that

$$g_1'(\theta_l^{(D)}) = 2\left(\frac{\cos\theta_l^{(D)}}{\alpha_l} + \cos\frac{3\theta_l^{(D)}}{2}\right) = 0 , \tag{5.3.26}$$

and this will provide the value of $\theta_l^{(D)}$ as a function of crack-tip velocity v. Now define

$$C(v) = \frac{1}{\alpha_l F(v)} \left\{ \frac{3.17}{g_1(\theta_l^{(D)})} \right\}^{5/2} ,$$

where $C(v)$ is a function of the crack-tip velocity, v. Equation (5.3.25) can be rewritten as

$$K_I^d(t) = C(v) \frac{D^{5/2}}{10.7 z_0 ch} , \tag{5.3.27}$$

which has the same form as that given by Rosakis *et al.* (1984). Equation (5.3.27) is the result of the classical analysis of the caustic pattern and is widely used in the experimental interpretation of caustics corresponding to elastodynamic crack propagation.

Moreover, as $v = 0$ (stationary crack), $\alpha_l = 1$, $F(v) = 1$, and $g_1'(\theta_l^{(D)}) = 0$ gives $\theta_l^{(D)} = \theta_0 = 72^o$, and $g_1(\theta_l^{(D)}) = 3.17$. Therefore, $C(0) = 1$ and (Theocaris, 1981 and Beinert and Kalthoff, 1981)

$$K_I^d(t) = \frac{2\sqrt{2\pi}}{3ch z_0} \left(\frac{D}{3.17} \right)^{5/2} . \tag{5.3.28}$$

This equation holds not only for the stationary crack subjected to dynamic loading, but also for static problem, where $K_I^d(t)$ should be replaced by K_I.

5.4 Multi-point measurement technique

5.4.1 Description of the multi-point measurement method

Traditionally, in experimental investigation of the dynamic propagation of a mode-I crack, by using the optical method of caustics, only one characteristic dimension of the caustic curve is measured. It is the maximum transverse diameter, D, and this dimension is directly related to the dynamic stress intensity factor, $K_I^d(t)$, at the propagating crack-tip by equation (5.3.27) given in the previous section. This

analysis of caustic pattern is based on the assumption that the deformation field near the propagating crack-tip is K_I^d–dominant, which means that the stress field at a finite region near the crack-tip can be approximated accurately by the elastodynamic asymptotic singular solution. This interpretation method is thus called classical analysis of method of caustics. By relaxing the assumption of K_I^d-dominance, we have developed a new interpretation method about the caustic patterns obtained from the dynamic fracture experiments. This new method is based on a fully transient higher order asymptotic expansion of the stress field around the propagating crack-tip. In this analysis, influence of transients resulting from the existence of non-uniform $K_I^d(t)$ and $v(t)$ histories (effects of $\dot{K}_I^d(t)$ and $\dot{v}(t)$) is included. In the new interpretation method, instead of just measuring one characteristic length, two caustic curve dimensions need to be measured. One is still the maximum transverse diameter, D, the other one is the distance between the point of intersection of the diameter, D, and the X_1–axis in the reference plane and the front point of the caustics, X (see FIGURE 5.2). The dynamic stress intensity factor at the crack-tip and the coefficient of the high order term can be explicitly related to these two dimensions.

Since the accurate measurement of the two geometrical dimensions, D and X, is a crucial aspect of the new interpretation method, one question has been asked. How can the two geometrical dimensions be measured very accurately, especially the distance between the point of intersection of the diameter, D, and the X_1-axis in the reference plane and the front point of the caustics, X, because practically, it is hard to tell the exact position of the diameter D. To cope with this problem, one option is the so-called multi-point over-deterministic data reduction technique. Recently, Rossmanith and Knasmillner (1991) have developed an interactive image processing system and studied the multi-point measurement technique systematically. The basic principle of this technique is measuring the coordinates of a series points along the caustic curve and substituting these coordinates into the mapping equations and the

initial curve equation. By solving the over-deterministic system of equations, the unknown coefficients in the mapping equations and the initial curve equation can be obtained, and therefore, the dynamic stress intensity factor can be determined. Liu (1989) has used the multi-point measurement technique to get the two dynamic stress intensity factors, $K_I^d(t)$ and $K_{II}^d(t)$, from the caustic patterns of a crack propagating along a curved path. Similar technique has also been used by Sanford and Dally (1979) in the photoelastic fringe patterns to determine the stress intensity factor at the crack-tip.

Unlike other optical techniques, such as photoelasticity and coherent gradient sensing technique (CGS), we have to consider two planes in the method of caustics. One is the specimen plane from where the information of deformation is picked up and some parameters have to be determined. The other one is the reference plane which is located some distance away from the specimen plane, and the distance is denoted by z_0. The mapping equations provide the corresponding relation between the points on the specimen plane and the points on the reference plane. The initial curve equation defines the region from where the information is conveyed. When we measured the coordinates of points along the caustic curve on the reference plane, because the coefficients are unknown, we do not know what points on the specimen plane are actually associated with those points on the caustic curve. If we directly substitute those coordinates into the mapping equations and the initial curve equation, we will end up to a huge, highly nonlinear system of equations.

To avoid solving a highly nonlinear system of equations, in this section, we will propose another approach which can be used to measure the two geometrical dimensions, D and X, very accurately, so that we can take the advantage of the explicitness of the interpretation method developed in the previous section. By using this approach, the dynamic stress intensity factor, $K_I^d(t)$, and the coefficient of the higher order term can be obtained directly. The basic idea of this approach is also measuring the coor-

dinates of a series points along the caustic curve. But instead of substituting them into the mapping equations and the initial curve equation, we try to find a curve in the reference plane that best fits those points. Whence this curve is found, the two geometrical dimensions, D and X, are measured numerically from this curve other than directly from the caustic pattern. Since with respect to the fitting curve, the numerically measured dimensions, D and X, can be thought as exact, the crucial aspect will become to the accurate measurement of the coordinates of points along the caustic curve. Based on today's image processing technique, this goal can be easily achieved.

5.4.2 Method of multi-point measurement

For measuring of the coordinates of points along a caustic curve, a Cartesian coordinate system $(\hat{X}_1, \hat{X}_2)$ is placed in the reference plane so that the $\hat{X}_1$-axis is parallel to the direction of crack propagation. Since we only consider the mode-I type of deformation, we can always choose that the $\hat{X}_1$-axis coincides with the crack line. Therefore, the caustic pattern is symmetric about the $\hat{X}_1$-axis, and this will simplify our analysis. If the location of the crack-tip were known, then system $(\hat{X}_1, \hat{X}_2)$ could be placed so that its origin is at the crack-tip. In general, however, the exact position of the crack-tip is unknown a prior, we can put the origin of system $(\hat{X}_1, \hat{X}_2)$ anywhere along the crack line (see FIGURE 5.3).

Suppose that along the caustic curve, the two polar coordinates are related by

$$\hat{r} = \sum_{n=1}^{N} \alpha_n f_n(\hat{\theta}) \ , \tag{5.4.1}$$

where $f_n(\hat{\theta})$, $n = 1, 2, \cdots, N$, are known functions of $\hat{\theta}$, and α_n, $n = 1, 2, \cdots, N$ are constants. For mode-I type of deformation and the choice of our coordinate system, we know that

$$f_n(-\hat{\theta}) = f_n(\hat{\theta}) \ , \qquad n = 1, 2, \cdots, N \ . \tag{5.4.2}$$

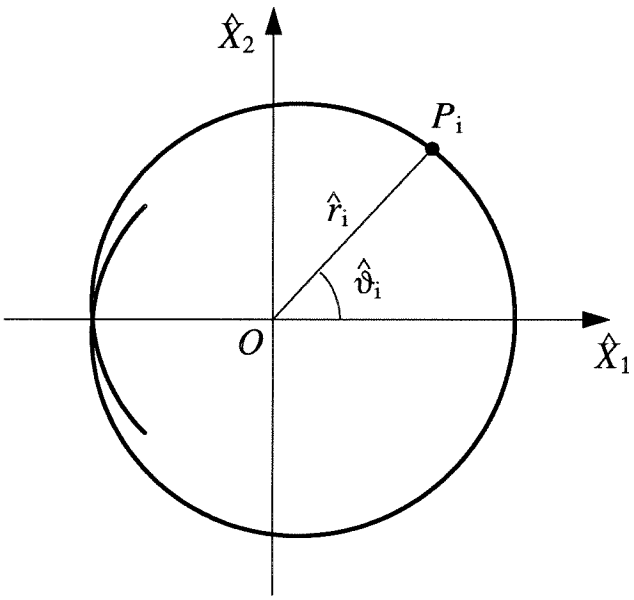

Figure 5.3: The choice of coordinate system and the multi-point measurement along the caustic curve.

Let $(\hat{r}_i, \hat{\theta}_i), i = 1, 2, \cdots, M$, be the coordinates of points measured along the caustic curve. Define a function

$$\Phi(\alpha_1, \alpha_2, \cdots, \alpha_N) = \sum_{i=1}^{M} \left[\hat{r}_i - \sum_{n=1}^{N} \alpha_n f_n(\hat{\theta}_i) \right]^2 . \tag{5.4.3}$$

The numbers $\alpha_n, n = 1, 2, \cdots, N$, are chosen such that $\Phi(\alpha_1, \alpha_2, \cdots, \alpha_N)$ is minimized, or the non-dimensional error function $\epsilon(N)$ yields minimum, where $\epsilon(N)$ is defined by

$$\epsilon(N) = \frac{1}{\alpha_1} \sqrt{\frac{\Phi}{M}} . \tag{5.4.4}$$

It can be shown that to minimize $\Phi(\alpha_1, \alpha_2, \cdots, \alpha_N)$, or $\epsilon(N)$, α_n $(n = 1, 2, \cdots, N)$ should satisfy a system of linear equations,

$$\sum_{m=1}^{N} A_{nm} \alpha_m = b_n , \qquad n = 1, 2, \cdots, N , \tag{5.4.5}$$

where

$$\left.\begin{aligned} A_{nm} &= \sum_{i=1}^{M} f_n(\hat{\theta}_i) f_m(\hat{\theta}_i) \\ b_n &= \sum_{i=1}^{M} \hat{r}_i f_n(\hat{\theta}_i) \end{aligned}\right\} . \tag{5.4.6}$$

By solving $\alpha_n, n = 1, 2, \cdots, N$, from equation (5.4.5), the two Cartesian coordinates that describe the fitting curve on the reference plane are given by

$$\left.\begin{aligned} \hat{X}_1(\hat{\theta}) &= \sum_{n=1}^{N} \alpha_n f_n(\hat{\theta}) \cos\hat{\theta} \\ \hat{X}_2(\hat{\theta}) &= \sum_{n=1}^{N} \alpha_n f_n(\hat{\theta}) \sin\hat{\theta} \end{aligned}\right\} . \tag{5.4.7}$$

If we solve the value $\hat{\theta}_0$, such that

$$\frac{\mathrm{d}}{\mathrm{d}\hat{\theta}} \left\{ \hat{X}_2(\hat{\theta}) \right\} = 0 , \qquad \text{as} \qquad \hat{\theta} = \hat{\theta}_0 , \tag{5.4.8}$$

then, the two characteristic dimensions of the caustic pattern, D and X, are given by

$$\left.\begin{aligned} D &= 2 \sum_{n=1}^{N} \alpha_n f_n(\hat{\theta}_0) \sin\hat{\theta}_0 \\ X &= \sum_{n=1}^{N} \alpha_n \left\{ f_n(0) - f_n(\hat{\theta}_0) \cos\hat{\theta}_0 \right\} \end{aligned}\right\} . \tag{5.4.9}$$

It is noted that the process from equation (5.4.7) to equation (5.4.9), is accurate within the error of the fitting, which can be characterized by the magnitude of the error function, $\epsilon(N)$. Also, there is no restrictions on how many terms of $f_n(\hat{\theta})$ and what kind of $f_n(\hat{\theta})$ we should use to fit the curve. Since we are seeking the fitting function with respect to each of the caustic pattern, we may choose any kind of $f_n(\hat{\theta})$, and the number of terms as many as we want, until each of the caustic pattern is best fitted.

5.4.3 An example

To illustrate the measurement method discussed above, we will consider an example and study the effects that will affect the accuracy of the measurement. The caustic pattern presented in FIGURE 5.4 is generated by the full solution of Broberg problem (we will discuss this solution in section 5.5), which includes the transient effect of the time derivative of the dynamic stress intensity factor. A Cartesian coordinate

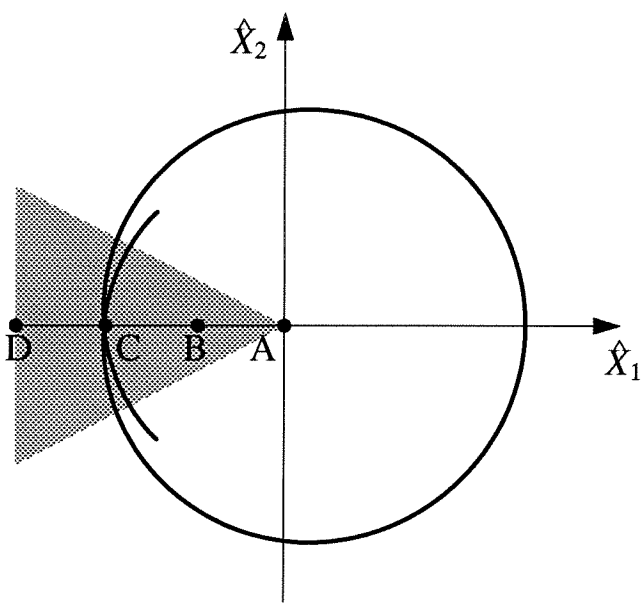

Figure 5.4: Caustic pattern generated from the full solution of Broberg problem.

system is chosen so that the caustic pattern is symmetric about the $\hat{X}_1$–axis. In order to study what influence of different position of the origin on the accuracy of the measurement, we put the origin of the coordinate system at four different locations: i) approximately at the center of the caustic pattern, A; ii) away from the center but still inside the caustic pattern, B; iii) at the edge of the caustic pattern, C; iv) outside the caustic pattern, D. From the practical experience, we will measure the points along the caustic curve but avoid the region that very close to the crack faces where the optical image will not be very clear (the shaded area in FIGURE 5.4). As

for the fitting function $f_n(\hat{\theta})$, we simply choose the polynomial, i.e.,

$$f_n(\hat{\theta}) = \hat{\theta}^{2(n-1)} , \qquad n = 1, 2, \cdots, N . \tag{5.4.10}$$

The total number of the measuring points is $M = 30$.

In FIGURE 5.5, the measuring points and the fitting curves are plotted. The

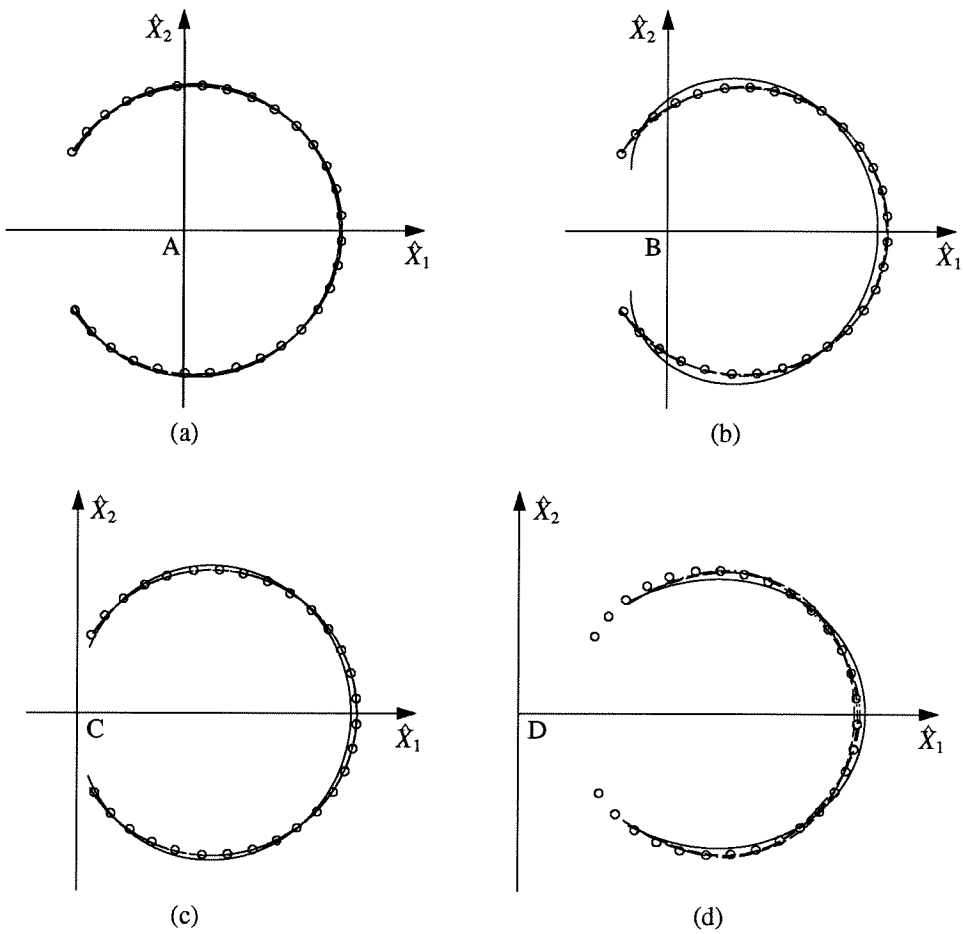

∘ measuring point, ——— $N = 2$, - - - - - $N = 3$, - - - - - - $N = 4$, - - - - - - - $N = 5$

Figure 5.5: The measuring points and the fitting curves with different term number, N: (a) the origin position is A; (b) the origin position is B; (c) the origin position is C; (d) the origin position is D.

number of terms associated with those fitting curves, N, varies from 2 to 5. When

the origin of the coordinate system is chosen approximately at the center of the caustic pattern, from FIGURE 5.5(a), we can see that even by using just two terms, the data points are fitted remarkably well. As the origin of the coordinate system is positioned at the other three locations, B, C, and D, it can be seen from FIGURES 5.5(b), (c), and (d), that when $N \geq 3$, the data points can be fitted quite well.

To make the observation more quantitatively, the variation of the error function $\epsilon(N)$ with respect to the number of terms, N, is presented in FIGURE 5.6. From this figure, we can see that when the origin is positioned at A, the magnitude of $\epsilon(N)$ is about 1% as $N = 2$, and then drops to the magnitude about 0.5% as $N \geq 3$. For the cases of B and C, the magnitude of $\epsilon(N)$ is 4% and 2% for $N = 2$, respectively, and then drops significantly as $N \geq 3$. We also observe that for the case that the origin is located at B, the magnitude of $\epsilon(N)$ is well below 0.5%. But as the origin is at the point D, the magnitude of $\epsilon(N)$ is always about 4%. From FIGURE 5.7, it can be observed that even when we use as many as 30 terms in the polynomial, the magnitude of $\epsilon(N)$ is still at the level of 3.5%, nevertheless, it declines very slowly. Above observations suggest that the best position of the origin of the coordinate system, is between the center and the tail of the caustic pattern. If the origin is outside the caustic curve, the fitting is relatively poor. However, if we choose other fitting functions instead of polynomials, this should be improved even when the origin is located outside the caustic pattern.

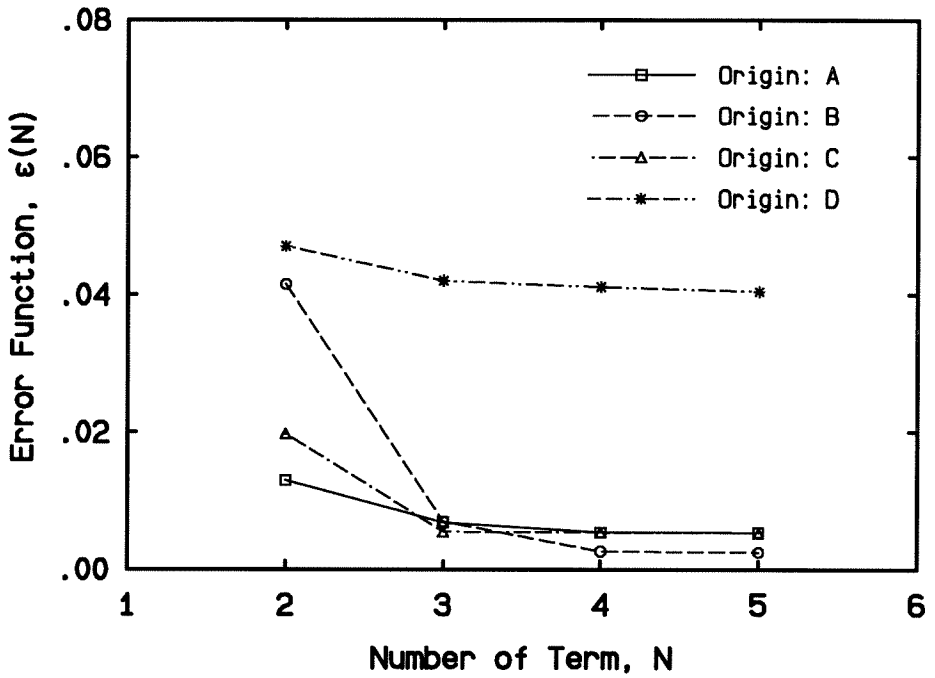

Figure 5.6: Variation of the error function $\epsilon(N)$ with the term number N for different locations of the origin.

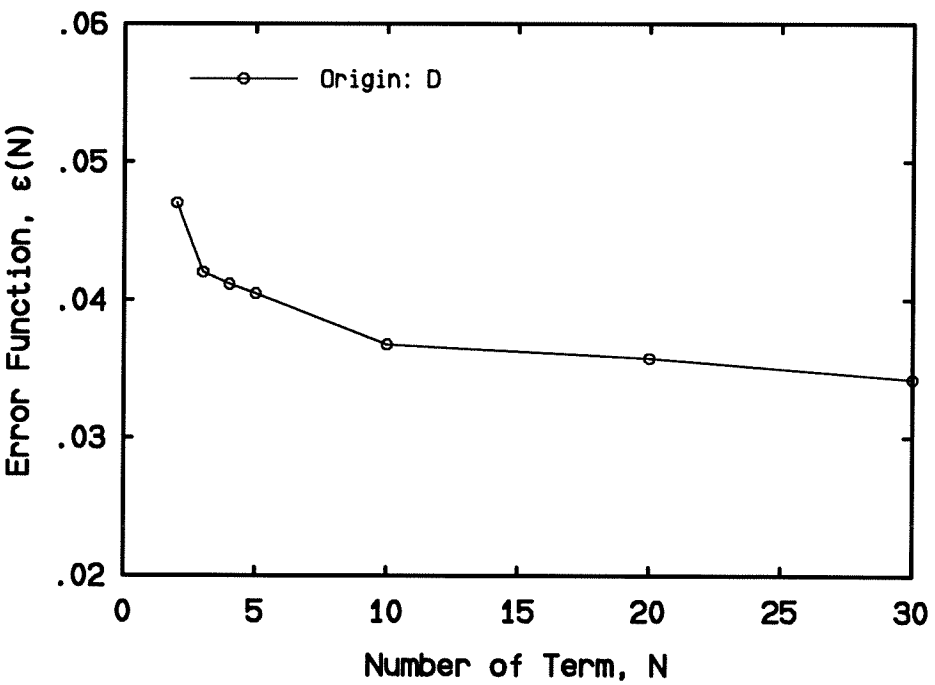

Figure 5.7: Variation of the error function $\epsilon(N)$ with the term number N as the origin is located at D.

5.5 Application of the modified interpretation method to Broberg problem

5.5.1 The caustic pattern corresponding to Broberg problem

In order to illustrate the effect of the higher order terms in caustic patterns obtained for the case of highly transient crack growth problems, and to check the ability of equations (5.3.19) and (5.3.20) to furnish the correct values of $K_I^d(t)$, the solution of a particular elastodynamic boundary value problem is considered. This is the plane stress problem of a crack growing symmetrically from zero initial length at constant velocity under uniform remote tensile stress σ_∞. The plane of deformation is the x_1', x_2'–plane and the crack lies in the interval $-vt < x_1' < vt$, $x_2' = 0$, where v is the constant speed of either crack-tip. This is the problem first analyzed by Broberg (1960) and later, by Cherepanov and Afanasev (1973) and Freund (1990) using a different approach.

An expression for the first stress invariant directly ahead of the crack tips is obtained by Freund (1990). On the line $x_2' = 0$,

$$\sigma_{11} + \sigma_{22} = -2\sigma_\infty \frac{I(v/c_s)}{v} \left(1 - \frac{c_s^2}{c_l^2}\right) \int_{1/c_l}^{t/x_1'} \frac{f(\xi)}{(v^{-1} - \xi)^{\frac{3}{2}}} \mathrm{d}\xi \ , \tag{5.5.1}$$

where $I(v/c_s)$ is a known function of v, and

$$f(\xi) = \frac{(c_s^{-2} - 2\xi^2)}{\left(\xi^2 - c_l^{-2}\right)^{\frac{1}{2}} (v^{-1} + \xi)^{\frac{3}{2}}} \ .$$

Focusing on the crack-tip moving in the positive x_1'-direction, and expanding equation (5.5.1) in powers of $x_1 = x_1' - vt$ near $x_1 = 0$, we obtain

$$\sigma_{11} + \sigma_{22} = W(v) \frac{K_I^d(t)}{\sqrt{2\pi}} \left\{ x_1^{-1/2} + \frac{1}{vt} \left[\frac{1}{2} + \frac{f'(1/v)}{v f(1/v)} \right] x_1^{1/2} \right\} + O\left(x_1^{3/2}\right) \ , \tag{5.5.2}$$

where

$$W(v) = \frac{2(1+\alpha_s^2)(\alpha_l^2-\alpha_s^2)}{D(v)} ,$$

and the dynamic stress intensity factor for this problem is

$$K_I^d(t) = \frac{c_s^2 I(v/c_s) D(v)}{\alpha_l v^2} \sigma_\infty \sqrt{\pi v t} . \tag{5.5.3}$$

If the expansion (5.5.2) is compared with the general expansion (5.3.3), in which $B_l(t) = 0$ ($\dot{v}(t) = 0$), and $\theta_l = 0$, $r_l = x_1$, and terms of like powers in distance from the crack-tip are collected, then explicit relations for the coefficients in the expansion are obtained as

$$\left.\begin{aligned}
\hat{A}_0(t) &= \frac{2}{3}\cdot\frac{W(v)}{\alpha_l^2-\alpha_s^2}\cdot\frac{K_I^d(t)}{\mu\sqrt{2\pi}} = \frac{2\sqrt{2}}{3}\cdot\frac{(1+\alpha_s^2)I(v/c_s)}{\alpha_l(1-\alpha_s^2)}\cdot\frac{\sigma_\infty}{\mu}\sqrt{vt} \\
D_l^1\{A_0(t)\} &= \left(1-\frac{1}{\alpha_l^2}\right)\frac{W(v)}{\alpha_l^2-\alpha_s^2}\cdot\frac{K_I^d(t)}{\mu\sqrt{2\pi}}\cdot\frac{1}{vt} \\
&= -\frac{\sqrt{2}(1-\alpha_l^2)(1+\alpha_s^2)I(v/c_s)}{\alpha_l^3(1-\alpha_s^2)}\cdot\frac{\sigma_\infty}{\mu}\cdot\frac{1}{\sqrt{vt}} \\
\hat{A}_1(t) &= 0 \\
\hat{A}_2(t) &= \frac{2}{15}\left\{\frac{5}{4}+\frac{5}{4\alpha_l^2}+\frac{f'(1/v)}{vf(1/v)}\right\}\frac{W(v)}{\alpha_l^2-\alpha_s^2}\cdot\frac{K_I^d(t)}{\mu\sqrt{2\pi}}\cdot\frac{1}{vt} \\
&= \frac{2\sqrt{2}}{15}\left\{\frac{5}{4}+\frac{5}{4\alpha_l^2}+\frac{f'(1/v)}{vf(1/v)}\right\}\frac{(1+\alpha_s^2)I(v/c_s)}{\alpha_l(1-\alpha_s^2)}\cdot\frac{\sigma_\infty}{\mu}\cdot\frac{1}{\sqrt{vt}}
\end{aligned}\right\} .$$

Since the coefficients $D_l^1\{A_0(t)\}$ and $\hat{A}_2(t)$ are proportional to $1/\sqrt{t}$, the third term in the near-tip asymptotic expansion of the first stress invariant is very large during the early stages of crack growth, possibly dominating the square root singular term. As a result, even though the crack-tip speed is constant, transient effects do exist in the near-tip field.

For this particular problem, we normalize the caustic mapping equations (5.3.4) and (5.3.5), and the initial curve equation (5.3.6) with the length $r_0 = \left(3\alpha_l \hat{K}/2\right)^{2/5}$.

This length is related to the value of the dynamic stress intensity factor, $K_I^d(t)$, of Broberg problem by equation (5.3.9).

The normalized caustic mapping equations and the initial curve equation then become

$$\left.\begin{aligned}\frac{X_1}{r_0} &= \left(\frac{r_l}{r_0}\right)\cos\theta_l + \frac{2}{3\alpha_l}\left(\frac{r_l}{r_0}\right)^{-3/2}\cos\frac{3\theta_l}{2} \\ &- \frac{2}{3\alpha_l}\left(\frac{r_0}{vt}\right)\left\{\left[\frac{5}{4}+\frac{5}{4\alpha_l^2}+\frac{f'(1/v)}{vf(1/v)}\right]\cos\frac{\theta_l}{2}\right. \\ &- \left.2\left[\left(1-\frac{v^2}{4c_l^2}\right)\cos\frac{\theta_l}{2}-\frac{v^2}{8c_l^2}\cos\frac{5\theta_l}{2}\right]\right\}\left(\frac{r_l}{r_0}\right)^{-1/2}\end{aligned}\right\}, \tag{5.5.4}$$

$$\left.\begin{aligned}\frac{X_2}{r_0} &= \left(\frac{r_l}{r_0}\right)\frac{\sin\theta_l}{\alpha_l} + \frac{2}{3}\left(\frac{r_l}{r_0}\right)^{-3/2}\sin\frac{3\theta_l}{2} \\ &- \frac{2}{3}\left(\frac{r_0}{vt}\right)\left\{\left[\frac{5}{4}+\frac{5}{4\alpha_l}+\frac{f'(1/v)}{vf(1/v)}\right]\sin\frac{\theta_l}{2}\right. \\ &- \left.2\left[\left(1-\frac{3v^2}{4c_l^2}\right)\sin\frac{\theta_l}{2}-\frac{v^2}{8c_l^2}\sin\frac{5\theta_l}{2}\right]\right\}\left(\frac{r_l}{r_0}\right)^{-1/2}\end{aligned}\right\}, \tag{5.5.5}$$

and

$$\left.\begin{aligned}&\left\{1-\frac{1}{\alpha_l}\left(\frac{v^2}{c_l^2}\right)\left(\frac{r_l}{r_0}\right)^{-5/2}\cos\frac{5\theta_l}{2}-\left(\frac{r_l}{r_0}\right)^{-5}\right\} \\ &+\frac{1}{3\alpha_l}\left(\frac{r_0}{vt}\right)\left\{\left[\left(\frac{v^2}{c_l^2}\right)\left(\frac{5}{4}+\frac{5}{4\alpha_l^2}+\frac{f'(1/v)}{vf(1/v)}\right)\cos\frac{3\theta_l}{2}\right.\right. \\ &\left.\frac{4}{\alpha_l}\left(f_{11}^d(\theta_l)+\alpha_l^2 f_{22}^d(\theta_l)\right)\right]\left(\frac{r_l}{r_0}\right)^{-3/2} \\ &+2\left[\left(\frac{5}{4}+\frac{5}{4\alpha_l^2}+\frac{f'(1/v)}{vf(1/v)}\right)\cos\theta_l+\frac{2}{\alpha_l^2}g_1^d(\theta_l)\right]\left(\frac{r_l}{r_0}\right)^{-4}\Bigg\} \\ &-\frac{1}{9}\left(\frac{r_0}{vt}\right)^2\left\{\left(\frac{5}{4}+\frac{5}{4\alpha_l^2}+\frac{f'(1/v)}{vf(1/v)}\right)^2+\frac{4}{\alpha_l^2}\left(\frac{5}{4}+\frac{5}{4\alpha_l^2}+\frac{f'(1/v)}{vf(1/v)}\right)g_2^d(\theta_l)\right. \\ &\left.-\frac{16}{\alpha_l^4}\left[f_{11}^d(\theta_l)f_{22}^d(\theta_l)-\left(f_{12}^d(\theta_l)\right)^2\right]\right\}\left(\frac{r_l}{r_0}\right)^{-3} = 0\end{aligned}\right\}, \tag{5.5.6}$$

where the functions $f^d_{\alpha\beta}(\theta_l)$, and $g^d_\alpha(\theta_l)$ have been defined in section 5.3 (see equation (5.3.6)). We can see that the coefficients of higher order terms in the nondimensional caustic mapping equations and the initial curve equation, are proportional to a nondimensional parameter r_0/vt. Relations (5.5.3) and (5.3.9) provide an expression of r_0/vt with respect to time after crack initiation and z_0 as follows,

$$\frac{r_0}{vt} = \left\{ \frac{3}{4\sqrt{2}} \cdot \frac{(1+\alpha_s^2) I(v/c_s)}{1-\alpha_s^2} \cdot \frac{c\sigma_\infty}{1-\nu} \right\}^{2/5} \left(\frac{\sqrt{z_0 h}}{c_s t} \right)^{4/5} , \qquad (5.5.7)$$

where c is a material constant and is given in equation (5.3.2). For a given experimental set up and specimen, c, σ_∞, and h are fixed. In particular, the distance between the specimen and the focal plane of the recording camera, z_0, is set prior to the experiment.

As $t \to \infty$, the ratio r_0/vt vanishes and equations (5.5.4) – (5.5.6) reduce to the classical analysis of dynamic caustics obtained on the basis of K^d_I-dominance. Indeed this is consistent with the fact that as $t \to \infty$,

$$\dot{K}^d_I(t) = \frac{\sqrt{\pi}}{2} \cdot \frac{I(v/c_s) D(v) \sigma_\infty}{\alpha_l (1-\alpha_s^2)} \sqrt{\frac{v}{t}} \to 0 ,$$

which indicates that steady state and K^d_I-dominant conditions are approached. For a fixed time $t > 0$, the ratio r_0/vt may vanish only as $z_0 \to 0$. For this case, the initial curve shrinks to the crack tip and even if $\dot{K}^d_I(t) \neq 0$, the caustic is generated from a K^d_I-dominant region. For a fixed z_0, at short times after crack initiation, $r_0/vt \to \infty$ ($\dot{K}^d_I(t) \to \infty$), and therefore transient effects are predominant. So the change of the nondimensional parameter r_0/vt from zero to infinity characterizes the relative influence of transients on caustic shape and size.

A qualitative discussion of the influence of higher order terms and crack tip velocity on the caustic and initial curve shapes is presented in FIGURE 5.8 and FIGURE 5.9. FIGURE 5.8 shows the influence of crack-tip speed on the caustic mapping for $r_0/vt = 0.3$. It is obvious that in the range $0.1 \leq v/c_s \leq 0.5$, changes in crack-tip velocity

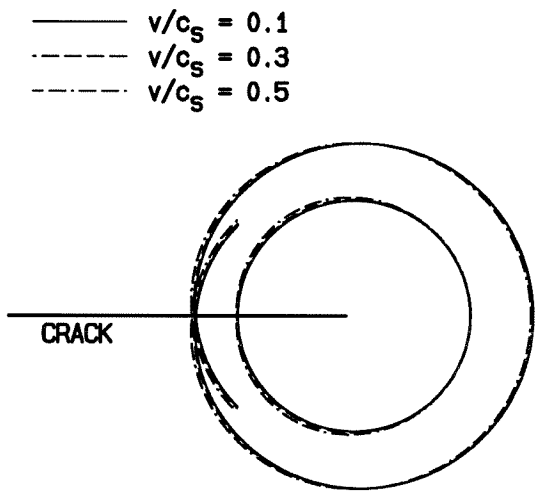

Figure 5.8: Three-term simulations of the initial and caustic curves corresponding to the Broberg problem for different crack-tip speeds, and for $r_0/vt = 0.3$.

do not markedly influence the caustic shape. The initial curve also remains almost circular. The results displayed in FIGURE 5.9 are more striking. Here, the crack-tip speed is fixed ($v/c_s = 0.3$). The ratio r_0/vt is varied to investigate the effect of transients. Indeed, variation of r_0/vt from 0 to 0.5 (see FIGURE 5.9(a)) creates rather large variations in caustic shape. The value of $r_0/vt = 0$ corresponds to caustic shape obtained by the classical (K_I^d-dominant) analysis of caustics. The differences in D and X observed for other values of r_0/vt are an indication of the error in K_I^d measurement if the classical analysis of caustics is used. On the other hand, it is very interesting to note that the initial curve is hardly influenced by the value of r_0/vt. It remains almost perfectly circular with a radius $r_l = r_0$ as assumed by equation (5.3.9) of our analysis. The major assumption pivotal to the derivation of the relation between $K_I^d(t)$, D, and X (equations (5.3.19) and (5.3.20)) is the circularity of the initial curve (equation (5.3.9)), and we feel that this provides a strong justification for our simplifying assumption. In FIGURE 5.9(b), r_0/vt is varied from 0 to 1.0. Here again the assumption of the circularity and size of the initial curve still remains valid. The

only difference to FIGURE 5.9(a) is that the center of the circle is slightly moved backwards. However the caustic shape changes drastically from the K_I^d-dominant shape.

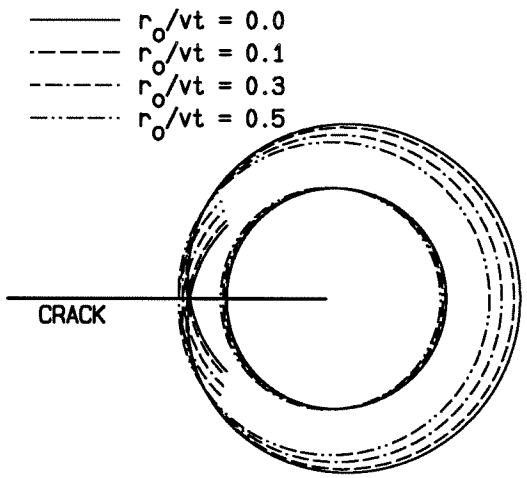

Poisson's ratio ν = 0.3, v/c_s = 0.3

(a)

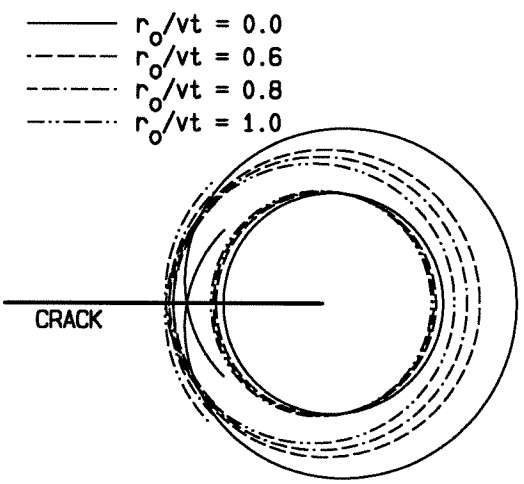

Poisson's ratio ν = 0.3, v/c_s = 0.3

(b)

Figure 5.9: Three-term simulations of the initial and caustic curves corresponding to the Broberg problem for different values of r_0/vt: (a), from 0 to 0.5; (b), from 0 to 1.0, which represents the scale of transient effects, and for $v/c_s = 0.3$.

5.5.2 Comparison of the dynamic stress intensity factor obtained from different measurement methods

The main purpose of this section is to verify the feasibility and accuracy of the measurement method proposed in section 5.3 (equations (5.3.19) and (5.3.20)). This method provides a relation between the dynamic stress intensity factor at the tip of a transiently propagating crack in terms of experimentally measurable dimensions of the caustic curve. We are also interested in comparing values of K_I^d obtained from various measurement techniques, and to access their relative accuracy. More specifically, the classical analysis of caustics, which is based on the assumption of K_I^d-dominance, will be compared with the method presented above. To implement this objective, the exact caustic patterns are generated for the Broberg problem by using equations (5.5.4) – (5.5.6). Then measurements are performed on these exact caustic patterns either by the classical analysis method or by the method proposed in section 5.3 combining with the multi-point measurement technique discussed in section 5.4.

In the classical analysis of the caustic pattern, the only quantity to be measured is the diameter of the caustics, D, and this quantity is related to the dynamic stress intensity factor, $K_I^d(t)$ by relation (5.3.27) for different crack propagating velocities. In the method presented in section 5.3 (equations (5.3.19) and (5.3.20)), the determination of $K_I^d(t)$ also requires the evaluation of another parameter, $\theta_l^{(\mathrm{D})}$. To calculate $\theta_l^{(\mathrm{D})}$, two dimensions of the caustic need to be measured. One is the transverse diameter, D, and the other, X, is the distance from the intersection of this diameter with the X_1-axis to the front point of the caustics. The parameter $\theta_l^{(\mathrm{D})}$ is then given by solving equation (5.3.20), which involves D and X as well as their ratio. Since the velocity of the crack is constant in the Broberg problem, equation (5.3.20) implies that $\theta_l^{(\mathrm{D})}$ is a function of the ratio X/D only. FIGURE 5.10 presents the variation of the parameter $\theta_l^{(\mathrm{D})}$ versus the ratio X/D for different crack-tip propagating velocities.

As we can see from this figure, the parameter $\theta_l^{(D)}$ is very sensitive to the ratio of X/D, but is not sensitive to the crack-tip speed. The effect of transience on X/D is shown in FIGURE 5.11. FIGURE 5.11 gives the variation relation between the ratio X/D and

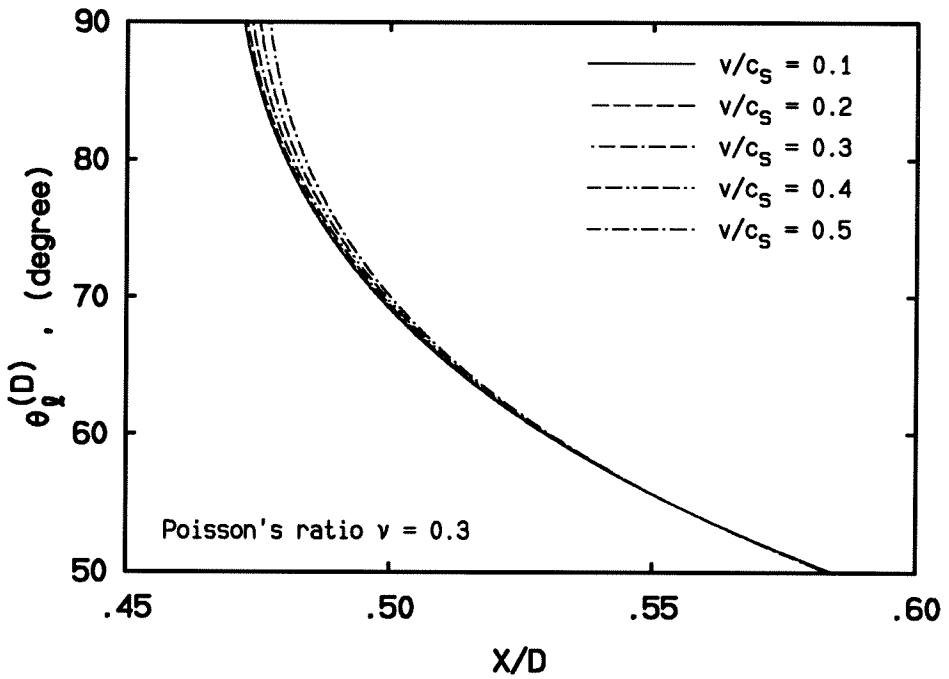

Figure 5.10: Value of the parameter $\theta_l^{(D)}$, solved from equation (5.3.20), versus the ratio X/D, for different crack-tip speeds.

the nondimensional parameter r_0/vt. It is shown that when the stress state around the crack tip deviates from K_I^d-dominance ($r_0/vt \to \infty$), the ratio X/D deviates from its steady state value which implies that the caustic becomes more elongated in the X_1-direction due to the existence of transient effects for this particular problem.

Quantitative estimates of the error incurred by the classical interpretation of caustics during crack growth are presented in FIGURE 5.12. Here the ratio

$$K^d_{I(\text{caustic})}/K^d_{I(\text{theo.})}$$

is presented as a function of the parameter r_0/vt for different crack-tip velocities. As anticipated earlier as $r_0/vt \to 0$, the classical analysis becomes accurate (either zero

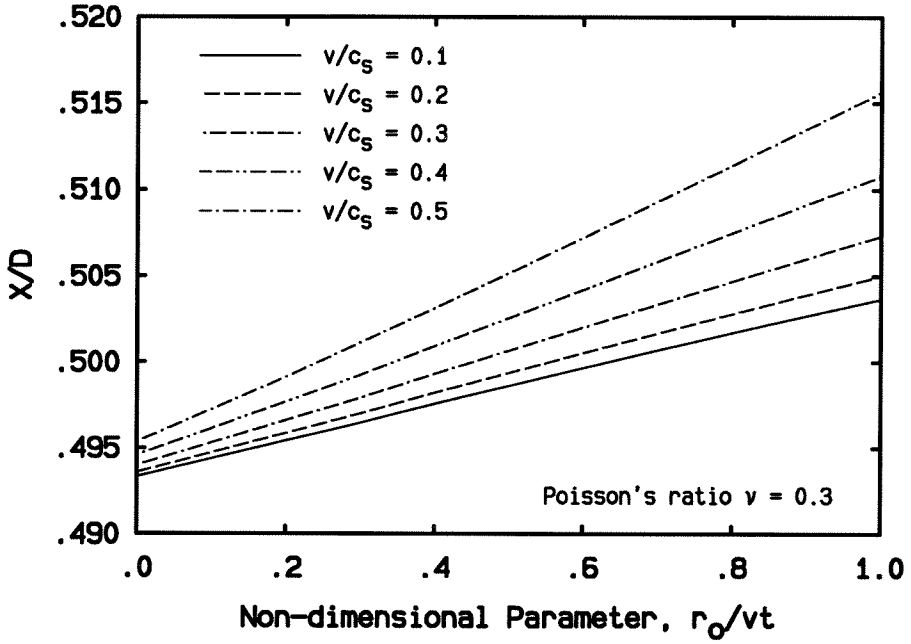

Figure 5.11: Ratio X/D versus the non-dimensional parameter r_0/vt for different crack-tip speeds.

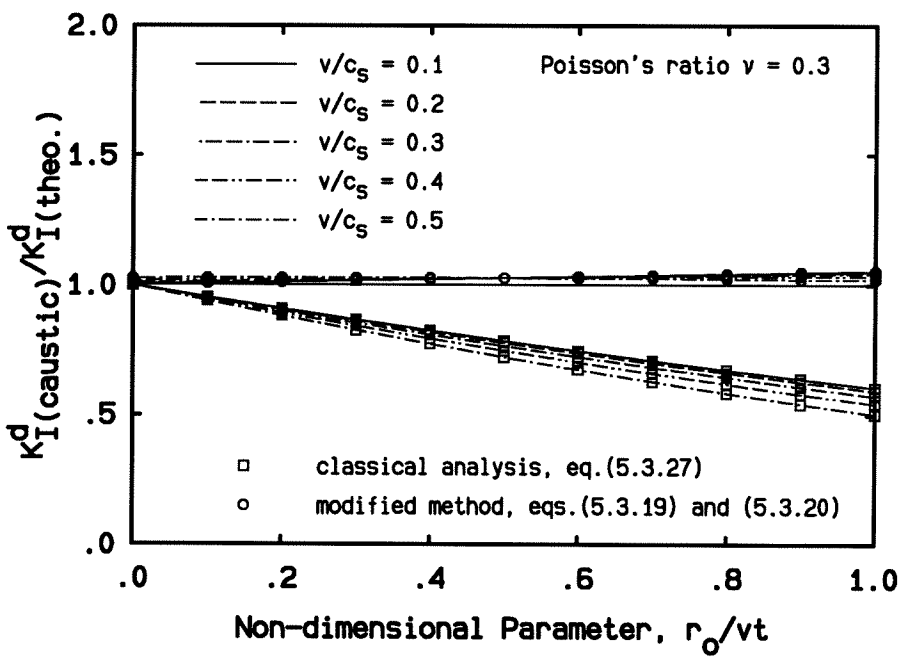

Figure 5.12: Comparison of the dynamic stress intensity factor inferred from the modified method and the classical analysis for different values of r_0/vt, and for different crack-tip speeds.

initial curve or long times after initiation). However as $r_0/vt \to \infty$, we observe large deviations of $K^d_{I(\text{caustic})}$ relative to $K^d_{I(\text{theo.})}$, which is known prior (see lines with square symbols). The figure also presents the same ratio obtained if the numerically constructed caustics are analyzed on the basis of our improved method (equations (5.3.19) and (5.3.20)). As it is obvious from the lines marked by the circles, errors of less than 5%, which are acceptable in the experimental investigation of dynamic fracture mechanics, are obtained. In both cases it is shown that the effect of velocity is small especially when the improved analysis is used.

An alternative representation of the above results is given in FIGURE 5.13, FIGURE 5.14, and FIGURE 5.15. Here $K^d_{I(\text{caustic})}/K^d_{I(\text{theo.})}$ is plotted versus time from

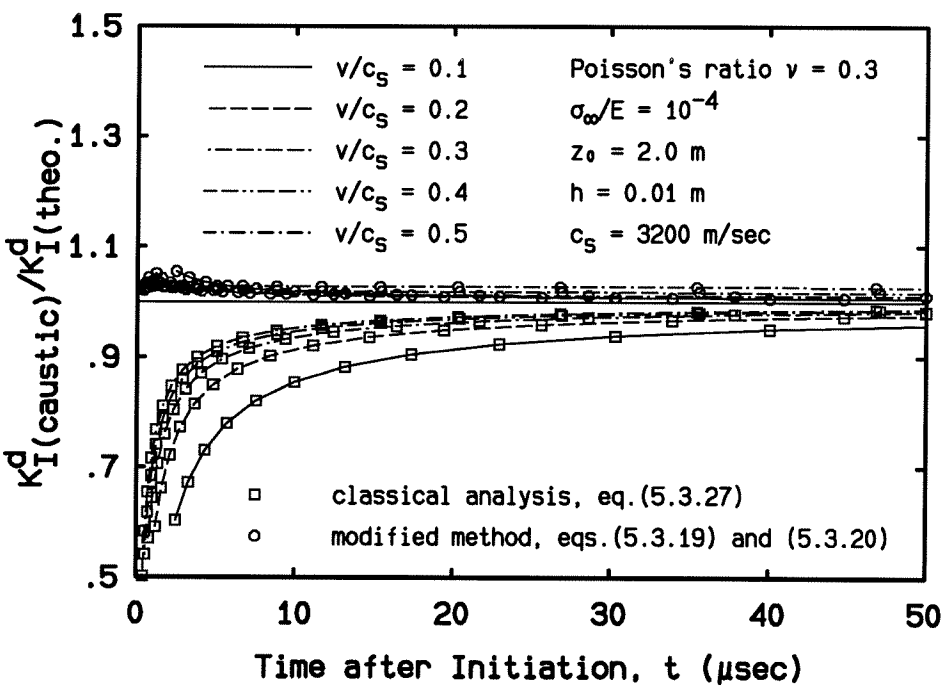

Figure 5.13: Variation of the ratio $K^d_{I(caustic)}/K^d_{I(theo.)}$ with the time after crack initiation for different crack-tip speeds. The material parameters correspond to 4340 steel.

crack initiation. The results of both improved and classical analyses of caustics are included. FIGURE 5.13 shows the variation of this ratio for a variety of crack-tip velocities for material parameters corresponding to 4340 steel, $z_0 = 2.0m$, and specimen

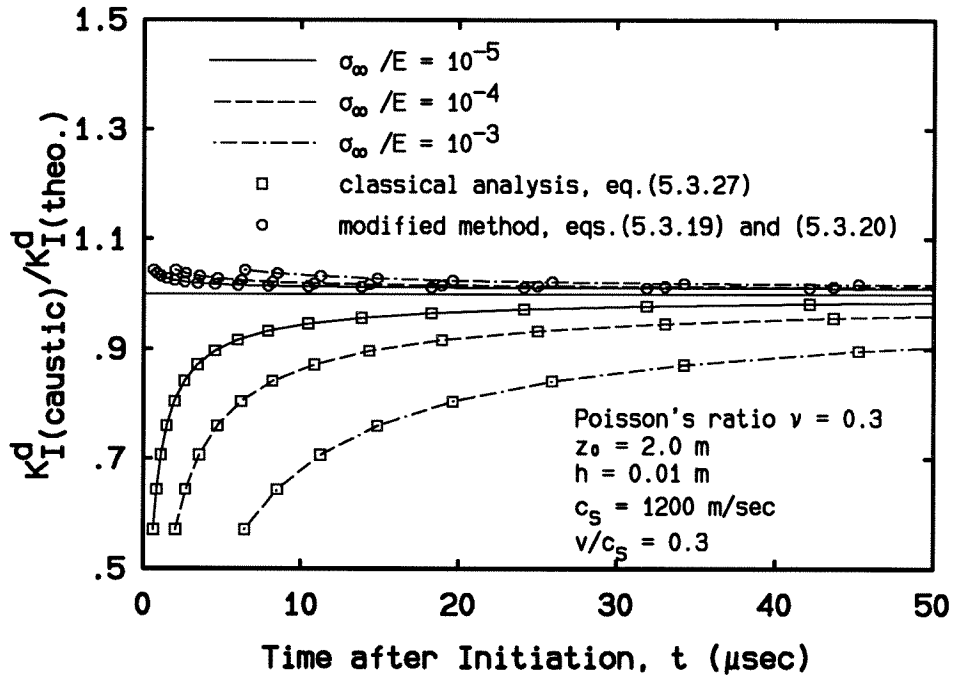

Figure 5.14: Variation of the ratio $K^d_{I(caustic)}/K^d_{I(theo.)}$ with the time after crack initiation for different load levels, σ_∞/E.

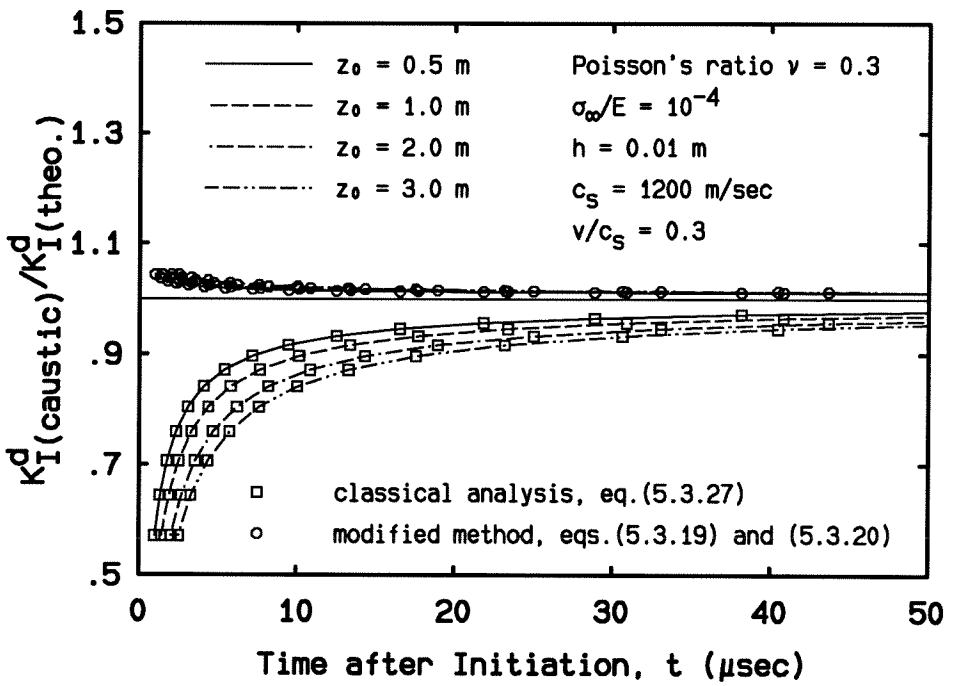

Figure 5.15: Variation of the ratio $K^d_{I(caustic)}/K^d_{I(theo.)}$ with the time after crack initiation for varying experimental parameter z_0.

thickness $h = 0.01m$. FIGURE 5.14 shows the same ratio as a function of time for different values of σ_∞/E, but the material parameters correspond to PMMA. This figure indicates that for higher load level, the transient effect is much more significant than that for the lower load level, especially at the time near the crack initiation. This reflects the fact that at a specific time t and fixed z_0, higher σ_∞/E implies larger initial curve radii (see equation (5.5.7)).

FIGURE 5.15 shows the dependence of this ratio on z_0. Here, it is evident that as z_0 is decreased (the initial curve shrinks to the crack-tip) the value of $K^d_{I(\text{caustic})}$ obtained from the classical analysis of caustics slowly approaches $K^d_{I(\text{theo.})}$. Nevertheless, large errors still persist near initiation. From the practical point of view, this is not a consolation since acceptable reductions of z_0 (and thus r_0) are limited by the size of the near tip three-dimensional zone ($\sim 0.5h$). Here the advantage of the modified interpretation becomes clear since accurate results can be obtained with relatively large values of z_0 corresponding to caustic measurements *outside* the near tip three-dimensional zone.

5.6 Discussion and concluding remarks

Motivated by recent experimental evidence (Krishnaswamy and Rosakis, 1991; Krishnaswamy *et al.*, 1990) that show the inadequacy of the classical analysis of caustics in furnishing accurate values of K^d_I in the presence of transient effects, a modified analysis of the technique is presented here. This analysis is based on a fully transient higher order expansion recently developed by Freund and Rosakis (1992) and by Liu and Rosakis (1992). The improved analysis of caustic patterns includes the influence of transients resulting because of the existence of non-uniform $K^d_I(t)$ and $v(t)$ histories (effects of $\dot{K}^d_I(t)$ and $\dot{v}(t)$). The analysis can be used to obtain $K^d_I(t)$ as well as the values of higher order terms in terms of the geometrical characteristics of the caustic

curves. The resulting expressions contain the classical results (static or dynamic K_I^d-dominant analyses) as special cases. The relative performance of the improved and the classical analyses is compared. This is done by considering the Broberg problem as an example model of transient crack growth. Based on the full Broberg solution, the caustic curves are first constructed numerically. These curves are then analyzed to obtain $K_I^d(t)$, as would be done in an experiment, and to compare with the theoretically known $K_I^d(t)$ time history. When the caustics are analyzed on the basis of equation (5.3.27) (classical K_I^d-dominant analysis) very large errors are obtained at times close to crack initiation. As a matter of fact, for this problem, such errors are unbounded as $t \to 0$. On the other hand, when equations (5.3.19) and (5.3.20) are used in the analysis of the caustic patterns, the measured $K_I^d(t)$ agrees very well with the theoretical value (to within 5%). This clearly indicates that the improved analysis of caustics, based on the higher order transient expansion, is capable of providing accurately the dynamic stress intensity factor history even if the crack growth event is very transient.

Another noteworthy fact is that the crack-tip propagating velocity is assumed to be known in the analysis. However in real applications, the crack-tip position is only approximately known, since the crack-tip is covered by the dark shadow spot. This problem can be overcome either by simultaneously using some other measurement techniques which can provide the crack-tip position at each instant of time, or by the following iteration procedure. At the beginning of the iteration process, we can assume that the caustic diameter D passes through the crack-tip. As a result, X represents the distance from the crack-tip to the front of the caustic curve. After the crack-tip position is determined by this assumption, an approximate crack-tip velocity history can be deduced. By carrying out the measurement method we proposed in section 3.3, all parameters will be determined. If we now go back to equation (5.3.11) to calculate the "real" distance from the crack-tip to the caustic front, then the

velocity history will be corrected. This procedure will be repeated until the crack-tip velocity converges at each instant of time.

The shortcomings of the classical analysis of caustics discussed in this chapter may have far-reaching consequences. In particular, caution should be exercised in the interpretation of experimental measurements obtained by caustics in the past, especially when highly transient crack problems were studied by the technique.

During the recent two decades, the optical method of caustics has been widely used in experimental solid mechanics, especially in the study of dynamic fracture processes. Another method, which is also widely adopted, is photoelasticity. The history of photoelasticity is much longer than the method of caustics and therefore can be thought as well developed. Nevertheless, due to the simplicity of the method of caustics either in the experimental set up, or in the data analysis, both techniques remain appealing as powerful candidates in the study of fracture processes. However, serious discrepancies have been reported in the literature by a number of different researchers using the classical interpretation of caustics or photoelasticity. Nigam and Shukla (1988) have compared the methods of photoelasticity and transmission caustics by performing experiments on identical specimens under identical loading. Their results show that while both methods work well for static problems, the method of photoelasticity gives values for the dynamic stress intensity factor which are about 30% – 50% different than those obtained through the method of caustics. In section 5.5, we have shown by using the Broberg problem, that for transient crack propagation with constant velocity, the value of the dynamic stress intensity factor obtained through the classical analysis of caustics can indeed produce differences of that magnitude or even higher. This provides a qualitative explanation to the different results in $K_I^d(t)$ obtained from these two techniques in Nigam and Shukla's paper. It should be pointed out that in the interpretation of their photoelastic fringes, Nigam and Shukla used a two-dimensional "higher-order" expansion suggested by Dally *et al.*

(1985). This expansion is based on the steady state asymptotic representation of the stresses around the crack-tip. As was shown in this chapter, only at the region very close to the crack-tip, the transient effects will not be felt strongly. Outside this region the dynamic transient effects will affect the stress distribution. This issue was also discussed by Krishnaswamy *et al.* (1990) by using the CGS method. It has also been shown by Rosakis *et al.* (1991) and Liu and Rosakis (1992), that the asymptotic expansion of stresses under the fully transient condition is different from that obtained under the steady state condition. The steady state, higher order expansion can be approximately used only when the time derivatives of all the coefficients are negligibly small and the crack-tip velocity is essentially constant. If these conditions are violated, the results of the steady state approximation are questionable. Nonetheless, use of a higher order steady state expansion is bound to be an improvement over the assumption of strict K_I^d-dominance. As a result, the values of $K_I^d(t)$ obtained by photoelasticity in Nigam and Shukla's paper are expected to be close to the real value of K_I^d rather than the one obtained by the classical analysis of caustics.

A long standing issue of fundamental importance in dynamic fracture research is the connection between the dynamic fracture toughness, K_{IC}^d, and the crack-tip speed. The debate, for the most part, has centered around the question of whether a unique, material dependent relationship exists between K_{IC}^d and v. Kobayashi and Dally (1980), Rosakis *et al.* (1984), and Zehnder and Rosakis (1990), among others, provide data sets that seem to indicate that a relation between K_{IC}^d and v exists and may reasonably be viewed as a material property. For most materials tested, K_{IC}^d was found to be a weakly increasing function of crack-tip velocity, for low velocities, followed by a strongly increasing branch as the crack-tip speed increases. The location of the steep branch depends on the material under consideration. The conclusion of the existence of a unique curve is usually made in the presence of experimental scatter in both K_{IC}^d and $v(t)$. In particular, it should be emphasized here that the data sets

provided by Rosakis *et al.* (1984) and Zehnder and Rosakis (1990) for AISI carbon steel, *if collectively viewed*, are characterized by a scatter in K_{IC}^d of the order of 30% for crack-tip velocities in the range of $400m/sec$ to $900m/sec$. Nonetheless it should also be remembered that the dynamic stress intensity factor was inferred by using the classical analysis of caustics which assumes K_I^d-dominance and neglects the history dependent, transient nature of the field. In addition, it should be recalled that two different specimen and loading geometries were used. Further, even within one specimen geometry, the resulting crack growth histories were intentionally varied (by controlling the starter notch radius), in order to span a representative range of crack-tip velocities. This is a common practice of most experimental investigations in this field. The above observations clearly indicate that each of these experiments was characterized by very distinct transient crack growth histories. Finally, and as was observed by Zehnder and Rosakis (1990), if data from a *single* specimen were used to explore the variation of K_{IC}^d and v, very smooth curves resulted. However, if such variations were collectively viewed, then the resulting data scatter was of the order of 30% in K_{IC}^d.

Given the above observations, it is therefore conceivable that the observed maximum scatter between tests may be due to phenomena of the type observed in section 5.5, i.e., to errors associated with the classical analysis of caustics when strict K_I^d-dominance is violated.

Another series of experiments leading to results that have yet to be explained are those reported by Dahlberg *et al.* (1980) and Kalthoff (1983), which seem to indicate that the dynamic fracture toughness could be specimen dependent. The claim of specimen dependence is made in the presence of 20% differences between curves obtained for each specimen configuration. In this case, as well, the observations related to the work of Rosakis *et al.* (1984) and of Zehnder and Rosakis (1990) are relevant. Here again the crack growth histories varied from configuration to

configuration and from specimen to specimen. As a result, it may be possible to attribute the apparent specimen dependence of K_{IC}^d vs. v to the specimen dependent transient nature of the region where the caustic measurement was made.

On the basis of some crack propagation experiments in which the optical method of caustics was used, Takahashi and Arakawa (1987) proposed that the instantaneous value of dynamic fracture toughness of their material depended on the instantaneous crack-tip acceleration. As shown in Freund and Rosakis (1992), Rosakis *et al.* (1991), and Liu and Rosakis (1992), however, the near-tip stress field expansion involves crack-tip acceleration in its third or higher order terms. As a result, caustic patterns obtained from regions where higher order terms are important will exhibit acceleration effects. However, if caustics from such a region are *interpreted* on the assumption of K_I^d-dominance then it would appear that the instantaneous value of stress intensity factor, and thus of fracture toughness of the material, depends on the instantaneous acceleration of the crack-tip.

The above comments are also relevant to the works of Kobayashi and Mall (1978) and Ravi-Chandar and Knauss (1984) who suggested that although an average increasing trend in K_{IC}^d with crack-tip velocity seems to exist, no clear, unique relation between K_{IC}^d and v could be found. Here again the question of transience in the interpretation of caustics becomes important. As discussed by Freund and Rosakis (1992), this becomes more transparent in the second reference, since there, the analytical time history of K_I^d is available to be compared with the one inferred based on caustics. Indeed it is shown that the classical analysis of caustics is adequate in predicting $K_I^d(t)$ during loading , up to the point of crack initiation. After initiation of dynamic crack growth differences of over 50% to the theoretical value are seen.

We would like to conclude this discussion by pointing out that the above observations on past experimentation (including our own work) are by no means meant to

discredit the use of caustics as an experimental tool in dynamic fracture studies. On the contrary we attempt to provide means to improve the accuracy of interpretation of this method which we believe to be a formidable tool for the study of transient crack problems. Indeed, given the extraordinary experimental simplicity of the technique and the large numbers of raw re-analyzable data already available, this seemed to be a worthwhile task. In addition, we believe that the time for taking final positions in the debate regarding the existence of a unique K_{IC}^{d} vs. v curve has not arrived yet. Our current observations merely suggest that the existing arguments (including our own in the past) based on experimental interpretations (for both photoelasticity and caustics) which neglect the transient nature of crack growth cannot be conclusive. We believe that further experimental study or even re-interpretation of raw experimental measurements using the recently available transient results is required to assess the possibilities and to resolve this issue once and for all.

Chapter 6

Highly Transient Elastodynamic Crack Growth in a Bimaterial Interface

6.1 Introduction

Advanced multiphase materials such as fiber or whisker reinforced composites have seen widespread applications in recent years. It has been recognized that interfacial fracture may play an important role in determining the overall mechanical response of such multiphase systems. It is the low fracture toughness of these materials, which may result from debonding between different phases, that limits their use in engineering applications. Therefore, the scientific understanding of the mechanics of crack formation, initiation, and crack growth in bimaterial interfaces is essential for the effective study of failure processes of these advanced composite materials.

The earliest study of interfacial fracture appears to be by Williams (1959), who examined the local fields near the tip of a traction free semi-infinite interfacial crack, lying between two otherwise perfectly bonded elastic half spaces. He observed that, unlike in homogeneous materials, the interfacial crack exhibits an oscillatory stress singularity. Since then, Sih and Rice (1964), and Rice and Sih (1965) have provided explicit expressions for the near-tip stresses and related them to remote elastic stress fields. The works of Erdogan (1965), England (1965), and Malyshev and Salganik

(1965) have also further examined two-dimensional singular models for single or multiple crack configurations in bimaterial systems. Recent progress in static interfacial fracture includes work by Rice (1988), Hutchinson and Suo (1991), and Shih (1991).

Depending on the nature of loads that the composite structure is subjected to, the debonding process may take place dynamically. If the interface is already weakened by pre-existing flaws, these flaws may serve as sites of initiation of cracks which propagate unstably along the interface under the right circumstances. Such situations have motivated attempts to analyze dynamic crack propagation in interfaces. However, due to the complexity of the problem, thus far, only a few theoretical results of dynamic bimaterial crack growth have been obtained. Among others, Gol'dstein (1967), Brock and Achenbach (1973), Willis (1971, 1973), and Atkinson (1977) have provided crack line solutions of particular fracture problems. Although these analytical results have provided some insights of the near-tip dynamic behavior, in order to effectively formulate and apply crack initiation and growth criteria in bimaterial systems, we need knowledge about the complete spatial structure of the field surrounding the moving interfacial crack-tip.

More recently, experimental investigations of interfacial crack-tip deformation fields have been carried out by Tippur and Rosakis (1991) and Rosakis *et al.* (1991) using the optical method of Coherent Gradient Sensing (CGS) (Rosakis, 1993) and high speed photography. The bimaterial system they used was a PMMA/aluminum combination. They observed substantial crack-tip speeds (up to $90\% c_R^{\mathrm{PMMA}}$) associated with crack initiation and growth. Motivated by these observations, Yang *et al.* (1991) provided the asymptotic structure of the most singular term of the steady state elastodynamic bimaterial crack-tip fields. In the work of Wu (1991), similar conclusions were reached. In addition, Deng (1992) obtained the asymptotic series representation of the stress field near the tip of a running interfacial crack in a bimaterial system under steady state conditions. Also motivated by the experiments of

Tippur and Rosakis (1991), Lo *et al.* (1992) have performed a numerical analysis of the same bimaterial system as was used in the experiments.

The question of whether there exists a K^d-dominant region surrounding the crack-tip (i.e., a region where the stress field can be well described by the leading singular term only), or in fact whether steady state crack propagation constitutes a good assumption in analysis, are issues to be verified by experimental observations. New experimental evidence, which will be described in this chapter, emphasize the existence of substantial crack-tip accelerations in addition to very high crack-tip speeds. The existence of high accelerations violates the conditions under which the steady state assumption may confidently be applied. Motivated by the above experimental evidence, in this chapter, we investigate the asymptotic structure of the near-tip field in a bimaterial system, where a highly transient elastodynamic crack growth history has occurred. To do so, we employ the asymptotic procedure proposed by Freund (1990) and utilized by Freund and Rosakis (1992) in studying the transient growth of a mode-I crack in a homogeneous isotropic material. The same procedure was employed by Liu and Rosakis (1992) in studying the mixed-mode transient growth of a crack along an arbitrary curved path in a homogeneous isotropic solid (see Chapter 2). For anisotropic solids, transient crack growth under mode-I conditions was recently explored by Willis (1992).

In Section 6.2 of the present study, the general formulation and properties of the asymptotic procedure are described. By using this asymptotic methodology, the equation of motion is reduced to a series of coupled partial differential equations. In Section 6.3, the solution for the higher order transient problem is obtained. By imposing the boundary conditions along the surface of the interfacial crack and the bonding conditions along the interface ahead of the crack-tip, our problem can be further recast into a Riemann-Hilbert problem. Upon solving the Riemann-Hilbert equation and evaluating the Stieltjes transforms, the higher order near-tip transient

elastodynamic asymptotic field can be obtained. In Section 6.4, the asymptotic elastodynamic stress field surrounding the interfacial crack-tip is studied. The first stress invariant is provided explicitly. The properties of the interfacial mismatch parameters are studied in Section 6.5. These depend on the properties of the bimaterial combination and the crack-tip speed. In some of the available experiments by Rosakis *et al.* (1991), and the experimental evidence described in this chapter, it has been observed that an interfacial crack can reach speeds amounting to a considerable fraction, or even exceeding the lower Rayleigh wave speed of the two constituents of the interface. Recognizing that our analysis need not be limited to a velocity regime below the lower Rayleigh wave speed, in Section 6.6, we extend our solution to the case when the crack is traveling at a speed between the lower Rayleigh and shear wave speeds. Finally, in Section 6.7, recent experimental evidence of a transient higher order stress field in bimaterial fracture specimens is presented. The transient theoretical fields obtained in previous sections are used to quantitatively analyze optical interferograms obtained in real time high speed photography of dynamic bimaterial experiments in a PMMA/steel system. In addition, we present experimental evidence of transonic crack growth histories involving maximum speeds between 60% and 80% of the *dilatational* wave speed of PMMA. For comparison purposes, one should note that typical terminal crack-tip speeds in homogeneous PMMA are of the order of only 20% of the dilatational wave speed.

6.2 General formulation

Consider a planar body composed of two homogeneous, isotropic, and linearly elastic materials which are bonded along a straight line interface. A crack propagates nonuniformly along the interface, see Figure 6.1. Introduce a fixed orthonormal Cartesian coordinate system (x_1, x_2) so that the x_1-axis lies on the interface and coincides with the direction of the propagating crack. Suppose that the crack propagates with a non-

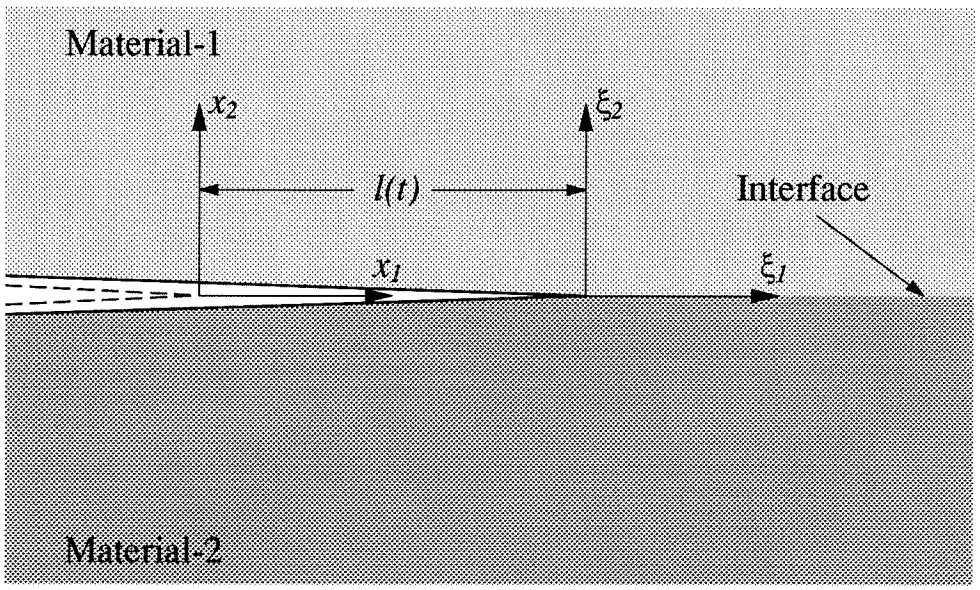

Figure 6.1: Schematic of dynamic growth of a crack along the bimaterial interface.

uniform speed, $v(t)$, and the crack faces satisfy traction free boundary conditions. At a time $t = 0$, the crack-tip happens to be at the origin of the system, so the growth of the interfacial crack at any $t > 0$ is characterized by the length $l(t)$ $(v(t) = \dot{l}(t))$, which is the distance from the origin to the moving crack-tip. If the deformation is assumed to be plane strain, for each of the two materials comprising the interface, the displacement field may be generated from two displacement potentials, $\phi_k(x_1, x_2, t)$ and $\psi_k(x_1, x_2, t)$, where $k \in \{1, 2\}$. Here, the integer k is assigned to distinguish between the two different materials. In Figure 1, material–1 is the one shown above while material–2 is the one shown below the interface. Then, in either one of the two materials, the two non-zero displacement components can be expressed as

$$u_\alpha(x_1, x_2, t) = \phi_{,\alpha}(x_1, x_2, t) + e_{\alpha\beta}\psi_{,\beta}(x_1, x_2, t) \ , \tag{6.2.1}$$

where α, $\beta \in \{1, 2\}$. Similarly, in either one of the two materials, the components of stress can also be expressed in terms of the displacement potentials which have been given in Chapter 2. The corresponding plane stress solution can be obtained

by changing some material constants. In the absence of body forces, the equation of motion for each material that constitutes the bimaterial system is the same as that given in Chapter 2.

We now introduce a new moving coordinate system, (ξ_1, ξ_2), by

$$\xi_1 = x_1 - l(t) \ , \qquad \xi_2 = x_2 \ . \tag{6.2.2}$$

This system is such that its origin is translating with the crack-tip. In this new system, the equations of motion for $\phi(\xi_1, \xi_2, t)$ and $\psi(\xi_1, \xi_2, t)$ become (Freund, 1990)

$$\left.\begin{aligned} \left(1 - \frac{v^2(t)}{c_l^2}\right)\phi_{,11} + \phi_{,22} + \frac{\dot{v}(t)}{c_l^2}\phi_{,1} + \frac{2v(t)}{c_l^2}\phi_{,1t} - \frac{1}{c_l^2}\phi_{,tt} &= 0 \\ \left(1 - \frac{v^2(t)}{c_s^2}\right)\psi_{,11} + \psi_{,22} + \frac{\dot{v}(t)}{c_s^2}\psi_{,1} + \frac{2v(t)}{c_s^2}\psi_{,1t} - \frac{1}{c_s^2}\psi_{,tt} &= 0 \end{aligned}\right\} . \tag{6.2.3}$$

Notice that, similar to the notation used in Chapter 2, we use $\partial/\partial t$, or $\{\ \}_{,t}$ to denote differentiation with respect to time, t, when the moving spatial coordinates (ξ_1, ξ_2) are held fixed. The notation $\{\ \dot{}\ \}$ denotes the same operation when the spatial coordinates (x_1, x_2) are held fixed.

Once again, like in Chapter 2, we employ the standard asymptotic device used by Freund and Rosakis (1992) for the analysis of transient crack growth in homogeneous materials. We assume that $\phi(\xi_1, \xi_2, t)$ and $\psi(\xi_1, \xi_2, t)$, for each material, can be asymptotically expanded as

$$\left.\begin{aligned} \phi(\xi_1, \xi_2, t) &= \sum_{m=0}^{\infty} \varepsilon^{p_m} \phi_m(\eta_1, \eta_2, t) \\ \psi(\xi_1, \xi_2, t) &= \sum_{m=0}^{\infty} \varepsilon^{p_m} \psi_m(\eta_1, \eta_2, t) \end{aligned}\right\} , \tag{6.2.4}$$

as $r = (\xi_1^2 + \xi_2^2)^{1/2} \to 0$, where $\eta_\alpha = \xi_\alpha/\varepsilon$, $\alpha \in \{1, 2\}$, and ε is a small arbitrary positive number. Under this asymptotic expansion, the crack line occupies the whole negative η_1-axis. By taking $\varepsilon = 1$, the above equations will provide the asymptotic

representation of the displacement potentials in the unscaled physical plane for each of the materials, respectively.

The asymptotic representation (6.2.4) possesses some properties, namely,

$$\left.\begin{aligned} & p_{m+1} = p_m + \frac{1}{2}\,, && m = 0,1,2,\cdots \\ & \frac{\varepsilon^{p_{m+n}}\phi_{m+n}(\eta_1,\eta_2,t)}{\varepsilon^{p_m}\phi_m(\eta_1,\eta_2,t)} \to 0\,, && \text{as} \quad \varepsilon \to 0 \\ & \frac{\phi_{m+n}(\xi_1,\xi_2,t)}{\phi_m(\xi_1,\xi_2,t)} \to 0\,, && \text{as} \quad r = \sqrt{\xi_1^2+\xi_2^2} \to 0 \end{aligned}\right\}\,, \tag{6.2.5}$$

for any positive integer n, and $1 < p_0 < 2$. Notice that from equation (6.2.5), in the physical plane, (ξ_1,ξ_2), $\phi_m(\xi_1,\xi_2,t)$ are ordered according to their contributions to the near-tip deformation field. The above properties for ϕ_m hold for ψ_m as well.

Substituting the asymptotic representations for $\phi(\xi_1,\xi_2,t)$ and $\psi(\xi_1,\xi_2,t)$, (6.2.4), into the equations of motion, (6.2.3), we obtain two equations whose left-hand side is an infinite power series in ε and whose right-hand side vanishes. Since ε is an arbitrary number, the coefficient of each power of ε should be zero. Therefore, the equations of motion reduce to a series of coupled differential equations for $\phi_m(\eta_1,\eta_2,t)$ and $\psi_m(\eta_1,\eta_2,t)$ as follows (Rosakis *et al.*, 1991; Freund and Rosakis, 1992):

$$\left.\begin{aligned} \phi_{m,11} + \frac{1}{\alpha_l^2(t)}\phi_{m,22} &= -\frac{2v^{1/2}(t)}{\alpha_l^2(t)c_l^2}\left\{v^{1/2}(t)\phi_{m-2,1}\right\}_{,t} + \frac{1}{\alpha_l^2(t)c_l^2}\phi_{m-4,tt} \\ \psi_{m,11} + \frac{1}{\alpha_s^2(t)}\psi_{m,22} &= -\frac{2v^{1/2}(t)}{\alpha_s^2(t)c_s^2}\left\{v^{1/2}(t)\psi_{m-2,1}\right\}_{,t} + \frac{1}{\alpha_s^2(t)c_s^2}\psi_{m-4,tt} \end{aligned}\right\}\,, \tag{6.2.6}$$

for $m = 0,1,2,\cdots$, and the quantities α_l and α_s depend on the crack-tip speed, and therefore on time t through

$$\alpha_{l,s}(t) = \left\{1 - \frac{v^2(t)}{c_{l,s}^2}\right\}^{1/2}\,. \tag{6.2.7}$$

Also

$$\phi_m = \begin{cases} \phi_m & \text{for } m \geq 0 \\ 0 & \text{for } m < 0 \end{cases}\,, \qquad \psi_m = \begin{cases} \psi_m & \text{for } m \geq 0 \\ 0 & \text{for } m < 0 \end{cases}\,. \tag{6.2.8}$$

Equation (6.2.6) can also be obtained from equations (2.2.16) and (2.2.17) by setting the curvature at the moving crack-tip, $k(t) = 0$, since we are considering a straight propagating crack.

In what will follow, for our convenience, we drop the subscript which is used to distinguish between the two materials. However, we should keep in mind that the above asymptotic form of the equations of motion (6.2.6) hold for each of the materials with the appropriate elastic constants. The term "coupled" is used above in the sense that the higher order solutions for ϕ_m and ψ_m will depend on the lower order solutions for the same quantities. It is noted that, for the special case of *steady state* crack growth, the crack-tip speed, v, will be a constant, and at the same time, $\phi_{m,t} = \psi_{m,t} = 0$, for $m = 0, 1, 2, \cdots$. This means that ϕ_m and ψ_m depend on t only through the spatial scaled coordinate η_1. In such a case, the equations in (6.2.6) are not coupled anymore, and each one reduces to Laplace's equation in the coordinates $(\eta_1, \alpha_l\eta_2)$ for ϕ_m and $(\eta_1, \alpha_s\eta_2)$ for ψ_m. For steady state conditions, the functions ϕ_m and ψ_m are independent of time in the moving coordinate system. For the transient case, however, the crack-tip speed, $v(t)$, may be an arbitrary smooth function of time, and also ϕ_m and ψ_m may depend on time explicitly in the moving coordinate system. The only uncoupled equations are those for $m = 0$ and $m = 1$. For $m > 1$, we can see from (6.2.6) that the solutions for ϕ_m, and ψ_m are composed of two parts. One is the particular solution which is wholly determined by lower order solutions for ϕ_m, and ψ_m. The other part is the homogeneous solution which satisfies Laplace's equation in the corresponding scaled coordinate plane. The combination of the particular and homogeneous solutions should satisfy the traction free conditions on the crack faces as well as the bonding conditions along the interface. In the following sections, we will solve for ϕ_m and ψ_m for the most general transient situation, and for both materials.

It should be noted that the steady state problem could be solved using the efficient Stroh formulation. This formulation reduces the two spatial and one temporal

variables to only two spatial variables and takes advantage of a well known formalism to solve the steady state crack problem (Yang *et al.*, 1991). However, this approach, although it can be easily be extended to anisotropic solids, is strictly restricted to steady state conditions and cannot be used for our present purposes.

6.3 Solution for the higher order transient problem

Similar to the procedures used in Chapter 2, in this section, we consider the situation of $m = 0$ and $m = 1$ first. After we get solutions for $m = 0$ and 1, we will subsequently solve for higher order ϕ_m and ψ_m in each material. The method and procedure used in this section are very similar, or even identical to those used in Chapter 2. However, because the situation becomes more complicated for the bimaterial system, for sake of self-containedness, I will repeat every step which is necessary to solve the problem.

6.3.1 Solutions for $\phi_m(\eta_1, \eta_2, t)$ and $\psi_m(\eta_1, \eta_2, t)$ for $m = 0$ and 1

For $m = 0$, or 1, (6.2.6) reduce to

$$\left.\begin{aligned} \phi_{m,11}(\eta_1, \eta_2, t) + \frac{1}{\alpha_l^2(t)}\phi_{m,22}(\eta_1, \eta_2, t) &= 0 \\ \psi_{m,11}(\eta_1, \eta_2, t) + \frac{1}{\alpha_s^2(t)}\psi_{m,22}(\eta_1, \eta_2, t) &= 0 \end{aligned}\right\} . \tag{6.3.1}$$

The above equations are Laplace's equations in the corresponding scaled planes $(\eta_1, \alpha_l\eta_2)$ for ϕ_m, and $(\eta_1, \alpha_s\eta_2)$ for ψ_m. As we have mentioned earlier, the subscript k is omitted here, but the above equations hold for both materials that constitute the bimaterial body.

The most general solutions for equations (6.3.1) can be expressed as

$$\phi_m(\eta_1,\eta_2,t) = \mathrm{Re}\{F_m(z_l;t)\}\ , \qquad \psi_m(\eta_1,\eta_2,t) = \mathrm{Im}\{G_m(z_s;t)\}\ , \tag{6.3.2}$$

where the two complex variables z_l and z_s are given by

$$z_l = \eta_1 + i\alpha_l\eta_2\ , \qquad z_s = \eta_1 + i\alpha_s\eta_2\ ,$$

and $i = \sqrt{-1}$. For the bimaterial system, $F_{mk}(z_l;t)$ and $G_{mk}(z_s;t)$ are analytic in the upper half complex z_{lk}–, or z_{sk}–planes for $k = 1$ (upper material), and analytic in the lower half complex z_{lk}–, or z_{sk}–planes for $k = 2$ (lower material). The complex conjugates of these functions are also analytic on the plane obtained by reflection along the real axis, e.g., $\overline{F}_{m1}(\overline{z}_l;t)$ is an analytic function on the $\overline{z}_l$ plane. Since α_l and α_s are different for each material, the scaled complex variables z_l and z_s will also be different. For fully transient problems, in the analytic functions $F_{mk}(z_l;t)$ and $G_{mk}(z_s;t)$, time t appears as a parameter. This suggests that these functions will depend on time t not only through the complex variables, z_l and z_s, but also directly through time t itself.

The displacement and stress components associated with these ϕ_m and ψ_m, are given by

$$\left.\begin{aligned} u_1^{(m)} &= \mathrm{Re}\left\{F_m'(z_l;t) + \alpha_s G_m'(z_s;t)\right\} \\ u_2^{(m)} &= -\mathrm{Im}\left\{\alpha_l F_m'(z_l;t) + G_m'(z_s;t)\right\} \end{aligned}\right\}\ , \tag{6.3.3}$$

and

$$\left.\begin{aligned} \sigma_{11}^{(m)} &= \mu\mathrm{Re}\left\{\left(1+2\alpha_l^2-\alpha_s^2\right)F_m''(z_l;t) + 2\alpha_s G_m''(z_s;t)\right\} \\ \sigma_{22}^{(m)} &= -\mu\mathrm{Re}\left\{\left(1+\alpha_s^2\right)F_m''(z_l;t) + 2\alpha_s G_m''(z_s;t)\right\} \\ \sigma_{12}^{(m)} &= -\mu\mathrm{Im}\left\{2\alpha_l F_m''(z_l;t) + \left(1+\alpha_s^2\right)G_m''(z_s;t)\right\} \end{aligned}\right\}\ , \tag{6.3.4}$$

where primes denote the derivative with respect to the corresponding complex arguments.

For any analytic function $\Omega(z)$, define the following,

$$\left.\begin{aligned}\lim_{\eta_2\to 0^+}\Omega(z)&=\Omega^+(\eta_1)\\ \lim_{\eta_2\to 0^-}\Omega(z)&=\Omega^-(\eta_1)\end{aligned}\right\}, \qquad z=\eta_1+i\eta_2\ .$$

For $\eta_1<0$ and $\eta_2\to 0^+$, the traction free condition on the upper crack face gives

$$\left\{\sigma_{22}^{(m)}\right\}_1=\left\{\sigma_{12}^{(m)}\right\}_1=0\ ,$$

or, in terms of the complex displacement potentials $F_m(z_l;t)$ and $G_m(z_s;t)$,

$$\left.\begin{aligned}&\left\{\mu(1+\alpha_s^2)\left[F_m'^{+}(\eta_1;t)+\overline{F}_m'^{-}(\eta_1;t)\right]+2\mu\alpha_s\left[G_m'^{+}(\eta_1;t)+\overline{G}_m'^{-}(\eta_1;t)\right]\right\}_1=0\\ &\left\{2\mu\alpha_l\left[F_m'^{+}(\eta_1;t)-\overline{F}_m'^{-}(\eta_1;t)\right]+\mu(1+\alpha_s^2)\left[G_m'^{+}(\eta_1;t)-\overline{G}_m'^{-}(\eta_1;t)\right]\right\}_1=0\end{aligned}\right\}, \tag{6.3.5}$$

For $\eta_1<0$ and $\eta_2\to 0^-$, the traction free condition on the lower crack face gives

$$\left\{\sigma_{22}^{(m)}\right\}_2=\left\{\sigma_{12}^{(m)}\right\}_2=0\ ,$$

or

$$\left.\begin{aligned}&\left\{\mu(1+\alpha_s^2)\left[F_m'^{-}(\eta_1;t)+\overline{F}_m'^{+}(\eta_1;t)\right]+2\mu\alpha_s\left[G_m'^{-}(\eta_1;t)+\overline{G}_m'^{+}(\eta_1;t)\right]\right\}_2=0\\ &\left\{2\mu\alpha_l\left[F_m'^{-}(\eta_1;t)-\overline{F}_m'^{+}(\eta_1;t)\right]+\mu(1+\alpha_s^2)\left[G_m'^{-}(\eta_1;t)-\overline{G}_m'^{+}(\eta_1;t)\right]\right\}_2=0\end{aligned}\right\}. \tag{6.3.6}$$

The above equations, (6.3.5) and (6.3.6), hold for $\eta_1<0$.

Along the interface, or $\eta_1>0$ and $\eta_2=0$, the bonding conditions should be satisfied, which implies that

$$\left.\begin{aligned}&\left\{\sigma_{22}^{(m)}\right\}_1-\left\{\sigma_{22}^{(m)}\right\}_2=0,\quad \left\{\sigma_{12}^{(m)}\right\}_1-\left\{\sigma_{12}^{(m)}\right\}_2=0\\ &\left\{u_1^{(m)}\right\}_1-\left\{u_1^{(m)}\right\}_2=0,\quad \left\{u_2^{(m)}\right\}_1-\left\{u_2^{(m)}\right\}_2=0\end{aligned}\right\},\ \forall\ \eta_1>0,\ \eta_2=0\ ,$$

or, in terms of $F_m(z_l;t)$ and $G_m(z_s;t)$, from traction continuity,

$$\left.\begin{aligned}
&\left\{\mu(1+\alpha_s^2)\left[F_m''^{+}(\eta_1;t)+\overline{F}_m''^{-}(\eta_1;t)\right]+2\mu\alpha_s\left[G_m''^{+}(\eta_1;t)+\overline{G}_m''^{-}(\eta_1;t)\right]\right\}_1\\
&-\left\{\mu(1+\alpha_s^2)\left[F_m''^{-}(\eta_1;t)+\overline{F}_m''^{+}(\eta_1;t)\right]+2\mu\alpha_s\left[G_m''^{-}(\eta_1;t)+\overline{G}_m''^{+}(\eta_1;t)\right]\right\}_2=0\\
&\left\{2\mu\alpha_l\left[F_m''^{+}(\eta_1;t)-\overline{F}_m''^{-}(\eta_1;t)\right]+\mu(1+\alpha_s^2)\left[G_m''^{+}(\eta_1;t)-\overline{G}_m''^{-}(\eta_1;t)\right]\right\}_1\\
&-\left\{2\mu\alpha_l\left[F_m''^{-}(\eta_1;t)-\overline{F}_m''^{+}(\eta_1;t)\right]+\mu(1+\alpha_s^2)\left[G_m''^{-}(\eta_1;t)-\overline{G}_m''^{+}(\eta_1;t)\right]\right\}_2=0
\end{aligned}\right\}, \tag{6.3.7}$$

and from displacement continuity,

$$\left.\begin{aligned}
&\left\{\left[F_m'^{+}(\eta_1;t)+\overline{F}_m'^{-}(\eta_1;t)\right]+\alpha_s\left[G_m'^{+}(\eta_1;t)+\overline{G}_m'^{-}(\eta_1;t)\right]\right\}_1\\
&-\left\{\left[F_m'^{-}(\eta_1;t)+\overline{F}_m'^{+}(\eta_1;t)\right]+\alpha_s\left[G_m'^{-}(\eta_1;t)+\overline{G}_m'^{+}(\eta_1;t)\right]\right\}_2=0\\
&\left\{\alpha_l\left[F_m'^{+}(\eta_1;t)-\overline{F}_m'^{-}(\eta_1;t)\right]+\left[G_m'^{+}(\eta_1;t)-\overline{G}_m'^{-}(\eta_1;t)\right]\right\}_1\\
&-\left\{\alpha_l\left[F_m'^{-}(\eta_1;t)-\overline{F}_m'^{+}(\eta_1;t)\right]+\left[G_m'^{-}(\eta_1;t)-\overline{G}_m'^{+}(\eta_1;t)\right]\right\}_2=0
\end{aligned}\right\}. \tag{6.3.8}$$

The above equations, (6.3.7) and (6.3.8), hold for $\eta_1 > 0$.

For simplicity, define the following matrices for each material, $k \in \{1,2\}$,

$$\boldsymbol{P}_k=\begin{bmatrix}\mu(1+\alpha_s^2) & 2\mu\alpha_s\\ 2\mu\alpha_l & \mu(1+\alpha_s^2)\end{bmatrix}_k,\qquad \boldsymbol{Q}_k=\begin{bmatrix}\mu(1+\alpha_s^2) & 2\mu\alpha_s\\ -2\mu\alpha_l & -\mu(1+\alpha_s^2)\end{bmatrix}_k,$$

$$\boldsymbol{U}_k=\begin{bmatrix}1 & \alpha_s\\ \alpha_l & 1\end{bmatrix}_k,\qquad \boldsymbol{V}_k=\begin{bmatrix}1 & \alpha_s\\ -\alpha_l & -1\end{bmatrix}_k.$$

Also define the following complex vector for each material,

$$\boldsymbol{f}_{mk}(z;t)=\left(\,F_{mk}(z;t),\;G_{mk}(z;t)\,\right)^{\mathsf{T}},$$

where $z=\eta_1+i\eta_2$. From above definitions, the boundary and bonding conditions, equations (6.3.5), (6.3.6), (6.3.7), and (6.3.8), can be rewritten as

$$\left.\begin{aligned}
&\boldsymbol{P}_1\boldsymbol{f}_{m1}''^{+}(\eta_1;t)+\boldsymbol{Q}_1\overline{\boldsymbol{f}}_{m1}''^{-}(\eta_1;t)=\boldsymbol{o}\\
&\boldsymbol{P}_2\boldsymbol{f}_{m2}''^{-}(\eta_1;t)+\boldsymbol{Q}_2\overline{\boldsymbol{f}}_{m2}''^{+}(\eta_1;t)=\boldsymbol{o}
\end{aligned}\right\},\qquad \forall\ \eta_1<0\,, \tag{6.3.9}$$

and

$$\left.\begin{aligned} \boldsymbol{P}_1\boldsymbol{f}''^{+}_{m1}(\eta_1;t) + \boldsymbol{Q}_1\overline{\boldsymbol{f}}''^{-}_{m1}(\eta_1;t) - \boldsymbol{P}_2\boldsymbol{f}''^{-}_{m2}(\eta_1;t) - \boldsymbol{Q}_2\overline{\boldsymbol{f}}''^{+}_{m2}(\eta_1;t) = \mathbf{o} \\ \boldsymbol{U}_1\boldsymbol{f}'^{+}_{m1}(\eta_1;t) + \boldsymbol{V}_1\overline{\boldsymbol{f}}'^{-}_{m1}(\eta_1;t) - \boldsymbol{U}_2\boldsymbol{f}'^{-}_{m2}(\eta_1;t) - \boldsymbol{V}_2\overline{\boldsymbol{f}}'^{+}_{m2}(\eta_1;t) = \mathbf{o} \end{aligned}\right\}, \ \forall\ \eta_1 > 0. \tag{6.3.10}$$

Further, the bonding conditions in (6.3.10) can be rearranged as

$$\left.\begin{aligned} \boldsymbol{P}_1\boldsymbol{f}''^{+}_{m1}(\eta_1;t) - \boldsymbol{Q}_2\overline{\boldsymbol{f}}''^{+}_{m2}(\eta_1;t) = \boldsymbol{P}_2\boldsymbol{f}''^{-}_{m2}(\eta_1;t) - \boldsymbol{Q}_1\overline{\boldsymbol{f}}''^{-}_{m1}(\eta_1;t) \\ \boldsymbol{U}_1\boldsymbol{f}'^{+}_{m1}(\eta_1;t) - \boldsymbol{V}_2\overline{\boldsymbol{f}}'^{+}_{m2}(\eta_1;t) = \boldsymbol{U}_2\boldsymbol{f}'^{-}_{m2}(\eta_1;t) - \boldsymbol{V}_1\overline{\boldsymbol{f}}'^{-}_{m1}(\eta_1;t) \end{aligned}\right\}, \ \forall\ \eta_1 > 0\ . \tag{6.3.11}$$

In the above equations (6.3.11), the left-hand sides are the limiting values of functions which are analytic in the *upper* half plane. The right-hand sides are the limiting values of functions which are analytic in the *lower* half plane. Since the limiting values are the same along the positive real axis, the function $\boldsymbol{P}_2\boldsymbol{f}''_{m2}(z;t) - \boldsymbol{Q}_1\overline{\boldsymbol{f}}''_{m1}(z;t)$ defined in the lower half plane, is the analytic continuation of the function $\boldsymbol{P}_1\boldsymbol{f}''_{m1}(z;t) - \boldsymbol{Q}_2\overline{\boldsymbol{f}}''_{m2}(z;t)$ which is defined in the upper half plane, and vice versa. This results from the continuation properties of analytic functions. As a result, we can write

$$\left.\begin{aligned} \boldsymbol{P}_1\boldsymbol{f}''_{m1}(z;t) - \boldsymbol{Q}_2\overline{\boldsymbol{f}}''_{m2}(z;t) = \boldsymbol{\kappa}_m(z;t)\ , \qquad z \in S^+ \\ \boldsymbol{P}_2\boldsymbol{f}''_{m2}(z;t) - \boldsymbol{Q}_1\overline{\boldsymbol{f}}''_{m1}(z;t) = \boldsymbol{\kappa}_m(z;t)\ , \qquad z \in S^- \end{aligned}\right\}, \tag{6.3.12}$$

and

$$\left.\begin{aligned} \boldsymbol{U}_1\boldsymbol{f}'_{m1}(z;t) - \boldsymbol{V}_2\overline{\boldsymbol{f}}'_{m2}(z;t) = \boldsymbol{\theta}_m(z;t)\ , \qquad z \in S^+ \\ \boldsymbol{U}_2\boldsymbol{f}'_{m2}(z;t) - \boldsymbol{V}_1\overline{\boldsymbol{f}}'_{m1}(z;t) = \boldsymbol{\theta}_m(z;t)\ , \qquad z \in S^- \end{aligned}\right\}, \tag{6.3.13}$$

where

$$S^{\pm} = \begin{cases} \{\ (\eta_1,\ i\eta_2)\ \mid\ -\infty < \eta_1 < \infty,\ \eta_2 \geq 0\ \} - C \\ \{\ (\eta_1,\ i\eta_2)\ \mid\ -\infty < \eta_1 < \infty,\ \eta_2 \leq 0\ \} - C \end{cases},$$

$$C = \{\ (\eta_1,\ i\eta_2)\ \mid\ -\infty < \eta_1 \leq 0,\ \eta_2 = 0\ \}\ .$$

$\boldsymbol{\kappa}_m(z;t)$ and $\boldsymbol{\theta}_m(z;t)$ are analytic functions throughout the z-plane except along the cut C which is the entire non-positive real axis. From the above equations, it can

be seen immediately that equations (6.3.10) are satisfied identically. So, the question now is to find the analytic functions $\boldsymbol{\kappa}_m(z;t)$ and $\boldsymbol{\theta}_m(z;t)$ in the cut-plane $S^+ \cup S^-$.

Solving for $\boldsymbol{f}''_{mk}(z;t)$ and $\overline{\boldsymbol{f}}''_{mk}(z;t)$ from equations (6.3.12) and (6.3.13), we get

$$\left.\begin{aligned} \boldsymbol{f}''_{m1}(z;t) &= \boldsymbol{P}_1^{-1}\boldsymbol{H}^{-1}\left\{\boldsymbol{\theta}'_m(z;t) - \overset{*}{\boldsymbol{L}}_2\,\boldsymbol{\kappa}_m(z;t)\right\} \\ \overline{\boldsymbol{f}}''_{m2}(z;t) &= \boldsymbol{Q}_2^{-1}\boldsymbol{H}^{-1}\left\{\boldsymbol{\theta}'_m(z;t) - \boldsymbol{L}_1\boldsymbol{\kappa}_m(z;t)\right\} \end{aligned}\right\}, \qquad z \in S^+ , \tag{6.3.14}$$

and

$$\left.\begin{aligned} \boldsymbol{f}''_{m2}(z;t) &= -\boldsymbol{P}_2^{-1}\,\overset{*}{\boldsymbol{H}}^{-1}\left\{\boldsymbol{\theta}'_m(z;t) - \overset{*}{\boldsymbol{L}}_1\,\boldsymbol{\kappa}_m(z;t)\right\} \\ \overline{\boldsymbol{f}}''_{m1}(z;t) &= -\boldsymbol{Q}_1^{-1}\,\overset{*}{\boldsymbol{H}}^{-1}\left\{\boldsymbol{\theta}'_m(z;t) - \boldsymbol{L}_2\boldsymbol{\kappa}_m(z;t)\right\} \end{aligned}\right\}, \qquad z \in S^- . \tag{6.3.15}$$

The definitions of matrices $\boldsymbol{L}_k$, $\overset{*}{\boldsymbol{L}}_k$, $\boldsymbol{H}$, and $\overset{*}{\boldsymbol{H}}$, as well as the properties of these matrices are given in Appendix A. Matrices $\boldsymbol{P}_k$ and $\boldsymbol{Q}_k$ have been defined above. In obtaining (6.3.14) and (6.3.15), we have assumed that the inverse matrices $\boldsymbol{P}_k^{-1}$ and $\boldsymbol{Q}_k^{-1}$ exist. Notice that the determinants of $\boldsymbol{P}_k$ and $\boldsymbol{Q}_k$ are both equal to $D_k(v)$, where

$$D_k(v) = \left\{4\alpha_l\alpha_s - \left(1+\alpha_s^2\right)^2\right\}_k .$$

Therefore, in this analysis, we exclude the situation where the interfacial crack propagates with either of the two Rayleigh wave speeds of the bimaterial system which are the real roots of $D_k(v) = 0$. This ensures the existence of $\boldsymbol{P}_k^{-1}$ and $\boldsymbol{Q}_k^{-1}$.

Substituting equations (6.3.14) and (6.3.15) into the traction free conditions on the crack faces, (6.3.9), we get

$$\left.\begin{aligned} \overset{*}{\boldsymbol{H}}\left\{\boldsymbol{\theta}'^{+}_m(\eta_1;t) - \overset{*}{\boldsymbol{L}}_2\,\boldsymbol{\kappa}^+_m(\eta_1;t)\right\} - \boldsymbol{H}\left\{\boldsymbol{\theta}'^{-}_m(\eta_1;t) - \boldsymbol{L}_2\boldsymbol{\kappa}^-_m(\eta_1;t)\right\} &= \mathbf{o} \\ \boldsymbol{H}\left\{\boldsymbol{\theta}'^{-}_m(\eta_1;t) - \overset{*}{\boldsymbol{L}}_1\,\boldsymbol{\kappa}^-_m(\eta_1;t)\right\} - \overset{*}{\boldsymbol{H}}\left\{\boldsymbol{\theta}'^{+}_m(\eta_1;t) - \boldsymbol{L}_1\boldsymbol{\kappa}^+_m(\eta_1;t)\right\} &= \mathbf{o} \end{aligned}\right\}, \quad \forall \eta_1 < 0. \tag{6.3.16}$$

Adding the two equations in (6.3.16), and using the fact that $\overset{*}{\boldsymbol{H}}\,\boldsymbol{H} \neq \mathbf{o}$ for a crack propagating with a nonzero speed, we obtain

$$\boldsymbol{\kappa}^+_m(\eta_1;t) - \boldsymbol{\kappa}^-_m(\eta_1;t) = \mathbf{o} , \qquad \forall\ \eta_1 < 0 . \tag{6.3.17}$$

This implies that $\boldsymbol{\kappa}_m(z;t)$ is continuous across the cut except at the crack-tip and therefore $\boldsymbol{\kappa}_m(z;t)$ is analytic in the entire complex plane except at $z = 0$. However, the condition of bounded displacement requires that $\mid \boldsymbol{\kappa}_m(z;t) \mid = O\ (\ |z|^{\alpha}\ )$ for some $\alpha > -1$, as $|z| \to 0$, so that any singularity of $\boldsymbol{\kappa}_m(z;t)$ at the crack-tip is removable. Therefore, $\boldsymbol{\kappa}_m(z;t)$ is an entire function. Now, both equations in (6.3.16) become

$$\overset{*}{\boldsymbol{H}}\ \boldsymbol{\theta}'^{+}_m(\eta_1;t) - \boldsymbol{H}\boldsymbol{\theta}'^{-}_m(\eta_1;t) = \boldsymbol{R}\boldsymbol{\kappa}_m(\eta_1;t)\ , \qquad \forall\ \eta_1 < 0\ , \tag{6.3.18}$$

where

$$\left.\begin{aligned} &\boldsymbol{\kappa}_m(\eta_1;t) = \boldsymbol{\kappa}^{+}_m(\eta_1;t) = \boldsymbol{\kappa}^{-}_m(\eta_1;t) \\ &\boldsymbol{R} = \overset{*}{\boldsymbol{H}}\overset{*}{\boldsymbol{L}}_2 - \boldsymbol{H}\boldsymbol{L}_2 = \overset{*}{\boldsymbol{H}}\ \boldsymbol{L}_1 - \boldsymbol{H}\ \overset{*}{\boldsymbol{L}}_1 \end{aligned}\right\}\ .$$

Equation (6.3.18) constitutes a Riemann-Hilbert problem. Its solution $\boldsymbol{\theta}'_m(z;t)$ is analytic in the cut-plane $S^+ \cup S^-$. Along the cut, $\boldsymbol{\theta}'_m(z;t)$ satisfies equation (6.3.18) for some arbitrary entire function $\boldsymbol{\kappa}_m(z;t)$. Also, from the requirement of bounded displacements at the crack-tip, as $|z| \to 0$,

$$\mid \boldsymbol{\theta}'_m(z;t) \mid = O\ (\ |z|^{\alpha}\ )\ , \tag{6.3.19}$$

for some $\alpha > -1$.

In equation (6.3.18), the solution $\boldsymbol{\theta}'_m(z;t)$ is composed of two parts, the homogeneous solution $\overset{\circ}{\boldsymbol{\theta}}{}'_m\ (z;t)$, and the particular solution $\hat{\boldsymbol{\theta}}'_m(z;t)$. We will consider these two solutions separately.

HOMOGENEOUS SOLUTION:

The homogeneous solution is obtained by solving

$$\overset{*}{\boldsymbol{H}}\overset{\circ}{\boldsymbol{\theta}}{}'^{+}_m\ (\eta_1;t) - \boldsymbol{H}\ \overset{\circ}{\boldsymbol{\theta}}{}'^{-}_m\ (\eta_1;t) = \mathbf{o}\ , \qquad \forall\ \eta_1 < 0\ . \tag{6.3.20}$$

By using the solution given in Appendix B and by imposing restriction (6.3.19), we can write the solution to the above equation as follows:

$$\overset{\circ}{\boldsymbol{\theta}}{}'_m\ (z;t) = z^{-\frac{1}{2}+i\epsilon}\ \overset{\circ}{A}_m\ (z;t)\boldsymbol{\zeta} + z^{-\frac{1}{2}-i\epsilon}\ \overset{\circ}{B}_m\ (z;t)\ \overset{*}{\boldsymbol{\zeta}}\ , \tag{6.3.21}$$

where

$$\left.\begin{aligned} &\epsilon = \frac{1}{2\pi}\ln\frac{1-\beta}{1+\beta}, \quad \beta = \frac{h_{11}}{\sqrt{h_{12}h_{21}}}, \\ &\boldsymbol{\zeta} = (\ 1,\ \eta\ )^{\top}, \qquad \overset{*}{\boldsymbol{\zeta}} = (\ 1,\ -\eta\ )^{\top}, \quad \eta = \sqrt{\frac{h_{21}}{h_{12}}} \end{aligned}\right\},$$

and $\overset{\circ}{A}_m\ (z;t)$, $\overset{\circ}{B}_m\ (z;t)$ are arbitrary entire functions. The parameters ϵ and η defined here are known functions of crack-tip speed, v, and material properties. Their functional dependence on these variables is discussed in Appendix A and Section 6.5. For $v = 0$, $\epsilon(v)$ reduces to ϵ_0 which is the oscillatory index that appears in the quasi-static interfacial crack problems (Williams, 1959; Rice, 1988).

By substituting equation (6.3.21) into equations (6.3.14) and (6.3.15), we get

$$\left.\begin{aligned} \overset{\circ}{\boldsymbol{f}}{}''_{m1}\ (z;t) &= \boldsymbol{P}_1^{-1}\boldsymbol{H}^{-1}\left\{z^{-\frac{1}{2}+i\epsilon}\ \overset{\circ}{A}_m\ (z;t)\boldsymbol{\zeta} + z^{-\frac{1}{2}-i\epsilon}\ \overset{\circ}{B}_m\ (z;t)\ \overset{*}{\boldsymbol{\zeta}}\right\} \\ \overline{\overset{\circ}{\boldsymbol{f}}}{}''_{m2}(z;t) &= \boldsymbol{Q}_2^{-1}\boldsymbol{H}^{-1}\left\{z^{-\frac{1}{2}+i\epsilon}\ \overset{\circ}{A}_m\ (z;t)\boldsymbol{\zeta} + z^{-\frac{1}{2}-i\epsilon}\ \overset{\circ}{B}_m\ (z;t)\ \overset{*}{\boldsymbol{\zeta}}\right\} \end{aligned}\right\}, \quad z \in S^+, \tag{6.3.22}$$

and

$$\left.\begin{aligned} \overset{\circ}{\boldsymbol{f}}{}''_{m2}\ (z;t) &= -\boldsymbol{P}_2^{-1}\ \overset{*}{\boldsymbol{H}}{}^{-1}\left\{z^{-\frac{1}{2}+i\epsilon}\ \overset{\circ}{A}_m\ (z;t)\boldsymbol{\zeta} + z^{-\frac{1}{2}-i\epsilon}\ \overset{\circ}{B}_m\ (z;t)\ \overset{*}{\boldsymbol{\zeta}}\right\} \\ \overline{\overset{\circ}{\boldsymbol{f}}}{}''_{m1}(z;t) &= -\boldsymbol{Q}_1^{-1}\ \overset{*}{\boldsymbol{H}}{}^{-1}\left\{z^{-\frac{1}{2}+i\epsilon}\ \overset{\circ}{A}_m\ (z;t)\boldsymbol{\zeta} + z^{-\frac{1}{2}-i\epsilon}\ \overset{\circ}{B}_m\ (z;t)\ \overset{*}{\boldsymbol{\zeta}}\right\} \end{aligned}\right\}, \quad z \in S^-. \tag{6.3.23}$$

Notice that the following identities hold,

$$\left.\begin{aligned} \boldsymbol{H}^{-1}\boldsymbol{\zeta} &= -\frac{\sqrt{h_{12}h_{21}}}{h_{11}^2 - h_{12}h_{21}}(1-\beta)\boldsymbol{\zeta}, \quad \boldsymbol{H}^{-1}\ \overset{*}{\boldsymbol{\zeta}} = \frac{\sqrt{h_{12}h_{21}}}{h_{11}^2 - h_{12}h_{21}}(1+\beta)\ \overset{*}{\boldsymbol{\zeta}} \\ \overset{*}{\boldsymbol{H}}{}^{-1}\ \boldsymbol{\zeta} &= \frac{\sqrt{h_{12}h_{21}}}{h_{11}^2 - h_{12}h_{21}}(1+\beta)\boldsymbol{\zeta}, \quad \overset{*}{\boldsymbol{H}}{}^{-1}\overset{*}{\boldsymbol{\zeta}} = -\frac{\sqrt{h_{12}h_{21}}}{h_{11}^2 - h_{12}h_{21}}(1-\beta)\ \overset{*}{\boldsymbol{\zeta}} \end{aligned}\right\},$$

and

$$1+\beta = \frac{e^{-\epsilon\pi}}{\cosh\epsilon\pi}\ , \qquad 1-\beta = \frac{e^{\epsilon\pi}}{\cosh\epsilon\pi}\ .$$

Without losing generality, we may absorb the factor $\sqrt{h_{12}h_{21}}/(h_{11}^2 - h_{12}h_{21})$ into the entire functions, $\overset{\circ}{A}_m\ (z;t)$ and $\overset{\circ}{B}_m\ (z;t)$. By taking the conjugate of the function

$\overset{\circ}{\overline{f}}{}''_{m1}(z;t)$ in equation (6.3.23) and comparing it with the function $\overset{\circ}{f}{}''_{m1}(z;t)$ in equation (6.3.22), and also by using the properties of matrices $\boldsymbol{P}_k$ and $\boldsymbol{Q}_k$, we can obtain a relationship between the entire functions $\overset{\circ}{A}_m(z;t)$ and $\overset{\circ}{B}_m(z;t)$ as follows,

$$\overset{\circ}{B}_m(z;t) = -\overset{\circ}{\overline{A}}_m(z;t) .$$

Meanwhile, by using the fact that

$$\boldsymbol{P}_k^{-1}\overset{*}{\boldsymbol{\zeta}} = \boldsymbol{Q}_k^{-1}\boldsymbol{\zeta} , \qquad \boldsymbol{Q}_k^{-1}\overset{*}{\boldsymbol{\zeta}} = \boldsymbol{P}_k^{-1}\boldsymbol{\zeta} ,$$

we can get the solutions,

$$\left.\begin{aligned}
\overset{\circ}{f}{}''_{m1}(z;t) &= \frac{e^{\epsilon\pi}\boldsymbol{P}_1^{-1}\boldsymbol{\zeta}}{\cosh\epsilon\pi} z^{-\frac{1}{2}+i\epsilon}\,\overset{\circ}{A}_m(z;t) + \frac{e^{-\epsilon\pi}\boldsymbol{Q}_1^{-1}\boldsymbol{\zeta}}{\cosh\epsilon\pi} z^{-\frac{1}{2}-i\epsilon}\overset{\circ}{\overline{A}}_m(z;t), \quad z\in S^+ \\
\overset{\circ}{f}{}''_{m2}(z;t) &= \frac{e^{-\epsilon\pi}\boldsymbol{P}_2^{-1}\boldsymbol{\zeta}}{\cosh\epsilon\pi} z^{-\frac{1}{2}+i\epsilon}\,\overset{\circ}{A}_m(z;t) + \frac{e^{\epsilon\pi}\boldsymbol{Q}_2^{-1}\boldsymbol{\zeta}}{\cosh\epsilon\pi} z^{-\frac{1}{2}-i\epsilon}\overset{\circ}{\overline{A}}_m(z;t), \quad z\in S^-
\end{aligned}\right\} , \tag{6.3.24}$$

or, in terms of $F_m(z_l;t)$ and $G_m(z_s;t)$, for the material above the interface,

$$\left.\begin{aligned}
\overset{\circ}{F}{}''_m(z_l;t) &= -\frac{[(1+\alpha_s^2)-2\eta\alpha_s]\,e^{\epsilon\pi}}{\mu D(v)\cosh\epsilon\pi} z_l^{-\frac{1}{2}+i\epsilon}\,\overset{\circ}{A}_m(z_l;t) \\
&\quad - \frac{[(1+\alpha_s^2)+2\eta\alpha_s]\,e^{-\epsilon\pi}}{\mu D(v)\cosh\epsilon\pi} z_l^{-\frac{1}{2}-i\epsilon}\overset{\circ}{\overline{A}}_m(z_l;t) \\
\overset{\circ}{G}{}''_m(z_s;t) &= \frac{[2\alpha_l-\eta(1+\alpha_s^2)]\,e^{\epsilon\pi}}{\mu D(v)\cosh\epsilon\pi} z_s^{-\frac{1}{2}+i\epsilon}\,\overset{\circ}{A}_m(z_s;t) \\
&\quad + \frac{[2\alpha_l+\eta(1+\alpha_s^2)]\,e^{-\epsilon\pi}}{\mu D(v)\cosh\epsilon\pi} z_s^{-\frac{1}{2}-i\epsilon}\overset{\circ}{\overline{A}}_m(z_s;t)
\end{aligned}\right\} . \tag{6.3.25}$$

For the material below the interface, the solution is also given by equation (6.3.25) with the parameter $\epsilon\pi$ changed to $-\epsilon\pi$.

PARTICULAR SOLUTION:

Since $\boldsymbol{\kappa}_m(z;t)$ is an entire function, the particular solution $\hat{\boldsymbol{\theta}}'_m(z;t)$ can be easily constructed. Suppose $\hat{\boldsymbol{\theta}}'_m(z;t)$ is also an entire function, which implies that

$$\hat{\boldsymbol{\theta}}'^{+}_m(\eta_1;t) = \hat{\boldsymbol{\theta}}'^{-}_m(\eta_1;t) = \hat{\boldsymbol{\theta}}'_m(\eta_1;t),$$

then from equation (6.3.18), we get

$$\hat{\boldsymbol{\theta}}'_m(\eta_1;t) = \left\{ \overset{*}{\boldsymbol{H}} - \boldsymbol{H} \right\}^{-1} \boldsymbol{R}\boldsymbol{\kappa}_m(\eta_1;t) \ , \qquad \forall\ \eta_1 < 0 \ . \tag{6.3.26}$$

By using the identity theorem for analytical functions, it can be shown that for any z,

$$\hat{\boldsymbol{\theta}}'_m(z;t) = \left\{ \overset{*}{\boldsymbol{H}} - \boldsymbol{H} \right\}^{-1} \boldsymbol{R}\boldsymbol{\kappa}_m(z;t) \ . \tag{6.3.27}$$

By substituting this particular solution into equations (6.3.14) and (6.3.15), we have

$$\left.\begin{aligned} \hat{\boldsymbol{f}}''_{m1}(z;t) &= \boldsymbol{P}_1^{-1} \left\{ \overset{*}{\boldsymbol{H}} - \boldsymbol{H} \right\}^{-1} \left\{ \overset{*}{\boldsymbol{L}}_2 - \boldsymbol{L}_2 \right\} \boldsymbol{\kappa}_m(z;t) \\ \overline{\hat{\boldsymbol{f}}}''_{m2}(z;t) &= -\boldsymbol{Q}_2^{-1} \left\{ \overset{*}{\boldsymbol{H}} - \boldsymbol{H} \right\}^{-1} \left\{ \overset{*}{\boldsymbol{L}}_1 - \boldsymbol{L}_1 \right\} \boldsymbol{\kappa}_m(z;t) \end{aligned}\right\} , \quad z \in S^+, \tag{6.3.28}$$

and

$$\left.\begin{aligned} \hat{\boldsymbol{f}}''_{m2}(z;t) &= \boldsymbol{P}_2^{-1} \left\{ \overset{*}{\boldsymbol{H}} - \boldsymbol{H} \right\}^{-1} \left\{ \overset{*}{\boldsymbol{L}}_1 - \boldsymbol{L}_1 \right\} \boldsymbol{\kappa}_m(z;t) \\ \overline{\hat{\boldsymbol{f}}}''_{m1}(z;t) &= -\boldsymbol{Q}_1^{-1} \left\{ \overset{*}{\boldsymbol{H}} - \boldsymbol{H} \right\}^{-1} \left\{ \overset{*}{\boldsymbol{L}}_2 - \boldsymbol{L}_2 \right\} \boldsymbol{\kappa}_m(z;t) \end{aligned}\right\} , \quad z \in S^-. \tag{6.3.29}$$

Notice that

$$\left\{ \overset{*}{\boldsymbol{H}} - \boldsymbol{H} \right\}^{-1} \left\{ \overset{*}{\boldsymbol{L}}_k - \boldsymbol{L}_k \right\} = \begin{bmatrix} \dfrac{(l_{21})_k}{h_{21}} & 0 \\ 0 & \dfrac{(l_{12})_k}{h_{12}} \end{bmatrix} , \qquad k \in \{1,2\} \ .$$

If the entire function $\boldsymbol{\kappa}_m(z;t)$ is expressed as

$$\boldsymbol{\kappa}_m(z;t) = \left(\ \kappa_m^{(1)}(z;t),\ \kappa_m^{(2)}(z;t) \ \right)^{\top} \ ,$$

then, it can be shown that by comparing the conjugate of $\overline{\hat{\boldsymbol{f}}}''_{m1}(z;t)$ in equation (6.3.29) with $\hat{\boldsymbol{f}}''_{m1}(z;t)$ in equation (6.3.28), we have

$$\kappa_m^{(1)}(z;t) + \overline{\kappa}_m^{(1)}(z;t) = 0 \ , \qquad \kappa_m^{(2)}(z;t) - \overline{\kappa}_m^{(2)}(z;t) = 0 \ .$$

Define a new entire function $\hat{A}_m(z;t)$ by

$$\hat{A}_m(z;t) = \frac{1}{4}\left\{\left[\kappa_m^{(1)}(z;t) - \overline{\kappa}_m^{(1)}(z;t)\right] + \left[\kappa_m^{(2)}(z;t) + \overline{\kappa}_m^{(2)}(z;t)\right]\right\} .$$

Also let

$$\boldsymbol{w}_k = \left(\frac{(l_{21})_k}{h_{21}}, \frac{(l_{12})_k}{h_{12}} \right)^\top .$$

By relating $\boldsymbol{\kappa}_m(z;t)$ to $\hat{A}_m(z;t)$, and by using the above definition, equations (6.3.28) and (6.3.29) give

$$\left.\begin{aligned} \hat{\boldsymbol{f}}''_{m1}(z;t) &= \boldsymbol{P}_1^{-1}\boldsymbol{w}_2\hat{A}_m(z;t) - \boldsymbol{Q}_1^{-1}\boldsymbol{w}_2\overline{\hat{A}}_m(z;t) , \quad z \in S^+ \\ \hat{\boldsymbol{f}}''_{m2}(z;t) &= \boldsymbol{P}_2^{-1}\boldsymbol{w}_1\hat{A}_m(z;t) - \boldsymbol{Q}_2^{-1}\boldsymbol{w}_1\overline{\hat{A}}_m(z;t) , \quad z \in S^- \end{aligned}\right\} . \tag{6.3.30}$$

In order to express the particular solution in terms of $F_m(z_l;t)$ and $G_m(z_s;t)$, we need to define two parameters, ω_l and ω_s that only depend on the crack-tip speed,

$$\omega_l = \frac{\left\{\dfrac{\alpha_l(1-\alpha_s^2)}{\mu D(v)}\right\}_1}{\left\{\dfrac{\alpha_l(1-\alpha_s^2)}{\mu D(v)}\right\}_2} , \qquad \omega_s = \frac{\left\{\dfrac{\alpha_s(1-\alpha_s^2)}{\mu D(v)}\right\}_1}{\left\{\dfrac{\alpha_s(1-\alpha_s^2)}{\mu D(v)}\right\}_2} .$$

Then, for the material above the interface, the particular solution can be expressed as

$$\left.\begin{aligned} \hat{F}''_m(z_l;t) &= -\frac{1}{\mu D(v)}\left\{\left(\frac{1+\alpha_s^2}{1+\omega_l} - \frac{2\alpha_s}{1+\omega_s}\right)\hat{A}_m(z_l;t) \right. \\ &\qquad \left. -\left(\frac{1+\alpha_s^2}{1+\omega_l} + \frac{2\alpha_s}{1+\omega_s}\right)\overline{\hat{A}}_m(z_l;t)\right\} \\ \hat{G}''_m(z_s;t) &= \frac{1}{\mu D(v)}\left\{\left(\frac{2\alpha_l}{1+\omega_l} - \frac{1+\alpha_s^2}{1+\omega_s}\right)\hat{A}_m(z_s;t) \right. \\ &\qquad \left. -\left(\frac{2\alpha_l}{1+\omega_l} + \frac{1+\alpha_s^2}{1+\omega_s}\right)\overline{\hat{A}}_m(z_s;t)\right\} \end{aligned}\right\} . \tag{6.3.31}$$

For the material below the interface, the particular solution is also given by equations (6.3.31) with ω_l and ω_s changed to ω_l^{-1} and ω_s^{-1}, respectively.

By adding the expressions in equations (6.3.25) and (6.3.31), and by integrating with respect to the corresponding arguments, the final solutions of $F_m(z_l;t)$ and

$G_m(z_s;t)$ for the material above the interface, for $m = 0,\ 1$, can be obtained as

$$\left.\begin{aligned} F_m(z_l;t) \;=\; & -\frac{[(1+\alpha_s^2)-2\eta\alpha_s]\,e^{\epsilon\pi}}{\mu D(v)\cosh\epsilon\pi} z_l^{\frac{3}{2}+i\epsilon} A_m(z_l;t) \\ & +\frac{[(1+\alpha_s^2)+2\eta\alpha_s]\,e^{-\epsilon\pi}}{\mu D(v)\cosh\epsilon\pi} z_l^{\frac{3}{2}-i\epsilon}\overline{A}_m(z_l;t) \\ & -\frac{1}{\mu D(v)}\left\{\left(\frac{1+\alpha_s^2}{1+\omega_l}-\frac{2\alpha_s}{1+\omega_s}\right)B_m(z_l;t)-\left(\frac{1+\alpha_s^2}{1+\omega_l}+\frac{2\alpha_s}{1+\omega_s}\right)\overline{B}_m(z_l;t)\right\} z_l^2 \end{aligned}\right\}, \tag{6.3.32}$$

and

$$\left.\begin{aligned} G_m(z_s;t) \;=\; & \frac{[2\alpha_l-\eta(1+\alpha_s^2)]\,e^{\epsilon\pi}}{\mu D(v)\cosh\epsilon\pi} z_s^{\frac{3}{2}+i\epsilon} A_m(z_s;t) \\ & +\frac{[2\alpha_l+\eta(1+\alpha_s^2)]\,e^{-\epsilon\pi}}{\mu D(v)\cosh\epsilon\pi} z_s^{\frac{3}{2}-i\epsilon}\overline{A}_m(z_s;t) \\ & +\frac{1}{\mu D(v)}\left\{\left(\frac{2\alpha_l}{1+\omega_l}-\frac{1+\alpha_s^2}{1+\omega_s}\right)B_m(z_s;t)-\left(\frac{2\alpha_l}{1+\omega_l}+\frac{1+\alpha_s^2}{1+\omega_s}\right)\overline{B}_m(z_s;t)\right\} z_s^2 \end{aligned}\right\}, \tag{6.3.33}$$

where the entire functions, $A_m(z;t)$ and $B_m(z;t)$ are defined by

$$\frac{\mathrm{d}^2}{\mathrm{d}z^2}\left\{z^{\frac{3}{2}+i\epsilon}A_m(z;t)\right\} = z^{-\frac{1}{2}+i\epsilon}\,\mathring{A}_m\,(z;t)\,, \qquad \frac{\mathrm{d}^2}{\mathrm{d}z^2}\left\{z^2 B_m(z;t)\right\} = \hat{A}_m(z;t)\,,$$

and they can only be determined by the far field conditions. The solutions for the two displacement potentials, $\phi_m(\eta_1,\eta_2,t)$ and $\psi_m(\eta_1,\eta_2,t)$, will be given by equations (6.3.2).

Since $A_m(z;t)$ and $B_m(z;t)$ are entire functions, they can be expanded into Taylor series,

$$\left.\begin{aligned} A_0(z;t) &= \sum_{n=0}^{\infty} A_0^{(n)}(t) z^n\,, \quad B_0(z;t) = \sum_{n=0}^{\infty} B_0^{(n)}(t) z^n \\ A_1(z;t) &= \sum_{n=0}^{\infty} A_1^{(n)}(t) z^n\,, \quad B_1(z;t) = \sum_{n=0}^{\infty} B_1^{(n)}(t) z^n \end{aligned}\right\}. \tag{6.3.34}$$

As we have mentioned in the previous section, in the unscaled physical plane, (ξ_1,ξ_2), $\phi_m(\xi_1,\xi_2,t)$ and $\psi_m(\xi_1,\xi_2,t)$ should be ordered according to their contributions to the near-tip deformation field. By imposing this property, i.e., equation (6.2.5), to

the representations of $\phi_m(\eta_1,\eta_2,t)$ and $\psi_m(\eta_1,\eta_2,t)$, for $m=0$ and 1, we can obtain restrictions on the entire functions $A_m(z;t)$ and $B_m(z;t)$. In the Taylor expansion (6.3.34), $A_0^{(0)}(t)\neq 0$ and $B_1^{(0)}(t)\neq 0$, but $A_1^{(0)}(t)=0$. In other words, the leading terms of ϕ_0 and ψ_0 are of order $z^{3/2}$, whereas the leading terms of ϕ_1 and ψ_1 are of order z^2. Meanwhile, it can be shown that the coefficient of the leading term, $A_0^{(0)}(t)$, in (6.3.32) and (6.3.33), is directly related to the complex dynamic stress intensity factor $K^d(t)$ defined by YANG *et al.* (1991) through the relation

$$A_0^{(0)}(t)=-\frac{1}{2\sqrt{2\pi}}\cdot\frac{K^d(t)}{\left(\frac{3}{2}+i\epsilon\right)\left(\frac{1}{2}+i\epsilon\right)}\,. \tag{6.3.35}$$

As a matter of fact, in the unscaled plane, (ξ_1,ξ_2), and for $m=0$, equations (6.3.32) and (6.3.33) are identical in spatial structure to the complete solution for the *steady state* propagating interfacial crack in a bimaterial. By using entirely different methodologies, the most singular solution of the steady state problem was obtained by Yang *et al.* (1991) and the complete solution of the steady state problem was given by Deng (1992). However, in the present analysis the functions $A_m^{(n)}(t)$ and $B_m^{(n)}(t)$ are allowed to be functions of time.

6.3.2 Solutions for $\phi_m(\eta_1,\eta_2,t)$ and $\psi_m(\eta_1,\eta_2,t)$ for $m=2$

For $m=2$, the equations of motion (6.2.6) are coupled. They take the form,

$$\left.\begin{aligned}\phi_{2,11}(\eta_1,\eta_2,t)+\frac{1}{\alpha_l^2}\phi_{2,22}(\eta_1,\eta_2,t) &= -\frac{2v^{1/2}}{\alpha_l^2c_l^2}\mathrm{Re}\left\{v^{1/2}F_0'(z_l;t)\right\}_{,t}\\ \psi_{2,11}(\eta_1,\eta_2,t)+\frac{1}{\alpha_s^2}\psi_{2,22}(\eta_1,\eta_2,t) &= -\frac{2v^{1/2}}{\alpha_s^2c_s^2}\mathrm{Im}\left\{v^{1/2}G_0'(z_s;t)\right\}_{,t}\end{aligned}\right\}\,, \tag{6.3.36}$$

where $F_0(z_l;t)$ and $G_0(z_s;t)$ correspond to the solution of (6.2.6) for $m=0$ and are given by equations (6.3.32) and (6.3.33).

In order to obtain the next most singular term in $\phi_2(\eta_1,\eta_2,t)$ and $\psi_2(\eta_1,\eta_2,t)$, we should only consider the most singular terms in $F_0(z_l;t)$ and $G_0(z_s;t)$. Therefore, for

the material above the interface,

$$\left.\begin{aligned} F_0(z_l;t) &= a_0(t)A_0(t)z_l^{\frac{3}{2}+i\epsilon} + b_0(t)\overline{A}_0(t)z_l^{\frac{3}{2}-i\epsilon} \\ G_0(z_s;t) &= c_0(t)A_0(t)z_s^{\frac{3}{2}+i\epsilon} + d_0(t)\overline{A}_0(t)z_s^{\frac{3}{2}-i\epsilon} \end{aligned}\right\}, \tag{6.3.37}$$

where $A_0(t) = A_0^{(0)}(t)$, given in (6.3.35), and

$$\begin{aligned} a_0(t) &= -\frac{[(1+\alpha_s^2) - 2\eta\alpha_s]\, e^{\epsilon\pi}}{\mu D(v)\cosh\epsilon\pi}\,, \\ b_0(t) &= -\frac{[(1+\alpha_s^2) + 2\eta\alpha_s]\, e^{-\epsilon\pi}}{\mu D(v)\cosh\epsilon\pi}\,, \\ c_0(t) &= \frac{[2\alpha_l - \eta(1+\alpha_s^2)]\, e^{\epsilon\pi}}{\mu D(v)\cosh\epsilon\pi}\,, \\ d_0(t) &= \frac{[2\alpha_l + \eta(1+\alpha_s^2)]\, e^{-\epsilon\pi}}{\mu D(v)\cosh\epsilon\pi}\,. \end{aligned}$$

For the material below the interface, we need to change the parameter $\epsilon\pi$ to $-\epsilon\pi$.

Substituting (6.3.37) into (6.3.36) and carrying out the differentiation with respect to time, (6.3.36) becomes

$$\left.\begin{aligned} &\phi_{2,11}(\eta_1,\eta_2,t) + \frac{1}{\alpha_l^2}\phi_{2,22}(\eta_1,\eta_2,t) = \\ &-\frac{2\sqrt{v}}{\alpha_l^2 c_l^2}\mathrm{Re}\left\{ i\dot{\epsilon}\sqrt{v}\left[\hat{A}_0(t)a_0(t)z_l^{i\epsilon} - \overline{\hat{A}}_0(t)b_0(t)z_l^{-i\epsilon}\right] z_l^{\frac{1}{2}}\ln z_l \right. \\ &-\frac{\sqrt{v}\dot{\alpha}_l}{2\alpha_l}\left[\hat{B}_0(t)a_0(t)z_l^{i\epsilon} + \overline{\hat{B}}_0(t)b_0(t)z_l^{-i\epsilon}\right] z_l^{-\frac{1}{2}}\overline{z}_l \\ &+\left[\frac{\mathrm{d}}{\mathrm{d}t}\left(\sqrt{v}\hat{A}_0(t)a_0(t)\right) + \frac{\sqrt{v}\dot{\alpha}_l}{2\alpha_l}\hat{B}_0(t)a_0(t)\right] z_l^{\frac{1}{2}+i\epsilon} \\ &\left.+\left[\frac{\mathrm{d}}{\mathrm{d}t}\left(\sqrt{v}\overline{\hat{A}}_0(t)b_0(t)\right) + \overline{\hat{B}}_0(t)b_0(t)\right] z_l^{\frac{1}{2}-i\epsilon}\right\} \end{aligned}\right\}, \tag{6.3.38}$$

and

$$\left.\begin{aligned}
&\psi_{2,11}(\eta_1,\eta_2,t)+\frac{1}{\alpha_s^2}\psi_{2,22}(\eta_1,\eta_2,t)= \\
&-\frac{2\sqrt{v}}{\alpha_s^2 c_s^2}\mathrm{Im}\left\{i\dot{\epsilon}\sqrt{v}\left[\hat{A}_0(t)c_0(t)z_s^{i\epsilon}-\overline{\hat{A}}_0(t)d_0(t)z_s^{-i\epsilon}\right]z_s^{\frac{1}{2}}\ln z_s\right. \\
&-\frac{\sqrt{v}\dot{\alpha}_s}{2\alpha_s}\left[\hat{B}_0(t)c_0(t)z_s^{i\epsilon}+\overline{\hat{B}}_0(t)d_0(t)z_s^{-i\epsilon}\right]z_s^{-\frac{1}{2}}\overline{z}_s \\
&+\left[\frac{\mathrm{d}}{\mathrm{d}t}\left(\sqrt{v}\hat{A}_0(t)c_0(t)\right)+\frac{\sqrt{v}\dot{\alpha}_s}{2\alpha_s}\hat{B}_0(t)c_0(t)\right]z_s^{\frac{1}{2}+i\epsilon} \\
&\left.+\left[\frac{\mathrm{d}}{\mathrm{d}t}\left(\sqrt{v}\overline{\hat{A}}_0(t)d_0(t)\right)+\frac{\sqrt{v}\dot{\alpha}_s}{2\alpha_s}\overline{\hat{B}}_0(t)d_0(t)\right]z_s^{\frac{1}{2}-i\epsilon}\right\}
\end{aligned}\right\}, \tag{6.3.39}$$

where

$$\hat{A}_0(t)=\left(\frac{3}{2}+i\epsilon\right)A_0(t)\ ,\quad \hat{B}_0(t)=\left(\frac{3}{2}+i\epsilon\right)\left(\frac{1}{2}+i\epsilon\right)A_0(t)\ .$$

The most general solutions to equations (6.3.38) and (6.3.39) are

$$\left.\begin{aligned}
\phi_2(\eta_1,\eta_2,t)&=\mathrm{Re}\left\{F_2(z_l;t)-\overline{z}_l\hat{F}(z_l;t)-\overline{z}_l^2\tilde{F}(z_l;t)\right\} \\
\psi_2(\eta_1,\eta_2,t)&=\mathrm{Im}\left\{G_2(z_s;t)-\overline{z}_s\hat{G}(z_s;t)-\overline{z}_s^2\tilde{G}(z_s;t)\right\}
\end{aligned}\right\}, \tag{6.3.40}$$

where

$$\left.\begin{aligned}
\hat{F}(z;t) &= D_l\{a_0(t)\}z^{\frac{3}{2}+i\epsilon}+\overline{D}_l\{b_0(t)\}z^{\frac{3}{2}-i\epsilon} \\
&+ \dot{\epsilon}\left\{K_l(t)a_0(t)z^{\frac{3}{2}+i\epsilon}+\overline{K}_l(t)b_0(t)z^{\frac{3}{2}-i\epsilon}\right\}\ln z \\
\hat{G}(z;t) &= D_s\{c_0(t)\}z^{\frac{3}{2}+i\epsilon}+\overline{D}_s\{d_0(t)\}z^{\frac{3}{2}-i\epsilon} \\
&+ \dot{\epsilon}\left\{K_s(t)c_0(t)z^{\frac{3}{2}+i\epsilon}+\overline{K}_s(t)d_0(t)z^{\frac{3}{2}-i\epsilon}\right\}\ln z
\end{aligned}\right\},$$

and

$$\left.\begin{aligned}
\tilde{F}(z;t) &= B_l(t)a_0(t)z^{\frac{1}{2}+i\epsilon}+\overline{B}_l(t)b_0(t)z^{\frac{1}{2}-i\epsilon} \\
\tilde{G}(z;t) &= B_s(t)c_0(t)z^{\frac{1}{2}+i\epsilon}+\overline{B}_s(t)d_0(t)z^{\frac{1}{2}-i\epsilon}
\end{aligned}\right\}.$$

The two operators $D_l\{\cdot\}$ and $D_s\{\cdot\}$ are given by

$$\left.\begin{aligned}
D_{l,s}\{p(t)\} &= \frac{v^{1/2}}{2\alpha_{l,s}^2c_{l,s}^2}\left\{\left(\frac{3}{2}+i\epsilon\right)^{-1}\frac{\mathrm{d}}{\mathrm{d}t}\left[v^{1/2}p(t)\left(\frac{3}{2}+i\epsilon\right)A_0(t)\right]\right. \\
&+ \left.\frac{v^{1/2}\dot{\alpha}_{l,s}}{2\alpha_{l,s}}p(t)\left(\frac{1}{2}+i\epsilon\right)A_0(t)\ +\ i\ \dot{\epsilon}v^{1/2}p(t)A_0(t)\right\}
\end{aligned}\right\},$$

where $p(t)$ is a real function of time t. Also

$$B_{l,s}(t) = -\frac{v\dot{\alpha}_{l,s}}{8\alpha_{l,s}^3 c_{l,s}^2}\left(\frac{3}{2} + i\epsilon\right) A_0(t) \ , \quad K_{l,s}(t) = \frac{ivA_0(t)}{2\alpha_{l,s}^2 c_{l,s}^2} \ .$$

In (6.3.40), $\hat{F}(z_l;t)$, $\tilde{F}(z_l;t)$, $\hat{G}(z_s;t)$, and $\tilde{G}(z_s;t)$ are totally determined by the complex potentials $F_0(z_l;t)$ and $G_0(z_s;t)$, given in equation (6.3.37). The coefficients of functions $\hat{F}(z_l;t)$, $\tilde{F}(z_l;t)$, $\hat{G}(z_s;t)$, and $\tilde{G}(z_s;t)$ are related to the crack-tip acceleration, the time derivative of $A_0(t)$, as well as the crack-tip speed and $A_0(t)$ themselves through the definitions of $D_{l,s}\{A_0(t)\}$, $B_{l,s}(t)$, and $K_{l,s}(t)$. It should be noted at this point that these definitions reduce to the equivalent ones corresponding to the transient crack growth in homogeneous materials. Indeed, if ϵ is set to be zero, the expressions for $D_{l,s}\{A_0(t)\}$ and $B_{l,s}(t)$ that appear in Freund and Rosakis (1992) are obtained. Once again, it is clear that for the steady state situation, functions $\hat{F}(z_l;t)$, $\tilde{F}(z_l;t)$, $\hat{G}(z_s;t)$, and $\tilde{G}(z_s;t)$ will vanish. The undetermined functions $F_2(z_l;t)$ and $G_2(z_s;t)$ are analytic in the upper half plane for the material above the interface, and in the lower half for the material below the interface. These functions are at the moment unknown and will be determined below by using the boundary and bonding conditions.

Associated with $\phi_2(\eta_1,\eta_2,t)$ and $\psi_2(\eta_1,\eta_2,t)$, the components of displacement will be

$$\left.\begin{aligned}
u_1^{(2)} &= \mathrm{Re}\Big\{F_2'(z_l;t) + \alpha_s G_2'(z_s;t) \\
&- \left[\overline{z}_l\hat{F}'(z_l;t) + \overline{z}_l^2\tilde{F}'(z_l;t) + \hat{F}(z_l;t) + 2\overline{z}_l\tilde{F}(z_l;t)\right] \\
&- \alpha_s\left[\overline{z}_s\hat{G}'(z_s;t) + \overline{z}_s^2\tilde{G}'(z_s;t) - \hat{G}(z_s;t) - 2\overline{z}_s\tilde{G}(z_s;t)\right]\Big\} \\
u_2^{(2)} &= \mathrm{Im}\Big\{\alpha_l F_2'(z_l;t) + G_2'(z_s;t) \\
&- \alpha_l\left[\overline{z}_l\hat{F}'(z_l;t) + \overline{z}_l^2\tilde{F}'(z_l;t) - \hat{F}(z_l;t) - 2\overline{z}_l\tilde{F}(z_l;t)\right] \\
&- \left[\overline{z}_s\hat{G}'(z_s;t) + \overline{z}_s^2\tilde{G}'(z_s;t) + \hat{G}(z_s;t) + 2\overline{z}_s\tilde{G}(z_s;t)\right]\Big\}
\end{aligned}\right\} , \qquad (6.3.41)$$

and the components of stress

$$\left.\begin{aligned}\sigma_{11}^{(2)} &= \mu \mathrm{Re}\Big\{ \left(1+2\alpha_l^2-\alpha_s^2\right) F_2''(z_l;t) + 2\alpha_s G_2''(z_s;t) \\ &- \left(1+2\alpha_l^2-\alpha_s^2\right)\left[\overline{z}_l \hat{F}''(z_l;t) + \overline{z}_l^2 \tilde{F}''(z_l;t) + 2\tilde{F}(z_l;t)\right] \\ &- 2\left[\left(1-\alpha_s^2\right) + \frac{2\alpha_l^2\left(\alpha_l^2-\alpha_s^2\right)}{1-\alpha_l^2}\right]\left[\hat{F}'(z_l;t) + 2\overline{z}_l \tilde{F}'(z_l;t)\right] \\ &- 2\alpha_s\left[\overline{z}_s \hat{G}''(z_s;t) + \overline{z}_s^2 \tilde{G}''(z_s;t) - 2\tilde{G}(z_s;t)\right]\Big\}\end{aligned}\right\}, \tag{6.3.42}$$

$$\left.\begin{aligned}\sigma_{22}^{(2)} &= -\mu \mathrm{Re}\Big\{ \left(1+\alpha_s^2\right) F_2''(z_l;t) + 2\alpha_s G_2''(z_s;t) \\ &- \left(1+\alpha_s^2\right)\left[\overline{z}_l \hat{F}''(z_l;t) + \overline{z}_l^2 \tilde{F}''(z_l;t) + 2\tilde{F}(z_l;t)\right] \\ &- 2\left[\left(1-\alpha_s^2\right) - \frac{2\left(\alpha_l^2-\alpha_s^2\right)}{1-\alpha_l^2}\right]\left[\hat{F}'(z_l;t) + 2\overline{z}_l \tilde{F}'(z_l;t)\right] \\ &- 2\alpha_s\left[\overline{z}_s \hat{G}''(z_s;t) + \overline{z}_s^2 \tilde{G}''(z_s;t) - 2\tilde{G}(z_s;t)\right]\Big\}\end{aligned}\right\}, \tag{6.3.43}$$

and

$$\left.\begin{aligned}\sigma_{12}^{(2)} &= -\mu \mathrm{Im}\Big\{ 2\alpha_l F_2''(z_l;t) + \left(1+\alpha_s^2\right) G_2''(z_s;t) \\ &- 2\alpha_l\left[\overline{z}_l \hat{F}''(z_l;t) + \overline{z}_l^2 \tilde{F}''(z_l;t) - 2\tilde{F}(z_l;t)\right] \\ &- \left(1+\alpha_s^2\right)\left[\overline{z}_s \hat{G}''(z_s;t) + \overline{z}_s^2 \tilde{G}''(z_s;t) + 2\tilde{G}(z_s;t)\right] \\ &- 2\left(1-\alpha_s^2\right)\left[\hat{G}'(z_s;t) + 2\overline{z}_s \tilde{G}'(z_s;t)\right]\Big\}\end{aligned}\right\}. \tag{6.3.44}$$

To produce a more compact form for the boundary and bonding conditions, one needs to define the following quantities: First let $\overset{*}{\boldsymbol{P}}_k$, $\overset{*}{\boldsymbol{Q}}_k$, $\overset{*}{\boldsymbol{U}}_k$, and $\overset{*}{\boldsymbol{V}}_k$ be obtained from matrices $\boldsymbol{P}_k$, $\boldsymbol{Q}_k$, $\boldsymbol{U}_k$, and $\boldsymbol{V}_k$, respectively, by changing the sign of the off-diagonal elements, and let

$$\boldsymbol{M}_k = \begin{bmatrix} \mu m(v) & 0 \\ 0 & \mu n(v) \end{bmatrix}_k, \qquad \boldsymbol{N}_k = \begin{bmatrix} \mu m(v) & 0 \\ 0 & -\mu n(v) \end{bmatrix}_k,$$

where

$$m(v) = \left(1-\alpha_s^2\right) - \frac{2\left(\alpha_l^2-\alpha_s^2\right)}{1-\alpha_l^2}, \qquad n(v) = 1-\alpha_s^2 .$$

Also, define complex vectors, $\boldsymbol{f}_k(z;t) = (F_{2k}(z;t), G_{2k}(z;t))^\top$, $\hat{\boldsymbol{f}}_k(z;t) = (\hat{F}_k(z;t), \hat{G}_k(z;t))^\top$, $\tilde{\boldsymbol{f}}_k(z;t) = (\tilde{F}_k(z;t), \tilde{G}_k(z;t))^\top$. Then, by using the above definitions, the traction free condition on the crack faces will be

$$\left.\begin{aligned}
&\boldsymbol{P}_1\left[\boldsymbol{f}_1''^{+}(\eta_1;t) - \eta_1\hat{\boldsymbol{f}}_1''^{+}(\eta_1;t) - \eta_1^2\tilde{\boldsymbol{f}}_1''^{+}(\eta_1;t)\right]\\
&+\boldsymbol{Q}_1\left[\overline{\boldsymbol{f}}_1''^{-}(\eta_1;t) - \eta_1\overline{\hat{\boldsymbol{f}}}_1''^{-}(\eta_1;t) - \eta_1^2\overline{\tilde{\boldsymbol{f}}}_1''^{-}(\eta_1;t)\right]\\
&-2\boldsymbol{M}_1\left[\hat{\boldsymbol{f}}_1'^{+}(\eta_1;t) + 2\eta_1\tilde{\boldsymbol{f}}_1'^{+}(\eta_1;t)\right] - 2\boldsymbol{N}_1\left[\overline{\hat{\boldsymbol{f}}}_1'^{-}(\eta_1;t) + 2\eta_1\overline{\tilde{\boldsymbol{f}}}_1'^{-}(\eta_1;t)\right]\\
&-2\overset{*}{\boldsymbol{P}}_1\,\tilde{\boldsymbol{f}}_1^{+}(\eta_1;t) - 2\overset{*}{\boldsymbol{Q}}_1\,\overline{\tilde{\boldsymbol{f}}}_1^{-}(\eta_1;t) = \mathbf{o}\\
&\boldsymbol{P}_2\left[\boldsymbol{f}_2''^{-}(\eta_1;t) - \eta_1\hat{\boldsymbol{f}}_2''^{-}(\eta_1;t) - \eta_1^2\tilde{\boldsymbol{f}}_2''^{-}(\eta_1;t)\right]\\
&+\boldsymbol{Q}_2\left[\overline{\boldsymbol{f}}_2''^{+}(\eta_1;t) - \eta_1\overline{\hat{\boldsymbol{f}}}_2''^{+}(\eta_1;t) - \eta_1^2\overline{\tilde{\boldsymbol{f}}}_2''^{+}(\eta_1;t)\right]\\
&-2\boldsymbol{M}_2\left[\hat{\boldsymbol{f}}_2'^{-}(\eta_1;t) + 2\eta_1\tilde{\boldsymbol{f}}_2'^{-}(\eta_1;t)\right] - 2\boldsymbol{N}_2\left[\overline{\hat{\boldsymbol{f}}}_2'^{+}(\eta_1;t) + 2\eta_1\overline{\tilde{\boldsymbol{f}}}_2'^{+}(\eta_1;t)\right]\\
&-2\overset{*}{\boldsymbol{P}}_2\,\tilde{\boldsymbol{f}}_2^{-}(\eta_1;t) - 2\overset{*}{\boldsymbol{Q}}_2\,\overline{\tilde{\boldsymbol{f}}}_2^{+}(\eta_1;t) = \mathbf{o}
\end{aligned}\right\},\ \forall\eta_1 < 0. \tag{6.3.45}$$

The continuity of traction along the interface will reduce to

$$\left.\begin{aligned}
&\Big\{\boldsymbol{P}_1\left[\boldsymbol{f}_1''^{+}(\eta_1;t) - \eta_1\hat{\boldsymbol{f}}_1''^{+}(\eta_1;t) - \eta_1^2\tilde{\boldsymbol{f}}_1''^{+}(\eta_1;t)\right]\\
&+\boldsymbol{Q}_1\left[\overline{\boldsymbol{f}}_1''^{-}(\eta_1;t) - \eta_1\overline{\hat{\boldsymbol{f}}}_1''^{-}(\eta_1;t) - \eta_1^2\overline{\tilde{\boldsymbol{f}}}_1''^{-}(\eta_1;t)\right]\\
&-2\boldsymbol{M}_1\left[\hat{\boldsymbol{f}}_1'^{+}(\eta_1;t) + 2\eta_1\tilde{\boldsymbol{f}}_1'^{+}(\eta_1;t)\right] - 2\boldsymbol{N}_1\left[\overline{\hat{\boldsymbol{f}}}_1'^{-}(\eta_1;t) + 2\eta_1\overline{\tilde{\boldsymbol{f}}}_1'^{-}(\eta_1;t)\right]\\
&-2\overset{*}{\boldsymbol{P}}_1\,\tilde{\boldsymbol{f}}_1^{+}(\eta_1;t) - 2\overset{*}{\boldsymbol{Q}}_1\,\overline{\tilde{\boldsymbol{f}}}_1^{-}(\eta_1;t)\Big\}\\
&-\Big\{\boldsymbol{P}_2\left[\boldsymbol{f}_2''^{-}(\eta_1;t) - \eta_1\hat{\boldsymbol{f}}_2''^{-}(\eta_1;t) - \eta_1^2\tilde{\boldsymbol{f}}_2''^{-}(\eta_1;t)\right]\\
&+\boldsymbol{Q}_2\left[\overline{\boldsymbol{f}}_2''^{+}(\eta_1;t) - \eta_1\overline{\hat{\boldsymbol{f}}}_2''^{+}(\eta_1;t) - \eta_1^2\overline{\tilde{\boldsymbol{f}}}_2''^{+}(\eta_1;t)\right]\\
&-2\boldsymbol{M}_2\left[\hat{\boldsymbol{f}}_2'^{-}(\eta_1;t) + 2\eta_1\tilde{\boldsymbol{f}}_2'^{-}(\eta_1;t)\right] - 2\boldsymbol{N}_2\left[\overline{\hat{\boldsymbol{f}}}_2'^{+}(\eta_1;t) + 2\eta_1\overline{\tilde{\boldsymbol{f}}}_2'^{+}(\eta_1;t)\right]\\
&-2\overset{*}{\boldsymbol{P}}_2\,\tilde{\boldsymbol{f}}_2^{-}(\eta_1;t) - 2\overset{*}{\boldsymbol{Q}}_2\,\overline{\tilde{\boldsymbol{f}}}_2^{+}(\eta_1;t)\Big\} = \mathbf{o}
\end{aligned}\right\},\ \forall\ \eta_1 > 0, \tag{6.3.46}$$

and the continuity of the displacement along the interface will be

$$\left.\begin{aligned}
&\Big\{\boldsymbol{U}_1\Big[\boldsymbol{f}_1'^{+}(\eta_1;t)-\eta_1\hat{\boldsymbol{f}}_1'^{+}(\eta_1;t)-\eta_1^2\tilde{\boldsymbol{f}}_1'^{+}(\eta_1;t)\Big]\\
&+\boldsymbol{V}_1\Big[\overline{\boldsymbol{f}}_1'^{-}(\eta_1;t)-\eta_1\overline{\hat{\boldsymbol{f}}}_1'^{-}(\eta_1;t)-\eta_1^2\overline{\tilde{\boldsymbol{f}}}_1'^{-}(\eta_1;t)\Big]\\
&-\overset{*}{\boldsymbol{U}}_1\Big[\hat{\boldsymbol{f}}_1^{+}(\eta_1;t)+2\eta_1\tilde{\boldsymbol{f}}_1^{+}(\eta_1;t)\Big]-\overset{*}{\boldsymbol{V}}_1\Big[\overline{\hat{\boldsymbol{f}}}_1^{-}(\eta_1;t)+2\eta_1\overline{\tilde{\boldsymbol{f}}}_1^{-}(\eta_1;t)\Big]\Big\}\\
&-\Big\{\boldsymbol{U}_2\Big[\boldsymbol{f}_2'^{-}(\eta_1;t)-\eta_1\hat{\boldsymbol{f}}_2'^{-}(\eta_1;t)-\eta_1^2\tilde{\boldsymbol{f}}_2'^{-}(\eta_1;t)\Big]\\
&+\boldsymbol{V}_2\Big[\overline{\boldsymbol{f}}_2'^{+}(\eta_1;t)-\eta_1\overline{\hat{\boldsymbol{f}}}_2'^{+}(\eta_1;t)-\eta_1^2\overline{\tilde{\boldsymbol{f}}}_2'^{+}(\eta_1;t)\Big]\\
&-\overset{*}{\boldsymbol{U}}_2\Big[\hat{\boldsymbol{f}}_2^{-}(\eta_1;t)+2\eta_1\tilde{\boldsymbol{f}}_2^{-}(\eta_1;t)\Big]-\overset{*}{\boldsymbol{V}}_2\Big[\overline{\hat{\boldsymbol{f}}}_2^{+}(\eta_1;t)+2\eta_1\overline{\tilde{\boldsymbol{f}}}_2^{+}(\eta_1;t)\Big]\Big\}=\mathbf{o}
\end{aligned}\right\},\ \forall\eta_1>0. \tag{6.3.47}$$

Similar to the procedure in the previous section, by rearranging the bonding condition (6.3.46) and (6.3.47), we may introduce two new functions $\boldsymbol{\kappa}(z;t)$ and $\boldsymbol{\theta}(z;t)$, which are analytic in the cut-plane $S^+\cup S^-$. In order to keep our notation short, we define some new quantities,

$$\left.\begin{aligned}
\boldsymbol{g}_k(z;t) &= \boldsymbol{f}_k''(z;t)-z\hat{\boldsymbol{f}}_k''(z;t)-z^2\tilde{\boldsymbol{f}}_k''(z;t)\\
&-\ 2\boldsymbol{P}_k^{-1}\boldsymbol{M}_k\Big[\hat{\boldsymbol{f}}_k'(z;t)+2z\tilde{\boldsymbol{f}}_k'(z;t)\Big]\ -\ 2\boldsymbol{P}_k^{-1}\overset{*}{\boldsymbol{P}}_k\,\tilde{\boldsymbol{f}}_k(z;t)
\end{aligned}\right\},\quad k\in\{1,2\}.$$

Therefore, we can write that

$$\left.\begin{aligned}
\boldsymbol{\kappa}(z;t)&=\boldsymbol{P}_1\boldsymbol{g}_1(z;t)-\boldsymbol{Q}_2\overline{\boldsymbol{g}}_2(z;t)\\
\boldsymbol{\theta}'(z;t)&=\boldsymbol{U}_1\boldsymbol{g}_1(z;t)-\boldsymbol{V}_2\overline{\boldsymbol{g}}_2(z;t)+\boldsymbol{q}_1(z;t)-\overline{\overset{*}{\boldsymbol{q}}}_2(z;t)
\end{aligned}\right\},\quad z\in S^+\,, \tag{6.3.48}$$

and

$$\left.\begin{aligned}
\boldsymbol{\kappa}(z;t)&=\boldsymbol{P}_2\boldsymbol{g}_2(z;t)-\boldsymbol{Q}_1\overline{\boldsymbol{g}}_1(z;t)\\
\boldsymbol{\theta}'(z;t)&=\boldsymbol{U}_2\boldsymbol{g}_2(z;t)-\boldsymbol{V}_1\overline{\boldsymbol{g}}_1(z;t)+\boldsymbol{q}_2(z;t)-\overline{\overset{*}{\boldsymbol{q}}}_1(z;t)
\end{aligned}\right\},\quad z\in S^-\,, \tag{6.3.49}$$

where

$$\left.\begin{aligned}
\boldsymbol{q}_k(z;t)&=2\left(\boldsymbol{L}_k\boldsymbol{M}_k-\boldsymbol{I}\right)\Big[\hat{\boldsymbol{f}}_k'(z;t)+2z\tilde{\boldsymbol{f}}_k'(z;t)\Big]+2\left(\boldsymbol{L}_k\overset{*}{\boldsymbol{P}}_k-\overset{*}{\boldsymbol{U}}_k\right)\tilde{\boldsymbol{f}}_k(z;t)\\
\overset{*}{\boldsymbol{q}}_k(z;t)&=2\left(\overset{*}{\boldsymbol{L}}_k\boldsymbol{N}_k-\boldsymbol{J}\right)\Big[\hat{\boldsymbol{f}}_k'(z;t)+2z\tilde{\boldsymbol{f}}_k'(z;t)\Big]+2\left(\overset{*}{\boldsymbol{L}}_k\overset{*}{\boldsymbol{Q}}_k-\overset{*}{\boldsymbol{V}}_k\right)\tilde{\boldsymbol{f}}_k(z;t)
\end{aligned}\right\}, \tag{6.3.50}$$

and

$$\boldsymbol{I} = \begin{bmatrix} 1 & 0 \\ 0 & 1 \end{bmatrix} , \qquad \boldsymbol{J} = \begin{bmatrix} 1 & 0 \\ 0 & -1 \end{bmatrix} .$$

Vector $\overset{*}{\boldsymbol{q}}_k\ (z;t)$ is related to vector $\boldsymbol{q}_k(z;t)$ by

$$\overset{*}{\boldsymbol{q}}_k\ (z;t) = \left(q_k^{(1)}(z;t),\ -q_k^{(2)}(z;t) \right)^{\top} , \quad \boldsymbol{q}_k(z;t) = \left(q_k^{(1)}(z;t),\ q_k^{(2)}(z;t) \right)^{\top} .$$

This notation will be used throughout the paper to signify this operation. In calculating $\overset{*}{\boldsymbol{q}}_k\ (z;t)$ and $\boldsymbol{q}_k(z;t)$ in equation (6.3.50), we have used the fact that

$$\boldsymbol{P}_k^{-1}\boldsymbol{M}_k = \boldsymbol{Q}_k^{-1}\boldsymbol{N}_k , \qquad \boldsymbol{P}_k^{-1}\ \overset{*}{\boldsymbol{P}}_k = \boldsymbol{Q}_k^{-1}\ \overset{*}{\boldsymbol{Q}}_k , \qquad k \in \{1,2\}.$$

By solving equations (6.3.48) and (6.3.49) for $\boldsymbol{g}_k(z;t)$ and $\overline{\boldsymbol{g}}_k(z;t)$, we obtain

$$\left.\begin{aligned} \boldsymbol{g}_1(z;t) &= \boldsymbol{P}_1^{-1}\boldsymbol{H}^{-1}\left\{\boldsymbol{\theta}'(z;t) - \overset{*}{\boldsymbol{L}}_2\ \boldsymbol{\kappa}(z;t) - \left[\boldsymbol{q}_1(z;t) - \overline{\overset{*}{\boldsymbol{q}}}_2(z;t)\right]\right\} \\ \overline{\boldsymbol{g}}_2(z;t) &= \boldsymbol{Q}_2^{-1}\boldsymbol{H}^{-1}\left\{\boldsymbol{\theta}'(z;t) - \boldsymbol{L}_1\boldsymbol{\kappa}(z;t) - \left[\boldsymbol{q}_1(z;t) - \overline{\overset{*}{\boldsymbol{q}}}_2(z;t)\right]\right\} \end{aligned}\right\}, \ z \in S^+, \tag{6.3.51}$$

and

$$\left.\begin{aligned} \boldsymbol{g}_2(z;t) &= -\boldsymbol{P}_2^{-1}\ \overset{*}{\boldsymbol{H}}^{-1}\left\{\boldsymbol{\theta}'(z;t) - \overset{*}{\boldsymbol{L}}_1\ \boldsymbol{\kappa}(z;t) - \left[\boldsymbol{q}_2(z;t) - \overline{\overset{*}{\boldsymbol{q}}}_1(z;t)\right]\right\} \\ \overline{\boldsymbol{g}}_1(z;t) &= -\boldsymbol{Q}_1^{-1}\ \overset{*}{\boldsymbol{H}}^{-1}\left\{\boldsymbol{\theta}'(z;t) - \boldsymbol{L}_2\boldsymbol{\kappa}(z;t) - \left[\boldsymbol{q}_2(z;t) - \overline{\overset{*}{\boldsymbol{q}}}_1(z;t)\right]\right\} \end{aligned}\right\}, z \in S^-. \tag{6.3.52}$$

It can be seen that the above equations are very similar to equations (6.3.14) and (6.3.15) with the exception of terms $\boldsymbol{q}_1(z;t) - \overline{\overset{*}{\boldsymbol{q}}}_2(z;t)$ and $\boldsymbol{q}_2(z;t) - \overline{\overset{*}{\boldsymbol{q}}}_1(z;t)$, which are totally determined by the solution for $m = 0$.

By substituting equations (6.3.51) and (6.3.52) into the traction free boundary condition (6.3.45), one can show that $\boldsymbol{\kappa}(z;t)$ is an entire function. As a result, the boundary condition (6.3.45) will reduce to

$$\overset{*}{\boldsymbol{H}}\ \boldsymbol{\theta}'^{+}(\eta_1;t) - \boldsymbol{H}\boldsymbol{\theta}'^{-}(\eta_1;t) = \boldsymbol{R}\boldsymbol{\kappa}(\eta_1;t) + \hat{\boldsymbol{\kappa}}(\eta_1;t) , \qquad \forall\ \eta_1 < 0 , \tag{6.3.53}$$

where

$$\hat{\boldsymbol{\kappa}}(\eta_1;t) = \overset{*}{\boldsymbol{H}} \left\{ \boldsymbol{q}_1^+(\eta_1;t) - \overline{\overset{*}{\boldsymbol{q}}}_2^+(\eta_1;t) \right\} - \boldsymbol{H} \left\{ \boldsymbol{q}_2^-(\eta_1;t) - \overline{\overset{*}{\boldsymbol{q}}}_1^-(\eta_1;t) \right\} .$$

Equation (6.3.53) also represents a Riemann-Hilbert problem for $\boldsymbol{\theta}'(z;t)$. It requires that $\boldsymbol{\theta}'(z;t)$ is analytic in the cut-plane $S^+ \cup S^-$, and along the cut satisfies the above equation. By using the properties of our asymptotic expansion, equation (6.2.5), it can be shown that $\boldsymbol{\theta}'(z;t)$ should vary as,

$$| \boldsymbol{\theta}'(z;t) | = O (|z|^{\alpha}) , \qquad \text{as} \quad |z| \to 0 , \tag{6.3.54}$$

for some $\alpha > 0$. The complete solution of (6.3.53) is generated by splitting the problem to the following two parts.

To obtain the first part, let $\overset{\circ}{\boldsymbol{\theta}}{}'(z;t)$ be an analytic function in the cut-plane $S^+ \cup S^-$, such that

$$\overset{*}{\boldsymbol{H}} \overset{\circ}{\boldsymbol{\theta}}{}'^{+}(\eta_1;t) - \boldsymbol{H}\, \overset{\circ}{\boldsymbol{\theta}}{}'^{-}(\eta_1;t) = \boldsymbol{R}\boldsymbol{\kappa}(\eta_1;t) , \qquad \forall\ \eta_1 < 0 . \tag{6.3.55}$$

This is exactly the same as equation (6.3.18). One basic difference, however, is that unlike the previous case, here $\overset{\circ}{\boldsymbol{\theta}}{}'(z;t)$ has to satisfy (6.3.54) (recall that before, $\alpha > -1$). As a result of this observation, in the material above the interface, the solution for $\overset{\circ}{\boldsymbol{g}}_1(z;t)$ is given by

$$\left.\begin{aligned}
&\overset{\circ}{g}{}_1^{(1)}(z;t) = -\frac{[(1+\alpha_s^2) - 2\eta\alpha_s]\, e^{\epsilon\pi}}{\mu D(v) \cosh \epsilon\pi} z^{\frac{1}{2}+i\epsilon}\, \overset{\circ}{A}_2(z;t) \\
&-\frac{[(1+\alpha_s^2) + 2\eta\alpha_s]\, e^{-\epsilon\pi}}{\mu D(v) \cosh \epsilon\pi} z^{\frac{1}{2}-i\epsilon}\, \overline{\overset{\circ}{A}}_2(z;t) \\
&-\frac{1}{\mu D(v)} \left\{ \left(\frac{1+\alpha_s^2}{1+\omega_l} - \frac{2\alpha_s}{1+\omega_s} \right) \overset{\circ}{B}_2(z;t) - \left(\frac{1+\alpha_s^2}{1+\omega_l} + \frac{2\alpha_s}{1+\omega_s} \right) \overline{\overset{\circ}{B}}_2(z;t) \right\} z
\end{aligned}\right\} , \tag{6.3.56}$$

and

$$\left.\begin{aligned} \overset{\circ}{g}{}_1^{(2)}(z;t) &= \frac{[2\alpha_l - \eta(1+\alpha_s^2)]\, e^{\epsilon\pi}}{\mu D(v)\cosh\epsilon\pi} z^{\frac{1}{2}+i\epsilon}\, \overset{\circ}{A}_2(z;t) \\ &+ \frac{[2\alpha_l + \eta(1+\alpha_s^2)]\, e^{-\epsilon\pi}}{\mu D(v)\cosh\epsilon\pi} z^{\frac{1}{2}-i\epsilon}\, \overline{\overset{\circ}{A}_2}(z;t) \\ &+ \frac{1}{\mu D(v)} \left\{ \left(\frac{2\alpha_l}{1+\omega_l} - \frac{1+\alpha_s^2}{1+\omega_s} \right) \overset{\circ}{B}_2(z;t) - \left(\frac{2\alpha_l}{1+\omega_l} + \frac{1+\alpha_s^2}{1+\omega_s} \right) \overline{\overset{\circ}{B}_2}(z;t) \right\} z \end{aligned} \right\}, \tag{6.3.57}$$

where

$$\overset{\circ}{\boldsymbol{g}}_1(z;t) = \left(\overset{\circ}{g}{}_1^{(1)}(z;t),\ \overset{\circ}{g}{}_1^{(2)}(z;t) \right)^{\mathsf{T}},$$

and the entire functions $\overset{\circ}{A}_2(z;t)$ and $\overset{\circ}{B}_2(z;t)$ can only be determined by the far field conditions. Similarly, the solution for $\overset{\circ}{\boldsymbol{g}}_2(z;t)$, in the material below the interface, can be obtained by changing the corresponding parameters in equations (6.3.56) and (6.3.57).

The second part of the solution is obtained by letting

$$\left.\begin{aligned} \hat{\boldsymbol{\theta}}'(z;t) &= \boldsymbol{\theta}'(z;t) - \overset{\circ}{\boldsymbol{\theta}}{}'(z;t) \\ \hat{\boldsymbol{g}}_k(z;t) &= \boldsymbol{g}_k(z;t) - \overset{\circ}{\boldsymbol{g}}_k(z;t) \end{aligned} \right\}.$$

Then, $\hat{\boldsymbol{\theta}}'(z;t)$ will be analytic in the cut-plane $S^+ \cup S^-$, and satisfy

$$\overset{*}{\boldsymbol{H}}\, \hat{\boldsymbol{\theta}}'^{+}(\eta_1;t) - \boldsymbol{H}\hat{\boldsymbol{\theta}}'^{-}(\eta_1;t) = \hat{\boldsymbol{\kappa}}(\eta_1;t)\,, \qquad \forall\ \eta_1 < 0\,. \tag{6.3.58}$$

Because the right-hand side of equation (6.3.58), $\hat{\boldsymbol{\kappa}}(\eta_1;t)$ is totally determined by the solutions $\phi_0(\eta_1,\eta_2,t)$ and $\psi_0(\eta_1,\eta_2,t)$, $\hat{\boldsymbol{\theta}}'(z;t)$, and therefore, $\hat{\boldsymbol{g}}_k(z;t)$ are also completely determined.

By using the results in Appendix B, we can write

$$\hat{\boldsymbol{\theta}}'(z;t) = \frac{1}{4\pi i}\int_{-\infty}^{0} \left\{ \frac{1}{\lambda_2}\cdot\frac{L(z)}{L^+(\eta_1)}\boldsymbol{\Gamma}\hat{\boldsymbol{\kappa}}(\eta_1;t) + \frac{1}{\lambda_1}\cdot\frac{\overline{L}(z)}{\overline{L}^+(\eta_1)}\, \overset{*}{\boldsymbol{\Gamma}}\, \hat{\boldsymbol{\kappa}}(\eta_1;t) \right\} \frac{\mathrm{d}\eta_1}{\eta_1 - z}\,, \tag{6.3.59}$$

where

$$L(z) = z^{\frac{1}{2}+i\epsilon} \ .$$

The explicit dependence of $\boldsymbol{q}_k(z;t)$ on z can be obtained from equation (6.3.50),

$$\left.\begin{aligned} \boldsymbol{q}_k(z;t) &= \boldsymbol{t}_k\{a_0(t), c_0(t)\} z^{\frac{1}{2}+i\epsilon} + \overline{\boldsymbol{t}}_k\{b_0(t), d_0(t)\} z^{\frac{1}{2}-i\epsilon} \\ &+ \dot{\epsilon}\,(3+2i\epsilon)(\boldsymbol{L}_k\boldsymbol{M}_k - \boldsymbol{I})\boldsymbol{k}_k\{a_0(t), c_0(t)\} z^{\frac{1}{2}+i\epsilon} \ln z \\ &+ \dot{\epsilon}\,(3-2i\epsilon)(\boldsymbol{L}_k\boldsymbol{M}_k - \boldsymbol{I})\overline{\boldsymbol{k}}_k\{b_0(t), d_0(t)\} z^{\frac{1}{2}-i\epsilon} \ln z \end{aligned}\right\} , \qquad (6.3.60)$$

where operators like $\boldsymbol{t}_k\{a_0(t), c_0(t)\}$ and $\boldsymbol{k}_k\{a_0(t), c_0(t)\}$, etc., are given in Appendix A. From the definitions for $\overset{*}{\boldsymbol{q}}_k\,(z;t)$ and the above, one can get

$$\left.\begin{aligned} \boldsymbol{q}_1(z;t) - \overline{\overset{*}{\boldsymbol{q}}}_2(z;t) &= \boldsymbol{\beta} z^{\frac{1}{2}+i\epsilon} - \overline{\overset{*}{\boldsymbol{\gamma}}} z^{\frac{1}{2}-i\epsilon} + \dot{\epsilon}\,\boldsymbol{\xi} z^{\frac{1}{2}+i\epsilon} \ln z - \dot{\epsilon}\,\overline{\overset{*}{\boldsymbol{\varsigma}}} z^{\frac{1}{2}-i\epsilon} \ln z \\ \boldsymbol{q}_2(z;t) - \overline{\overset{*}{\boldsymbol{q}}}_1(z;t) &= \boldsymbol{\gamma} z^{\frac{1}{2}+i\epsilon} - \overline{\overset{*}{\boldsymbol{\beta}}} z^{\frac{1}{2}-i\epsilon} + \dot{\epsilon}\,\boldsymbol{\varsigma} z^{\frac{1}{2}+i\epsilon} \ln z - \dot{\epsilon}\,\overline{\overset{*}{\boldsymbol{\xi}}} z^{\frac{1}{2}-i\epsilon} \ln z \end{aligned}\right\} , \qquad (6.3.61)$$

where quantities of $\boldsymbol{\beta}$, $\boldsymbol{\gamma}$, $\boldsymbol{\xi}$, and $\boldsymbol{\varsigma}$ are also given in Appendix A. It should be noted here that $\boldsymbol{\beta}$ and $\boldsymbol{\gamma}$ depend on the crack-tip speed and the complex parameter $A_0(t)$, as well as their time derivatives. However, $\boldsymbol{\xi}$ and $\boldsymbol{\varsigma}$ depend only on the crack-tip speed and the complex parameter $A_0(t)$. The right-hand side of equation (6.3.58), $\hat{\boldsymbol{\kappa}}(\eta_1;t)$, becomes

$$\left.\begin{aligned} \hat{\boldsymbol{\kappa}}(\eta_1;t) &= \dot{\epsilon}\,\boldsymbol{\omega}_d(-\eta_1)^{\frac{1}{2}+i\epsilon} \ln(-\eta_1) + \dot{\epsilon}\,\overline{\overset{*}{\boldsymbol{\omega}}}_d(-\eta_1)^{\frac{1}{2}-i\epsilon} \ln(-\eta_1) \\ &+ \boldsymbol{\omega}_t(-\eta_1)^{\frac{1}{2}+i\epsilon} + \overline{\overset{*}{\boldsymbol{\omega}}}_t(-\eta_1)^{\frac{1}{2}-i\epsilon} \end{aligned}\right\} , \quad \forall\ \eta_1 < 0 \ , \qquad (6.3.62)$$

where

$$\left.\begin{aligned} \boldsymbol{\omega}_d &= i\left\{e^{-\epsilon\pi}\ \overset{*}{\boldsymbol{H}}\,\boldsymbol{\xi} + e^{\epsilon\pi}\boldsymbol{H}\boldsymbol{\varsigma}\right\} \\ \boldsymbol{\omega}_t &= i\left\{e^{-\epsilon\pi}\ \overset{*}{\boldsymbol{H}}\,\boldsymbol{\beta} + e^{\epsilon\pi}\boldsymbol{H}\boldsymbol{\gamma}\right\} - \pi\dot{\epsilon}\left\{e^{-\epsilon\pi}\ \overset{*}{\boldsymbol{H}}\,\boldsymbol{\xi} - e^{\epsilon\pi}\boldsymbol{H}\boldsymbol{\varsigma}\right\} \end{aligned}\right\} .$$

Once again, it can be seen that $\boldsymbol{\omega}_d$ does not depend on the time derivatives of the complex parameter $A_0(t)$ and the crack-tip speed, while $\boldsymbol{\omega}_t$ depends on these quantities.

The functions inside the integrand of equation (6.3.59) can be rewritten as

$$\left.\begin{aligned}
\frac{\hat{\boldsymbol{\kappa}}(\eta_1;t)}{L^+(\eta_1)} &= -ie^{\pi\epsilon}\left\{\dot{\epsilon}\,\boldsymbol{\omega}_d\ln(-\eta_1)+\dot{\epsilon}\,\overline{\overset{*}{\boldsymbol{\omega}}}_d(-\eta_1)^{-2i\epsilon}\ln(-\eta_1)\right.\\
&\quad\left.+\boldsymbol{\omega}_t+\overline{\overset{*}{\boldsymbol{\omega}}}_t(-\eta_1)^{-2i\epsilon}\right\}\\
\frac{\hat{\boldsymbol{\kappa}}(\eta_1;t)}{\overline{L}^+(\eta_1)} &= -ie^{-\pi\epsilon}\left\{\dot{\epsilon}\,\boldsymbol{\omega}_d(-\eta_1)^{2i\epsilon}\ln(-\eta_1)+\dot{\epsilon}\,\overline{\overset{*}{\boldsymbol{\omega}}}_d\ln(-\eta_1)\right.\\
&\quad\left.+\boldsymbol{\omega}_t(-\eta_1)^{2i\epsilon}+\overline{\overset{*}{\boldsymbol{\omega}}}_t\right\}
\end{aligned}\right\}. \tag{6.3.63}$$

In order to obtain the solution for $\hat{\boldsymbol{\theta}}'(z;t)$, we recast equation (6.3.59) into the form of a Stieltjes transform by using (6.3.63). However, one can see that for our case, a closed form evaluation of the Stieltjes transform integral is very difficult. At the beginning of this section, it has been mentioned that only the most singular terms in the solution of $F_0(z;t)$ and $G_0(z;t)$ are considered. This implies that we are only interested in the region where $|z|\to 0$, i.e., very close to the interfacial crack-tip. As a result, instead of evaluating the entire Stieltjes transform, we only need to study the asymptotic behavior of that transform as $|z|\to 0$. The details of this asymptotic analysis are given in Appendix C. If only the leading terms in the Stieltjes transform are retained, by using the results provided in Appendix C, the solution for $\hat{\boldsymbol{\theta}}'(z;t)$ can be obtained as

$$\left.\begin{aligned}
\hat{\boldsymbol{\theta}}'(z;t) &= \dot{\epsilon}\left[\boldsymbol{\zeta}_d z^{\frac{1}{2}+i\epsilon}-\overline{\overset{*}{\boldsymbol{\zeta}}}_d z^{\frac{1}{2}-i\epsilon}\right](\ln z)^2+\left[\boldsymbol{\zeta}_t z^{\frac{1}{2}+i\epsilon}-\overline{\overset{*}{\boldsymbol{\zeta}}}_t z^{\frac{1}{2}-i\epsilon}\right]\ln z\\
&+\left[\boldsymbol{\zeta}_{tt} z^{\frac{1}{2}+i\epsilon}-\overline{\overset{*}{\boldsymbol{\zeta}}}_{tt} z^{\frac{1}{2}-i\epsilon}\right]+O\left(|z|\right)
\end{aligned}\right\}, \tag{6.3.64}$$

where in developing the above equation, the relation

$$\frac{e^{\pi\epsilon}}{\lambda_2}=-\frac{e^{-\pi\epsilon}}{\lambda_1},$$

has been used, and the following notations have been defined:

$$\left.\begin{aligned}
\boldsymbol{\zeta}_d &= \frac{e^{-\pi\epsilon}}{8\pi\lambda_1}\boldsymbol{\Gamma}\boldsymbol{\omega}_d \\
\boldsymbol{\zeta}_t &= \frac{e^{-\pi\epsilon}}{4\pi\lambda_1}\left\{\boldsymbol{\Gamma}\boldsymbol{\omega}_t - \frac{i\pi\dot{\epsilon}}{\sinh(2\pi\epsilon)}\overset{*}{\boldsymbol{\Gamma}}\boldsymbol{\omega}_d\right\} \\
\boldsymbol{\zeta}_{tt} &= \frac{e^{-\pi\epsilon}}{4\pi\lambda_1}\left\{\left[\frac{\pi\dot{\epsilon}}{6}\boldsymbol{\Gamma}\boldsymbol{\omega}_d - \frac{\dot{\epsilon}}{4\epsilon^2}\boldsymbol{\Gamma}\overline{\overset{*}{\boldsymbol{\omega}}}_d - \frac{i}{2\epsilon}\boldsymbol{\Gamma}\overline{\overset{*}{\boldsymbol{\omega}}}_t\right]\right. \\
&+ \left.\left[\frac{\pi^2\dot{\epsilon}\cosh(2\pi\epsilon)}{\sinh^2(2\pi\epsilon)}\overset{*}{\boldsymbol{\Gamma}}\boldsymbol{\omega}_d + \frac{i\pi}{\sinh(2\pi\epsilon)}\overset{*}{\boldsymbol{\Gamma}}\boldsymbol{\omega}_t\right]\right\}
\end{aligned}\right\}.$$

In constructing the entire solution for $\boldsymbol{g}_1(z;t)$ and $\boldsymbol{g}_2(z;t)$, the leading terms in (6.3.56) and (6.3.57), are considered. This is consistent with the fact that (6.3.64) contains only leading terms of the same order. The final solutions for $\boldsymbol{g}_1(z;t)$ and $\boldsymbol{g}_2(z;t)$, are therefore

$$\left.\begin{aligned}
\boldsymbol{g}_1(z;t) &= \dot{\epsilon}\left\{\boldsymbol{P}_1^{-1}\boldsymbol{H}^{-1}\boldsymbol{\zeta}_d z^{\frac{1}{2}+i\epsilon} - \boldsymbol{Q}_1^{-1}\overset{*}{\boldsymbol{H}}^{-1}\overline{\boldsymbol{\zeta}}_d z^{\frac{1}{2}-i\epsilon}\right\}(\ln z)^2 \\
&+ \left\{\boldsymbol{P}_1^{-1}\boldsymbol{H}^{-1}\left(\boldsymbol{\zeta}_t - \dot{\epsilon}\,\boldsymbol{\xi}\right)z^{\frac{1}{2}+i\epsilon} - \boldsymbol{Q}_1^{-1}\overset{*}{\boldsymbol{H}}^{-1}\left(\overline{\boldsymbol{\zeta}}_t - \dot{\epsilon}\,\overline{\boldsymbol{\varsigma}}\right)z^{\frac{1}{2}-i\epsilon}\right\}\ln z \\
&+ \left\{\boldsymbol{P}_1^{-1}\boldsymbol{H}^{-1}\left(\boldsymbol{\zeta}_{tt} - \boldsymbol{\beta}\right)z^{\frac{1}{2}+i\epsilon} - \boldsymbol{Q}_1^{-1}\overset{*}{\boldsymbol{H}}^{-1}\left(\overline{\boldsymbol{\zeta}}_{tt} - \overline{\boldsymbol{\gamma}}\right)z^{\frac{1}{2}-i\epsilon}\right\} \\
&+ \frac{e^{\epsilon\pi}\boldsymbol{P}_1^{-1}\boldsymbol{\zeta}}{\cosh\epsilon\pi}z^{\frac{1}{2}+i\epsilon}\overset{\circ}{A}_2(t) + \frac{e^{-\epsilon\pi}\boldsymbol{Q}_1^{-1}\boldsymbol{\zeta}}{\cosh\epsilon\pi}z^{\frac{1}{2}-i\epsilon}\overline{\overset{\circ}{A}}_2(t) + O\left(|z|\right)
\end{aligned}\right\},\quad z\in S^+, \tag{6.3.65}$$

and

$$\left.\begin{aligned}
\boldsymbol{g}_2(z;t) &= -\dot{\epsilon}\left\{\boldsymbol{P}_2^{-1}\overset{*}{\boldsymbol{H}}^{-1}\boldsymbol{\zeta}_d z^{\frac{1}{2}+i\epsilon} - \boldsymbol{Q}_2^{-1}\boldsymbol{H}^{-1}\overline{\boldsymbol{\zeta}}_d z^{\frac{1}{2}-i\epsilon}\right\}(\ln z)^2 \\
&- \left\{\boldsymbol{P}_2^{-1}\overset{*}{\boldsymbol{H}}^{-1}\left(\boldsymbol{\zeta}_t - \dot{\epsilon}\,\boldsymbol{\varsigma}\right)z^{\frac{1}{2}+i\epsilon} - \boldsymbol{Q}_2^{-1}\boldsymbol{H}^{-1}\left(\overline{\boldsymbol{\zeta}}_t - \dot{\epsilon}\,\overline{\boldsymbol{\xi}}\right)z^{\frac{1}{2}-i\epsilon}\right\}\ln z \\
&- \left\{\boldsymbol{P}_2^{-1}\overset{*}{\boldsymbol{H}}^{-1}\left(\boldsymbol{\zeta}_{tt} - \boldsymbol{\gamma}\right)z^{\frac{1}{2}+i\epsilon} - \boldsymbol{Q}_2^{-1}\boldsymbol{H}^{-1}\left(\overline{\boldsymbol{\zeta}}_{tt} - \overline{\boldsymbol{\beta}}\right)z^{\frac{1}{2}-i\epsilon}\right\} \\
&+ \frac{e^{-\epsilon\pi}\boldsymbol{P}_2^{-1}\boldsymbol{\zeta}}{\cosh\epsilon\pi}z^{\frac{1}{2}+i\epsilon}\overset{\circ}{A}_2(t) + \frac{e^{\epsilon\pi}\boldsymbol{Q}_2^{-1}\boldsymbol{\zeta}}{\cosh\epsilon\pi}z^{\frac{1}{2}-i\epsilon}\overline{\overset{\circ}{A}}_2(t) + O\left(|z|\right)
\end{aligned}\right\},\quad z\in S^-, \tag{6.3.66}$$

where $\overset{\circ}{A}_2(t) = \overset{\circ}{A}_2(0;t)$.

Our final target is to find the complex potentials $\boldsymbol{f}_k(z;t)$, $k \in \{1,2\}$. After some manipulations, $\boldsymbol{f}_1''(z;t)$ and $\boldsymbol{f}_2''(z;t)$ can be expressed as

$$\left.\begin{aligned}
\boldsymbol{f}_1''(z;t) = {} & \dot{\epsilon}\left\{\boldsymbol{P}_1^{-1}\boldsymbol{H}^{-1}\boldsymbol{\zeta}_d z^{\frac{1}{2}+i\epsilon} - \boldsymbol{Q}_1^{-1}\overset{*}{\boldsymbol{H}}^{-1}\overline{\boldsymbol{\zeta}}_d z^{\frac{1}{2}-i\epsilon}\right\}(\ln z)^2 \\
& + \left\{\left[\boldsymbol{P}_1^{-1}\boldsymbol{H}^{-1}\left(\boldsymbol{\zeta}_t - \dot{\epsilon}\,\boldsymbol{\xi}\right) + \dot{\epsilon}\,\boldsymbol{w}_{d1}\{a_0(t), c_0(t)\}\right] z^{\frac{1}{2}+i\epsilon}\right. \\
& \left. - \left[\boldsymbol{Q}_1^{-1}\overset{*}{\boldsymbol{H}}^{-1}\left(\overline{\boldsymbol{\zeta}}_t - \dot{\epsilon}\,\overline{\boldsymbol{\varsigma}}\right) - \dot{\epsilon}\,\overline{\boldsymbol{w}}_{d1}\{b_0(t), d_0(t)\}\right] z^{\frac{1}{2}-i\epsilon}\right\}\ln z \\
& + \left\{\left[\boldsymbol{P}_1^{-1}\boldsymbol{H}^{-1}\left(\boldsymbol{\zeta}_{tt} - \boldsymbol{\beta}\right) + \boldsymbol{w}_{t1}\{a_0(t), c_0(t)\}\right] z^{\frac{1}{2}+i\epsilon}\right. \\
& \left. - \left[\boldsymbol{Q}_1^{-1}\overset{*}{\boldsymbol{H}}^{-1}\left(\overline{\boldsymbol{\zeta}}_{tt} - \overline{\boldsymbol{\gamma}}\right) - \overline{\boldsymbol{w}}_{t1}\{b_0(t), d_0(t)\}\right] z^{\frac{1}{2}-i\epsilon}\right\} \\
& + \frac{e^{\epsilon\pi}\boldsymbol{P}_1^{-1}\boldsymbol{\zeta}}{\cosh\epsilon\pi} z^{\frac{1}{2}+i\epsilon}\,\overset{\circ}{A}_2\,(t) + \frac{e^{-\epsilon\pi}\boldsymbol{Q}_1^{-1}\boldsymbol{\zeta}}{\cosh\epsilon\pi} z^{\frac{1}{2}-i\epsilon}\overline{\overset{\circ}{A}}_2(t) + O\,(\,|z|\,)
\end{aligned}\right\},\quad z \in S^+, \quad (6.3.67)$$

and

$$\left.\begin{aligned}
\boldsymbol{f}_2''(z;t) = {} & -\dot{\epsilon}\left\{\boldsymbol{P}_2^{-1}\overset{*}{\boldsymbol{H}}^{-1}\boldsymbol{\zeta}_d z^{\frac{1}{2}+i\epsilon} - \boldsymbol{Q}_2^{-1}\boldsymbol{H}^{-1}\overline{\boldsymbol{\zeta}}_d z^{\frac{1}{2}-i\epsilon}\right\}(\ln z)^2 \\
& - \left\{\left[\boldsymbol{P}_2^{-1}\overset{*}{\boldsymbol{H}}^{-1}\left(\boldsymbol{\zeta}_t - \dot{\epsilon}\,\boldsymbol{\varsigma}\right) - \dot{\epsilon}\,\boldsymbol{w}_{d2}\{a_0(t), c_0(t)\}\right] z^{\frac{1}{2}+i\epsilon}\right. \\
& \left. - \left[\boldsymbol{Q}_2^{-1}\boldsymbol{H}^{-1}\left(\overline{\boldsymbol{\zeta}}_t - \dot{\epsilon}\,\overline{\boldsymbol{\xi}}\right) + \dot{\epsilon}\,\overline{\boldsymbol{w}}_{d2}\{b_0(t), d_0(t)\}\right] z^{\frac{1}{2}-i\epsilon}\right\}\ln z \\
& - \left\{\left[\boldsymbol{P}_2^{-1}\overset{*}{\boldsymbol{H}}^{-1}\left(\boldsymbol{\zeta}_{tt} - \boldsymbol{\gamma}\right) - \boldsymbol{w}_{t2}\{a_0(t), c_0(t)\}\right] z^{\frac{1}{2}+i\epsilon}\right. \\
& \left. - \left[\boldsymbol{Q}_2^{-1}\boldsymbol{H}^{-1}\left(\overline{\boldsymbol{\zeta}}_{tt} - \overline{\boldsymbol{\beta}}\right) + \overline{\boldsymbol{w}}_{t2}\{b_0(t), d_0(t)\}\right] z^{\frac{1}{2}-i\epsilon}\right\} \\
& + \frac{e^{-\epsilon\pi}\boldsymbol{P}_2^{-1}\boldsymbol{\zeta}}{\cosh\epsilon\pi} z^{\frac{1}{2}+i\epsilon}\,\overset{\circ}{A}_2\,(t) + \frac{e^{\epsilon\pi}\boldsymbol{Q}_2^{-1}\boldsymbol{\zeta}}{\cosh\epsilon\pi} z^{\frac{1}{2}-i\epsilon}\overline{\overset{\circ}{A}}_2(t) + O\,(\,|z|\,)
\end{aligned}\right\},\quad z \in S^-, \quad (6.3.68)$$

where the operators $\boldsymbol{w}_{dk}(\cdot,\cdot)$ and $\boldsymbol{w}_{tk}(\cdot,\cdot)$ are given in Appendix A. By integrating the above two expressions with respect to the complex argument z, we can finally obtain the complex potential $\boldsymbol{f}_k(z;t) = (\,F_{2k}(z;t), G_{2k}(z;t)\,)^\top$ for both materials.

Since equations (6.3.67) and (6.3.68) are directly related to the stress components around the interfacial crack-tip, some of the noteworthy features of the asymptotic

field can be studied through them. The most interesting feature is that there exist two terms in the above equations, which are totally different in nature from the terms found in the solution of a crack propagating transiently in a homogeneous material. The first of these terms is that associated with $z^{1/2}(\ln z)^2$. This term is clearly associated with the interfacial nature of crack growth since it is proportional to the quantity $\dot{\epsilon}$. This quantity is also related to the transient nature (existence of non-zero accelerations) of the problem. By observing that

$$\dot{\epsilon} = \frac{\mathrm{d}\epsilon}{\mathrm{d}v} \cdot \frac{\mathrm{d}v}{\mathrm{d}t} \ .$$

One can easily see that $\dot{\epsilon}$ and thus the $z^{1/2}(\ln z)^2$ term vanish either when the crack-tip speed is constant and/or when the material mismatch parameter ϵ vanishes.

The second term is that associated with $z^{1/2}\ln z$. The coefficient of this term is related to the complex parameter $A_0(t)$ and also depends on the crack-tip speed, as well as on their time derivatives. So it depends on both $\dot{v}(t)$ and $\dot{K}^d(t)$. It can be seen that for constant speed transient crack growth ($\dot{v} = 0$, $\dot{K}_d \neq 0$), this term will still be present. Indeed the $r^{1/2}\ln r$ term has been observed by Willis (1973), who studied a particular constant velocity, transient interfacial crack growth problem. Both of these two terms which include logarithms will vanish at the same time only if the situation is strictly *steady state.* Otherwise one or both will be present. These logarithmic singularities are the consequences of the existence of both the interface and the transient nature of the propagating crack. For the case of crack growth in a homogeneous material ($\epsilon = 0$), $\boldsymbol{\beta} = \boldsymbol{\gamma}$ and $\boldsymbol{\xi} = \boldsymbol{\varsigma}$, see Appendix A. This is true even if crack propagation is transient. As a result, it can be shown that $\boldsymbol{\omega}_d = \boldsymbol{\omega}_t = \mathbf{o}$, and consequently, $\boldsymbol{\zeta}_d$, $\boldsymbol{\zeta}_t$, and $\boldsymbol{\zeta}_{tt}$ will vanish. The logarithmic terms also disappear. In this case, the transient field reduces to the one obtained by Liu and Rosakis (1992) which does not feature any logarithms. It should be stated at this point that transient higher order terms involving logarithmic singularities have also been observed in the solution of dislocation lines propagating transiently in elastic solids (Callias *et al.*,

1990, and Markenscoff and Ni, 1990). These terms were shown to vanish when the dislocations propagated with constant speed.

In this section, we have provided a procedure which allows us to investigate higher order transient effects systematically. By imposing the boundary and bonding conditions on the complex potentials, the problem was recast into the Riemann-Hilbert problem. By solving the Riemann-Hilbert equations, and by evaluating the Stieltjes transforms, the higher order terms were obtained.

6.4 The asymptotic elastodynamic field around a non-uniformly propagating interfacial crack-tip

In the Cartesian coordinate system (ξ_1, ξ_2) which is translating with the interfacial crack-tip, let $\phi_m(\xi_1, \xi_2, t)$ and $\psi_m(\xi_1, \xi_2, t)$ be solutions of equations (6.2.6), $m = 0, 1, 2, \cdots$, such that

$$\left.\begin{array}{l} \dfrac{\phi_{m+n}(\xi_1, \xi_2, t)}{\phi_m(\xi_1, \xi_2, t)} \to 0 \\ \dfrac{\psi_{m+n}(\xi_1, \xi_2, t)}{\psi_m(\xi_1, \xi_2, t)} \to 0 \end{array}\right\} , \quad \text{as } r = \sqrt{\xi_1^2 + \xi_2^2} \to 0 , \quad m = 0, 1, 2, \cdots , \tag{6.4.1}$$

for any positive integer n, and define $\phi(\xi_1, \xi_2, t)$ and $\psi(\xi_1, \xi_2, t)$ by

$$\left.\begin{array}{rcl} \phi(\xi_1, \xi_2, t) & = & \displaystyle\sum_{m=0}^{\infty} \phi_m(\xi_1, \xi_2, t) \\ \psi(\xi_1, \xi_2, t) & = & \displaystyle\sum_{m=0}^{\infty} \psi_m(\xi_1, \xi_2, t) \end{array}\right\} . \tag{6.4.2}$$

Then, as discussed in Chapter 2, the asymptotic elastodynamic state surrounding the interfacial crack-tip can be constructed.

For its importance in the experimental investigation described in Section 6.7, we only provide the asymptotic expression of the first stress invariant around the

interfacial crack-tip. However, in order to shorten our expression, some notation needs to be defined first. In the expressions below, the superscript (1) or (2) denotes the components of the vectors defined in Appendix A and in previous sections. For the material above the interface, we may define the following quantities,

$$\begin{aligned}
\Omega_d(t) &= -\frac{1}{\mu D(v)\lambda_1\lambda_2}\Big\{\left[(1+\alpha_s^2)h_{11}+2\alpha_s h_{21}\right]\zeta_d^{(1)} \\
&\quad -\left[(1+\alpha_s^2)h_{12}+2\alpha_s h_{11}\right]\zeta_d^{(2)}\Big\}\ , \\
\overset{*}{\Omega}_d(t) &= -\frac{1}{\mu D(v)\lambda_1\lambda_2}\Big\{\left[(1+\alpha_s^2)h_{11}+2\alpha_s h_{21}\right]\overline{\zeta}_d^{(1)} \\
&\quad +\left[(1+\alpha_s^2)h_{12}+2\alpha_s h_{11}\right]\overline{\zeta}_d^{(2)}\Big\}\ , \\
\Omega_t(t) &= -\frac{1}{\mu D(v)\lambda_1\lambda_2}\Big\{\left[(1+\alpha_s^2)h_{11}+2\alpha_s h_{21}\right]\left(\zeta_t^{(1)}-\dot{\epsilon}\,\xi^{(1)}\right) \\
&\quad -\left[(1+\alpha_s^2)h_{12}+2\alpha_s h_{11}\right]\left(\zeta_t^{(2)}-\dot{\epsilon}\,\xi^{(2)}\right)\Big\}+\dot{\epsilon}\,w_d^{(1)}\{a_0(t),c_0(t)\}\ , \\
\overset{*}{\Omega}_t(t) &= -\frac{1}{\mu D(v)\lambda_1\lambda_2}\Big\{\left[(1+\alpha_s^2)h_{11}+2\alpha_s h_{21}\right]\left(\overline{\zeta}_t^{(1)}-\dot{\epsilon}\,\overline{\varsigma}^{(1)}\right) \\
&\quad +\left[(1+\alpha_s^2)h_{12}+2\alpha_s h_{11}\right]\left(\overline{\zeta}_t^{(2)}-\dot{\epsilon}\,\overline{\varsigma}^{(2)}\right)\Big\}-\dot{\epsilon}\,\overline{w}_d^{(1)}\{b_0(t),d_0(t)\}\ , \\
\Omega_{tt}(t) &= -\frac{1}{\mu D(v)\lambda_1\lambda_2}\Big\{\left[(1+\alpha_s^2)h_{11}+2\alpha_s h_{21}\right]\left(\zeta_{tt}^{(1)}-\beta^{(1)}\right) \\
&\quad -\left[(1+\alpha_s^2)h_{12}+2\alpha_s h_{11}\right]\left(\zeta_{tt}^{(2)}-\beta^{(2)}\right)\Big\}+w_t^{(1)}\{a_0(t),c_0(t)\}\ , \\
\overset{*}{\Omega}_{tt}(t) &= -\frac{1}{\mu D(v)\lambda_1\lambda_2}\Big\{\left[(1+\alpha_s^2)h_{11}+2\alpha_s h_{21}\right]\left(\overline{\zeta}_{tt}^{(1)}-\overline{\gamma}^{(1)}\right) \\
&\quad +\left[(1+\alpha_s^2)h_{12}+2\alpha_s h_{11}\right]\left(\overline{\zeta}_{tt}^{(2)}-\overline{\gamma}^{(2)}\right)\Big\}-\overline{w}_t^{(1)}\{b_0(t),d_0(t)\}\ .
\end{aligned}$$

Now, one can show that by using equations (6.3.32) and (6.3.67), the first stress invariant in the material above the interface will be given by

$$\frac{\sigma_{11}+\sigma_{22}}{2\mu\left(\alpha_l^2-\alpha_s^2\right)} = \mathrm{Re}\Big\{\overset{\circ}{A}_0(t)a_0(t)z_l^{-\frac{1}{2}+i\epsilon}+\overline{\overset{\circ}{A}_0}(t)b_0(t)z_l^{-\frac{1}{2}-i\epsilon}$$

$$
\begin{aligned}
&+ \quad \frac{2\alpha_s}{\mu D(v)(1+\omega_s)} \left(\overset{\circ}{A}_1\,(t) + \overline{\overset{\circ}{A}}_1(t) \right) \\
&+ \quad \overset{\circ}{A}_2\,(t) a_0(t) z_l^{\frac{1}{2}+i\epsilon} + \overline{\overset{\circ}{A}}_2(t) b_0(t) z_l^{\frac{1}{2}-i\epsilon} \\
&+ \quad \Big[A_{tt}(t) z_l^{\frac{1}{2}+i\epsilon} + B_{tt}(t) \overline{z}_l z_l^{-\frac{1}{2}+i\epsilon} + C_{tt}(t) \overline{z}_l^2 z_l^{-\frac{3}{2}+i\epsilon} \\
&- \quad \overset{*}{A}_{tt}\,(t) z_l^{\frac{1}{2}-i\epsilon} - \overset{*}{B}_{tt}\,(t) \overline{z}_l z_l^{-\frac{1}{2}-i\epsilon} - \overset{*}{C}_{tt}\,(t) \overline{z}_l^2 z_l^{-\frac{3}{2}-i\epsilon} \Big] \\
&+ \quad \Big[A_t(t) z_l^{\frac{1}{2}+i\epsilon} + B_t(t) \overline{z}_l z_l^{-\frac{1}{2}+i\epsilon} - \overset{*}{A}_t\,(t) z_l^{\frac{1}{2}-i\epsilon} - \overset{*}{B}_t\,(t) \overline{z}_l z_l^{-\frac{1}{2}-i\epsilon} \Big] \ln z_l \\
&+ \quad \dot{\epsilon} \left[\Omega_d(t) z_l^{\frac{1}{2}+i\epsilon} - \overset{*}{\Omega}_d\,(t) z_l^{\frac{1}{2}-i\epsilon} \right] (\ln z_l)^2 \Big\} + O\,(\,|z_l|\,)\,. \qquad (6.4.3)
\end{aligned}
$$

where

$$
\begin{aligned}
A_{tt}(t) &= \Omega_{tt}(t) - \frac{2(1+\alpha_l^2)}{1-\alpha_l^2} \left\{ \left(\frac{3}{2} + i\epsilon \right) D_l\{a_0(t)\} + \dot{\epsilon}\, K_l(t) a_0(t) \right\} - 2B_l(t) a_0(t)\,, \\
\overset{*}{A}_{tt}\,(t) &= \overset{*}{\Omega}_{tt}\,(t) + \frac{2(1+\alpha_l^2)}{1-\alpha_l^2} \left\{ \left(\frac{3}{2} - i\epsilon \right) \overline{D}_l\{b_0(t)\} + \dot{\epsilon}\, \overline{K}_l(t) b_0(t) \right\} + 2\overline{B}_l(t) b_0(t)\,, \\
B_{tt}(t) &= -\left(\frac{3}{2} + i\epsilon \right) \left(\frac{1}{2} + i\epsilon \right) D_l\{a_0(t)\} - 2\dot{\epsilon}(1+i\epsilon) K_l(t) a_0(t) \\
&\quad - \frac{2(1+\alpha_l^2)}{1-\alpha_l^2} \left(\frac{1}{2} + i\epsilon \right) B_l(t) a_0(t)\,, \\
\overset{*}{B}_{tt}\,(t) &= \left(\frac{3}{2} - i\epsilon \right) \left(\frac{1}{2} - i\epsilon \right) \overline{D}_l\{b_0(t)\} + 2\dot{\epsilon}(1-i\epsilon) \overline{K}_l(t) b_0(t) \\
&\quad + \frac{2(1+\alpha_l^2)}{1-\alpha_l^2} \left(\frac{1}{2} - i\epsilon \right) \overline{B}_l(t) b_0(t)\,, \\
C_{tt}(t) &= \left(\frac{1}{4} + \epsilon^2 \right) B_l(t) a_0(t)\,, \qquad \overset{*}{C}_{tt}\,(t) = -\left(\frac{1}{4} + \epsilon^2 \right) \overline{B}_l(t) b_0(t)\,, \\
A_t(t) &= \Omega_t(t) - \frac{2(1+\alpha_l^2)\dot{\epsilon}}{1-\alpha_l^2} \left(\frac{3}{2} + i\epsilon \right) K_l(t) a_0(t)\,, \\
\overset{*}{A}_t\,(t) &= \overset{*}{\Omega}_t\,(t) + \frac{2(1+\alpha_l^2)\dot{\epsilon}}{1-\alpha_l^2} \left(\frac{3}{2} - i\epsilon \right) \overline{K}_l(t) b_0(t)\,,
\end{aligned}
$$

$$B_t(t) = -\dot{\epsilon}\left(\frac{3}{2}+i\epsilon\right)\left(\frac{1}{2}+i\epsilon\right)K_l(t)a_0(t)\ ,$$

$$\overset{*}{B}_t\ (t) = \dot{\epsilon}\left(\frac{3}{2}-i\epsilon\right)\left(\frac{1}{2}-i\epsilon\right)\overline{K}_l(t)b_0(t)\ ,$$

$$K_l(t) = -i\frac{v}{4\sqrt{2\pi}\alpha_l^2 c_l^2}\cdot\frac{K^d(t)}{\left(\frac{3}{2}+i\epsilon\right)\left(\frac{1}{2}+i\epsilon\right)}\ .$$

In expression (6.4.3), functions of time $\overset{\circ}{A}_0\ (t)$, $\overset{\circ}{A}_1\ (t)$, and $\overset{\circ}{A}_2\ (t)$ are undetermined by the asymptotic analysis. On the other hand, functions $A_{tt}(t)$, $B_{tt}(t)$, $C_{tt}(t)$, $\overset{*}{A}_{tt}\ (t)$, $\cdots$, are known in terms of $\overset{\circ}{A}_0\ (t)$, the crack-tip acceleration $\dot{v}(t)$, and the time derivative of $\overset{\circ}{A}_0\ (t)$. As a result, these functions are also undetermined by the asymptotic analysis. However, their dependence on time derivatives of $v(t)$ and $\overset{\circ}{A}_0\ (t)$ constitutes the mathematical demonstration of transient effects.

It is often convenient to express the first stress invariant in terms of real quantities. For any complex function of time $W(t)$, let its magnitude be denoted by $|W|$, and its phase be denoted by $\Phi(W)$. Meanwhile, a scaled polar coordinate system (r_l, θ_l) centered at the moving crack-tip is defined by

$$r_l = \left\{\xi_1^2 + \alpha_l^2\xi_2^2\right\}^{1/2}\ , \qquad \theta_l = \tan^{-1}\frac{\alpha_l\xi_2}{\xi_1}\ .$$

The first stress invariant in the material above the interface can therefore be expressed as

$$\begin{aligned}\frac{\sigma_{11}+\sigma_{22}}{2\mu\,(\alpha_l^2-\alpha_s^2)} &= |\ \overset{\circ}{A}_0\ (t)|\left\{\Sigma_0(\theta_l)\cos(\epsilon\ln r_l)+\overset{*}{\Sigma}_0\ (\theta_l)\sin(\epsilon\ln r_l)\right\}r_l^{-1/2}\\ &+ \frac{4\alpha_s}{\mu D(v)(1+\omega_s)}|\ \overset{\circ}{A}_1\ (t)|\cos\Phi(\overset{\circ}{A}_1)\\ &+ \dot{\epsilon}\left\{\Sigma_d(\theta_l)\cos(\epsilon\ln r_l)+\overset{*}{\Sigma}_d\ (\theta_l)\sin(\epsilon\ln r_l)\right\}r_l^{1/2}(\ln r_l)^2\\ &+ \left\{\Sigma_t(\theta_l)\cos(\epsilon\ln r_l)+\overset{*}{\Sigma}_t\ (\theta_l)\sin(\epsilon\ln r_l)\right\}r_l^{1/2}\ln r_l\end{aligned}$$

$$+ \quad \left\{\Sigma_{tt}(\theta_l)\cos(\epsilon \ln r_l) + \overset{*}{\Sigma}_{tt}(\theta_l)\sin(\epsilon \ln r_l)\right\} r_l^{1/2}$$

$$+ \quad |\overset{\circ}{A}_2(t)| \left\{\Sigma_2(\theta_l)\cos(\epsilon \ln r_l) + \overset{*}{\Sigma}_2(\theta_l)\sin(\epsilon \ln r_l)\right\} r_l^{1/2}$$

$$+ \quad O(r_l)\,, \tag{6.4.4}$$

where

$$\Sigma_0(\theta_l) = a_0(t)e^{-\epsilon\theta_l}\cos\left(\frac{\theta_l}{2} - \Phi(\overset{\circ}{A}_0)\right) + b_0(t)e^{\epsilon\theta_l}\cos\left(\frac{\theta_l}{2} + \Phi(\overset{\circ}{A}_0)\right),$$

$$\overset{*}{\Sigma}_0(\theta_l) = a_0(t)e^{-\epsilon\theta_l}\sin\left(\frac{\theta_l}{2} - \Phi(\overset{\circ}{A}_0)\right) - b_0(t)e^{\epsilon\theta_l}\sin\left(\frac{\theta_l}{2} + \Phi(\overset{\circ}{A}_0)\right),$$

$$\Sigma_2(\theta_l) = a_0(t)e^{-\epsilon\theta_l}\cos\left(\frac{\theta_l}{2} + \Phi(\overset{\circ}{A}_2)\right) + b_0(t)e^{\epsilon\theta_l}\cos\left(\frac{\theta_l}{2} - \Phi(\overset{\circ}{A}_2)\right),$$

$$\overset{*}{\Sigma}_2(\theta_l) = -\left\{a_0(t)e^{-\epsilon\theta_l}\sin\left(\frac{\theta_l}{2} + \Phi(\overset{\circ}{A}_2)\right) - b_0(t)e^{\epsilon\theta_l}\sin\left(\frac{\theta_l}{2} - \Phi(\overset{\circ}{A}_0)\right)\right\},$$

$$\Sigma_d(\theta_l) = |\Omega_d(t)|e^{-\epsilon\theta_l}\cos\left(\frac{\theta_l}{2} + \Phi(\Omega_d)\right) - |\overset{*}{\Omega}_d(t)|e^{\epsilon\theta_l}\cos\left(\frac{\theta_l}{2} + \Phi(\overset{*}{\Omega}_d)\right),$$

$$\overset{*}{\Sigma}_d(\theta_l) = -\left\{|\Omega_d(t)|e^{-\epsilon\theta_l}\sin\left(\frac{\theta_l}{2} + \Phi(\Omega_d)\right) + |\overset{*}{\Omega}_d(t)|e^{\epsilon\theta_l}\sin\left(\frac{\theta_l}{2} + \Phi(\overset{*}{\Omega}_d)\right)\right\},$$

$$\begin{aligned}\Sigma_t(\theta_l) &= |A_t(t)|e^{-\epsilon\theta_l}\cos\left(\frac{\theta_l}{2} + \Phi(A_t)\right) - |\overset{*}{A}_t(t)|e^{\epsilon\theta_l}\cos\left(\frac{\theta_l}{2} + \Phi(\overset{*}{A}_t)\right)\\ &+ |B_t(t)|e^{-\epsilon\theta_l}\cos\left(\frac{3\theta_l}{2} - \Phi(B_t)\right) - |\overset{*}{B}_t(t)|e^{\epsilon\theta_l}\cos\left(\frac{3\theta_l}{2} - \Phi(\overset{*}{B}_t)\right)\\ &- 2\dot{\epsilon}\left\{|\Omega_d(t)|e^{-\epsilon\theta_l}\sin\left(\frac{\theta_l}{2} + \Phi(\Omega_d)\right) - |\overset{*}{\Omega}_d(t)|e^{\epsilon\theta_l}\sin\left(\frac{\theta_l}{2} + \Phi(\overset{*}{\Omega}_d)\right)\right\}\theta_l,\end{aligned}$$

$$\begin{aligned}\overset{*}{\Sigma}_t(\theta_l) &= -\left\{|A_t(t)|e^{-\epsilon\theta_l}\sin\left(\frac{\theta_l}{2} + \Phi(A_t)\right) + |\overset{*}{A}_t(t)|e^{\epsilon\theta_l}\sin\left(\frac{\theta_l}{2} + \Phi(\overset{*}{A}_t)\right)\right\}\\ &+ |B_t(t)|e^{-\epsilon\theta_l}\sin\left(\frac{3\theta_l}{2} - \Phi(B_t)\right) + |\overset{*}{B}_t(t)|e^{\epsilon\theta_l}\sin\left(\frac{3\theta_l}{2} - \Phi(\overset{*}{B}_t)\right)\\ &- 2\dot{\epsilon}\left\{|\Omega_d(t)|e^{-\epsilon\theta_l}\cos\left(\frac{\theta_l}{2} + \Phi(\Omega_d)\right) + |\overset{*}{\Omega}_d(t)|e^{\epsilon\theta_l}\cos\left(\frac{\theta_l}{2} + \Phi(\overset{*}{\Omega}_d)\right)\right\}\theta_l,\end{aligned}$$

$$
\begin{aligned}
\Sigma_{tt}(\theta_l) &= |A_{tt}(t)|e^{-\epsilon\theta_l}\cos\left(\frac{\theta_l}{2}+\Phi(A_{tt})\right) - |\overset{*}{A}_{tt}(t)|e^{\epsilon\theta_l}\cos\left(\frac{\theta_l}{2}+\Phi(\overset{*}{A}_{tt})\right) \\
&+ |B_{tt}(t)|e^{-\epsilon\theta_l}\cos\left(\frac{3\theta_l}{2}-\Phi(B_{tt})\right) - |\overset{*}{B}_{tt}(t)|e^{\epsilon\theta_l}\cos\left(\frac{3\theta_l}{2}-\Phi(\overset{*}{B}_{tt})\right) \\
&+ |C_{tt}(t)|e^{-\epsilon\theta_l}\cos\left(\frac{7\theta_l}{2}-\Phi(C_{tt})\right) - |\overset{*}{C}_{tt}(t)|e^{\epsilon\theta_l}\cos\left(\frac{7\theta_l}{2}-\Phi(\overset{*}{C}_{tt})\right) \\
&- \left\{|A_t(t)|e^{-\epsilon\theta_l}\sin\left(\frac{\theta_l}{2}+\Phi(A_t)\right) - |\overset{*}{A}_t(t)|e^{\epsilon\theta_l}\sin\left(\frac{\theta_l}{2}+\Phi(\overset{*}{A}_t)\right)\right\}\theta_l \\
&+ \left\{|B_t(t)|e^{-\epsilon\theta_l}\sin\left(\frac{3\theta_l}{2}-\Phi(B_t)\right) - |\overset{*}{B}_t(t)|e^{\epsilon\theta_l}\sin\left(\frac{3\theta_l}{2}-\Phi(\overset{*}{B}_t)\right)\right\}\theta_l \\
&- \dot{\epsilon}\left\{|\Omega_d(t)|e^{-\epsilon\theta_l}\cos\left(\frac{\theta_l}{2}+\Phi(\Omega_d)\right) - |\overset{*}{\Omega}_d(t)|e^{\epsilon\theta_l}\cos\left(\frac{\theta_l}{2}+\Phi(\overset{*}{\Omega}_d)\right)\right\}\theta_l^2, \\
\overset{*}{\Sigma}_{tt}(\theta_l) &= -\left\{|A_{tt}(t)|e^{-\epsilon\theta_l}\sin\left(\frac{\theta_l}{2}+\Phi(A_{tt})\right) + |\overset{*}{A}_{tt}(t)|e^{\epsilon\theta_l}\sin\left(\frac{\theta_l}{2}+\Phi(\overset{*}{A}_{tt})\right)\right\} \\
&+ |B_{tt}(t)|e^{-\epsilon\theta_l}\sin\left(\frac{3\theta_l}{2}-\Phi(B_{tt})\right) + |\overset{*}{B}_{tt}(t)|e^{\epsilon\theta_l}\sin\left(\frac{3\theta_l}{2}-\Phi(\overset{*}{B}_{tt})\right) \\
&+ |C_{tt}(t)|e^{-\epsilon\theta_l}\sin\left(\frac{7\theta_l}{2}-\Phi(C_{tt})\right) + |\overset{*}{C}_{tt}(t)|e^{\epsilon\theta_l}\sin\left(\frac{7\theta_l}{2}-\Phi(\overset{*}{C}_{tt})\right) \\
&- \left\{|A_t(t)|e^{-\epsilon\theta_l}\cos\left(\frac{\theta_l}{2}+\Phi(A_t)\right) + |\overset{*}{A}_t(t)|e^{\epsilon\theta_l}\cos\left(\frac{\theta_l}{2}+\Phi(\overset{*}{A}_t)\right)\right\}\theta_l \\
&- \left\{|B_t(t)|e^{-\epsilon\theta_l}\cos\left(\frac{3\theta_l}{2}-\Phi(B_t)\right) + |\overset{*}{B}_t(t)|e^{\epsilon\theta_l}\cos\left(\frac{3\theta_l}{2}-\Phi(\overset{*}{B}_t)\right)\right\}\theta_l \\
&+ \dot{\epsilon}\left\{|\Omega_d(t)|e^{-\epsilon\theta_l}\sin\left(\frac{\theta_l}{2}+\Phi(\Omega_d)\right) + |\overset{*}{\Omega}_d(t)|e^{\epsilon\theta_l}\sin\left(\frac{\theta_l}{2}+\Phi(\overset{*}{\Omega}_d)\right)\right\}\theta_l^2.
\end{aligned}
$$

The first term in equation (6.4.4) has a square root singularity and oscillatory nature. It is associated with the complex dynamic stress intensity factor $K^d(t)$ (defined by Yang *et al.*, 1991) which is related to the complex coefficient $\overset{\circ}{A}_0(t)$ by

$$K^d(t) = -2\sqrt{2\pi}\,\overset{\circ}{A}_0(t)\,.$$

The second term is the so-called T-stress term, and is independent of position. The

first two terms have the same spatial form as those obtained under steady state conditions by Deng (1992). However, the remaining four terms, proportional to the square root of the radial distance from the crack-tip, are more complicated and have some unusual features. The part associated with $|\overset{\circ}{A}_2(t)|$ has the same form as that predicted by the steady state solution and is of order $r^{1/2}$. The term of order $r^{1/2}(\ln r)^2$ has a coefficient proportional to $\dot{\epsilon} = \epsilon'(v)\dot{v}(t)$. This term vanishes either when $\dot{v} = 0$ and/or $\epsilon = 0$. The remaining two terms contain the functions $\Sigma_t(\theta_l)$, $\overset{*}{\Sigma}_t(\theta_l)$, $\Sigma_{tt}(\theta_l)$, and $\overset{*}{\Sigma}_{tt}(\theta_l)$ which depend on the time derivatives of the complex dynamic stress intensity factor and the crack-tip speed, i.e., they depend on transient effects. These parts also vanish for steady state crack growth. The term of order $r^{1/2}\ln r$ was first observed by Willis (1973) who analyzed the stresses in the case of constant speed, transient interfacial crack growth. In this case, $\dot{v} = 0$, $\dot{K}^d \neq 0$, and the only surviving terms will be of order $r^{1/2}\ln r$ and $r^{1/2}$. If the two elastic materials that constitute the bimaterial system become identical, the terms associated with $r^{1/2}(\ln r)^2$ and $r^{1/2}\ln r$ will disappear. However, in this case, the functions $\Sigma_{tt}(\theta_l)$ and $\overset{*}{\Sigma}_{tt}(\theta_l)$ do not vanish and reduce to the ordinary transient term given by Liu and Rosakis (1992) in studying the transient growth of a crack in homogeneous materials. It is significant to note at this point that transient effects may noticeably change the r and θ structure of the field from that predicted by the steady state approximation (e.g., existence of logarithmic $r^{1/2}\ln r$ and $r^{1/2}(\ln r)^2$ terms).

6.5 Properties of the mismatch parameters in dynamic interfacial fracture

In the analysis of an interfacial crack dynamically propagating along the interface, there are two mismatch parameters which depend not only on the properties of the materials that constitute the bimaterial system, but also on the crack-tip velocity. The properties of these parameters are very important since we have seen that the

asymptotic representation of the crack-tip field is drastically changed due to their presence. One of these parameters is defined by

$$\epsilon = \frac{1}{2\pi} \ln \frac{1-\beta}{1+\beta} , \qquad \beta = \frac{h_{11}}{\sqrt{h_{12} h_{21}}} , \tag{6.5.1}$$

while the other one by

$$\eta = \sqrt{\frac{h_{21}}{h_{12}}} . \tag{6.5.2}$$

In the above two definitions,

$$\left.\begin{aligned} h_{11} &= \left\{ \frac{2\alpha_l \alpha_s - (1+\alpha_s^2)}{\mu D(v)} \right\}_1 - \left\{ \frac{2\alpha_l \alpha_s - (1+\alpha_s^2)}{\mu D(v)} \right\}_2 \\ h_{12} &= \left\{ \frac{\alpha_s (1-\alpha_s^2)}{\mu D(v)} \right\}_1 + \left\{ \frac{\alpha_s (1-\alpha_s^2)}{\mu D(v)} \right\}_2 \\ h_{21} &= \left\{ \frac{\alpha_l (1-\alpha_s^2)}{\mu D(v)} \right\}_1 + \left\{ \frac{\alpha_l (1-\alpha_s^2)}{\mu D(v)} \right\}_2 \end{aligned}\right\} , \tag{6.5.3}$$

where

$$\alpha_l = \left(1 - \frac{v^2}{c_l^2}\right)^{1/2} , \quad \alpha_s = \left(1 - \frac{v^2}{c_s^2}\right)^{1/2} , \quad D(v) = 4\alpha_l \alpha_s - \left(1+\alpha_s^2\right)^2 .$$

To illustrate the properties of the mismatch parameters, we choose a bimaterial system composed of PMMA and AISI 4340 steel. We denote PMMA as material–1, and AISI 4340 steel as material–2. The mechanical properties for these two materials are listed in the table below.

Table: Properties of selected materials[1]

Parameter	$\mu(GPa)$	ν	$c_l(m/s)^*$	$c_l(m/s)^{**}$	$c_s(m/s)$	$c_R(m/s)$	$\rho(kg/m^3)$
PMMA	1.20	0.35	2081.7	1761.5	1004.0	937.8	1190.0
AISI 4340	80.0	0.30	5978.8	5401.9	3195.8	2959.8	7833.0

*plane-strain **plane-stress

For both plane strain and plane stress, FIGURE 6.2 presents the variation of the parameter η with respect to the crack-tip speed. We can see that η varies smoothly

[1]The parameters for PMMA are from CYRO Industries, Woodcliff Lake, NJ 06675; The parameters for AISI 4340 steel are from *Aerospace Structural Metals Handbook*, Battelle Columbus Laboratories, Columbus, Ohio

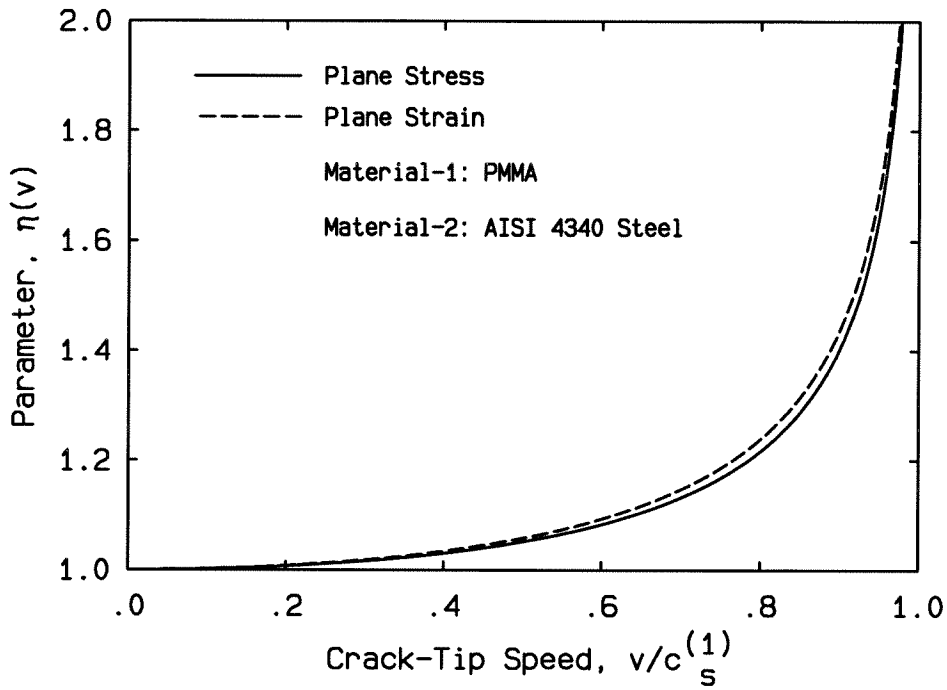

Figure 6.2: Velocity dependence of mismatch parameter η for plane stress and plane strain.

from 1.0 for the stationary interfacial crack, to ∞ as the crack-tip speed approaches the shear wave speed of PMMA ($c_s^{(1)}$). However, the situation is different for the parameter β. In FIGURE 6.3, we can observe that if the crack-tip speed is less than the Rayleigh wave speed of PMMA ($c_R^{(1)}$), β varies smoothly and tends to -1 when the crack-tip speed is very close to $c_R^{(1)}$. Since $D_1(v)$ will change sign as the crack-tip speed crosses $c_R^{(1)}$, β jumps from -1 to 1, and then tends to ∞ as the crack-tip speed tends to $c_s^{(1)}$. FIGURE 6.4 shows the variation of β when the crack-tip speed is bigger than $c_R^{(1)}$. FIGURE 6.5 presents the behavior of the parameter ϵ when the crack-tip speed is below the Rayleigh wave speed of PMMA. It shows that ϵ tends to ∞ as the crack-tip speed is very close to $c_R^{(1)}$. However, as the crack-tip speed crosses the speed $c_R^{(1)}$, since β is larger than 1, ϵ will become complex, and thus ϵ can be written as

$$\epsilon = \overset{*}{\epsilon} + \frac{1}{2}i\,, \qquad \overset{*}{\epsilon} = \frac{1}{2\pi}\ln\frac{\beta-1}{\beta+1}\,. \tag{6.5.4}$$

FIGURE 6.6 gives the variation of the real part of ϵ (i.e., $\overset{*}{\epsilon}$) with respect to the crack-tip

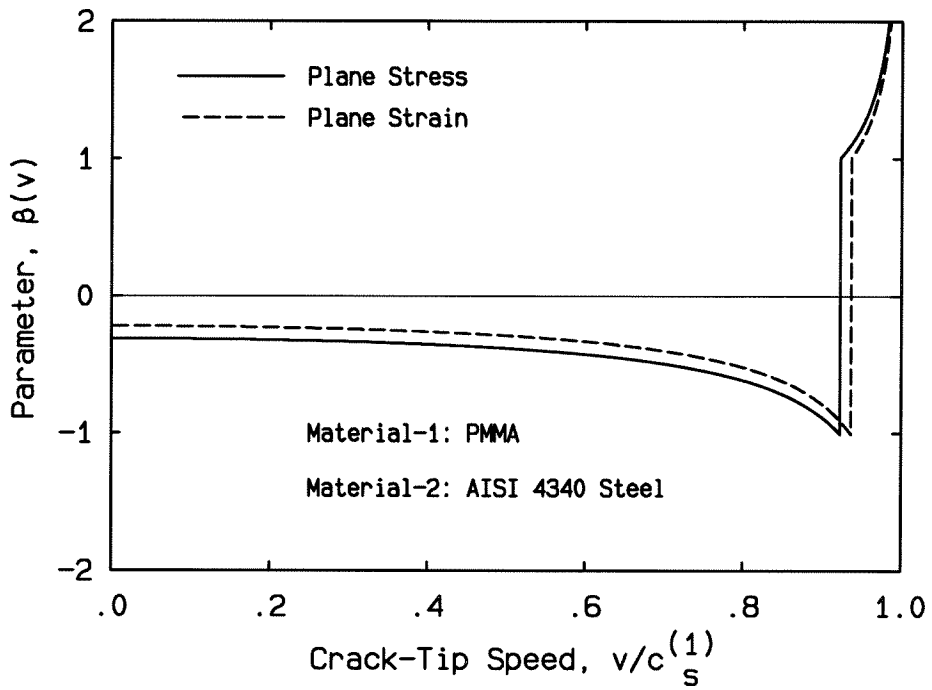

Figure 6.3: Velocity dependence of mismatch parameter β for plane stress and plane strain.

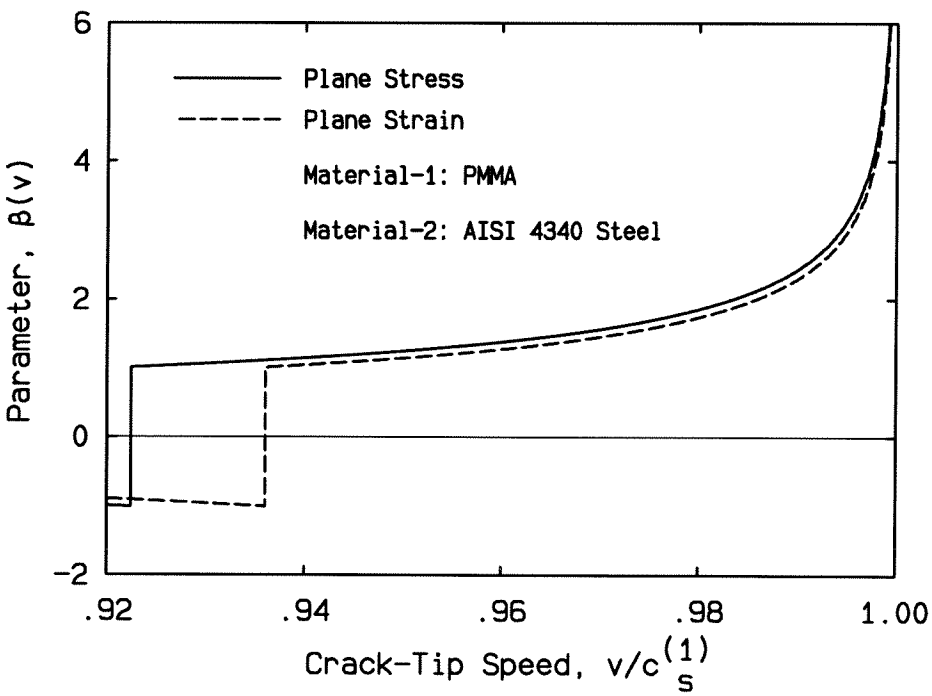

Figure 6.4: Velocity dependence of mismatch parameter β for plane stress and plane strain at the vicinity of the shear wave speed of PMMA.

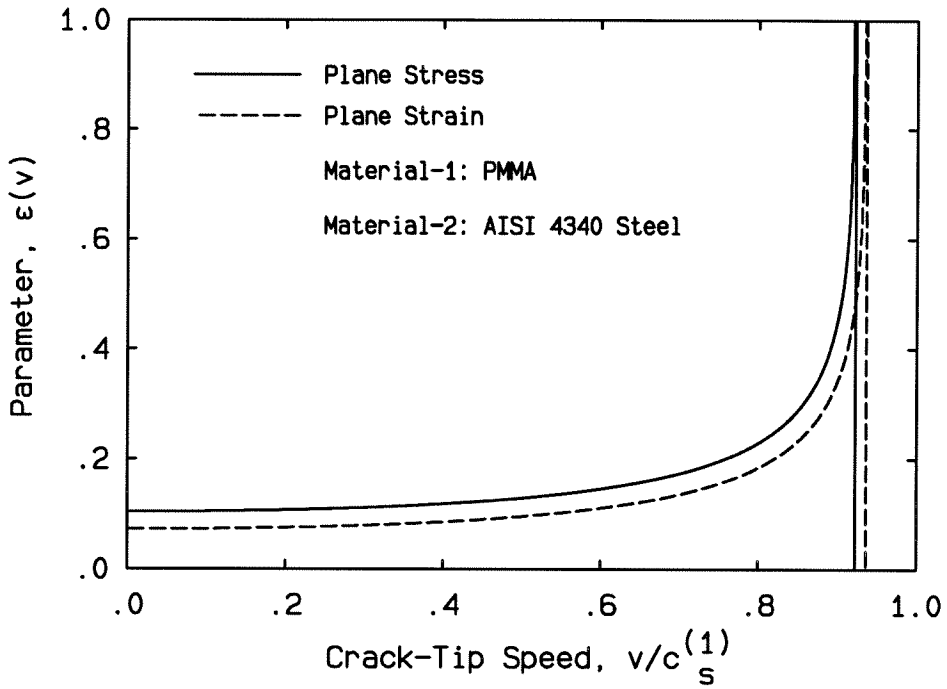

Figure 6.5: Velocity dependence of mismatch parameter ϵ for plane stress and plane strain.

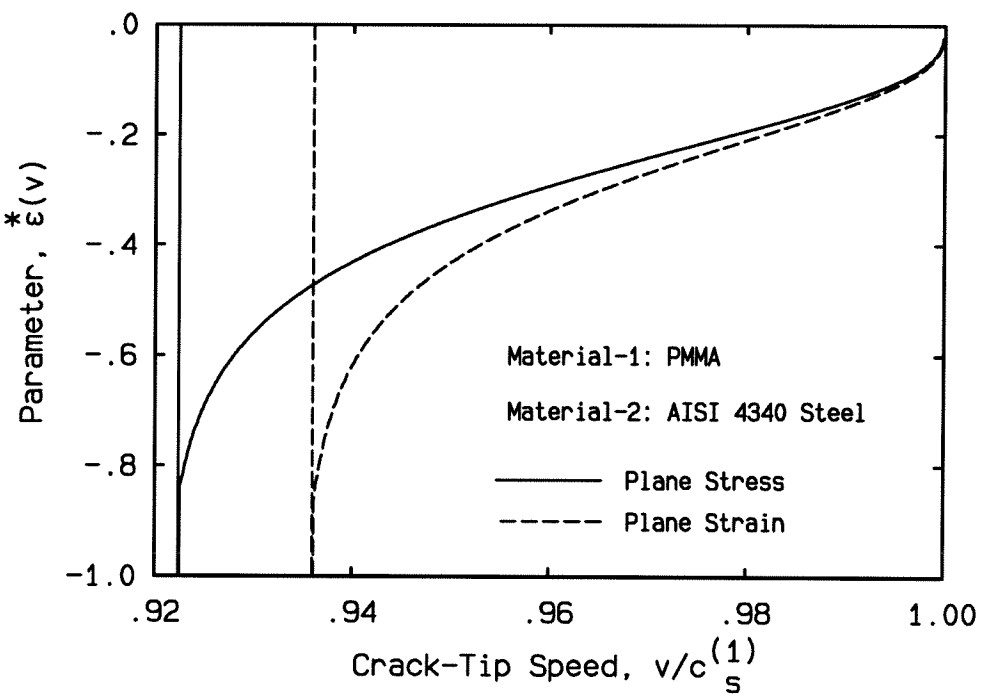

Figure 6.6: Velocity dependence of the real part of mismatch parameter ϵ for plane stress and plane strain at the vicinity of the shear wave speed of PMMA.

speed when the interfacial crack is running at speeds between $c_R^{(1)}$ and $c_s^{(1)}$. We can see that the real part of ϵ changes from $-\infty$ to 0 when the crack-tip speed is in the range of $c_R^{(1)} < v < c_s^{(1)}$.

6.6 The asymptotic field of an interfacial crack propagating at a speed between the lower Rayleigh and shear wave speeds

In recent experimental investigations, described in Section 6.7, bimaterial specimens composed of PMMA and AISI 4340 steel have been tested dynamically. This bimaterial combination exhibits a remarkable stiffness mismatch. It was observed that under impact loading conditions, interfacial cracks may propagate at speeds exceeding $c_R^{(1)}$, see Section 6.7. This experimental observation motivates our attempt to investigate dynamic crack growth in interfaces at speeds exceeding the lower Rayleigh wave speed. In homogeneous materials, an infinite amount of energy has to be transmitted to the crack-tip to maintain extension at the Rayleigh wave speed if the dynamic stress intensity factor is non-zero (Freund, 1990). This makes it impossible for a crack in a homogeneous solid to exceed the Rayleigh wave speed of that material. However, for a crack growing along a bimaterial interface, it has been shown that as the crack-tip speed approaches the lower Rayleigh wave speed, say $c_R^{(1)}$, only a finite amount of energy has to be transmitted to the crack-tip if the dynamic stress intensity factor is non-zero (see Yang *et al.*, 1991). Accordingly, there is no energetic restriction for an interfacial crack to exceed the lower Rayleigh wave speed. Indeed, the experimentally obtained velocity histories reported in Section 6.7, see FIGURE 6.14, are seen to largely exceed the Rayleigh wave speed of PMMA.

In the analysis of previous sections, the governing equations hold for crack-tip speeds in the range $0 < v < c_s^{(1)}$, if material–1 is more compliant than material–2.

Also, the development of the asymptotic stress field around the tip of a non-uniformly propagating interfacial crack is dependent on the complete solution of the Riemann-Hilbert problem. However, from the procedure provided in Appendix II, we can see that there are no restrictions imposed on crack-tip speed from this procedure. The only consequence of the restriction that the crack-tip speed is in the range of $0 < v < c_R^{(1)}$, is that all parameters appearing in the solution are real. Nevertheless, the mathematical approach is not limited by this restriction, even if some of the parameters become complex. Therefore, we can directly extend our solution to the case where the crack-tip speed exceeds the lower Rayleigh wave speed.

Suppose the properties of the materials constituting the interface are such that $c_s^{(1)} < c_R^{(2)}$, and $c_R^{(1)} < v < c_s^{(1)}$. As we have shown in the previous section, the parameter η remains real, but ϵ becomes complex and is given by equation (6.5.4). If only the leading term is considered, under the requirement of bounded displacement, or integrable mechanical energy density (Freund, 1990), the two complex displacement potentials in equation (6.3.32) for the material above the interface, become

$$\left.\begin{aligned} F_0(z_l;t) \;=\; & -\frac{[(1+\alpha_s^2)-2\eta\alpha_s]\,e^{\overset{*}{\epsilon}\pi}}{(2+i\overset{*}{\epsilon})(1+i\overset{*}{\epsilon})\mu D(v)\sinh\overset{*}{\epsilon}\pi} z_l^{2+i\overset{*}{\epsilon}} A_0(t) \\ & + \frac{[(1+\alpha_s^2)+2\eta\alpha_s]\,e^{-\overset{*}{\epsilon}\pi}}{(2-i\overset{*}{\epsilon})(1-i\overset{*}{\epsilon})\mu D(v)\sinh\overset{*}{\epsilon}\pi} z_l^{2-i\overset{*}{\epsilon}} \overline{A}_0(t) \end{aligned}\right\}, \tag{6.6.1}$$

and

$$\left.\begin{aligned} G_0(z_s;t) \;=\; & \frac{[2\alpha_l-\eta(1+\alpha_s^2)]\,e^{\overset{*}{\epsilon}\pi}}{(2+i\overset{*}{\epsilon})(1+i\overset{*}{\epsilon})\mu D(v)\sinh\overset{*}{\epsilon}\pi} z_s^{2+i\overset{*}{\epsilon}} A_0(t) \\ & - \frac{[2\alpha_l+\eta(1+\alpha_s^2)]\,e^{-\overset{*}{\epsilon}\pi}}{(2-i\overset{*}{\epsilon})(1-i\overset{*}{\epsilon})\mu D(v)\sinh\overset{*}{\epsilon}\pi} z_s^{2-i\overset{*}{\epsilon}} \overline{A}_0(t) \end{aligned}\right\}, \tag{6.6.2}$$

for an arbitrary complex function $A_0(t)$. To obtain this result, the definition of ϵ in the speed range $c_R^{(1)} < v < c_s^{(1)}$, equation (6.5.4), has been used. For the material below the interface, we need to change $\overset{*}{\epsilon}\,\pi$ to $-\overset{*}{\epsilon}\,\pi$ in the above expressions. By setting

$$A_0(t) = A(t)e^{i\Phi(t)}\,,$$

the first invariant of stress for the material above the interface becomes

$$\left.\begin{aligned}\sigma_{11}+\sigma_{22} &= \frac{4\left(\alpha_l^2-\alpha_s^2\right)A(t)}{D(v)\sinh \overset{*}{\epsilon}\,\pi}\left\{2\eta\alpha_s\cosh\left[\overset{*}{\epsilon}\,(\pi-\theta_l)\right]\right. \\ &- \left.(1+\alpha_s^2)\sinh\left[\overset{*}{\epsilon}\,(\pi-\theta_l)\right]\right\}\cos\left(\overset{*}{\epsilon}\ln r_l+\Phi(t)\right)\end{aligned}\right\}. \tag{6.6.3}$$

It can be observed that oscillations still exist along the radial direction. However, there is no singularity at the propagating crack-tip.

At a position, r, ahead of the interfacial crack-tip, the traction on the interface can be expressed as

$$\eta\sigma_{22}(r;t)+i\sigma_{12}(r;t)=-2\eta r^{i\overset{*}{\epsilon}}A_0(t)\ . \tag{6.6.4}$$

At a position, r, behind the interfacial crack-tip, the crack face displacement difference is found to be

$$\delta_1(r;t)-i\frac{\delta_2(r;t)}{\eta}=\frac{2\eta h_{12}}{\sinh \overset{*}{\epsilon}\,\pi}\cdot\frac{r^{1+i\overset{*}{\epsilon}}}{1+i\overset{*}{\epsilon}}A_0(t)\ . \tag{6.6.5}$$

If the interfacial crack extended an amount δ, then the energy released by this extension, $\Delta W(\delta)$ can be calculated by

$$\Delta W(\delta)=\frac{1}{2}\int_0^\delta\left\{\sigma_{22}(\xi_1;t)\delta_2(\delta-\xi_1;t)+\sigma_{12}(\xi_1;t)\delta_1(\delta-\xi_1;t)\right\}\mathrm{d}\xi_1\ . \tag{6.6.6}$$

By using (6.6.4) and (6.6.5), we can express the above equation as

$$\Delta W(\delta)=\frac{2\eta^2h_{12}|A_0(t)|^2}{\sinh \overset{*}{\epsilon}\,\pi}\mathrm{Im}\left\{\int_0^\delta\frac{(\delta-\xi_1)^{1+i\overset{*}{\epsilon}}\xi_1^{-i\overset{*}{\epsilon}}}{1+i\overset{*}{\epsilon}}\mathrm{d}\xi_1\right\}\ . \tag{6.6.7}$$

Further, it can be shown that

$$\int_0^\delta\frac{(\delta-\xi_1)^{1+i\overset{*}{\epsilon}}\xi_1^{-i\overset{*}{\epsilon}}}{1+i\overset{*}{\epsilon}}\mathrm{d}\xi_1=\int_0^\delta\frac{(\delta-\xi_1)^{1-i\overset{*}{\epsilon}}\xi_1^{i\overset{*}{\epsilon}}}{1-i\overset{*}{\epsilon}}\mathrm{d}\xi_1\ .$$

Therefore, the energy release rate at the tip of an interfacial crack moving at speeds in the range $c_R^{(1)}<v<c_s^{(1)}$, $\mathcal{G}$, will be

$$\mathcal{G}=\lim_{\delta\to0}\frac{\Delta W(\delta)}{\delta}=0\ . \tag{6.6.8}$$

This result may be anticipated since in this range of speeds, both stress and strain are bounded. Equation (6.6.8) states that if the speed of the interfacial crack is in the range $c_R^{(1)}<v<c_s^{(1)}$, no energy is needed to create new surfaces.

6.7 Experimental evidence for the importance of transient effects in the dynamic fracture of bimaterials

To investigate the validity of the analysis presented in this work, a sequence of dynamic impact experiments of bimaterial specimens has been performed by Rosakis and Lambros (1993), Rosakis *et al.* (1993), and Lambros and Rosakis (1994). Stress waves generated by impact, load an interfacial pre-crack, which subsequently propagates dynamically along the bimaterial interface. High speed interferograms of the near-tip region of the propagating crack are recorded. The optical method used is the newly developed method of Coherent Gradient Sensing (CGS) (Tippur *et al.*, 1991; Rosakis, 1993) described below.

6.7.1 Experimental technique (transmission CGS)

Consider a planar wavefront normally incident on an optically and mechanically isotropic, transparent plate of initial uniform thickness h and refractive index n. As shown in FIGURE 6.7, the specimen occupies the (x_1, x_2) plane in the undeformed configuration. When the specimen undergoes any kind of deformation (static or dynamic), the transmitted wavefront can be expressed as $S(x_1, x_2, x_3) = x_3 + \triangle S(x_1, x_2) = \text{constant}$, where $\triangle S$ is the optical path change acquired during refraction. As discussed in detail by Rosakis (1993), $\triangle S$ is related to the deformation state by the relation,

$$\triangle S(x_1, x_2) = 2h(n-1)\int_0^{1/2} \epsilon_{33}\mathrm{d}(x_3/h) + 2h\int_0^{1/2} \triangle n\mathrm{d}(x_3/h)\ . \qquad (6.7.1)$$

The first term of equation (6.7.1) represents the net optical path difference due to the plate thickness change caused by the strain component ϵ_{33}. The second term is

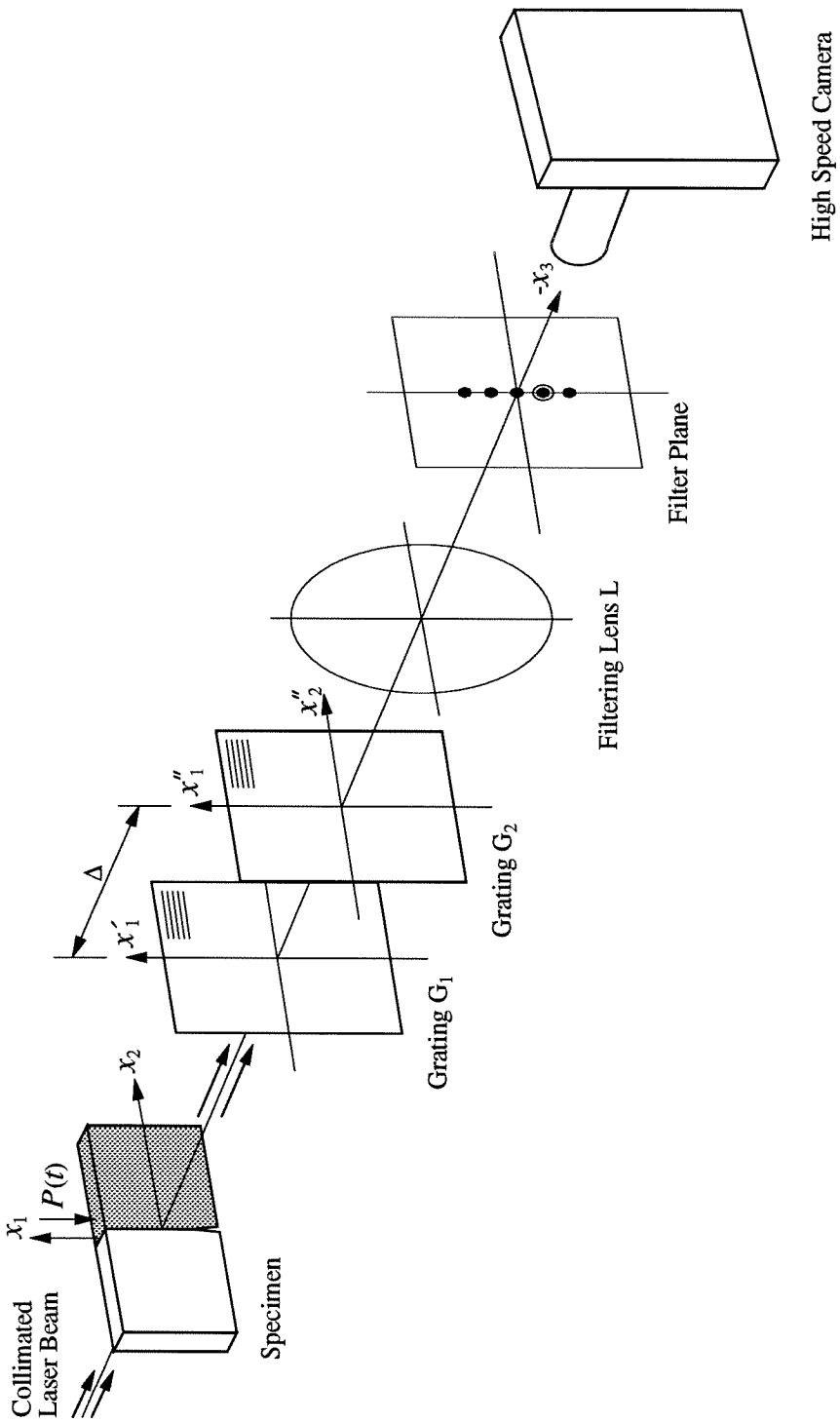

Figure 6.7: Schematic of the optical set-up for CGS in transmission.

due to the stress induced change of refractive index of the material. This change in refractive index $\triangle n$ is given by the Maxwell relation,

$$\triangle n = D_1 \left(\sigma_{11} + \sigma_{22} + \sigma_{33}\right) \ , \tag{6.7.2}$$

where D_1 is the stress optic coefficient and σ_{ij} are Cartesian components of the nominal stress tensor. The above relation is strictly true for isotropic, linearly elastic solids. For such solids, the strain component ϵ_{33} can also be related to the stresses, and equation (6.7.1) then becomes:

$$\triangle S(x_1, x_2) = 2hc_\sigma \int_0^{1/2} \left\{ (\sigma_{11} + \sigma_{22}) \left[1 - D_2 \left(\frac{\sigma_{33}}{\nu(\sigma_{11} + \sigma_{22})} \right) \right] \right\} \mathrm{d}(x_3/h) \ , \tag{6.7.3}$$

where

$$c_\sigma = D_1 - \frac{\nu(n-1)}{E} \ , \qquad D_2 = -\frac{\nu D_1 + \dfrac{\nu(n-1)}{E}}{\dfrac{\nu(n-1)}{E} D_1} \ ,$$

and E, ν, and c_σ are the Young's modulus, Poisson's ratio and stress optical coefficient of the material, respectively.

A schematic of the experimental apparatus is also shown in FIGURE 6.7. When the transmitted wavefront emerges from the specimen after being distorted, it passes through two high density gratings, G_1 and G_2 of pitch p, separated by a distance Δ. The gratings have their rulings parallel to either the x_1 or x_2 directions. The action of the gratings is to displace (shear) the diffracted beam and recombine it with itself, thus creating an interferogram after G_2. The filtering lens L processes the light emerging from G_2 and its frequency content (diffraction spots) is displayed on the back focal plane of L. By physically blocking all diffraction orders except for either the ± 1 orders, information regarding the gradient components of $\triangle S(x_1, x_2)$ along either the x_1 or x_2-axis is obtained on the image plane. The camera is kept focused on the specimen plane. For grating rulings perpendicular to the x_α-axis, the resulting fringe pattern is proportional to $\partial(\triangle S)/\partial x_\alpha$, $\alpha \in \{1, 2\}$.

A first order analysis described by Tippur *et al.* (1991), or a higher order Fourier optics analysis by Lee *et al.* (1993), have shown that the resulting fringes can be related to gradients of $\triangle S(x_1, x_2)$ as follows:

$$\frac{\partial(\triangle S)}{\partial x_\alpha} = \frac{k_\alpha p}{\Delta} , \qquad \alpha \in \{1, 2\} , \tag{6.7.4}$$

where

$$k_\alpha = \begin{cases} m & \text{for} \quad \alpha = 1, \ m = 0, \pm 1, \pm 2, \cdots \\ n & \text{for} \quad \alpha = 2, \ n = 0, \pm 1, \pm 2, \cdots \end{cases}$$

and m and n are the fringe orders for the x_1, x_2 gradient contours respectively.

Invariably a near-tip three-dimensional region will exist in any real specimen geometry. However, outside this three-dimensional zone, a plane stress approximation will be valid. A numerical study of each particular specimen configuration is needed to identify the extent and exact location of such a plane stress region. Such a calculation has been performed by Lee and Rosakis (1992) for a three point bend bimaterial specimen. A rather large two-dimensional plane stress region was seen over a significant portion of the specimen. In this region, $\sigma_{33}/\nu(\sigma_{11} + \sigma_{22})$ (a measure of three-dimensionality) tends to zero. For points outside the three-dimensional region $(\sigma_{33}/\nu(\sigma_{11} + \sigma_{22}) \to 0)$, the optical path difference in equation (6.7.3) will simplify to

$$\triangle S(x_1, x_2) \simeq c_\sigma h \left\{ \hat{\sigma}_{11}(x_1, x_2) + \hat{\sigma}_{22}(x_1, x_2) \right\} , \tag{6.7.5}$$

where $\hat{\sigma}_{11}$ and $\hat{\sigma}_{22}$ are *thickness averages* of the stress components in the plate.

As a result, for points outside the near-tip three-dimensional region, the CGS patterns assume a simple interpretation in terms of two-dimensional stress field approximations. In particular, equations (6.7.4) and (6.7.5) now indicate that fringes obtained from regions surrounding the three-dimensional zone can be related to the in-plane gradients of $\hat{\sigma}_{11} + \hat{\sigma}_{22}$ as follows:

$$\left.\begin{aligned} c_\sigma h \frac{\partial(\hat{\sigma}_{11} + \hat{\sigma}_{22})}{\partial x_1} &= \frac{mp}{\Delta} \\ c_\sigma h \frac{\partial(\hat{\sigma}_{11} + \hat{\sigma}_{22})}{\partial x_2} &= \frac{np}{\Delta} \end{aligned}\right\} , \quad m, n = 0, \pm 1, \pm 2, \cdots \tag{6.7.6}$$

where in the case of transmission c_σ is the stress optical coefficient of the material (e.g., PMMA).

6.7.2 Experimental set-up and procedure

Bimaterial specimens used in the dynamic experiments are of the three point or one point bend configuration and are made from 9mm thickness sheets of commercially available poly-methylmethacrylate (PMMA) (material–1) and AISI 4340 steel (material–2). The bonding procedure is outlined in Tippur and Rosakis (1990). A bond strength calibration experiment was also performed in that study, demonstrating that the bond toughness was at least as much as that of a homogeneous PMMA specimen. This fact testifies to the strength of the bond and becomes important in the discussion of the dynamic experiments presented bellow.

The bimaterial specimens have either a pre-cut edge notch, or a sharp pre-crack of length 25mm along the interface. The specimens are either impact loaded in a drop weight tower (Dynatup-8100A) or a high speed gas gun. After the impact event, the crack propagates dynamically along the interface. The transmission CGS technique in conjunction with high speed photography is used to record dynamic fields around the crack-tip (only on the PMMA side, of course). A rotating mirror high speed camera (Cordin model 330A) is used. A Spectra-Physics Argon-ion pulse laser (model 166) is used as the light source. By using short pulses of 30nsec duration, we are able to freeze even the fastest of running cracks and thus produce a sharp interference pattern during crack growth. The interframe time (controlled by the interval between pulses) is typically set at 1μsec for a total recording time of 80μsec. The laser pulsing is triggered by a strain gauge on the specimen that senses the impact.

True symmetric one or three point bend loading cannot be achieved since it is extremely difficult to apply the impact load exactly on the interface, which is very

thin. In addition since the wave speeds of PMMA and steel are vastly different, the loading history at the crack-tip would be completely different if the specimen were impacted on the PMMA or the steel side. Thus it was chosen to impact the specimen a small distance (7mm) into the steel side of the bond.

A sequence of high speed interferograms from a PMMA/steel test is shown in FIGURE 6.8. This is a three point bend test conducted in a drop weight tower. The impact speed was 4m/sec. When the crack initiates (t = 0μsec), intense stress waves emanate from the crack-tip. These waves are visible in FIGURE 6.8 as discrete kinks in otherwise smooth fringes and as circular lines centered at points along the crack line (see frames at $t = 16.5\mu$sec and $t = 23\mu$sec). This observation is a reliable sign of a highly dynamic event, as will be discussed later.

6.7.3 Analysis of experimental data

In subsequent sections we shall present an analysis of CGS interferograms of dynamic bimaterial specimens first using a K^d-dominant assumption and then using the higher order transient field described in Section 6.4.

Singular field (K^d-dominance)

The governing relations for CGS (6.7.6) can be used to estimate fracture parameters from points outside the three-dimensional zone of a given interferogram. One could expect that the plane stress region surrounding the near-tip three-dimensional region would be well described by the most singular term in the asymptotic expansion for stress, i.e., that a K^d-dominant region would exist somewhere around the crack-tip. This is something to be verified though and should not be taken for granted, especially in regions relatively far from the crack-tip or in experiments showing transient effects

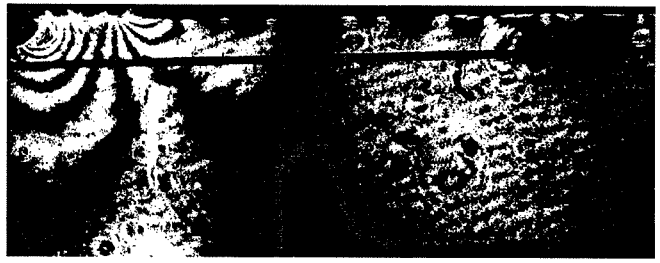

$t = 9.5$ μsec, $v = 640$ m/sec

$t = 16.5$ μsec, $v = 790$ m/sec

$t = 23$ μsec, $v = 800$ m/sec

$t = 32$ μsec, $v = 880$ m/sec

Figure 6.8: Selected sequence of CGS interferograms of a growing crack in a three point bend interfacial drop weight tower experiment. (Only PMMA side of PMMA/steel specimen is shown)

(e.g., rapidly changing crack-tip speed). In such cases the deformation field around the crack-tip may be better described by a higher order analysis.

As was stated earlier (see Section 6.4), for cracks propagating dynamically under *steady state* conditions in bimaterial specimens, Yang *et al.* (1991) and the first part of the present analysis observed that near the crack-tip the stress field assumes the form,

$$\sigma_{\alpha\beta} = \mathrm{Re}\left\{\frac{K^d r^{i\epsilon}}{\sqrt{2\pi r}}\right\}\tilde{\sigma}^{(I)}_{\alpha\beta}(\theta, v) + \mathrm{Im}\left\{\frac{K^d r^{i\epsilon}}{\sqrt{2\pi r}}\right\}\tilde{\sigma}^{(II)}_{\alpha\beta}(\theta, v)\ , \tag{6.7.7}$$

where (r, θ) are polar coordinates of a coordinate system translating with the crack-tip at speed v, and K^d is the complex dynamic stress intensity factor. The material mismatch parameter $\epsilon = \epsilon(v)$ is now a function of crack-tip speed and of the elastic moduli of the materials of the bimaterial system. Analytical expressions for $\tilde{\sigma}^{(I)}_{\alpha\beta}$ and $\tilde{\sigma}^{(II)}_{\alpha\beta}$ are given by Yang *et al.* (1991).

By using equation (6.7.7) and after some algebraic manipulations, $\hat{\sigma}_{11} + \hat{\sigma}_{22}$ can be written as

$$\left.\begin{aligned}\hat{\sigma}_{11} + \hat{\sigma}_{22} \;=\; & \frac{A(t)}{\sqrt{2\pi r_l}}\left\{\left(1 + \alpha_s^2 - 2\eta\alpha_s\right) e^{\epsilon(\pi-\theta_l)} \cos\left(\frac{\theta_l}{2} - \Phi(t) - \epsilon \ln r_l\right)\right. \\ & + \left.\left(1 + \alpha_s^2 + 2\eta\alpha_s\right) e^{-\epsilon(\pi-\theta_l)} \cos\left(\frac{\theta_l}{2} + \Phi(t) + \epsilon \ln r_l\right)\right\}\end{aligned}\right\}\ , \tag{6.7.8}$$

where

$$A(t) = \frac{(\alpha_l^2 - \alpha_s^2)\,|K^d(t)|}{D(v)\cosh(\epsilon\pi)}\ , \quad K^d(t) = K_1^d(t) + iK_2^d(t)\ , \quad \Phi(t) = \tan^{-1}\frac{K_2^d(t)}{K_1^d(t)}\ ,$$

and $\alpha_{l,s}$, $r_{l,s}$, and $\theta_{l,s}$ have been defined in previous sections. The mismatch parameters η and ϵ are functions of crack-tip speed and of material properties. These functions are given in Section 6.5 and appear in FIGURES 6.3 and 6.5, respectively. Note that equation (6.7.8) is the first part of equation (6.4.4) in Section 6.4. The field quantity of interest in analyzing the CGS patterns for material–1 is $c_\sigma h \partial(\hat{\sigma}_{11} + \hat{\sigma}_{22})/\partial x_1$. By

differentiating equation (6.7.8) with respect to x_1, we have

$$\left.\begin{aligned} c_\sigma h \frac{\partial(\hat{\sigma}_{11}+\hat{\sigma}_{22})}{\partial x_1} &= \frac{c_\sigma h r_l^{-3/2} e^{-\epsilon(\pi-\theta_l)} A(t)}{2\sqrt{2\pi}} \\ &\times \left\{ -\left(1+\alpha_s^2-2\eta\alpha_s\right) e^{2\epsilon(\pi-\theta_l)} \cos\left(\frac{3\theta_l}{2}-\Phi(t)-\epsilon\ln r_l\right)\right. \\ &-\left(1+\alpha_s^2+2\eta\alpha_s\right)\cos\left(\frac{3\theta_l}{2}+\Phi(t)+\epsilon\ln r_l\right) \\ &+2\epsilon\left(1+\alpha_s^2-2\eta\alpha_s\right) e^{2\epsilon(\pi-\theta_l)} \sin\left(\frac{3\theta_l}{2}-\Phi(t)-\epsilon\ln r_l\right) \\ &\left.-2\epsilon\left(1+\alpha_s^2+2\eta\alpha_s\right)\sin\left(\frac{3\theta_l}{2}+\Phi(t)+\epsilon\ln r_l\right)\right\} \end{aligned}\right\}, \qquad (6.7.9)$$

where $A(t)$ is as defined in equation (6.7.8) and $0 \le \theta_l \le \pi$.

From the above discussion it becomes obvious that extraction of parameters like K^d is now possible *provided* that experimental data are gathered from a region near the moving crack-tip characterized by the structure presented in equations (6.7.8) and (6.7.9). In a laboratory specimen of finite size where transient effects may be important, the field may not be K^d-dominant and the use of a higher order analysis may be necessary. The necessity of a higher order analysis in the interpretation of optical data from crack growth in homogeneous specimens was demonstrated by Freund and Rosakis (1992) and Krishnaswamy and Rosakis (1991). An equivalent analysis for a transiently propagating interfacial crack has been provided in previous sections and its effect on data interpretation is discussed in the next section.

Higher order transient analysis

In Section 6.4, a higher order expansion for the trace of the stress tensor in plane stress is shown in equation (6.4.4). By differentiating with respect to the x_1 coordinate, we obtain a relation for the x_1-gradient of $\hat{\sigma}_{11}+\hat{\sigma}_{22}$, which is relevant to the analysis of

CGS interferograms,

$$\left.\begin{aligned}
\frac{(\sigma_{11}+\sigma_{22})_{,1}}{2\mu\,(\alpha_l^2-\alpha_s^2)} &= |\mathcal{A}_0(t)|\left\{\Pi_0(\theta_l)\cos(\epsilon\ln r_l)+\overset{*}{\Pi}_0(\theta_l)\sin(\epsilon\ln r_l)\right\} r_l^{-3/2} \\
&+ \dot{\epsilon}\left\{\Pi_d(\theta_l)\cos(\epsilon\ln r_l)+\overset{*}{\Pi}_d(\theta_l)\sin(\epsilon\ln r_l)\right\} r_l^{-1/2}(\ln r_l)^2 \\
&+ \left\{\Pi_t(\theta_l)\cos(\epsilon\ln r_l)+\overset{*}{\Pi}_t(\theta_l)\sin(\epsilon\ln r_l)\right\} r_l^{-1/2}\ln r_l \\
&+ \left\{\Pi_{tt}(\theta_l)\cos(\epsilon\ln r_l)+\overset{*}{\Pi}_{tt}(\theta_l)\sin(\epsilon\ln r_l)\right\} r_l^{-1/2} \\
&+ |\mathcal{A}_2(t)|\left\{\Pi_2(\theta_l)\cos(\epsilon\ln r_l)+\overset{*}{\Pi}_2(\theta_l)\sin(\epsilon\ln r_l)\right\} r_l^{-1/2} \\
&+ O(r_l)
\end{aligned}\right\}, \tag{6.7.10}$$

where

$$\begin{aligned}
\Pi_0(\theta_l) &= a_0(t)e^{-\epsilon\theta_l}\cos\left(\frac{3\theta_l}{2}-\Phi(\mathcal{A}_0)\right)+b_0(t)e^{\epsilon\theta_l}\cos\left(\frac{3\theta_l}{2}+\Phi(\mathcal{A}_0)\right), \\
\overset{*}{\Pi}_0(\theta_l) &= a_0(t)e^{-\epsilon\theta_l}\sin\left(\frac{3\theta_l}{2}-\Phi(\mathcal{A}_0)\right)-b_0(t)e^{\epsilon\theta_l}\sin\left(\frac{3\theta_l}{2}+\Phi(\mathcal{A}_0)\right), \\
\Pi_2(\theta_l) &= a_0(t)e^{-\epsilon\theta_l}\cos\left(\frac{\theta_l}{2}-\Phi(\mathcal{A}_2)\right)+b_0(t)e^{\epsilon\theta_l}\cos\left(\frac{\theta_l}{2}+\Phi(\mathcal{A}_2)\right), \\
\overset{*}{\Pi}_2(\theta_l) &= a_0(t)e^{-\epsilon\theta_l}\sin\left(\frac{\theta_l}{2}-\Phi(\mathcal{A}_2)\right)-b_0(t)e^{\epsilon\theta_l}\sin\left(\frac{\theta_l}{2}+\Phi(\mathcal{A}_2)\right), \\
\Pi_d(\theta_l) &= |\mathcal{Q}_d(t)|e^{-\epsilon\theta_l}\cos\left(\frac{\theta_l}{2}-\Phi(\mathcal{Q}_d)\right)-|\overset{*}{\mathcal{Q}}_d(t)|e^{\epsilon\theta_l}\cos\left(\frac{\theta_l}{2}+\Phi(\overset{*}{\mathcal{Q}}_d)\right), \\
\overset{*}{\Pi}_d(\theta_l) &= |\mathcal{Q}_d(t)|e^{-\epsilon\theta_l}\sin\left(\frac{\theta_l}{2}-\Phi(\mathcal{Q}_d)\right)+|\overset{*}{\mathcal{Q}}_d(t)|e^{\epsilon\theta_l}\sin\left(\frac{\theta_l}{2}+\Phi(\overset{*}{\mathcal{Q}}_d)\right), \\
\Pi_t(\theta_l) &= |\mathcal{A}_t(t)|e^{-\epsilon\theta_l}\cos\left(\frac{\theta_l}{2}-\Phi(\mathcal{A}_t)\right)-|\overset{*}{\mathcal{A}}_t(t)|e^{\epsilon\theta_l}\cos\left(\frac{\theta_l}{2}-\Phi(\overset{*}{\mathcal{A}}_t)\right) \\
&+ |\mathcal{B}_t(t)|e^{-\epsilon\theta_l}\cos\left(\frac{5\theta_l}{2}-\Phi(\mathcal{B}_t)\right)-|\overset{*}{\mathcal{B}}_t(t)|e^{\epsilon\theta_l}\cos\left(\frac{5\theta_l}{2}-\Phi(\overset{*}{\mathcal{B}}_t)\right) \\
&+ 2\dot{\epsilon}\left\{|\mathcal{Q}_d(t)|e^{-\epsilon\theta_l}\sin\left(\frac{\theta_l}{2}-\Phi(\mathcal{Q}_d)\right)-|\overset{*}{\mathcal{Q}}_d(t)|e^{\epsilon\theta_l}\sin\left(\frac{\theta_l}{2}-\Phi(\overset{*}{\mathcal{Q}}_d)\right)\right\}\theta_l,
\end{aligned}$$

$$
\begin{aligned}
\overset{*}{\Pi}_t(\theta_l) &= |\mathcal{A}_t(t)|e^{-\epsilon\theta_l}\sin\left(\frac{\theta_l}{2}-\Phi(\mathcal{A}_t)\right)+|\overset{*}{\mathcal{A}}_t(t)|e^{\epsilon\theta_l}\sin\left(\frac{\theta_l}{2}-\Phi(\overset{*}{\mathcal{A}}_t)\right)\\
&+ |\mathcal{B}_t(t)|e^{-\epsilon\theta_l}\sin\left(\frac{5\theta_l}{2}-\Phi(\mathcal{B}_t)\right)+|\overset{*}{\mathcal{B}}_t(t)|e^{\epsilon\theta_l}\sin\left(\frac{5\theta_l}{2}-\Phi(\overset{*}{\mathcal{B}}_t)\right)\\
&- 2\dot{\epsilon}\left\{|\mathcal{Q}_d(t)|e^{-\epsilon\theta_l}\cos\left(\frac{\theta_l}{2}-\Phi(\mathcal{Q}_d)\right)+|\overset{*}{\mathcal{Q}}_d(t)|e^{\epsilon\theta_l}\cos\left(\frac{\theta_l}{2}-\Phi(\overset{*}{\mathcal{Q}}_d)\right)\right\}\theta_l,\\
\Pi_{tt}(\theta_l) &= |\mathcal{A}_{tt}(t)|e^{-\epsilon\theta_l}\cos\left(\frac{\theta_l}{2}-\Phi(\mathcal{A}_{tt})\right)-|\overset{*}{\mathcal{A}}_{tt}(t)|e^{\epsilon\theta_l}\cos\left(\frac{\theta_l}{2}-\Phi(\overset{*}{\mathcal{A}}_{tt})\right)\\
&+ |\mathcal{B}_{tt}(t)|e^{-\epsilon\theta_l}\cos\left(\frac{5\theta_l}{2}-\Phi(\mathcal{B}_{tt})\right)-|\overset{*}{\mathcal{B}}_{tt}(t)|e^{\epsilon\theta_l}\cos\left(\frac{5\theta_l}{2}-\Phi(\overset{*}{\mathcal{B}}_{tt})\right)\\
&+ |\mathcal{C}_{tt}(t)|e^{-\epsilon\theta_l}\cos\left(\frac{9\theta_l}{2}-\Phi(\mathcal{C}_{tt})\right)-|\overset{*}{\mathcal{C}}_{tt}(t)|e^{\epsilon\theta_l}\cos\left(\frac{9\theta_l}{2}-\Phi(\overset{*}{\mathcal{C}}_{tt})\right)\\
&+ \left\{|\mathcal{A}_t(t)|e^{-\epsilon\theta_l}\sin\left(\frac{\theta_l}{2}-\Phi(\mathcal{A}_t)\right)-|\overset{*}{\mathcal{A}}_t(t)|e^{\epsilon\theta_l}\sin\left(\frac{\theta_l}{2}-\Phi(\overset{*}{\mathcal{A}}_t)\right)\right\}\theta_l\\
&+ \left\{|\mathcal{B}_t(t)|e^{-\epsilon\theta_l}\sin\left(\frac{5\theta_l}{2}-\Phi(\mathcal{B}_t)\right)-|\overset{*}{\mathcal{B}}_t(t)|e^{\epsilon\theta_l}\sin\left(\frac{5\theta_l}{2}-\Phi(\overset{*}{\mathcal{B}}_t)\right)\right\}\theta_l\\
&- \dot{\epsilon}\left\{|\mathcal{Q}_d(t)|e^{-\epsilon\theta_l}\cos\left(\frac{\theta_l}{2}-\Phi(\mathcal{Q}_d)\right)-|\overset{*}{\mathcal{Q}}_d(t)|e^{\epsilon\theta_l}\cos\left(\frac{\theta_l}{2}-\Phi(\overset{*}{\mathcal{Q}}_d)\right)\right\}\theta_l^2,\\
\overset{*}{\Pi}_{tt}(\theta_l) &= |\mathcal{A}_{tt}(t)|e^{-\epsilon\theta_l}\sin\left(\frac{\theta_l}{2}-\Phi(\mathcal{A}_{tt})\right)+|\overset{*}{\mathcal{A}}_{tt}(t)|e^{\epsilon\theta_l}\sin\left(\frac{\theta_l}{2}-\Phi(\overset{*}{\mathcal{A}}_{tt})\right)\\
&+ |\mathcal{B}_{tt}(t)|e^{-\epsilon\theta_l}\sin\left(\frac{5\theta_l}{2}-\Phi(\mathcal{B}_{tt})\right)+|\overset{*}{\mathcal{B}}_{tt}(t)|e^{\epsilon\theta_l}\sin\left(\frac{5\theta_l}{2}-\Phi(\overset{*}{\mathcal{B}}_{tt})\right)\\
&+ |\mathcal{C}_{tt}(t)|e^{-\epsilon\theta_l}\sin\left(\frac{9\theta_l}{2}-\Phi(\mathcal{C}_{tt})\right)+|\overset{*}{\mathcal{C}}_{tt}(t)|e^{\epsilon\theta_l}\sin\left(\frac{9\theta_l}{2}-\Phi(\overset{*}{\mathcal{C}}_{tt})\right)\\
&- \left\{|\mathcal{A}_t(t)|e^{-\epsilon\theta_l}\cos\left(\frac{\theta_l}{2}-\Phi(\mathcal{A}_t)\right)+|\overset{*}{\mathcal{A}}_t(t)|e^{\epsilon\theta_l}\cos\left(\frac{\theta_l}{2}+\Phi(\overset{*}{\mathcal{A}}_t)\right)\right\}\theta_l\\
&- \left\{|\mathcal{B}_t(t)|e^{-\epsilon\theta_l}\cos\left(\frac{5\theta_l}{2}-\Phi(\mathcal{B}_t)\right)+|\overset{*}{\mathcal{B}}_t(t)|e^{\epsilon\theta_l}\cos\left(\frac{5\theta_l}{2}-\Phi(\overset{*}{\mathcal{B}}_t)\right)\right\}\theta_l\\
&- \dot{\epsilon}\left\{|\mathcal{Q}_d(t)|e^{-\epsilon\theta_l}\sin\left(\frac{\theta_l}{2}-\Phi(\mathcal{Q}_d)\right)+|\overset{*}{\mathcal{Q}}_d(t)|e^{\epsilon\theta_l}\sin\left(\frac{\theta_l}{2}-\Phi(\overset{*}{\mathcal{Q}}_d)\right)\right\}\theta_l^2,
\end{aligned}
$$

The functions of time $\mathcal{A}_0(t)$, $\mathcal{A}_2(t)$, $\mathcal{A}_{tt}(t)$, $\cdots$, that appear in the above expressions, are related to functions $A_0(t)$, $A_2(t)$, $A_{tt}(t)$, $\cdots$, in equation (6.4.3) by

$$\mathcal{A}_0(t) = \left(-\frac{1}{2}+i\epsilon\right)\overset{\circ}{A}_0(t)\,, \qquad \mathcal{A}_2(t) = \left(\frac{1}{2}+i\epsilon\right)\overset{\circ}{A}_2(t)\,,$$

$$\mathcal{A}_{tt}(t) = \left(\frac{1}{2}+i\epsilon\right)A_{tt}(t) + A_t(t) + B_{tt}(t)\,,$$

$$\overset{*}{\mathcal{A}}_{tt}(t) = \left(\frac{1}{2}-i\epsilon\right)\overset{*}{A}_{tt}(t) + \overset{*}{A}_t(t) + \overset{*}{B}_{tt}(t)\,,$$

$$\mathcal{B}_{tt}(t) = \left(-\frac{1}{2}+i\epsilon\right)B_{tt}(t) + B_t(t) + 2C_{tt}(t)\,,$$

$$\overset{*}{\mathcal{B}}_{tt}(t) = \left(-\frac{1}{2}-i\epsilon\right)\overset{*}{B}_{tt}(t) + \overset{*}{B}_t(t) + 2\,\overset{*}{C}_{tt}(t)\,,$$

$$\mathcal{C}_{tt}(t) = \left(-\frac{3}{2}+i\epsilon\right)C_{tt}(t)\,, \qquad \overset{*}{\mathcal{C}}_{tt}(t) = \left(-\frac{3}{2}-i\epsilon\right)\overset{*}{C}_{tt}(t)\,,$$

$$\mathcal{A}_t(t) = \left(\frac{1}{2}+i\epsilon\right)A_{tt}(t) + 2\dot{\epsilon}\Omega_d(t) + B_t(t)\,,$$

$$\overset{*}{\mathcal{A}}_t(t) = \left(\frac{1}{2}-i\epsilon\right)\overset{*}{A}_{tt}(t) + 2\dot{\epsilon}\,\overset{*}{\Omega}_d(t) + \overset{*}{B}_t(t)\,,$$

$$\mathcal{B}_t(t) = \left(-\frac{1}{2}+i\epsilon\right)B_t(t)\,, \qquad \overset{*}{\mathcal{B}}_t(t) = \left(-\frac{1}{2}-i\epsilon\right)\overset{*}{B}_t(t)\,,$$

$$\mathcal{Q}_d(t) = \left(\frac{1}{2}+i\epsilon\right)\Omega_d(t)\,, \qquad \overset{*}{\mathcal{Q}}_d(t) = \left(\frac{1}{2}-i\epsilon\right)\overset{*}{\Omega}_d(t)\,.$$

This gradient contains 4 orders in r_l. They are $r_l^{-3/2}$, $r_l^{-1/2}(\ln r_l)^2$, $r_l^{-1/2}\ln r_l$, and $r_l^{-1/2}$. It also contains 28 undetermined constants. The first two constants $|\mathcal{A}_0|$ and $\Phi(\mathcal{A}_0)$ are related to $|K^d|$ and Φ (or K_1^d, K_2^d) of the expression of Yang *et al.* (1991) (see equation (6.7.9)). In fact the most singular term of equation (6.7.10) reduces to equation (6.7.9). Under steady state conditions, equation (6.7.10) reduces to an expression with 4 terms which are identical to the first 4 terms of the higher order steady state expression derived by Deng (1992). The transient contributions to the expression for the gradient (6.7.9) are those that exhibit an $r_l^{-1/2}(\ln r_l)^2$ and $r_l^{-1/2}\ln r_l$ radial dependence. It is worth noting that most of these transient terms are multiplied by the quantity $\dot{\epsilon}$, the rate of change of the oscillatory index with time

($\dot{\epsilon} = \epsilon'(v)\dot{v}$). Thus, to a certain extent, $\dot{\epsilon}$ is a measure of transience of the propagating crack. If $\dot{\epsilon} = 0$, most, but not all transient terms disappear. Those that remain are those related to the rate of change of the complex stress intensity factor. Note that it is possible for $\dot{\epsilon}$ to be small even if a large acceleration exists, but $\epsilon'(v)$ is small. Conversely it is possible to have a large $\dot{\epsilon}$ corresponding to small $\dot{v}$ but large $\epsilon'(v)$. It should be noted that $\epsilon'(v)$ tends to infinity as v tends to $c_R^{(1)}$, see Figure 5. Whether or not $\dot{\epsilon}$ can be used as a reliable measure of transience will be investigated in the subsequent section.

It is clear at this point that analysis of the fringe patterns obtained from a dynamic experiment can be made using either equation (6.7.9) or equation (6.7.10). The choice of one or the other depends on whether a region of K^d-dominance has been established somewhere outside the near-tip three-dimensional zone. Use of either equation allows estimation of the time variation of the relevant parameters. This is done by performing a least squares fitting procedure to data points digitized from the CGS interferograms obtained during an experiment. Of course the crack-tip speed $v(t)$ is measured independently. There are 2 undetermined parameters in equation (6.7.9) and 28 undetermined constants in equation (6.7.10).

6.7.4 Results and discussion

The velocity and acceleration histories corresponding to the sequence of photographs in FIGURE 6.8 are shown in FIGURES 6.9(a) and 6.9(b). This is a test performed in a drop weight tower under the relatively small impact speed of 4m/sec. Indeed the terminal speed in this test seem to be about 90% of the Rayleigh wave speed of PMMA, $c_R^{(1)}$, see FIGURE 6.9(a). In contrast, previous experience with dynamic crack growth in *homogeneous* PMMA specimens of the same configuration show a maximum speed of about $0.35c_R^{(1)}$. Note also that in this particular bimaterial case

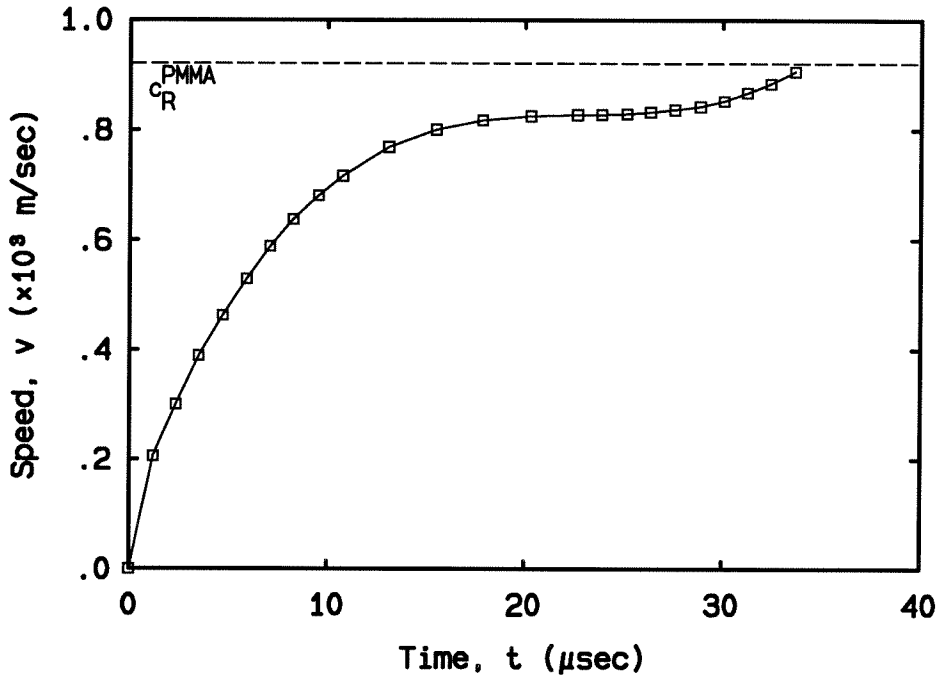

(a)

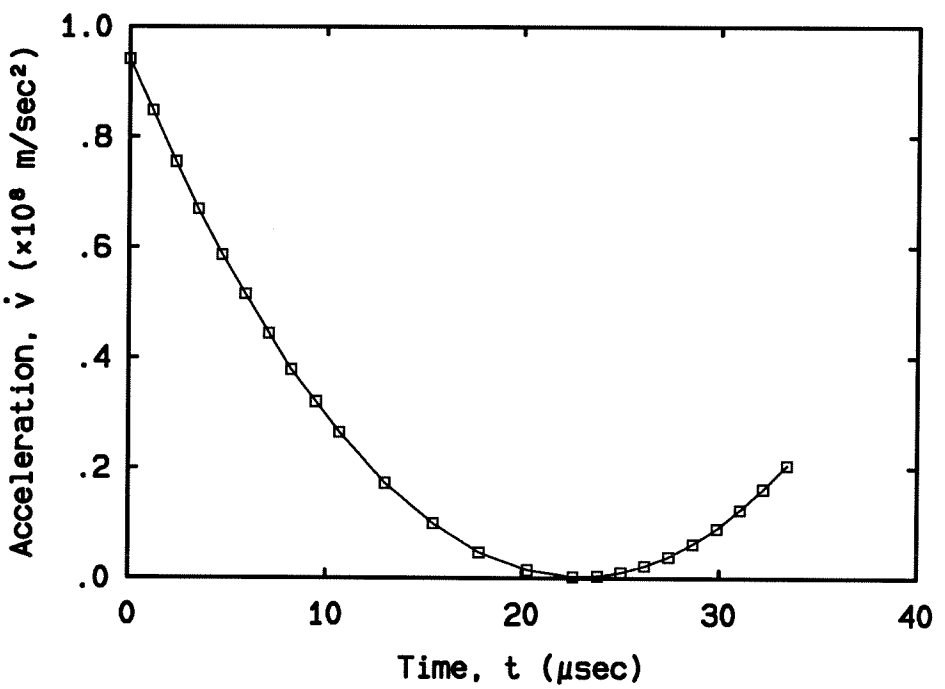

(b)

Figure 6.9: Velocity, (a) and acceleration, (b) time histories for the experiment shown in FIGURE 6.8.

there is a very large crack-tip acceleration (approximately $10^7\mathbf{g}$, where $\mathbf{g}$ is the acceleration of gravity) immediately after the crack initiates, see FIGURE 6.9(b). This would suggest that transient effects would be present close to initiation ($t = 0\mu$sec). As was mentioned earlier the rate of change of the oscillatory index with time ($\dot{\epsilon}$) may be considered a partial measure of transience. For the same test as FIGURE 6.8, we have plotted ϵ and $\dot{\epsilon}$ versus time in FIGURES 6.10(a) and 6.10(b). In FIGURE 6.10(b), $\dot{\epsilon}$ exhibits a local maximum at about $t = 10\mu$sec after initiation. It then starts increasing again after 25μsec. At short times after initiation, $\epsilon'(v)$ is close to zero although $\dot{v}$ is large ($10^7\mathbf{g}$). This accounts for the initially low values of $\dot{\epsilon}$. In this regime transient effects are demonstrated through large changes in the complex dynamic stress intensity factor. As time increases the combination of $\epsilon'(v)$ and $\dot{v}$ results in a local maximum in $\dot{\epsilon}$. At later times ($t > 25\mu$sec) and as the crack-tip velocity approaches the Rayleigh wave speed of PMMA, $\dot{\epsilon}$ increases again.

To demonstrate the need of a transient analysis in interpreting experimental data, let us now attempt to analyze the frame of FIGURE 6.8 at $t = 9.5\mu$sec. This corresponds to a local maximum value of $\dot{\epsilon}$ in this particular test. By following the fitting procedure described in Section 6.7.3, we can obtain the coefficients of either equation (6.7.9) or equation (6.7.10). The result of such a fit for the K^d-dominant field (equation (6.7.9)) is shown in FIGURE 6.11(a). The diamonds are digitized data points from the interferogram at $t = 9.5\mu$sec. The solid line is the contour of the quantity $\partial(\hat{\sigma}_{11} + \hat{\sigma}_{22})/\partial x_1$ calculated numerically by using the results for K^d from the fit generated by the same data points. As can be clearly seen, equation (6.7.9) cannot represent the data to any reasonable extent. The deformation field of this particular picture therefore is nowhere near K^d-dominant. In fact the main feature which is that the fringes vertically approach the interface cannot be captured at all by equation (6.7.9). The result of the fit of the transient higher order field (equation (6.7.10)) derived earlier is shown in FIGURE 6.11(b). The data points are exactly the

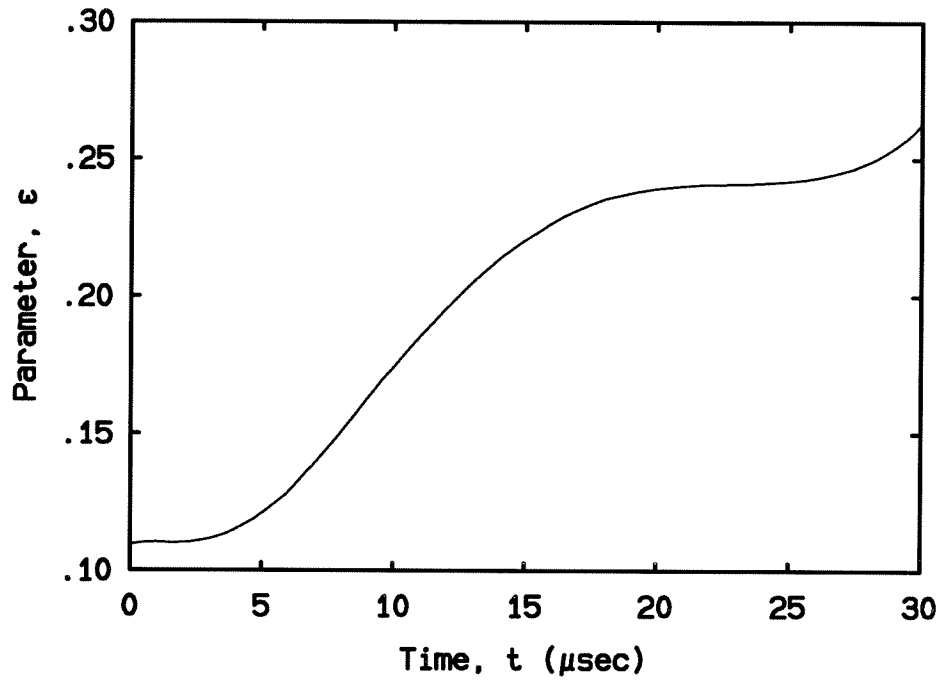

(a)

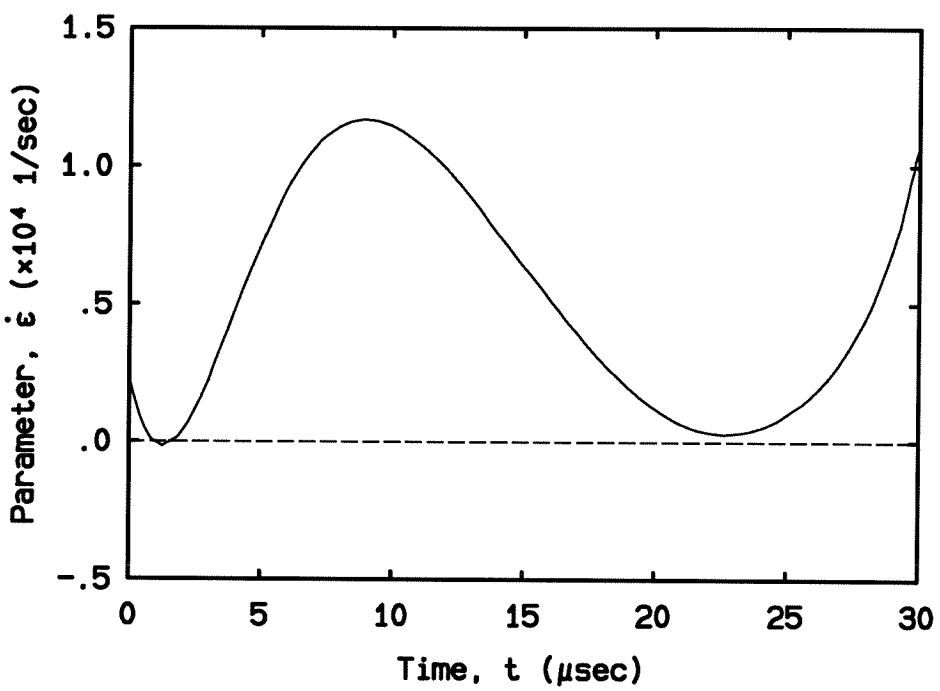

(b)

Figure 6.10: Time histories of mismatch parameter ϵ, (a) and its time derivative, (b) for the experiment shown in FIGURE 6.8.

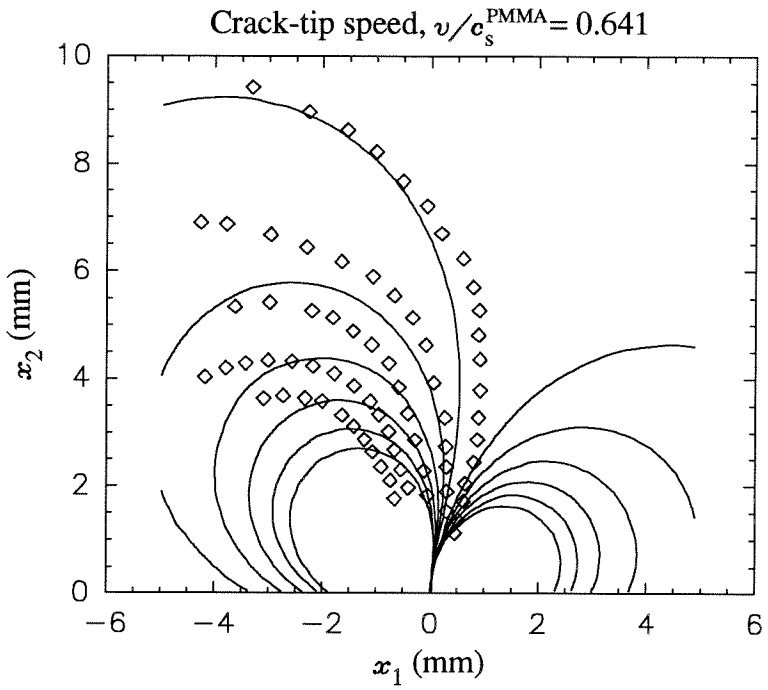

(a)

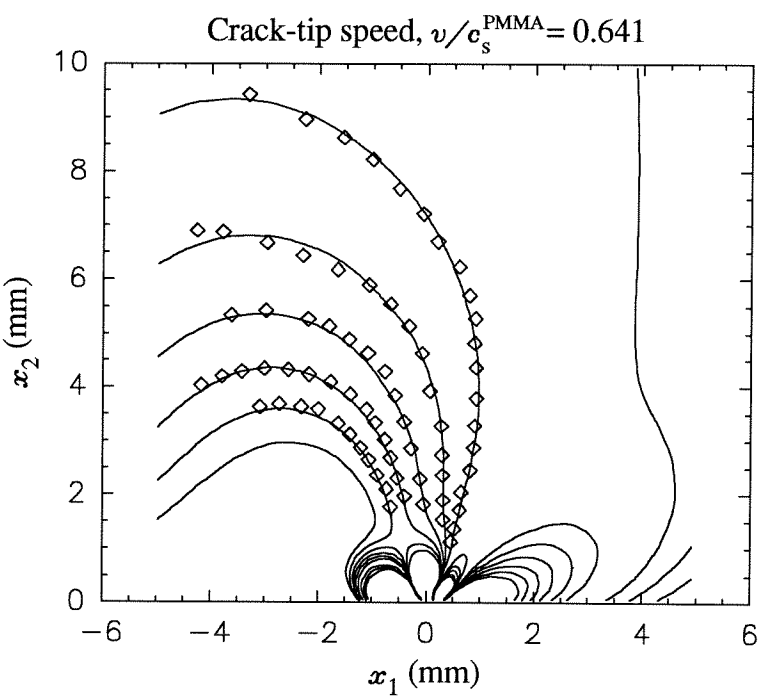

(b)

Figure 6.11: Comparison of digitized data points from the interferogram corresponding to $t = 9.5\mu$sec in FIGURE 6.8 with, (a) a K^d-dominant fit, equation (6.7.9); (b) a higher order transient analysis fit, equation (6.7.10). (Crack lies along the negative x_1-axis)

same as before and the solid line is the result of the fit. Clearly the fit is very good over a large area of the specimen. All features of the field are successfully captured by equation (6.7.10). This shows that the K^d-dominant analysis cannot be used for cases where $\dot{\epsilon}$ is high.

To further investigate the effect of $\dot{\epsilon}$ on the interpretation of optical data, we chose to analyze an interferogram corresponding to the minimum value of $\dot{\epsilon}$ within the duration of the test. This occurs at $t = 23\mu$sec. FIGURE 6.12(a) shows the result of the K^d-dominant fit to the experimental data. As the crack-tip is approached, equation (6.7.9) seems to adequately describe the experimental measurement. However, as the distance from the crack-tip is increased, K^d-dominance is lost. Nevertheless, the lack of K^d-dominance in FIGURE 6.12(a) ($\dot{\epsilon} \sim 1.0 \times 10^2 \text{sec}^{-1}$) is not as dramatic as in FIGURE 6.11(a) ($\dot{\epsilon} \sim 1.2 \times 10^4 \text{sec}^{-1}$). FIGURE 6.12(b) shows the result of the fit of the transient higher order field to the same experimental data as FIGURE 6.12(a). The fit is now much better over the whole range of radii. The above observations show that in general a transient analysis of data is necessary if fracture parameters such as K^d are to be obtained with confidence.

6.7.5 Transonic terminal speeds

The next cycle of experimentation involved bimaterial specimens loaded at higher loading rates than in a drop weight tower. This was achieved by using a high speed gas gun. A one point bend impact geometry was used. Again the issues of crack-tip loading history, as dependent upon PMMA or steel side impact, arise. It was chosen to impact the specimens on the steel side, to remain consistent with the drop weight tower tests. The gas gun projectile was 50mm in diameter and the impact velocity was 20m/sec, thus resulting in considerably larger near-tip loading rates than in the drop weight device. A sequence of interferograms from such a test is shown in

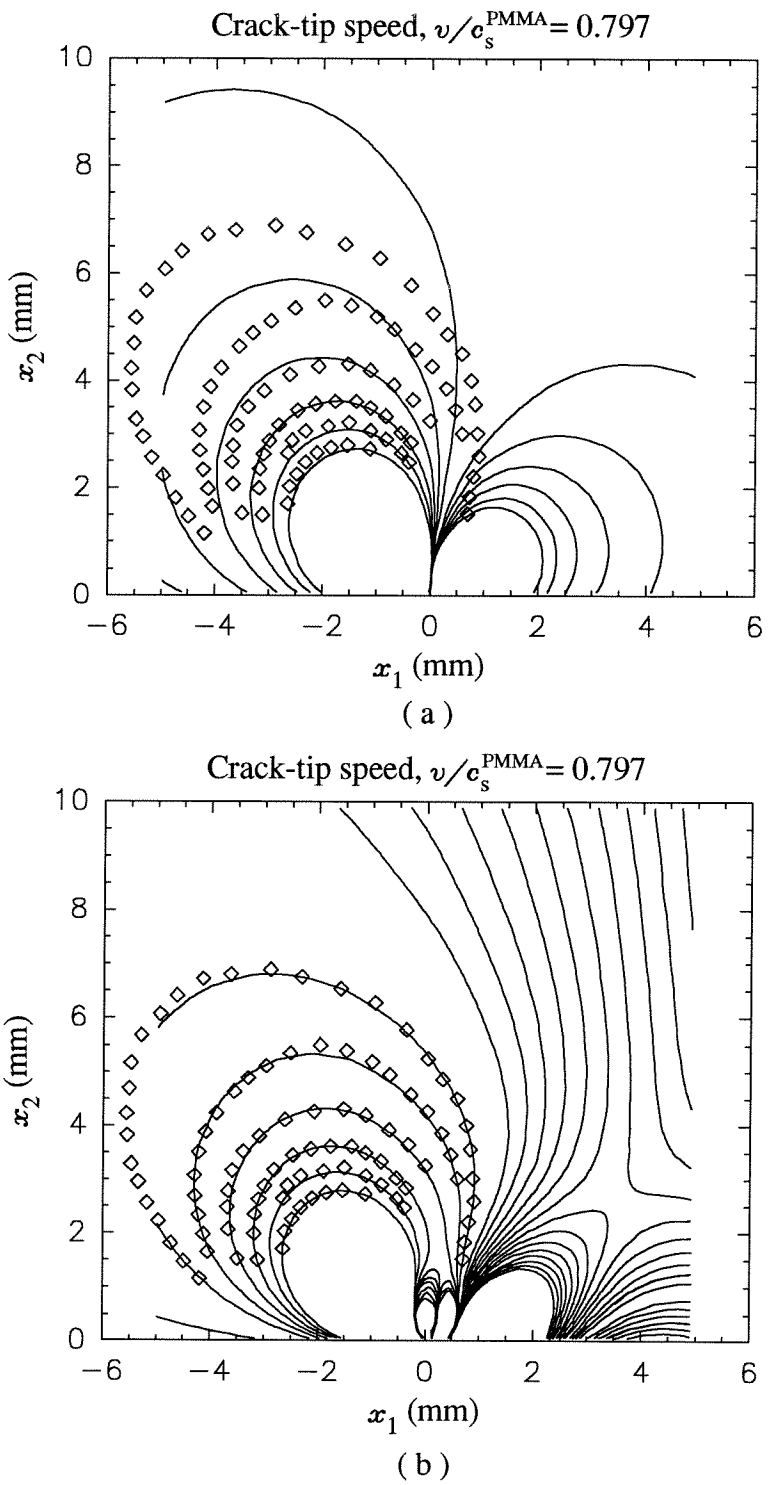

Figure 6.12: Comparison of digitized data points from the interferogram corresponding to $t = 23\mu$sec in FIGURE 6.8 with, (a) a K^d-dominant fit, equation (6.7.9); (b) a higher order transient analysis fit, equation (6.7.10). (Crack lies along the negative x_1-axis)

FIGURE 6.13. Its corresponding $v(t)$, $\dot{v}(t)$, $\epsilon(t)$ and $\dot{\epsilon}(t)$ plots are shown in FIGURES 6.14(a), (b), and 6.15(a), (b). In general terms the results are similar to those obtained from the drop weight tower experiments. A main difference is that the speed and acceleration are much higher. In fact the crack-tip speed seems to exceed the Rayleigh wave speed of PMMA after a relatively short time. In some cases (as in FIGURE 6.14) the velocity even exceeds the shear wave speed and approaches the longitudinal wave speed of PMMA, thus entering the transonic speed range for the PMMA side.

For a crack speed less than the Rayleigh wave speed, we can repeat a fitting procedure exactly as before. For the frame at $t = 8\mu$sec in FIGURE 6.13, the result of such a fit is shown in FIGURE 6.16. Here the white lines, obtained from plotting the field of equation (6.7.10) using the values of the fitted parameters, are superposed on the actual picture (instead of the digitized points as in FIGURES 6.11 and 6.12). The illustration is the same though, i.e., that a transient field is necessary to describe a picture such as this which corresponds to a high $\dot{\epsilon}$ and acceleration.

Unfortunately given the existing theoretical analyses, we do not have the tools to fit any field to interferograms having a speed in the transonic range for PMMA ($c_s^{(1)} < v < c_l^{(1)}$). These large speeds were observed in a number of tests involving one point bend interfacial specimens containing *sharp* pre-cracks lying along the interface. When a specimen containing a blunt starter notch was impacted, recorded crack-tip terminal speeds were even higher; at some cases approaching the longitudinal wave speed of PMMA. Such a velocity history is given in FIGURE 6.17. Here the maximum crack-tip speed is estimated to be $0.9c_l^{(1)}$. These observations are very interesting because to our knowledge no evidence of transonic or supersonic crack propagation has ever been seen in homogeneous materials even though a large number of the theoretical studies exist on the subject (Freund, 1990). It is believed that transonic crack growth is possible in a bimaterial situation because of an energy transfer mechanism from

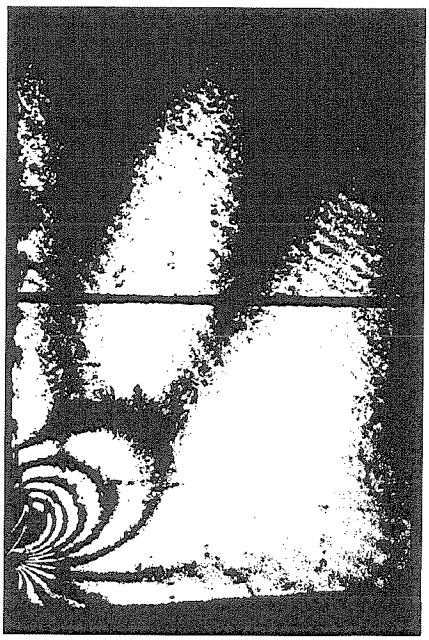

$t = 3$ μsec, $v = 140$ m/sec

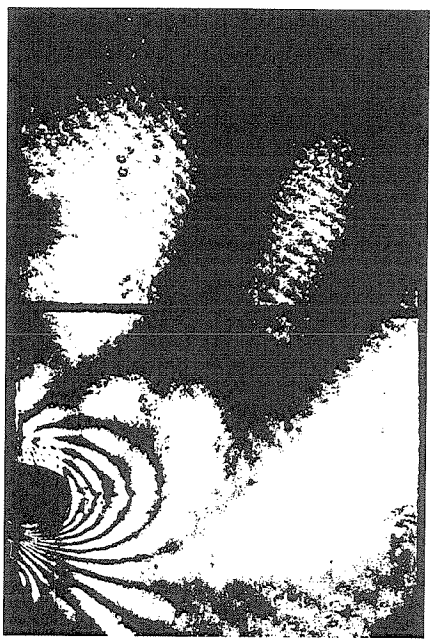

$t = 8$ μsec, $v = 720$ m/sec

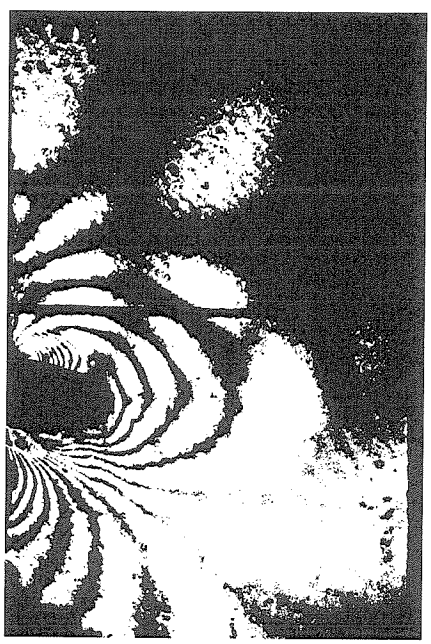

$t = 13$ μsec, $v = 1100$ m/sec

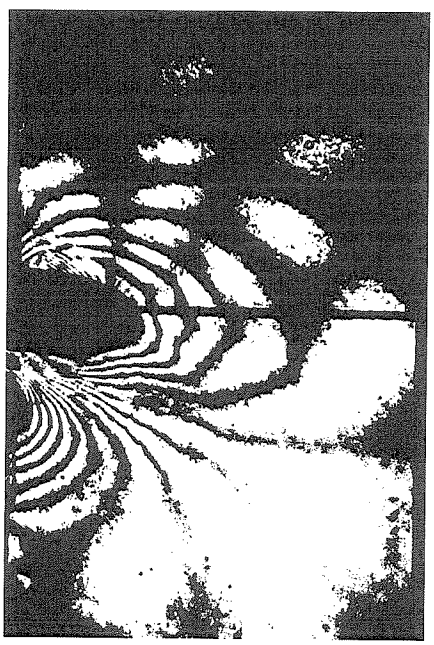

$t = 16.5$ μsec, $v = 1100$ m/sec

Figure 6.13: Selected sequence of CGS interferogram of a growing crack in a one point bend interfacial gas gun experiment. (Only PMMA side of PMMA/steel specimen is shown)

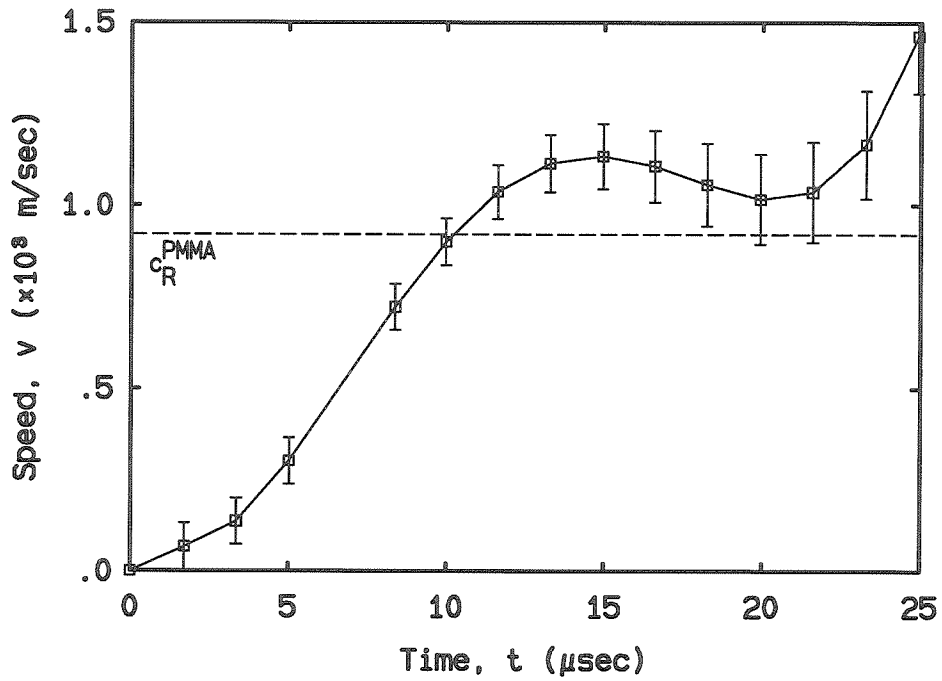

(a)

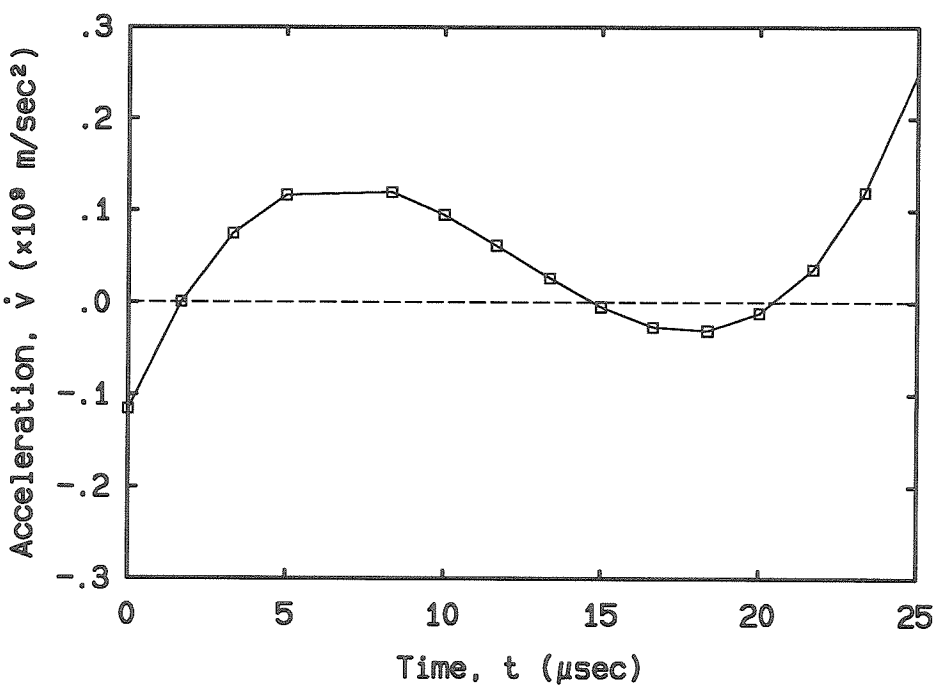

(b)

Figure 6.14: Velocity, (a) and acceleration, (b) time histories for the experiment shown in FIGURE 6.13.

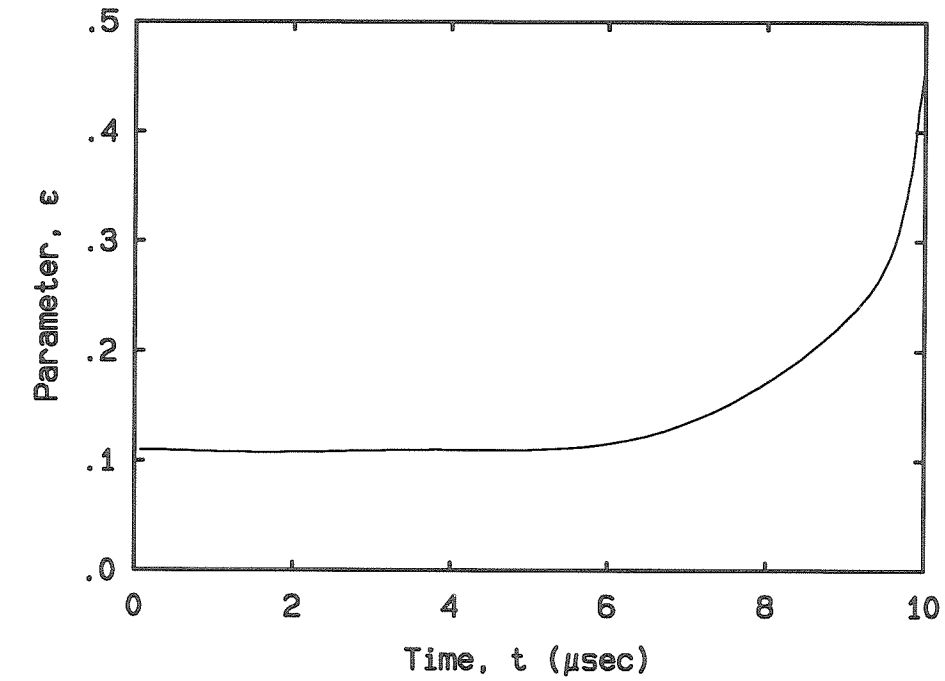

(a)

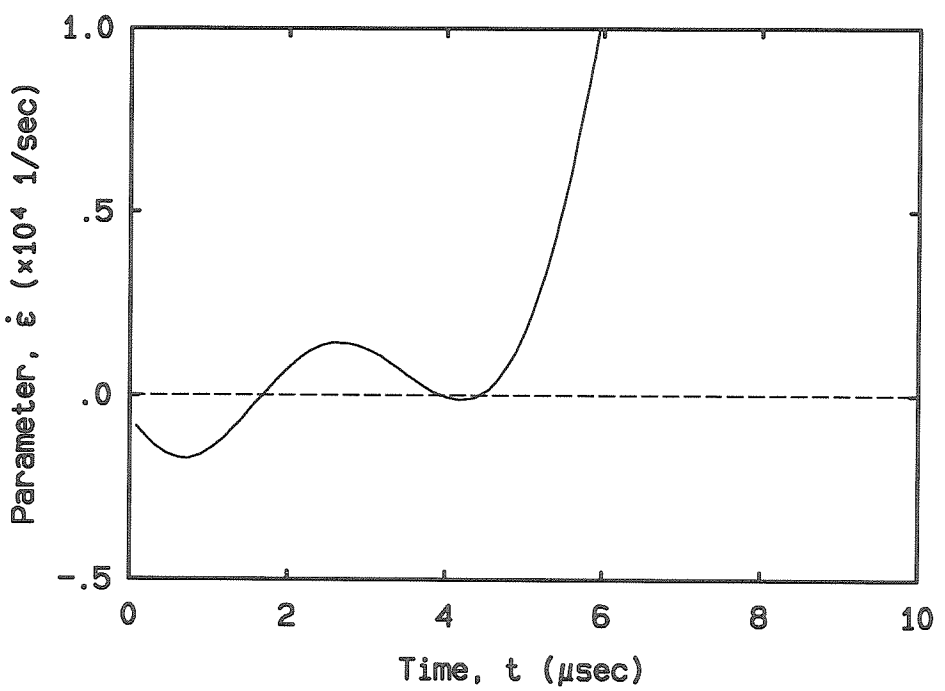

(b)

Figure 6.15: Time histories of mismatch parameter ϵ, (a) and its time derivative, (b) for the experiment shown in FIGURE 6.13.

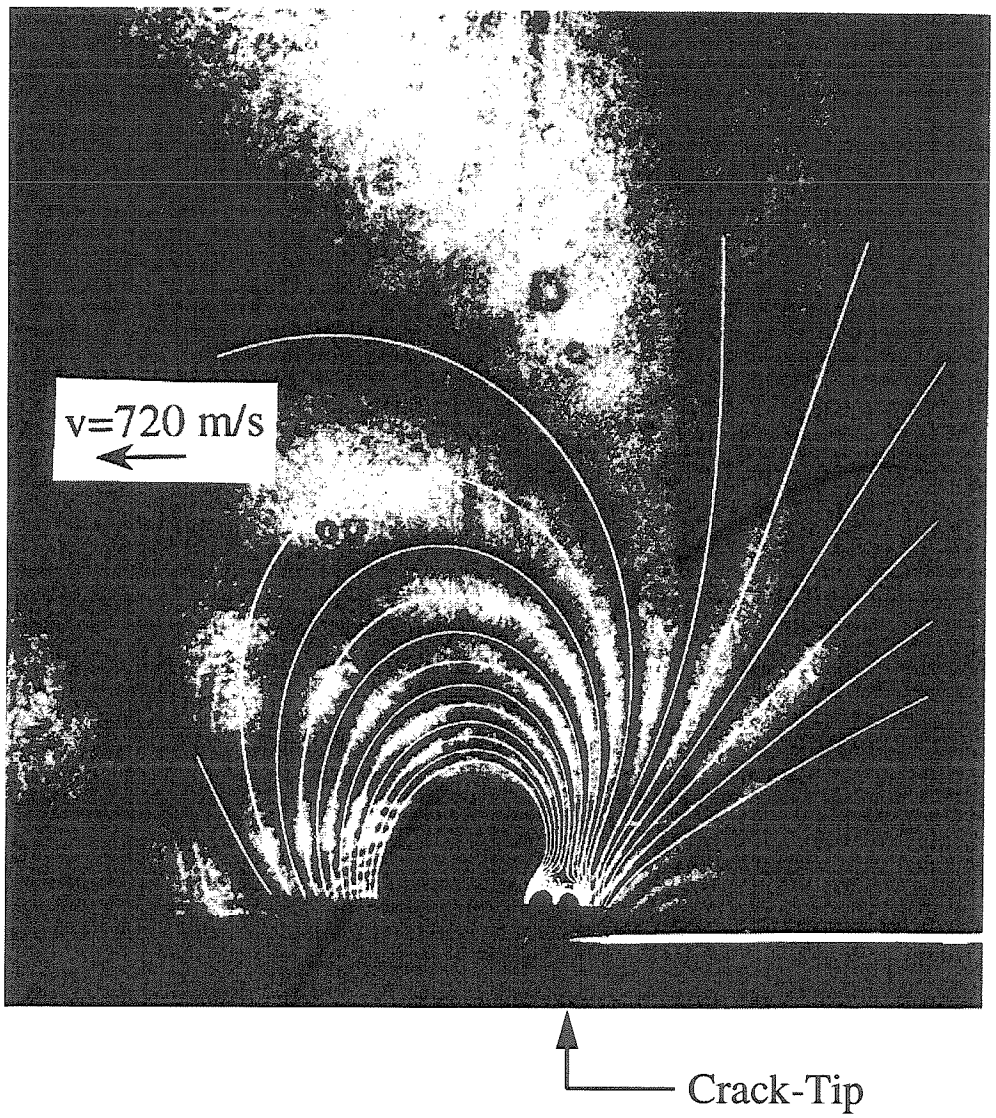

Figure 6.16: Comparison between the CGS fringe pattern and the fitted higher order transient stress field, equation (6.7.10), for a propagating crack in a PMMA/steel interface.

the stiffer to the softer material. It can be seen in FIGURE 6.13 that the nature of the fringes changes, approximately around the time at which the crack-tip speed exceeds the Rayleigh wave speed. A sequence corresponding to the same test whose velocity is shown in FIGURE 6.17(blunt starter notch) is presented in FIGURE 6.18. In these pictures, we see an even more drastic change in the nature of the fringe

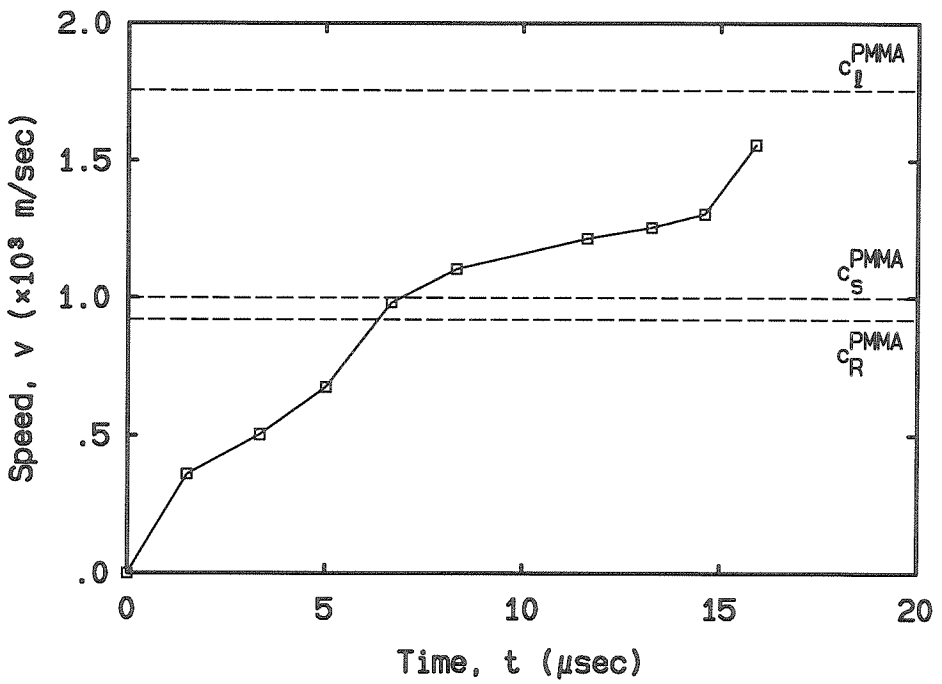

Figure 6.17: Velocity time history for the experiment shown in FIGURE 6.18.

patterns as the crack-tip speed exceeds both Rayleigh and shear wave speeds. To see this effect clearly, compare the second frame in FIGURE 6.18 to the sixth frame. Finally, additional visual proof of the existence of large transient effects is shown in FIGURE 6.19. We are now in the process of developing an analysis for the propagation of an interfacial crack at speeds exceeding $c_s^{(1)}$. It is hoped to be able to predict fringe patterns as those observed in FIGURES 6.13, 6.18, and 6.19.

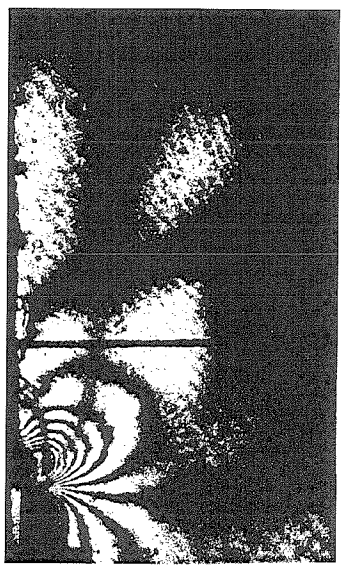

$t = 0$ μsec, $v = 0$ m/sec

$t = 1.5$ μsec, $v = 360$ m/sec

$t = 5$ μsec, $v = 670$ m/sec

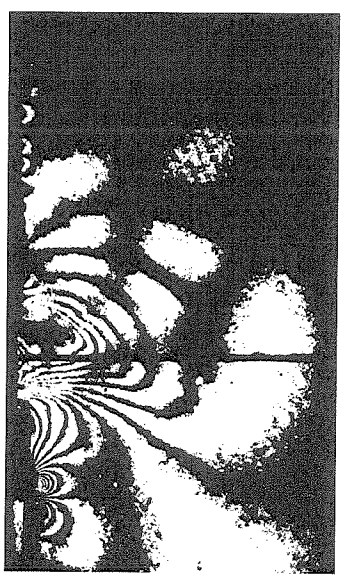

$t = 8.5$ μsec, $v = 1100$ m/sec

$t = 11.5$ μsec, $v = 1210$ m/sec

$t = 15$ μsec, $v = 1300$ m/sec

Figure 6.18: Selected sequence of CGS interferograms of a growing crack in a one point bend interfacial gas gun experiment. (A blunt starter notch was used)

$t = 10$ μsec, $v = 1000$ m/sec

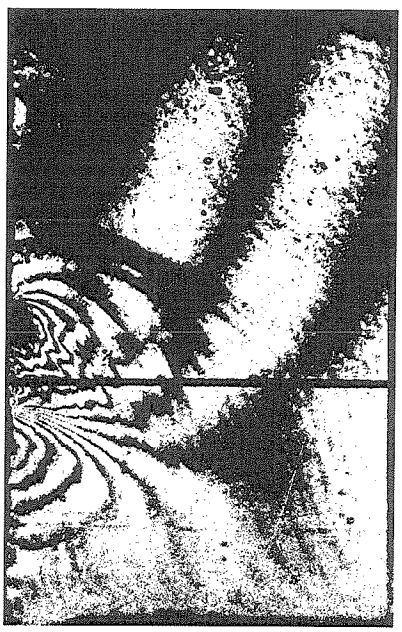

$t = 12.5$ μsec, $v = 1170$ m/sec

$t = 15.5$ μsec, $v = 1190$ m/sec

$t = 18.5$ μsec, $v = 1470$ m/sec

Figure 6.19: CGS interferograms providing visual evidence of the highly transient nature of dynamic interfacial crack growth.

6.8 Conclusions

Experimental observations of high speed (transonic terminal speeds) and high acceleration (10^8m/sec^2) crack growth in PMMA/steel interfaces are reported for the first time. Motivated by these observations, a fully transient higher order asymptotic analysis of dynamic interfacial crack growth is performed. This analysis is valid for crack-tip speed in the range $0 < v < c_s^{(1)}$ ($c_s^{(1)}$ is the shear wave speed of PMMA). Explicit expressions for stresses are provided. In addition to the classical $r^{-1/2}$, r^0, and $r^{1/2}$, $\cdots$, terms of steady state expansion for the stresses, new transient contributions of order $r^{1/2}\ln r$ and $r^{1/2}(\ln r)^2$ appear. The structure of the near-tip field obtained by the analysis is found to describe well the experimentally obtained stress fields. For subsonic crack growth, the experiments demonstrate the necessity of employing the fully transient expression in the analysis of optical experimental data. Terminal speeds of up to 90% of the plane stress dilatational wave speeds of PMMA are observed.

Appendices

A Definitions and properties of matrices used in Section 6.3

Let $\boldsymbol{P}_k$, $\boldsymbol{Q}_k$, $\boldsymbol{U}_k$, and $\boldsymbol{V}_k$ be defined as in Section 6.3, and $\boldsymbol{L}_k$ and $\overset{*}{\boldsymbol{L}}_k$ be given by

$$\boldsymbol{L}_k = \boldsymbol{U}_k \boldsymbol{P}_k^{-1} , \qquad \overset{*}{\boldsymbol{L}}_k = \boldsymbol{V}_k \boldsymbol{Q}_k^{-1} .$$

Matrices $\boldsymbol{H}$ and $\overset{*}{\boldsymbol{H}}$ are defined as,

$$\boldsymbol{H} = \boldsymbol{L}_1 - \overset{*}{\boldsymbol{L}}_2 , \qquad \overset{*}{\boldsymbol{H}} = \overset{*}{\boldsymbol{L}}_1 - \boldsymbol{L}_2 .$$

By algebraic calculations, it can be shown that for $k \in \{1, 2\}$,

$$\boldsymbol{L}_k = \begin{bmatrix} (l_{11})_k & (l_{12})_k \\ (l_{21})_k & (l_{11})_k \end{bmatrix} , \qquad \overset{*}{\boldsymbol{L}}_k = \begin{bmatrix} (l_{11})_k & -(l_{12})_k \\ -(l_{21})_k & (l_{11})_k \end{bmatrix} ,$$

where

$$(l_{11})_k = \left\{ \frac{2\alpha_l \alpha_s - (1+\alpha_s^2)}{\mu D(v)} \right\}_k , \; (l_{12})_k = \left\{ \frac{\alpha_s (1-\alpha_s^2)}{\mu D(v)} \right\}_k , \; (l_{21})_k = \left\{ \frac{\alpha_l (1-\alpha_s^2)}{\mu D(v)} \right\}_k ,$$

and

$$D(v) = 4\alpha_l \alpha_s - (1+\alpha_s^2)^2 .$$

Therefore,

$$\boldsymbol{H} = \begin{bmatrix} h_{11} & h_{12} \\ h_{21} & h_{11} \end{bmatrix} , \qquad \overset{*}{\boldsymbol{H}} = \begin{bmatrix} h_{11} & -h_{12} \\ -h_{21} & h_{11} \end{bmatrix} ,$$

where

$$h_{11} = (l_{11})_1 - (l_{11})_2 , \qquad h_{12} = (l_{12})_1 + (l_{12})_2 , \qquad h_{21} = (l_{21})_1 + (l_{21})_2 .$$

Notice that

$$\boldsymbol{H}\, \overset{*}{\boldsymbol{H}} = \overset{*}{\boldsymbol{H}}\, \boldsymbol{H} = (h_{11}^2 - h_{12} h_{21}) \boldsymbol{I} ,$$

where I is the 2×2 identity matrix. Thus,

$$H^{-1} = \frac{1}{h_{11}^2 - h_{12}h_{21}} \overset{*}{H} , \qquad \overset{*}{H}^{-1} = \frac{1}{h_{11}^2 - h_{12}h_{21}} H .$$

Also, it can be shown that

$$L_k \overset{*}{L}_k = \overset{*}{L}_k L_k , \qquad k \in \{1, 2\}.$$

A sequence of operator definitions follows. These are related to the analysis in Section 6.3.2. Let $p(t)$ and $q(t)$ be two real functions of time t and define the vector operators

$$\begin{aligned} d_k\{p(t), q(t)\} &= \{ D_l\{p(t)\},\ D_s\{q(t)\} \}_k^\top , \\ k_k\{p(t), q(t)\} &= \{ K_l(t)p(t),\ K_s(t)q(t) \}_k^\top , \\ b_k\{p(t), q(t)\} &= \{ B_l(t)p(t),\ B_s(t)q(t) \}_k^\top , \end{aligned}$$

where operators $D_{l,s}\{\cdot\}$ and functions $K_{l,s}(t)$ and $B_{l,s}(t)$ have been defined in Section 6.3.2. With the above definitions,

$$\begin{aligned} t_k\{p(t), q(t)\} &= (3 + 2i\epsilon)\,(L_k M_k - I)\, d_k\{p(t), q(t)\} \\ &+ 2\dot{\epsilon}\,(L_k M_k - I)\, k_k\{p(t), q(t)\} \\ &+ 2\left\{(1 + 2i\epsilon)\,(L_k M_k - I) + L_k \overset{*}{P}_k - \overset{*}{U}_k\right\} b_k\{p(t), q(t)\} , \end{aligned}$$

where M_k, $\overset{*}{P}_k$, and $\overset{*}{U}_k$ have also been defined in Section 6.3.2. In addition, for any given operator

$$m_k\{p(t), q(t)\} = \left\{ m_k^{(1)}\{p(t), q(t)\},\ m_k^{(2)}\{p(t), q(t)\} \right\}^\top ,$$

the associated operator $\overset{*}{m}_k\{p(t), q(t)\}$ is defined as

$$\overset{*}{m}_k\{p(t), q(t)\} = \left\{ m_k^{(1)}\{p(t), q(t)\},\ -m_k^{(2)}\{p(t), q(t)\} \right\}^\top .$$

Also vectors $\boldsymbol{\beta}$, $\boldsymbol{\gamma}$, $\boldsymbol{\xi}$, and $\boldsymbol{\varsigma}$, are defined as

$$\left.\begin{aligned}
\boldsymbol{\beta} &= \boldsymbol{t}_1\{a_0(t), c_0(t)\} - \overset{*}{\boldsymbol{t}}_2\,\{b_0(t), d_0(t)\} \\
\boldsymbol{\gamma} &= \boldsymbol{t}_2\{a_0(t), c_0(t)\} - \overset{*}{\boldsymbol{t}}_1\,\{b_0(t), d_0(t)\} \\
\boldsymbol{\xi} &= (3+2i\epsilon)\left\{(\boldsymbol{L}_1\boldsymbol{M}_1 - \boldsymbol{I})\,\boldsymbol{k}_1\{a_0(t), c_0(t)\} - \left(\overset{*}{\boldsymbol{L}}_2\,\boldsymbol{M}_2 - \boldsymbol{I}\right)\overset{*}{\boldsymbol{k}}_2\,\{b_0(t), d_0(t)\}\right\} \\
\boldsymbol{\varsigma} &= (3+2i\epsilon)\left\{(\boldsymbol{L}_2\boldsymbol{M}_2 - \boldsymbol{I})\,\boldsymbol{k}_2\{a_0(t), c_0(t)\} - \left(\overset{*}{\boldsymbol{L}}_1\,\boldsymbol{M}_1 - \boldsymbol{I}\right)\overset{*}{\boldsymbol{k}}_1\,\{b_0(t), d_0(t)\}\right\}
\end{aligned}\right\},$$

and operators $\boldsymbol{w}_{dk}\{p(t), q(t)\}$ and $\boldsymbol{w}_{tk}\{p(t), q(t)\}$ as

$$\left.\begin{aligned}
\boldsymbol{w}_{dk}\{p(t), q(t)\} &= \left(\frac{3}{2} + i\epsilon\right)\left\{2\boldsymbol{P}_k^{-1}\boldsymbol{M}_k + \left(\frac{1}{2} + i\epsilon\right)\boldsymbol{I}\right\}\boldsymbol{k}_k\{p(t), q(t)\} \\
\boldsymbol{w}_{tk}\{p(t), q(t)\} &= \left(\frac{3}{2} + i\epsilon\right)\left\{2\boldsymbol{P}_k^{-1}\boldsymbol{M}_k + \left(\frac{1}{2} + i\epsilon\right)\boldsymbol{I}\right\}\boldsymbol{d}_k\{p(t), q(t)\} \\
&+ 2\dot{\epsilon}\left\{\boldsymbol{P}_k^{-1}\boldsymbol{M}_k + (1+i\epsilon)\boldsymbol{I}\right\}\boldsymbol{k}_k\{p(t), q(t)\} \\
&+ \left\{2\boldsymbol{P}_k^{-1}\,\overset{*}{\boldsymbol{P}}_k + 2(1+2i\epsilon)\boldsymbol{P}_k^{-1}\boldsymbol{M}_k - \left(\frac{1}{4} + \epsilon^2\right)\boldsymbol{I}\right\}\boldsymbol{b}_k\{p(t), q(t)\}
\end{aligned}\right\}.$$

B Solution of the Riemann-Hilbert problem

Consider the problem formulated as following: Find a function

$$\boldsymbol{\theta}(z) = (\ \theta_1(z),\ \theta_2(z)\ )^{\mathsf{T}}\ ,$$

$z = \eta_1 + i\eta_2$, which is analytic in the whole z-plane except along the branch cut $-\infty < \eta_1 \leq 0$, $\eta_2 = 0$, and satisfies the equation,

$$\overset{*}{\boldsymbol{H}}\,\boldsymbol{\theta}^{+}(\eta_1) - \boldsymbol{H}\boldsymbol{\theta}^{-}(\eta_1) = \boldsymbol{\kappa}(\eta_1)\ , \qquad \forall\ \eta_1 < 0\ , \tag{B.1}$$

where $\overset{*}{\boldsymbol{H}}$ and $\boldsymbol{H}$ are 2×2 matrices, defined in Appendix I, and

$$\boldsymbol{\kappa}(\eta_1) = (\ \kappa_1(\eta_1),\ \kappa_2(\eta_1)\ )^{\mathsf{T}}\ ,$$

with κ_1 and κ_2 are known functions of η_1. Near the origin, function $\theta(z)$ should satisfy the requirement that

$$| \theta(z) | = O (|z|^{\alpha}) , \qquad \text{as } |z| \to 0 , \tag{B.2}$$

for some real number α, and generally, $\alpha > -1$.

In order to obtain the solution to the above Riemann-Hilbert problem, the eigen-values and eigen-vectors of $\boldsymbol{H}$, and $\overset{*}{\boldsymbol{H}}$ need to be studied first. By solving the equation

$$\det \{\boldsymbol{H} - \lambda \boldsymbol{I}\} = 0 , \tag{B.3}$$

where $\boldsymbol{I}$ is the identity matrix, the eigen-values for $\boldsymbol{H}$ are found to be

$$\lambda_{1,2} = h_{11} \pm \sqrt{h_{12} h_{21}} . \tag{B.4}$$

The expressions of functions h_{11}, h_{12}, and h_{21} in our problem are dependent upon the mechanical properties of the constituents of the bimaterial system and the speed of propagation of the interfacial crack. h_{11}, h_{12}, and h_{21} ensure that the eigen-values, λ_1 and λ_2, are real, provided that the crack-tip speed is less than the lower Rayleigh wave speed of the bimaterial. The corresponding eigen-vectors are

$$\boldsymbol{w}^{(1,2)} = (1, \pm \eta)^{\top} , \tag{B.5}$$

where the parameter η is defined by

$$\eta = \sqrt{\frac{h_{21}}{h_{12}}} .$$

It can be shown that the eigen-values for $\overset{*}{\boldsymbol{H}}$ are the same as those for $\boldsymbol{H}$, which are given in (B.4), while the corresponding eigen-vectors are

$$\overset{*}{\boldsymbol{w}}^{(1,2)} = (1, \mp \eta)^{\top} . \tag{B.6}$$

Define the matrix $\boldsymbol{B}$, by

$$\boldsymbol{B} = \begin{bmatrix} 1 & 1 \\ \eta & -\eta \end{bmatrix} ,$$

and set

$$\overset{*}{\boldsymbol{H}}{}' = \boldsymbol{B}^{-1}\,\overset{*}{\boldsymbol{H}}\,\boldsymbol{B}\ , \qquad \boldsymbol{H}' = \boldsymbol{B}^{-1}\boldsymbol{H}\boldsymbol{B}\ ,$$

and

$$\overset{\diamond}{\boldsymbol{\theta}}\,(z) = \boldsymbol{B}^{-1}\boldsymbol{\theta}(z)\ , \qquad \overset{\diamond}{\boldsymbol{\kappa}}\,(\eta_1) = \boldsymbol{B}^{-1}\boldsymbol{\kappa}(\eta_1)\ .$$

Then, equation (B.1) becomes

$$\overset{*}{\boldsymbol{H}}{}'\overset{\diamond}{\boldsymbol{\theta}}{}^{+}\,(\eta_1) - \boldsymbol{H}'\,\overset{\diamond}{\boldsymbol{\theta}}{}^{-}\,(\eta_1) = \overset{\diamond}{\boldsymbol{\kappa}}\,(\eta_1)\ , \qquad \forall\ \eta_1 < 0\ , \tag{B.7}$$

or, in component form,

$$\left.\begin{aligned} \lambda_2\,\overset{\diamond}{\theta}{}_1^{+}\,(\eta_1) - \lambda_1\,\overset{\diamond}{\theta}{}_1^{-}\,(\eta_1) &= \overset{\diamond}{\kappa}_1\,(\eta_1) \\ \lambda_1\,\overset{\diamond}{\theta}{}_2^{+}\,(\eta_1) - \lambda_2\,\overset{\diamond}{\theta}{}_2^{-}\,(\eta_1) &= \overset{\diamond}{\kappa}_2\,(\eta_1) \end{aligned}\right\}\ , \qquad \forall\ \eta_1 < 0\ . \tag{B.8}$$

It can be seen from above analysis that $\boldsymbol{H}$ and $\overset{*}{\boldsymbol{H}}$ can be diagonalized simultaneously by the same transformation. Therefore, the originally coupled equations (B.1) can be reduced to the uncoupled equations (B.8).

If we express the ratio λ_1/λ_2 as having the following dependence on β:

$$-\frac{\lambda_1}{\lambda_2} = \frac{1+\beta}{1-\beta}\ ,$$

then the parameter β must be expressed as,

$$\beta = \frac{h_{11}}{\sqrt{h_{12}h_{21}}}\ .$$

As a result, the solution for the first equation in (B.8) can be obtained as

$$\frac{\overset{\diamond}{\theta}_1\,(z)}{L(z)} = \frac{1}{2\pi i}\int_C \frac{\overset{\diamond}{\kappa}_1\,(\tau)\mathrm{d}\tau}{\lambda_2 L^{+}(\tau)(\tau - z)} + \overset{\diamond}{A}\,(z)\ , \tag{B.9}$$

where $\overset{\diamond}{A}\,(z)$ is an arbitrary entire function. C is a contour along the entire branch cut, and extends from negative infinity to the interfacial crack-tip. The function $L(z)$ is given by

$$L(z) = z^{-\frac{1}{2}+k_1+i\epsilon}\ , \tag{B.10}$$

where

$$\epsilon = \frac{1}{2\pi} \ln \frac{1-\beta}{1+\beta} ,$$

and k_1 is an real integer. Integer k_1 is chosen so that

$$| L(z) | = O (|z|^{\alpha}) , \qquad \text{as } |z| \to 0 ,$$

which complies with the restriction of equation (B.2).

Similarly, we can obtain that

$$\frac{\overset{\diamond}{\theta}_2 (z)}{\overline{L}(z)} = \frac{1}{2\pi i} \int_C \frac{\overset{\diamond}{\kappa}_2 (\tau) d\tau}{\lambda_1 \overline{L}^+(\tau)(\tau - z)} + \overset{\diamond}{B} (z) , \tag{B.11}$$

where $\overset{\diamond}{B} (z)$ is also an arbitrary entire function. $\overline{L}$ stands for the complex conjugate of L.

Returning to the original function $\boldsymbol{\theta}(z)$,

$$\left.\begin{aligned} \boldsymbol{\theta}(z) \;&=\; \frac{1}{4\pi i} \int_C \left\{ \frac{1}{\lambda_2} \cdot \frac{L(z)}{L^+(\tau)} \boldsymbol{\Gamma} \boldsymbol{\kappa}(\tau) + \frac{1}{\lambda_1} \cdot \frac{\overline{L}(z)}{\overline{L}^+(\tau)} \overset{*}{\boldsymbol{\Gamma}} \boldsymbol{\kappa}(\tau) \right\} \frac{d\tau}{\tau - z} \\ &+\; L(z) \overset{\diamond}{A} (z) \boldsymbol{\zeta} + \overline{L}(z) \overset{\diamond}{B} (z) \overset{*}{\boldsymbol{\zeta}} \end{aligned}\right\} , \tag{B.12}$$

where

$$\boldsymbol{\Gamma} = \begin{bmatrix} 1 & \frac{1}{\eta} \\ \eta & 1 \end{bmatrix} , \qquad \overset{*}{\boldsymbol{\Gamma}} = \begin{bmatrix} 1 & -\frac{1}{\eta} \\ -\eta & 1 \end{bmatrix} ,$$

and

$$\boldsymbol{\zeta} = (1, \eta)^{\top} , \qquad \overset{*}{\boldsymbol{\zeta}} = (1, -\eta)^{\top} .$$

C Some asymptotic results of the Stieltjes transform

In solving the Riemann-Hilbert problem, we need to evaluate the integral

$$I(z) = \int_{-\infty}^{0} \frac{f(-\eta_1)}{\eta_1 - z} d\eta_1 . \tag{C.1}$$

Setting $t = -\eta_1$, we get

$$I(z) = -\int_0^\infty \frac{f(t)}{t+z}\mathrm{d}t \ . \tag{C.2}$$

As we can see from equation (C.2), $-I(z)$ is the Stieltjes transform of function $f(t)$. Here we want to study the asymptotic behavior of the Stieltjes transform as $z \to 0$. Alternatively, we may set $\lambda = 1/z$ to get

$$I(z) = -\lambda H[f;\lambda] \ , \tag{C.3}$$

where

$$H[f;\lambda] = \int_0^\infty \frac{f(t)}{1+\lambda t}\mathrm{d}t \ . \tag{C.4}$$

Studying the asymptotic behavior of (C.2) as $z \to 0$ is equivalent to studying the asymptotic behavior of (C.4) as $\lambda \to \infty$.

Suppose that $f(t)$ is locally integrable in $(0,\infty)$. Recall that the Mellin transform of $f(t)$ is defined by

$$M[f;s] = \int_0^\infty t^{s-1} f(t)\mathrm{d}t \ , \tag{C.5}$$

and set

$$h(t) = \frac{1}{1+t} \ .$$

Then, by using the Parseval formula, we can obtain that

$$H[f;\lambda] = \frac{1}{2\pi i}\int_{r-i\infty}^{r+i\infty} \lambda^{-s} M[h;s]M[f;1-s]\mathrm{d}s \ , \tag{C.6}$$

where the constant r is such that $\mathrm{Re}(s) = r$ lies in the common strip of analyticity of the Mellin transforms $M[h;s]$ and $M[f;1-s]$.

After some manipulations, it can be shown that

$$M[h;s] = \frac{\pi}{\sin \pi s} \ , \tag{C.7}$$

where $M[h;s]$ is analytic in the strip $0 < \mathrm{Re}(s) < 1$. In analogy to the particular problem of interfacial fracture that we are interested in, we will define the function

$f(t)$ as,

$$f(t) = t^{i\alpha}\,(\ln t)^{\beta} \ , \tag{C.8}$$

where $\alpha = \pm 2\epsilon$, or 0, and $\beta = 0$, or 1. For this function, the Mellin transform $M[f;s]$ only exits in the generalized sense. Let

$$f_1(t) = \begin{cases} f(t), & t \in (0,1] \\ \\ 0, & t \in [1,\infty) \end{cases} \quad ; \qquad f_2(t) = \begin{cases} 0, & t \in (0,1] \\ \\ f(t), & t \in [1,\infty) \end{cases} \ .$$

Then, we may write

$$H[f_j;\lambda] = L_j(\lambda) = \int_0^{\infty} \frac{f_j(t)}{1+\lambda t}\mathrm{d}t \ , \qquad j = 1,\ 2 \ , \tag{C.9}$$

and

$$H[f;\lambda] = L_1(\lambda) + L_2(\lambda) \ . \tag{C.10}$$

Also let

$$G_j(s) = M[h;s]M[f_j;1-s] \ , \qquad j = 1,\ 2 \ . \tag{C.11}$$

Then,

$$G(s) = M[h;s]M[f;1-s] = G_1(s) + G_2(s) \ .$$

In addition, from the Parseval formula,

$$L_j(\lambda) = \frac{1}{2\pi i}\int_{r_j-i\infty}^{r_j+i\infty} \lambda^{-s} G_j(s)\mathrm{d}s \ , \qquad j = 1,\ 2 \ , \tag{C.12}$$

and

$$H[f;\lambda] = \frac{1}{2\pi i}\sum_{j=1}^{2}\int_{r_j-i\infty}^{r_j+i\infty} \lambda^{-s} G_j(s)\mathrm{d}s \ . \tag{C.13}$$

Using the specific function $f(t)$ chosen in (C.8), it can be shown that

$$G_1(s) = -\frac{1}{[s-(1+i\alpha)]^{\beta+1}} \cdot \frac{\pi}{\sin \pi s} \ . \tag{C.14}$$

In the above we can see that $G_1(s)$ is analytic in the strip $0 < \mathrm{Re}(s) < 1$. Since $M[f_2;1-s]$ is analytic in the half plane $\mathrm{Re}(s) > 1$, and $M[h;s]$ can be analytically

continued into the entire s–plane as a meromorphic function, $G_2(s)$ is a meromorphic function in the half plane $\mathrm{Re}(s) > 1$ with simple poles at $s = 2, 3, \cdots$. Then in equation (C.12), we can always choose that $0 < r_1 < 1$ and $r_2 > r_1$. Observe that if $s = s_1 + is_2$, $G_1(s)$ has the property

$$\lim_{|s_2|\to\infty} G_1(s_1 + is_2) = 0 \ , \qquad r_1 < s_1 < r_2 \ . \tag{C.15}$$

Therefore, we can apply Cauchy's integral theorem to equation (C.13), which results in

$$H[f;\lambda] = \sum_{r_1<\mathrm{Re}(s)<r_2} \mathrm{res}\left\{-\lambda^{-s}G_1(s)\right\} + \frac{1}{2\pi i}\int_{r_2-i\infty}^{r_2+i\infty} \lambda^{-s}G(s)\mathrm{d}s \ . \tag{C.16}$$

For our case, it is easy to show that $G(s) = 0$. So finally, we get

$$H[f;\lambda] = \sum_{r_1<\mathrm{Re}(s)<r_2} \mathrm{res}\left\{\frac{\lambda^{-s}}{[s-(1+i\alpha)]^{\beta+1}}\cdot\frac{\pi}{\sin\pi s}\right\} \ . \tag{C.17}$$

Letting $r_2 \to +\infty$, we get an infinite asymptotic series for $H[f;\lambda]$ as $\lambda \to \infty$.

By applying the above analysis to our particular problem, for $\alpha \neq 0$, we will obtain following asymptotic results:

$$\left.\begin{aligned}
\int_{-\infty}^{0} \frac{(-\eta_1)^{i\alpha}\ln(-\eta_1)}{\eta_1 - z}\mathrm{d}\eta_1 &= \frac{i\pi}{\sinh\pi\alpha} z^{i\alpha}\ln z - \frac{\pi^2\cosh\pi\alpha}{\sinh^2\pi\alpha} z^{i\alpha} - \frac{1}{\alpha^2} \\
&+ O(\,|z|\,) \\
\int_{-\infty}^{0} \frac{(-\eta_1)^{i\alpha}}{\eta_1 - z}\mathrm{d}\eta_1 &= -\frac{i\pi}{\sinh\pi\alpha} z^{i\alpha} + \frac{i}{\alpha} + O(\,|z|\,) \\
\int_{-\infty}^{0} \frac{\ln(-\eta_1)}{\eta_1 - z}\mathrm{d}\eta_1 &= \frac{1}{2}(\ln z)^2 + \frac{\pi^2}{6} + O(\,|z|\,) \\
\int_{-\infty}^{0} \frac{1}{\eta_1 - z}\mathrm{d}\eta_1 &= \ln z + O(\,|z|\,)
\end{aligned}\right\} , \text{ as } z \to 0. \tag{C.18}$$

Chapter 7

Summary

The purpose of this investigation was to understand the influence of transient effects during the process of dynamic fracture in homogeneous solids and bimaterial combinations. The first effort was to develop a fully transient representation of the asymptotic field surrounding the moving crack-tip. This asymptotic representation is able to take all the transient effects into account, including the crack-tip acceleration, the time derivative of the dynamic stress intensity factors, and the geometrical characteristics of the crack path. All these effects, actually, represent the past history of the growing crack. This is unlike the representation which is based on the assumption of the existence of a region dominated by only first term of the asymptotic K_I^d-dominant field. After this transient asymptotic representation was established, we continued our effort in justifying the necessity of applying it to the interpretation of experimental observations of dynamic fracture. To do so, we reconsidered the issue of the domain of dominance of the K_I^d-dominant field and showed that the K_I^d-dominant assumption is insufficient to describe the near-tip deformation field. In addition, we have shown that the new higher order transient asymptotic representation can successfully characterize the near-tip field. This was achieved by comparison of our higher order expansion to known full field analytical solutions and to actual experimental measurements obtained by means of high speed photography and optical methods. As a result, it becomes apparent that accurate extraction of fracture parameters from

experimental measurements requires the use of the higher order transient representation. For dynamic fracture along bimaterial interfaces, similar considerations were emphasized.

In particular, the basic issues studied in this thesis can be summarized as follows:

A. Homogeneous Solids

1. Establishment of a higher order fully transient asymptotic expansion at the vicinity of a crack-tip propagating dynamically along a smooth arbitrary path.
2. Use of known full field solutions of particular transient problems to verify the necessity of the transient expansion and to investigate regions of K_I^d-dominance.
3. Interpretation of plate impact experiments using the higher order transient analysis.
4. Analysis of the optical method of caustics using the transient expansion and investigation of errors resulting from use of the classical (K_I^d-dominant) analysis of caustics.

B. Bimaterial Systems

1. Establishment of the higher order transient asymptotic expansion for cracks propagating dynamically in bimaterial interfaces. Study of the interplay of transients and materials property mismatch.
2. Direct comparison of the predicted analytical near-tip structure to the results of optical CGS experiments in PMMA/steel bimaterial interfaces.
3. Investigation of the conditions under which CGS experiments should be analyzed by taking transients into account and study of regimes of K^d-dominance.

Bibliography

Achenbach, J. D., (1973), *Wave Propagation in Elastic Solids*, North-Holland.

Achenbach, J.D. and Nuismer, R., (1971), "Fracture Generated by a Dilatational Wave," *International Journal of Fracture* **7**, pp.77–88.

Atkinson, C., (1977), "Dynamic Crack Problems in Dissimilar Media," in *Mechanics of Fracture*, **4**, edited by Sih, G.C., Leyden: Noordhoff, pp.213–248.

Baker, B. R., (1962), "Dynamic Stresses Created by a Moving Crack," *Journal of Applied Mechanics*, **29**(3), pp.449–458.

Beinert, J. and Kalthoff, J. F., (1981), "Experimental Determination of Dynamic Stress-Intensity Factors by the Method of Shadow Patterns," in *Mechanics of Fracture*, Vol. VII, edited by Sih, G. C., Sijthoff and Noordhoff, Rockville, USA.

Broberg, K. B., (1960), "The Propagation of a Brittle Crack," *Archiv fur Fysik*, **18**, pp.159–192.

Brock, L.M. and Achenbach, J.D., (1973), "Extension of an Interface Flaw Under the Influence of Transient Waves," *International Journal of Solids and Structures*, **9**, pp.53–67.

Callias, C., Markenscoff, X., and Ni, L., (1990), "A Singular Asymptotic Expansion for the Field Near a Moving Dislocation Loop," *Quarterly of Applied Mathematics*, **48**(1), pp.113–132.

Chona, R. and Shukla, A., (1986), "Determining the Stress Field Parameters Associated with Curving Cracks," in the Proceedings of the 1986 SEM Spring Conference on Experimental Mechanics, New Orleans, Louisiana, June 8–13, 1986, pp.537–545.

Cotterell, B. and Rice, J. R., (1980), "Slightly Curved or Kinked Cracks," *International Journal of Fracture*, **16**(2), pp.155–169.

Craggs, J. W., (1960), "On the Propagation of a Crack in an Elastic-Brittle Material," *Journal of the Mechanics and Physics of Solids*, **8**, pp.66–75.

Dahlberg, L., Nilsson, F., and Brickstad, B., (1980), "Influence of Specimen Geometry on Crack Propagation and Arrest Toughness," in *Crack Arrest Methodology and Applications*, edited by Hahn, G.T., et al., **ASTM STP 711**, pp.89–108.

Dally, J. W., Fourney, W. L., and Irwin, G. R., (1985), "On the Uniqueness of K_{ID}–$\dot{a}$ Relation," *International Journal of Fracture*, **27**, pp.159–168.

Dally, J. W., (1987), "Dynamic Photoelasticity and Its Application to Stress Wave Propagation, Fracture Mechanics and Fracture Control," in *Static and Dynamic Photoelasticity and Caustics*, edited by Lagarde, A., Springer, New York, p.247–406.

Deng, X., (1992), "Complete Complex Series Expansions of Near-Tip Fields for Steadily Growing Interface Cracks in Dissimilar Isotropic Materials," *Engineering Fracture Mechanics*, **42**(2), pp.237–242.

England, A. H., (1965), "A Crack Between Dissimilar Media," *Journal of Applied Mechanics*, **32**, pp.400–402.

Erdogan, F., (1965), "Stress Distribution in Bonded Dissimilar Materials with Cracks," *Journal of Applied Mechanics*, **32**(2), pp.403–410.

Freund, L. B., (1972), "Propagation of a Crack in an Elastic Solid Subjected to General Loading – I. Constant Rate of Extension," *Journal of the Mechanics and Physics of Solids*, **20**(3), pp.129–140.

Freund, L. B., (1973), "Crack Propagation in an Elastic Solid Subjected to General Loading. III. Stress Wave Loading," *Journal of the Mechanics and Physics of Solids* **21**, pp.47–61.

Freund, L. B., (1990), *Dynamic Fracture Mechanics*, Cambridge University Press.

Freund, L. B. and Clifton, R. J., (1974), "On the Uniqueness of Plane Elastodynamic Solutions for Running Cracks," *Journal of Elasticity*, **4**(4), pp.293–299.

Freund, L. B. and Rosakis, A. J., (1990), "The Influence of Transient Effects on the Asymptotic Crack Tip Field during Dynamic Crack Growth," Eleventh National Congress of Applied Mechanics, Tucson, Arizona, May.

Freund, L. B. and Rosakis, A. J., (1992), "The Structure of the Near-Tip Field During Transient Elastodynamic Crack Growth," *Journal of the Mechanics and Physics of Solids*, **40**(3), pp.699–719.

Gol'dstein, R. V., (1967), "On Surface Waves in Jointed Elastic Materials and Their Relation to Crack Propagation Along the Junction," *Applied Mathematics and Mechanics*, **31**, pp.496–502.

Goldsmith, W. and Katsamanis, F., (1979), "Fracture of Notched Polymeric Beams due to Central Impact," *Experimental Mechanics*, **18**, pp.235–244.

Griffith, A. A., (1921), "The Phenomena of Rupture and Flow in Solids," *Philosophical Transactions of the Royal Society of London*, **A221**, pp.163–197.

Hutchinson, J. W. and Suo, Z., (1992), "Mixed Mode Cracking in Layered Materials," in *Advances in Applied Mechanics*, **29**, edited by J. W. Hutchinson and T. Y. Wu, New York: Academic Press, pp.163–191.

Irwin, G. R., (1957), "Analysis of Stresses and Strains Near the End of a Crack Transversing a Plate," *Journal of Applied Mechanics*, **24**, pp.361–364.

Kalthoff, J. F., Winkler, S., and Beinert, J., (1976), "Dynamic Stress - Intensity Factors for Arresting Cracks in DCB Specimens," *International Journal of Fracture*, **12**, pp.317–319.

Kalthoff, J.F., Beinert, J., and Winkler, S.,(1978) , "Influence of Dynamic Effects on Crack Arrest," Institut für Festkörpermechanik, Tech. Report, August.

Kalthoff, J.F., Beinert, J., and Winkler, S.,(1979), "Analysis of Fast Running Arresting Cracks by the Shadow-Optical Method of Caustics," *Proceedings of the IUTAM symposium on Optical Methods in Mechanics of Solids*, edited by Lagarde, A., Poitiers, France, pp.497–508.

Kalthoff, J. F., (1983), "On Some Current Problems in Experimental Fracture Mechanics," in *Workshop on Dynamic Fracture*, edited by Knauss, W.G., *et al.*, California Institute of Technology, pp.11–35.

Katsamanis, F., Raftopoulos, D., and Theocaris, P. S., (1977), "Static and Dynamic Stress Intensity Factors by the Method of Transmitted Caustics," *Journal of Engineering Materials and Technology*, **99**, pp.105–109.

Kim, K. -S., (1985), "Dynamic Fracture under Normal Impact Loading of the Crack Faces," *Journal of Applied Mechanics* **52**, pp.585–92.

Kobayashi, A. S. and Mall, S., (1978), "Dynamic Fracture Toughness of Homalite 100," *Experimental Mechanics*, **18**, pp.11–18.

Kobayashi, T. and Dally, J.W., (1980), "Dynamic Photo-elastic Determination of the $\dot{a}-K$ Relation for the 4340 Steel," in *Crack Arrest Methodology and Applications*, edited by Hahn, G. T., et al., **ASTM STP 711**, pp.189–210.

Krishnaswamy, S. and Rosakis, A. J., (1991), "On the Extent of Dominance of Asymptotic Elastodynamic Crack-Tip Fields: Part I – An Experimental Study Using Bifocal Caustics," *Journal of Applied Mechanics*, **58**(1), pp.87–94.

Krishnaswamy, S., Tippur, H. V. and Rosakis, A. J., (1992), "Measurement of Transient Crack Tip Deformation Fields Using the Method of Coherent Gradient Sensing," *Journal of the Mechanics and Physics of Solids*, 40(2), pp.339–372.

Lambros, J. and Rosakis, A. J., (1994), "Dynamic Decohesion of Bimaterials: Experimental Observations and Failure Criteria," NSF/ONR Symposium on Dynamic Failure of Modern Materials, California Institute of Technology, February 3 – 5, 1994. (Also to appear in a special volume of the *International Journal of Solids and Structures* devoted to Dynamic Failure of Modern Materials, 1994.)

Lee, Y. J., Lambros, J., and Rosakis, A. J., (1993), "Analysis of Coherent Gradient Sensing (CGS) by Fourier Optics," submitted to the *Journal of Applied Optics.*

Lee, Y. J. and Rosakis, A. J., (1992), "Interfacial Cracks in Plates: A Three-Dimensional Numerical Investigation," submitted to the *International Journal of Solids and Structures.*

Liu, C. and Rosakis, A. J., (1992), "On the Higher Order Asymptotic Analysis of a Non-Uniformly Propagating Dynamic Crack Along an Arbitrary Path," SM Report 92–45, Graduate Aeronautical Laboratories, California Institute of Technology. To appear in the *Journal of Elasticity* (1993).

Liu, C. and Rosakis, A. J., (1993), "Dynamic Crack Initiation and Transient Crack Growth Under Stress Wave Loading Conditions: Part I – A Full Field Analytical Solution and an Investigation of Transient Effects," SM Report 93–5, Graduate Aeronautical Laboratories, California Institute of Technology.

Liu, C., Rosakis, A. J., and Freund, L. B., (1993) , "The Interpretation of Optical Caustics in the Presence of Dynamic Non-Uniform Crack-Tip Motion Histories: A Study Based on a Higher Order Transient Crack-Tip Expansion," *International Journal of Solids and Structures*, **30**(7), pp.875–897.

Lo, C. Y., Nakamura, T., and Kushner, A., (1992), "Computational Analysis of Dynamic Crack Propagation Along Bimaterial Interface," to appear in *International Journal of Solids and Structures* (1993).

Ma, C. C. and Freund, L. B., (1986), "The Extent of the Stress Intensity Factor Field During Crack Growth under Dynamic Loading Conditions," *Journal of Applied Mechanics* **53**, pp.303–310.

Malyshev, B. M. and Salganik, R. L., (1965), "The Strength of Adhesive Joints Using the Theory of Crack," *International Journal of Fracture Mechanics*, **1**, pp.114–128.

Manogg, P., (1964), "Anwendungen der Schattenoptik zur Untersuchung des Zerreissvorgags von Platten", Dissertationsschrift an der Universität Freiburg, Germany.

Markenscoff, X. and Ni, L., (1990), "The Singular Nature of the Stress Field Near an Arbitrarily Moving Dislocation Loop," *Journal of the Mechanics and Physics of Solids*, **38**(4), pp.481–490.

Mott, N. F., (1948), "Fracture of Metals: Theoretical Considerations," *Engineering*, **165**, pp.16–18.

Muskhelishvili, N. I., (1953), *Some Basic Problems in the Mathematical Theory of Elasticity* (J. R. M. Radok, trans.), Noordhoff, Groningen, Holland.

Nigam, H. and Shukla, A., (1988), "Comparison of the Techniques of Transmitted Caustics and Photoelasticity as Applied to Fracture," *Experimental Mechanics*, **28**(2), pp.123–133.

Nishioka, T. and Atluri, S. N., (1983), "Path-Independent Integrals, Energy Release Rates, and General Solutions of Near-Tip Fields in Mixed-Mode Dynamic Fracture Mechanics," *Engineering Fracture Mechanics*, **18**(1), pp.1–22.

Prakash, V. and Clifton, R. J., (1992), "Experimental and Analytical Investigation of Dynamic Fracture Under Conditions of Plane Strain," *Fracture Mechanics: Twenty-Second Symposium (Volume I), ASTM STP 1131*, edited by Ernst, H. A. *et al.*, American Society for Testing and Materials, Philadelphia, 1992, pp.412–444.

Prakash, V., Freund, L. B., and Clifton, R. J., (1992), "Stress Wave Radiation From a Crack Tip During Dynamic Initiation," *Journal of Applied Mechanics*, **59**(2), pp.356–365.

Ravi-Chandar, K. and Knauss, W.G.,(1982), "Dynamic Crack-Tip Stresses Under Stress Wave Loading – A Comparison of Theory and Experiment," *International Journal of Fracture* **20**, pp.209–222.

Ravi-Chandar, K. and Knauss, W. G., (1984), "An Experimental Investigation into the Mechanics of Dynamic Fracture: I. Crack Initiation and Arrest," *International Journal of Fracture*, **25**, pp.247–262.

Ravichandran, G. and Clifton, R. J., (1989), "Dynamic Fracture Under Plane Wave Loading," *International Journal of Fracture*, **40**, pp.157–201.

Rice, J.R., (1988), "Elastic Fracture Mechanics Concept for Interfacial Cracks," *Journal of Applied Mechanics*, **55**(1), pp.98–103.

Rice, J. R. and Sih, G. C., (1965), "Plane Problems of Cracks in Dissimilar Media," *Journal of Applied Mechanics*, **32**(2), pp.418–423.

Rosakis, A.J., (1980), "Analysis of the Optical Method of Caustics for Dynamic Crack Propagation," *Engineering Fracture Mechanics*, **13**, pp.331–347.

Rosakis, A. J., (1993), "Two Optical Techniques Sensitive to Gradients of Optical Path Difference: The Method of Caustics and the Coherent Gradient Sensor (CGS)," in *Experimental Techniques in Fracture*, **3**, edited by J. Epstein, Chapter 10, pp.327–425.

Rosakis, A.J., Duffy, J., and Freund, L.B., (1984), "The Determination of Dynamic Fracture Toughness of AISI 4340 Steel by the Shadow Spot Method," *Journal of the Mechanics and Physics of Solids*, **32**, pp.443–460.

Rosakis, A. J., Krishnaswamy, S., and Tippur, H. V., (1990), "On the Application of the Optical Method of Caustics to the Investigation of Transient Elastodynamic Crack Problems: Limitations of the Classical Interpretation," *Optics and Lasers in Engineering*, **13**, pp.183–210.

Rosakis, A.J. and Lambros, J., (1993), "Dynamic Failure of Bimaterials and Composites," Proceedings of the 9th International Conference on Composite Materials (ICCM), Madrid, Spain, July 12 – 16, 1993.

Rosakis, A.J., Lee, Y.J., and Lambros, J.,(1991), "Dynamic Crack Growth in Bimaterial Interfaces," in *Experiments in Micromechanics of Failure Resistant Materials*, AMD-Vol 130, AMSE 1991, edited by K.-S. Kim, pp.17–23.

Rosakis, A. J., Liu, C., and Freund, L. B., (1991), "A Note on the Asymptotic Stress Field of a Non-Uniformly Propagating Dynamic Crack," *International Journal of Fracture*, **50**, R39–R45.

Rosakis, A. J. and Ravi-Chandar, K., (1986), "On Crack-Tip Stress State: An Experimental Evaluation of Three-Dimensional Effects," *International Journal of Solids and Structures*, **22**(2), pp.121–134.

Rosakis, A. J. and Zehnder, A. T., (1985), "On the Method of Caustics: An Exact Analysis Based on Geometrical Optics," *Journal of Elasticity*, **15**(4), pp.347–368.

Rossmanith, H. P., (1983), "How 'Mixed' Is Dynamic Mixed-Mode Crack Propagation?" *Journal of the Mechanics and Physics of Solids*, **31**(3), pp.251–260.

Schardin, H., (1959), "Velocity Effects in Fracture," in *Fracture*, edited by Averback, B. L., *et al.*, John Wiley and Sons, New York.

Shih, C. F., (1991), "Cracks on Bimaterial Interfaces: Elasticity and Plasticity Aspects," *Material Science and Engineering*, **A143**, pp.77–90.

Sih, G. C. and Rice, J. R., (1964), "Bending of Plates of Dissimilar Materials with Cracks," *Journal of Applied Mechanics*, **31**, pp.477–482.

Shukla, A. and Chona, R., (1988), "The Stress Field Surrounding a Rapidly Propagating Curving Crack," *Fracture Mechanics: Eighteenth Symposium, ASTM STP 945*, edited by Read, D. T. and Reed, R. P., American Society for Testing and Materials, Philadelphia, 1988, pp.86–99.

Takahashi, K. and Arakawa, K., (1987), "Dependence of Crack Acceleration on the Dynamic Stress-Intensity Factor in Polymers," *Experimental Mechanics*, **27**(2), pp.195–199.

Theocaris, P. S., (1970), "Local Yielding around a Crack Tip in Plexiglas," *Journal of Applied Mechanics*, **37**, pp.409–415.

Theocaris, P. S., (1971), "Reflected Shadow Method for the Study of Constrained Zones in Cracked Plates," *Applied Optics*, **10**, pp.2240–2247.

Theocaris, P. S., (1978), "Dynamic Propagation and Arrest Measurements by the Method of Caustics on Overlapping Skew-Parallel Cracks," *International Journal of Solids and Structures*, **14**, pp.639–653.

Theocaris, P. S., (1981), "Elastic Stress Intensity Factors Evaluated by Caustics," in *Mechanics of Fracture*, Vol. VII, edited by Sih, G.C., Sijthoff and Noordhoff, Rockville, USA.

Theocaris, P.S. and Gdoutos, E.E., (1974), "The Modified Dugdale-Barenblatt Model Adapted to Various Fracture Configurations in Metals," *International Journal of Fracture*, **10**, pp.549–564.

Tippur, H. V., Krishnaswamy, S., and Rosakis, A. J., (1991), "A Coherent Gradient Sensor for Crack Tip Measurements: Analysis and Experimental Results," *International Journal of Fracture*, **48**, pp.193–204.

Tippur, H.V. and Rosakis, A.J., (1991), "Quasi-Static and Dynamic Crack Growth Along Bimaterial Interfaces: A Note on Crack-Tip Field Measurements Using Coherent Gradient Sensing," *Experimental Mechanics*, **31**(3), pp.243–251.

Wheeler, L.T. and Sternberg, E., (1968), "Some Theorems in Classical Elastodynamics," *Archive for Rational Mechanics and Analysis*, **31**(1), pp.51–90.

Williams, M. L., (1957), "On the Stress Distribution at the Base of a Stationary Crack," *Journal of Applied Mechanics*, **24**, pp.109–114.

Williams, M. L., (1959), "The Stresses Around a Fault or Crack in Dissimilar Media," *Bulletin of the Seismological Society of America*, **49**(2), pp.199–203.

Willis, J. R., (1971), "Fracture Mechanics of Interfacial Cracks," *Journal of the Mechanics and Physics of Solids*, **19**, pp.353–368.

Willis, J. R., (1973), "Self-Similar Problems in Elastodynamics," *Philosophical Transactions of the Royal Society* (London), **274**, pp.435–491.

Willis, J. R., (1992), "The Stress Field Near the Tip of an Accelerating Crack," *Journal of the Mechanics and Physics of Solids*, **40**(7), pp.1671–1681.

Wu, K. C., (1991), "Explicit Crack-Tip Fields of an Extending Interface Crack in an Anisotropic Bimaterial," *International Journal of Solids and Structures*, **27**(4), pp.455–466.

Yang, W. and Freund, L. B., (1985), "Transverse Shear Effects for through Cracks in an Elastic Plate," *International Journal of Solids and Structures*, **21**(9), pp.977–994.

Yang, W., Suo, Z., and Shih, C. F., (1991) , "Mechanics of Dynamic Debonding," *Proceedings of the Royal Society of London* **A**, **433**, pp.679–697.

Yoffe, E. H., (1951), "The Moving Griffith Crack," *Philosophical Magazine*, **42**, pp.739–750.

Zehnder, A.T. and Rosakis, A.J., (1990), "Dynamic Fracture Initiation and Propagation in 4340 Steel under Impact Loading," *International Journal of Fracture*, **43**(4), pp.271–285.